



The University of Manchester

School of Chemistry

**The use of Optical Microscopy, X-ray Powder Diffraction, and
Single Crystal Diffraction to Identify and Structurally
Characterize Novel Transition Metal Benzoates.**

*A thesis submitted to the University of Manchester for the degree of
Doctor of Philosophy in Faculty of Science and Engineering*

By

Motunrayo Ololade Ladele

Main Supervisor: Dr. Robin G. Pritchard

Co-Supervisor: Dr. Frank S. Mair

The University of Manchester

School of Chemistry

**The use of Optical Microscopy, X-ray Powder Diffraction,
and Single Crystal Diffraction to Identify and Structurally
Characterize Novel Transition Metal Benzoates.**

*A thesis submitted to the University of Manchester for the degree of
Doctor of Philosophy in Faculty of Science and Engineering*

Motunrayo Ololade Ladele

2018

Table of Contents

Contents

Table of Contents.....	2
Dedication.....	7
Notations.....	8
Abstract.....	10
Declaration.....	11
Copyright Statement.....	12
Software Used.....	13
<i>Acknowledgment</i>	14
Chapter 1	15
Coordination Polymers of 1st-row Transition Metals and Substituted Benzoic Acids (1D, 2D, and 3D)	15
1.0. Introduction.....	16
1.1. The Chemistry of Carboxylate Based Ligands.....	21
1.2. The Chemistry of 1 st -row 3d Transition Metals.....	26
1.3. Coordination Polymers.....	35
1.4. Metal-Organic Frameworks.....	38
1.5. Chemical Interactions in Crystal Structures and MOFs.....	42
1.6. Studying the Formation of MOFs in Manchester.....	45
Chapter 2	47
The Theory and Practice of X-ray Single Crystal Diffraction	47
2.1. Introduction.....	48
2.2. The Crystallographic Concepts.....	49
2.2.1. Lattices and Unit Cells.....	49
2.2.2. Miller Indices.....	52
2.3. Symmetry and Space groups.....	53
2.3.1. Point Groups.....	53

2.3.2. Space Groups	54
2.4. Crystallization with particular reference to the techniques used in this study.	55
2.4.1. Crystal Growth.....	55
2.4.2. Characteristics of Crystals	56
2.4.3. Properties of Crystals.....	56
2.5. Crystallization Techniques commonly used for Small Molecules in the Chemical Laboratory	58
2.6. Introduction to X-ray Crystallography.....	59
2.6.1. Bragg's Law and Diffraction	59
2.6.2. Deriving Bragg's Law.....	59
2.7. Single Crystal Diffraction of X-rays	61
2.7.1. Production of X-rays.....	62
2.7.2. X-ray Scattering from the Crystal.....	63
2.7.3. Detection of X-rays.....	66
2.8. Single Crystal X-ray Diffraction Practice	67
2.8.1. Measuring and Obtaining Single Crystal X-Ray Diffraction Data	67
2.8.2. X-ray Crystal Structure Determination	67
2.8.3. Crystal Structure Analysis	69
2.9. Powder X-ray Diffraction (PXRD).....	71
Chapter 3	73
The Reaction of Substituted Benzoic Acids with a range of 1st-row Transition Metals and Investigation of the Products using Optical Microscopy and Single Crystal X-ray Diffraction..	73
3.1. Introduction.....	74
3.2. Result and Discussion.....	77
3.2.1. Reactive Crystallization and Crystal Structure of $[\text{Zn}(\text{C}_8\text{H}_5\text{NO}_4)(\text{H}_2\text{O})]_n$	77
3.2.1.1. Introduction.....	77
3.2.1.2. Crystal Structure Determination of Complex 1	78
3.2.2. Reactive Crystallization and Crystal Structure of $(\text{C}_8\text{H}_6\text{O}_6).(\text{Me}_2\text{NCHO})$	81
3.2.2.1. Introduction.....	81
3.2.2.2. Crystal Structure Determination of Complex 2	81

3.2.3. Reactive Crystallization and Crystal Structure of $[\text{Co}(\text{C}_8\text{H}_4\text{O}_6)(\text{C}_3\text{H}_7\text{NO})_2(\text{H}_2\text{O})_2]_n$	88
3.2.3.1. Introduction.....	88
3.2.3.2. Crystal Structure Determination of Complex 3	90
3.2.4. Reactive Crystallization and Crystal Structure of $\text{Na}_2(\text{C}_8\text{H}_6\text{NO}_4)_2(\text{C}_8\text{H}_7\text{NO}_4)_2(\text{H}_2\text{O})_6$	101
3.2.4.1. Introduction.....	101
3.2.4.2. Crystal Structure Determination of Complex 4	101
3.3. Summary.....	107
Chapter 4	108
The Small-scale Crystallization of MSO_4, where M = Cu, Co, Zn, and Ni Hydrates with NaAMB from Aqueous Solution in order to screen for Mixed Metal Compounds, Polymorphs, and Solvates	108
4.1. Introduction.....	109
4.2. Results and Discussion	111
4.2.1. Reactive Crystallization and Crystal Structure of $[\text{Cu}(\text{C}_8\text{H}_8\text{NO}_2)_2]_n$	111
4.2.1.1. Introduction.....	111
4.2.1.2. Crystal Structure Determination of Complexes 5a , 5b , 5c and, DUKTIM	112
4.2.2. Reactive Crystallization and Crystal Structures of Novel Hydrated CuAMB Complexes $[\text{Cu}(\text{C}_8\text{H}_8\text{NO}_2)\cdot\text{H}_2\text{O}]_2$, $\{[\text{Cu}(\text{C}_8\text{H}_8\text{NO}_2)_2]_2\cdot 8/3\text{H}_2\text{O}\}_n$ and $\{[\text{Cu}(\text{C}_8\text{H}_8\text{NO}_2)_2]_2\cdot 13/5\text{H}_2\text{O}\}_n$	116
4.2.2.1. Structural Characterization of $[\text{Cu}(\text{C}_8\text{H}_8\text{NO}_2)\cdot\text{H}_2\text{O}]_2$	116
4.2.2.2. Introduction.....	116
4.2.2.3. Crystal Structure Determination of Complex 6	117
4.2.3. Structural Characterization of $\{[\text{Cu}(\text{C}_8\text{H}_8\text{NO}_2)_2]_2\cdot 8/3\text{H}_2\text{O}\}_n$	126
4.2.3.1. Introduction.....	126
4.2.3.2. Crystal Structure Determination of Complex 7	126
4.2.3.3. Structural Characterization of $\{[\text{Cu}(\text{C}_8\text{H}_8\text{NO}_2)_2]_2\cdot 13/5\text{H}_2\text{O}\}_n$	134
4.2.3.4. Introduction.....	134
4.2.4.2. Crystal Structure Determination of Complex 8	135
4.2.5. Reactive Crystallization of Anhydrous ZnAMB $[\text{Zn}(\text{C}_8\text{H}_8\text{NO}_2)_2]_n$	148
4.2.5.1. Introduction.....	148
4.2.5.2. Structural Characterization of Anhydrous ZnAMB $[\text{Zn}(\text{C}_8\text{H}_8\text{NO}_2)_2]_n$	148
4.2.5.3. Introduction.....	148

4.2.5.4.	Crystal Structure Determination of Complex 9	148
4.2.6.	Reactive Crystallization and Crystal Structure of Novel Anhydrous and Hydrated CoAMB $[\text{Co}(\text{C}_8\text{H}_8\text{NO}_2)_2]_n$ and $\{[\text{Co}(\text{C}_8\text{H}_8\text{NO}_2)_2]\cdot\text{H}_2\text{O}\}_n$	157
4.2.6.1.	Introduction	157
4.2.6.2.	Structural Characterization of Hydrated CoAMB Structure $\{[\text{Co}(\text{C}_8\text{H}_8\text{NO}_2)_2]\cdot\text{H}_2\text{O}\}_n$ 159	
4.2.6.3.	Introduction	159
4.2.6.4.	Crystal Structure Determination of Complex 10	160
4.2.7.	Structural Characterization of Anhydrous CoAMB $[\text{Co}(\text{C}_8\text{H}_8\text{NO}_2)_2]_n$	167
4.2.7.1.	Introduction	167
4.2.7.2.	Crystal Structure Determination of Complex 11	167
4.2.8.	Reactive Crystallization of Novel Hydrated NiAMB $\text{Ni}(\text{C}_8\text{H}_8\text{NO}_2)(\text{H}_2\text{O})_2\cdot 2\text{H}_2\text{O}$	174
4.2.8.1.	Introduction	174
4.2.8.2.	Structural Characterization of Complex 12	174
4.2.8.3.	Crystal Structure Determination of Complex 12	175
4.3.	Summary	187
Chapter 5		201
Small-scale Crystallization of MSO_4 and MnCO_3 Hydrates with Benzoic Acid from Aqueous Solution in order to screen for Polymorphs and Solvates		201
5.1.	Introduction	202
5.2.	Results and Discussion	206
5.2.1.	Structural Characterization of $[\text{Mn}_2(\text{C}_6\text{H}_5\text{CO}_2)_4(\text{H}_2\text{O})_6]\cdot(\text{H}_2\text{O})_2$	206
5.2.1.1.	Introduction	206
5.2.1.2.	Crystal Structure Determination of Complex 13	206
5.2.2.	Structure Determination of $[\text{Mn}_2(\text{C}_6\text{H}_5\text{CO}_2)_4(\text{H}_2\text{O})_4]_n$	215
5.2.2.1.	Introduction	215
5.2.2.2.	Crystal Structure Determination of Complex 14	215
5.3.	Summary	226
Chapter 6		229
Experimental		229
6.1.	General Experimental Methods	230

6.2. Solvents and Reagents	230
6.3. Reactive Crystallization of Complexes 1, 2, 3 and 4	231
6.3.1. Reactive Crystallization of Metal Halides: ZnCl ₂ and CoCl ₂ .6H ₂ O with Five Substituted Benzoic Acid Ligands in Water, in DMF and in 50:50 Water/Methanol	231
6.3.2. Reactive Crystallization of Zinc Chloride (ZnCl ₂) with Five Substituted Benzoic Acid Ligands	232
6.3.3. Reactive Crystallization of Cobalt(II)Chloride Hexahydrate (CoCl ₂ .6H ₂ O) with Five Substituted Benzoic Acid.....	232
6.3.4. Reactive Crystallization of Different 1 st -row 3d Transition Metals and 5-aminoisophthalic acid in Water and in 50:50 H ₂ O/MeOH.....	233
6.4. Reactive Crystallization of Anhydrous and Hydrated M(AMB) _n	236
6.4.1. The Small-scale Crystallization of MSO ₄ , where M = Cu, Co, Zn, and Ni Hydrates with NaAMB from Aqueous Solution in order to screen for mixed Metal Compounds, Polymorphs, and Solvate	236
6.5. Small-scale Crystallization of MSO ₄ and MnCO ₃ Hydrates with Benzoic Acid from Aqueous Solution in order to screen for Polymorphs and Solvates	241
6.6. X-ray Structure Determination.....	244
Chapter 7	245
Conclusion and Suggestion for Future Work.....	245
7.1. Conclusion	246
7.2. Suggestion for further work	249
Appendix 1	250
Appendix 2.....	251
References.....	252

Dedication

This thesis is dedicated to the memory of my mother. The legacy you left behind has helped me to go this far.

Florence Oluyemisi Ladele

1948 – 2001

Notations

Abbreviation	Definition
λ	Wavelength
\AA	Angstrom
ω	Angular frequency
Θ	Bragg angle
$^{\circ}$	Degree
T	Temperature in Kelvin
Σ	Summation sign (Sigma)
C	C-face centered
Exp	Exponential function
F	Face-centered lattice
I	Body-centered Lattice
n	Any integer
m	Mirror planes
P	Primitive
V	Unit cell volume
δ	Interbond angle
XRD	X-ray Diffraction
SXRD	Single Crystal X-ray Diffraction
CCD	Charge Coupled Device
μ	X-ray Absorption Coefficient
s.u	Standard Uncertainty
R	Residual (R-factor)
${}_o$	Subscript: observed, as in $jF_o(hkl)_j$
l	Miller index parallel to the z-axis
R	Primitive Rhombohedral
R	Reliability factor
a, b, c	Unit-cell vectors of direct lattice
D	The distance between two diffracting slits
$d(hkl)$	The interplanar spacing of the (hkl)
(hkl)	Indices of a crystal face or of a single plane or of a set of parallel planes

f_j	Atomic scattering factor / for the j^{th} atom
$F(hkl)$	Structure factor for the hkl spectrum referred to one unit cell
H	Vector with components h, k, l in reciprocal space
h	Miller index parallel to the x -axis; Planck's constant
$I_o(hkl)$	the Observed intensity of reflection from the (hkl) planes referred to one unit cell
x, y, z	Coordination of any of a series of systematically spaced points expressed as a fraction of a, b, c filling the unit cell at a regular interval
α, β, γ	Interaxial angles between $b-c, a-c$ and $a-b$ respectively (alpha, beta, gamma).
CSD	Cambridge structure database
$\text{CuK}\alpha$	Copper Radiation
$\text{MoK}\alpha$	Molybdenum Radiation
Z	The number of formula units in the unit cell
Z'	The number of formula units in the asymmetric unit
$\rho(xyz)$	Electron density at the point x, y, z (units are length)
1D, 2D, 3D	One-, two-, and three-dimension
CCDC	Cambridge Crystallographic Data Centre
CIF	Crystallographic information file. It contains all the important information on the crystal
Me	Methyl
CPs	Coordination polymers
MOFs	Metal-Organic Frameworks
AMB	2-methyl-3-aminobenzoic acid
(H_2BDC)	Benzene-1,4-dicarboxylic acid

Abstract

This research investigated medium scale synthesis and crystallization, followed by structural characterization, as a means of discovering new solid-state products, with a series of controlled micro-scale reaction/crystallization experiments using various reagent ratios whilst monitoring changes using optical microscopy. By characterizing any crystals formed, the products (monomers, dimers, polymers, clusters, solvates, and polymorphs) were mapped in terms of reaction conditions (reagent ratios, solvent, temperature, time in solution).

Chapter 1 of this thesis covers the coordination polymer of 1st-row 3d transition metals and substituted benzoic acids. (1D, 2D, and 3D).

Chapter 2 describes the theory and practice of X-ray single crystal diffraction.

Chapter 3 describes the crystallization reaction of the substituted benzoic acids such as $\text{HOC}_6\text{H}_3\text{-1,3-(CO}_2\text{H)}_2$, $\text{H}_2\text{NC}_6\text{H}_3\text{-1,3-(CO}_2\text{H)}_2$, $(\text{HO})_2\text{C}_6\text{H}_2\text{-1,4-(CO}_2\text{H)}_2$, $\text{C}_6\text{H}_4\text{-1,4-(CO}_2\text{H)}_2$ and $\text{C}_6\text{H}_4\text{-1,3-(CO}_2\text{H)}_2$ with a range of 1st-row 3d transition metal halide/acetate such as CuCl_2 , $\text{CoCl}_2 \cdot 6\text{H}_2\text{O}$, ZnCl_2 , FeCl_2 , VCl_3 , NiCl_2 , CoCl_2 and $\text{Zn}(\text{CH}_3\text{COO})_2 \cdot 2\text{H}_2\text{O}$ in H_2O and in 50:50 $\text{H}_2\text{O}/\text{MeOH}$. These metal-ligand reactions produced known $[\text{Zn}(\text{C}_8\text{H}_5\text{NO}_4)(\text{H}_2\text{O})]_n$, $[\text{Co}(\text{C}_8\text{H}_4\text{O}_6)(\text{Me}_2\text{NCHO})_2(\text{H}_2\text{O})_2]_n$ and unknown $(\text{C}_8\text{H}_6\text{O}_6) \cdot 2(\text{Me}_2\text{NCHO})$ metal complexes that were investigated using optical microscopy and single crystal X-ray diffraction.

Chapter 4 describes the small-scale crystallization of MSO_4 hydrates, where $\text{M} = \text{Cu, Co, Zn, and Ni}$ (as a pure metal and as a bimetallic reaction) with sodium 2-amine-3-methylbenzoate (NaAMB) from aqueous solution in order to screen for mixed metal compounds, polymorphs, and solvates. These pure and bimetallic metal-ligand reactions produced known and unknown hydrate and anhydrous metal complexes: $[\text{Cu}(\text{C}_8\text{H}_8\text{NO}_2)_2]_n$, $[\text{Cu}(\text{C}_8\text{H}_8\text{NO}_2)_2 \cdot 2\text{H}_2\text{O}]_2$, $\{\text{Cu}(\text{C}_8\text{H}_8\text{NO}_2)_2\}_n \cdot \frac{8}{3}\text{H}_2\text{O}$, $\{\text{Cu}(\text{C}_8\text{H}_8\text{NO}_2)_2\}_n \cdot \frac{13}{5}\text{H}_2\text{O}$, $[\text{Zn}(\text{C}_8\text{H}_8\text{NO}_2)_2]_n$, $\{\text{Co}(\text{C}_8\text{H}_8\text{NO}_2)_2\}_n$, $\{\text{Co}(\text{C}_8\text{H}_8\text{NO}_2)_2 \cdot \text{H}_2\text{O}\}_n$ and $[\text{Ni}(\text{C}_8\text{H}_8\text{NO}_2)_2(\text{H}_2\text{O})_2] \cdot 2\text{H}_2\text{O}$.

Chapter 5 describes the small-scale crystallization of MnSO_4 and MnCO_3 hydrates with benzoic acid from aqueous solution to screen for polymorphs and solvates. These reactions produced two manganese benzoate linear chain polymers $[\text{Mn}_2(\text{C}_6\text{H}_5\text{CO}_2)_4(\text{H}_2\text{O})_6] \cdot [\text{H}_2\text{O}]_2$ and $\{\text{Mn}_2(\text{C}_6\text{H}_5\text{CO}_2)_4(\text{H}_2\text{O})_4\}_n$.

Chapter 7 concludes the thesis and suggests further work.

Declaration

No portion of the work referred to in this thesis has been submitted in support of an application for another degree or qualification of this or any other university or another institute of learning.

.....
Motunrayo Ololade Ladele

Copyright Statement

- i. The author of this thesis (including any appendices and/or schedules to this thesis) owns certain copyright or related rights in it (the “Copyright”) and s/he has given The University of Manchester certain rights to use such Copyright, including for administrative purposes.
- ii. Copies of this thesis, either in full or in extracts and whether in hard or electronic copy, may be made only in accordance with the Copyright, Designs and Patents Act 1988 (as amended) and regulations issued under it or, where appropriate, in accordance Presentation of Theses Policy.
- iii. The ownership of certain Copyright, patents, designs, trademarks and other intellectual property (the “Intellectual Property”) and any reproductions of copyright works in the thesis, for example graphs and tables (“Reproductions”), which may be described in this thesis, may not be owned by the author and may be owned by third parties. Such Intellectual Property and Reproductions cannot and must not be made available for use without the prior written permission of the owner(s) of the relevant Intellectual Property and/or Reproductions.
- iv. Further information on the conditions under which disclosure, publication, and commercialization of this thesis, the Copyright and any Intellectual Property and/or Reproductions described in it may take place is available in the University IP Policy in any relevant Thesis restriction declarations deposited in the University of Manchester Library, The University Library’s regulations and in The university’s policy on Presentation of Thesis.

Software Used

The software used in this study is described as follows:

1. **CrysAlis Pro:** It is software used for data collection and for the processing of small molecule and protein crystallography. It features automatic crystal screening, data collection, and strategy modules. Information such as intensity estimation by resolution range, unit cell parameters and suggested frame exposure times for the full data collection can be obtained in CrysAlis Pro.
2. **Olex2:** This program provides comprehensive tools for refinement and for solving molecular structures. CIF File data of the final molecular structure can be obtained in Olex2.
3. **SHELX:** SHELX programs are used for determining small and macro-crystal structures using single crystal X-ray diffraction data. The different SHELX program includes SHELXS, SHELXL, SHELXD, and SHELXT.
4. **PLATON:** It is a versatile SHELXL compatible multipurpose crystallographic tool.
5. **ConQuest:** This is a primary program used for searching and retrieving of information from the Cambridge Structural Database (CSD). ConQuest provides an extensive range of flexible search options such as locating structures based on compound name, formula, and the elemental.
6. **Mercury:** Mercury is a comprehensive tool for 3D structure visualization and the exploration of crystal packing within the crystallographic community. Also, quality images used in publications can be produced using Mercury. It is also be used to define and visualize a wide range of operations such as Miller planes, to generate packing diagrams, to build and explore networks of intermolecular contacts.
7. **PublCIF:** It is an application that accepts a crystallographic information file (CIF) and prepares a formatted paper (Preprint) in the style of Acta Crystallographic Sections C and E, with IUCr (International Union of Crystallography) format data.
8. **ChemBioDraw:** This software is the drawing tool employed for creating scientific drawings. Chemical information such as the name of the structure, molecular formula, formula weight, and element analysis can be performed in ChemBioDraw.

Acknowledgment

I would like to take this opportunity to thank everyone that supported me during my studies especially Mrs. Lara Ayodele for caring for my son whenever I am away in the laboratory or library.

I wouldn't have achieved this success if not for the supports and unrelenting efforts of my supervisor Dr. Robin .G. Pritchard (retired). Thank you for standing by me and rendered supports that promote the quality of my study. I appreciate your kind-heartedness and your zeal to support me in my dark times when I ought to have pulled out. I also appreciate my co-supervisor Dr. Frank S. Mair for reading through my work at odd times and made sure I have a standard Ph.D. thesis. I appreciate colleagues in my research group, especially Mona Saad Binkadem, thank you for always making out time to help.

I appreciate the countless support I received from the Postgraduate Support Team in the person of Helen Kreissl and Angela Dermody. You both make sure I always soar high in the face of challenges. You both are the best part of my life during my studies.

I appreciate The Nigeria Government under the past administration for awarding me a full scholarship to embark on this study.

I am grateful to the University of Manchester Management for not logging me out of the University system when the Nigeria Government abandoned and refused to pay my tuition. It is a rare privilege that I so much cherish.

I am so indebted to my father and siblings for their prayers and support. Thank you so much Dr. & Mrs. Dotun Akinlade for supporting me always. Thank you so much Dr. & Mrs. Tunde Adegbola, you are a rare gem sent to me by God.

My special thanks go to my son, my best friend, my supporter, and encourager, Master Gideon Eyitayo, you doubled up as everything to me. Your joy keeps me going daily. Your 'mummy don't worry' pushed me through. For wiping my tears and for always giving me curdles when I cry, I love you endlessly. You are the best in the whole wide world.

I appreciate God the giver of life and opportunity. His Lordship over my life brought me this far. I give HIM all the glory.

Chapter 1

Coordination Polymers of 1st-row Transition Metals and Substituted Benzoic Acids (1D, 2D, and 3D)

1.0. Introduction

The study of coordination polymers (CPs) has been a thing of great interest in the Chemistry world in the past years because they have the potential to function as materials used in organic chemistry (coordination compounds are made from the reaction between an organic ligands and transition metals), inorganic chemistry, biochemistry, material science,¹ as precursors for the preparation of nanomaterials,² electrochemistry and pharmacology, (active pharmaceutical ingredients can be screened for unexpected co-crystal formation when they are mixed with “inactive” ingredients in a formulation) with many other potential applications such as separation processes as in gas separation,³ non-linear optics or zeolitic behaviour,⁴ magnetism,⁵ catalysis,⁶ and drug delivery.⁷ The intriguing structural architectures and topologies coupled with the interdisciplinary nature of coordination polymers made their study to be extensive and popular in the recent time.⁸

The construction of coordination polymers depends mainly on the structural chemistry of the organic ligands, the nature of the metal centre as nodes, metal centre oxidation state, their preferred geometry environment, the character of the solvent,⁵ and the reaction conditions such as temperature,⁹ the metal-ligand ratio (concentration), counter anions, the pH value and reaction time.¹⁰

The most important factor in the construction of CPs and MOFs is the organic ligands because of their length, steric effect, and flexibility which normally lead to diverse structures of coordination polymers.¹¹ Ligands have been confirmed to play an important role in the construction of the structure, the topology and the functionality of CPs and MOFs.¹² When constructing coordination polymers, multidentate ligands with two or more donor atoms must be used since the ligand is expected to bridge between two metal ions. Depending on the number of donor atoms, the bridging ligands could be di-, tri- or tetrapopic.¹² To assemble a fantastic MOFs structure with desirable properties, controlling the properties of ligands such as the shape, functionality, flexibility, conformation, and symmetry should be considered.¹³

Organic ligands such as pure carboxylate ligands, amine substituted carboxylate ligands, methyl-substituted poly-carboxylate ligands and aromatic multi-carboxylate ligands (illustrated in figure 1-1) are the major carboxylate based ligands used in the construction of coordination polymers.

Symmetric carboxylate ligands often directly contribute to the formation of 3D frameworks with high symmetry, high surface area, and high pore volumes. For example, an aromatic polycarboxylic acid such as biphenyl-3,3',5,5'-tetracarboxylic acid (H_4bpta) with D_{2h} symmetry have been used on many occasions in the past to construct interesting frameworks with high pore volume for gas absorption¹³ while a low symmetry carboxylate ligand with three functional carboxylate groups such as 1,2,4-benzenetricarboxylic acid (H_3BTC) can devote from one to six oxygen atoms to coordinate to metal ions either as monodentate, bidentate, tridentate, tetradentate, pentadentate and hexadentate modes respectively.¹⁴

Aromatic carboxylate ligands such as 2,2'-biphenyldicarboxylic acid (H_2dpa) are excellent building blocks in the construction of coordination polymers due to their different coordination modes, self-penetration, versatile bridging fashions and their application as functional materials.¹⁵⁻¹⁶

Dicarboxylate ligands such as 1,4-dicarboxylic acid and pyridine-2,3-dicarboxylic acid have attracted much interest in coordination chemistry because they are a very important bridging ligand that displays various coordination modes. Likewise, multidentate ligands in coordination polymers have the ability to form multiple coordination bonds and act as a bridge between monomeric or multiple metal centres.¹⁰

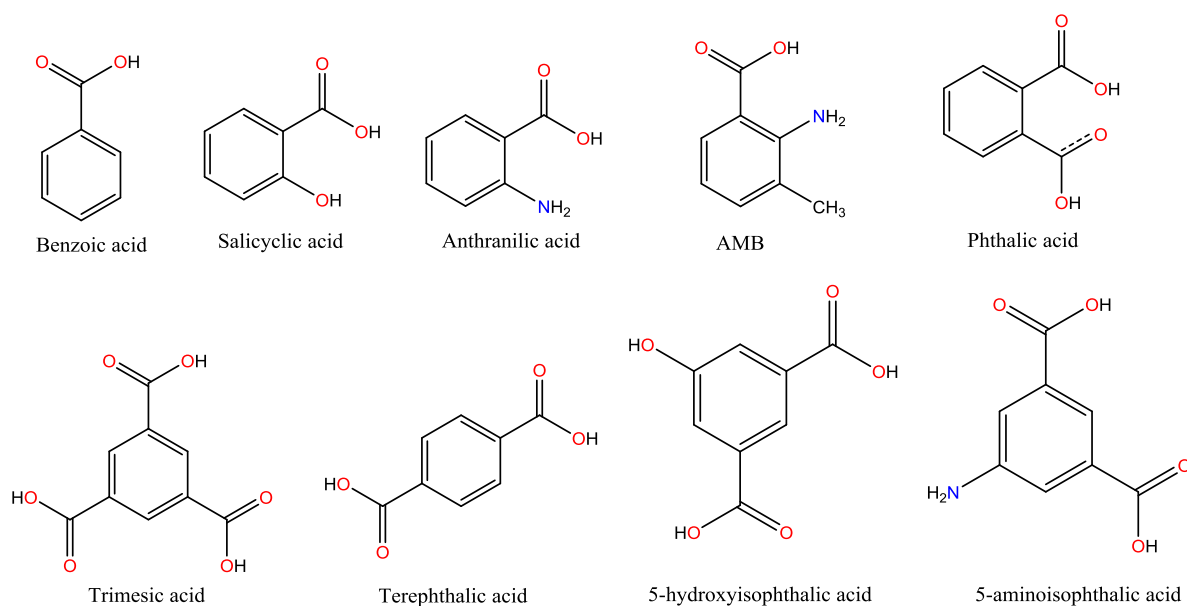


Figure 1-1: Examples of monodentate, bidentate and polydentate organic ligands.

Benzoic acid can act as a monodentate ligand by binding to a metal centre at one of its carboxylate oxygen atom or as a bidentate ligand by binding to the metal centre through both carboxylate oxygen atoms.

Carboxylate groups can display a wide variety of coordination modes such as *terminal* coordination mode in *the* monodentate ligand, *bridging*, *chelating* and with several configurations like *syn-syn* bidentate bridging mode, *syn-anti* bidentate bridging mode, and *anti-anti* bidentate bridging mode. Organic ligands such as AMB, anthranilic acid and ethylenediamine can act as bidentate or tridentate ligand binding to two different metal centres in different conformation such as *syn-syn* or *syn-anti* bidentate bridging mode while ligands such as trimesic acid and 5-aminoisophthalic acid could be tridentate or polydentate, binding to the metal centre at one or two of both of their carboxylate group and at the amino group depending on the coordination mode of the metal centre.¹⁷

The mono- and tri-atomic *syn-syn* conformations usually favour the formation of dinuclear complexes while the *anti-anti* and *syn-anti* triatomic conformations generally correspond to chain or layer compounds.¹⁸ Efforts have been channeled toward the use of dicarboxylic acid to study how the incorporation of this ligand type might affect the structures and the physical properties of the coordination polymers of metal-organic frameworks.¹⁹

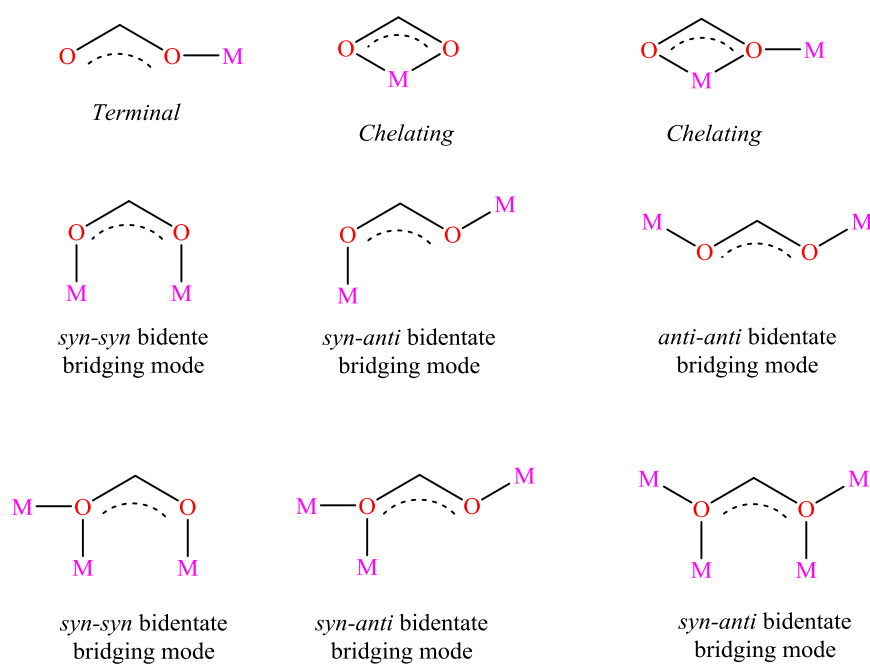


Figure 1-2: Different possible coordination modes of carboxylate groups.⁶

Simple benzoic acid, dibenzoic acids (including terephthalic acid and isophthalic acid) and more substituted cases such as AMB and 5-aminoisophthalic acid (figure 1-1) have all been used as ligands previously in the construction of coordination polymers. This study seeks to extend the use of such ligands, widening and deepening the knowledge of their coordination chemistry. The conjugate bases of all of these ligands can act as monodentate, bidentate or polydentate ligands when crystallized with a range of metal ions as illustrated in figure 1-2.

For example, isophthalic acid has various bridging abilities and rich coordination modes with multiple coordination sites that may generate structures of higher dimensions. The structure consists of two carboxylate groups, one or both of which may be deprotonated and thus results in acidity-dependent coordination modes.²⁰

All carboxylic acids in neutral form or in protonated form are self-complimentary in terms of H-bonding being both a C-O...H H-bond donor and a C=O: H-bond acceptor. This results in the common carboxylic acid dimer motif shown in figure 1-3. Such motifs give rise to short bridges where only a single carboxylate is present, but can also give long bridges via the benzene ring if there are more than one carboxylates.

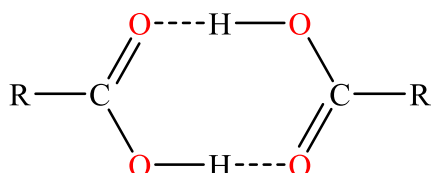


Figure 1-3: Self-complementary H-bonding in a neutral carboxylic acid.²¹

Deprotonated carboxylates, in contrast, have H-bond accepting character. The capacity for their oxygen central lone pairs to accept H-bonds is combined with a capacity to accept other Lewis acids such as metal ions. A range of bridging motifs is possible through combinations of the modes. Both the short bridges as in **A** and the long bridges as in **B** as illustrated in figure 1-4 are possible.

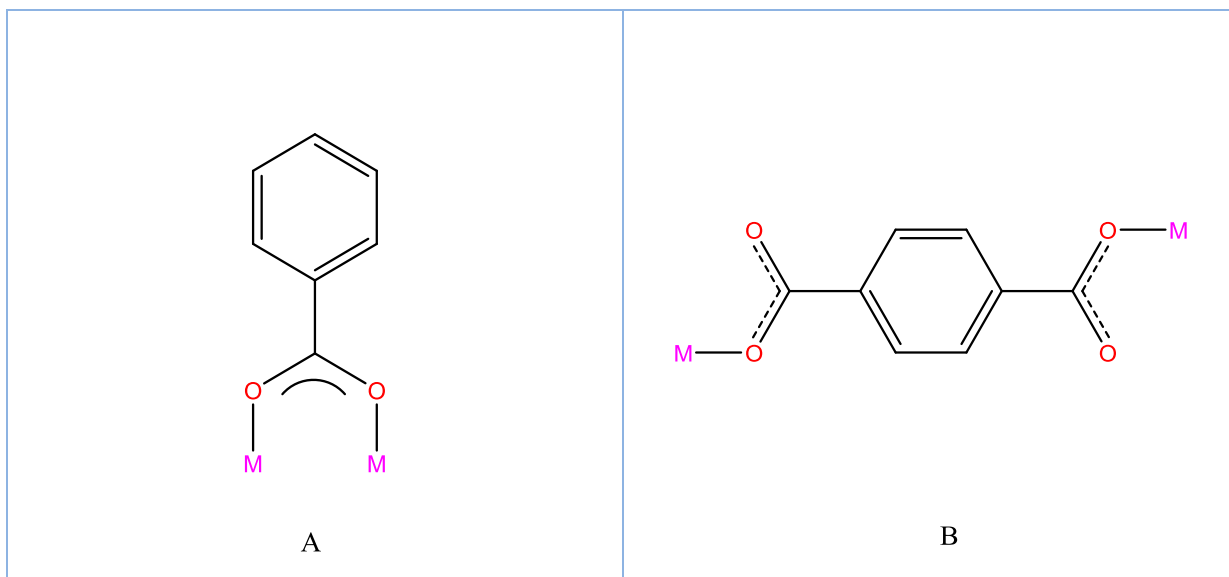


Figure 1-4: Figures showing short bridges and long bridges in the coordination mode of the deprotonated carboxylates.

In coordination polymers, ligands are attached to the metal ion through their donor atoms. These donor atoms are mainly group 14–17 elements on the periodic table. They could either be monoatomic ions such as F^- or Cl^- , polyatomic anions such as CN^- , CH_3^- or SCN^- , neutral molecules such as NH_3 , OH_2 or CO or cations such as NO^+ .²²

When more than one carboxyl group are present on the ligand in a different orientation, the construction of 1D- chain, 2D- net or 3D- frameworks are permitted and they can further be reinforced by the H-bonds and other weak interactions such as π - π interactions.²³

1.1. The Chemistry of Carboxylate Based Ligands

In recent years, a lot of focus have been on carboxylate based ligands either monocarboxylate such as benzoic acid and AMB or dicarboxylate such as isophthalic acid ²⁰ and terephthalic acid ²⁴ for the preparation of coordination polymers and metal-organic frameworks in order to see how incorporation of this ligand type might affect the physical properties of the structures obtained.¹⁸

Varieties of 1st-row 3d transition metal complexes that contained carboxylate based ligands which formed different coordination polymers and metal-organic frameworks have been constructed in the past. A search of the Cambridge Crystallographic Database for complexes made from the reaction of any of 1st-row 3d transition metals with carboxylate based ligands such as substituted benzoic acid, as shown in figure 1-5 revealed that 36,980 structures have been previously studied. This is an indication that a large number of transition metal complexes (coordination polymers) have been made and studied extensively in the time past and is still ongoing in the chemistry world.

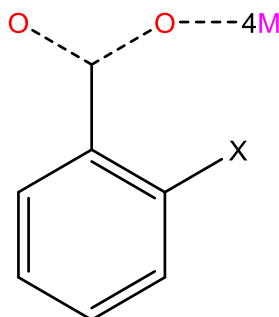


Figure 1-5: Query built for the statistics of coordination compounds studied and deposited in the Cambridge Crystallographic Database.

Ligands are referred to as Lewis bases when bonded to the metal ion because they possess one or more lone pairs.²² When carboxylate based ligands, either pure carboxylate ligands, amine-substituted ligands, poly-carboxylate ligands or aromatic multi-carboxylate ligands react with transition metals, they form a one-, two- or three-dimensional polymeric chain or layered structures, coordination polymers (CPs) or metal-organic frameworks (MOFs).²³

A typical example of carboxylate based ligand reacting with a transition metal to produce coordination polymers was found in the Cambridge Crystallographic Database search. Four intriguing structures were synthesized by Lia and Du. These structures were made using two different crystallization methods (solution method and solvothermal reaction) using ZnCl_2 and 2-carboxyphenoxy acetic acid in MeOH, adjusted with KOH and kept under pressure at 130°C (solvothermal reaction), crystals were obtained from the filtrate after slow evaporation. The same procedure was repeated with $\text{CoCl}_2 \cdot 6\text{H}_2\text{O}$. Likewise, same starting materials (metal-ligand) were used to grow crystals in a solution using H_2O in place of MeOH and also adjusted with KOH as illustrated in figure 1-6.²³

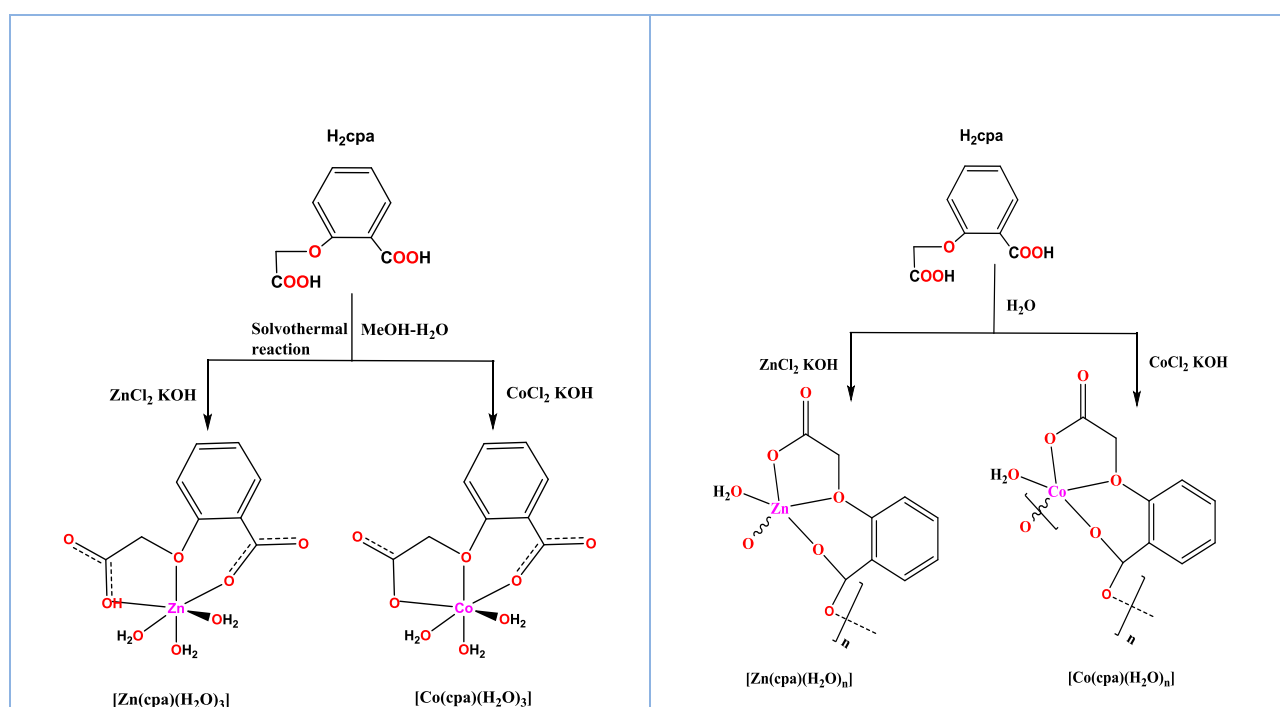


Figure 1-6: Schematic of solvothermal reaction in MeOH that produces six-coordinate Zn and Co complexes (left) and the reaction in deionized water that produces polymeric five-coordinate Zn and Co complexes at room temperature (right).²³

These two crystallization reaction methods produced four intriguing metal complexes which were characterized for further studies. In the structures obtained, reactions carried out in MeOH produced a six-coordinate metal complex while the reaction in H_2O produced a square based pyramidal metal complex, as illustrated in figure 1-7.²³

It is evident that the crystallization methods have a strong effect on the coordination ability and the coordination pattern of the ligands. Likewise, it plays an important part in the construction of structurally different complexes or polymorphs formed by the same metal salt and carboxylate ligands in a way that the solvothermal reaction of the same carboxylate ligand and metal salt in MeOH produced a monomeric six-coordinate complex while the reaction in deionized water at room temperature produced a polymeric five-coordinate complex as shown in figures 1-6 and 1-7.²³

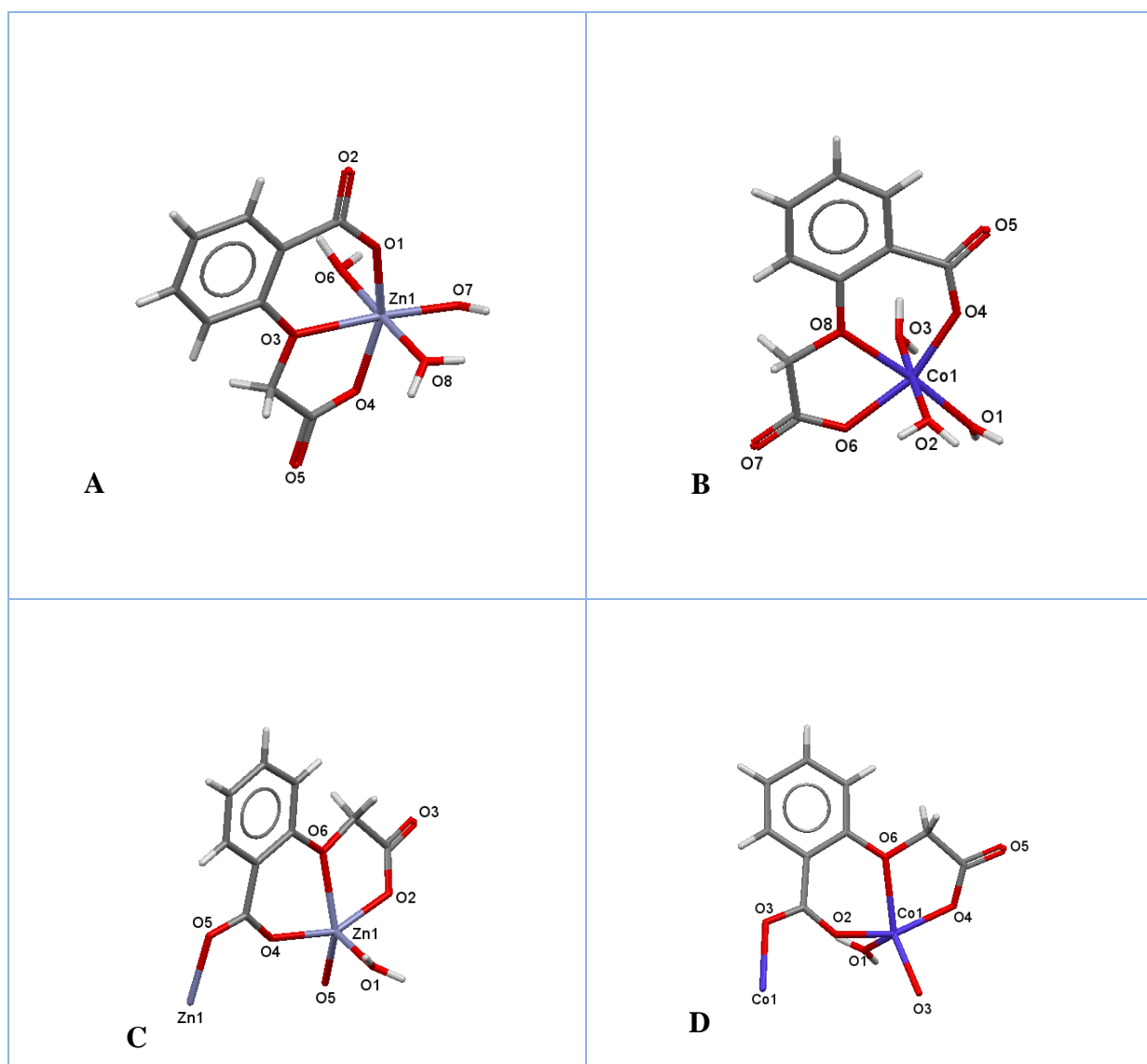
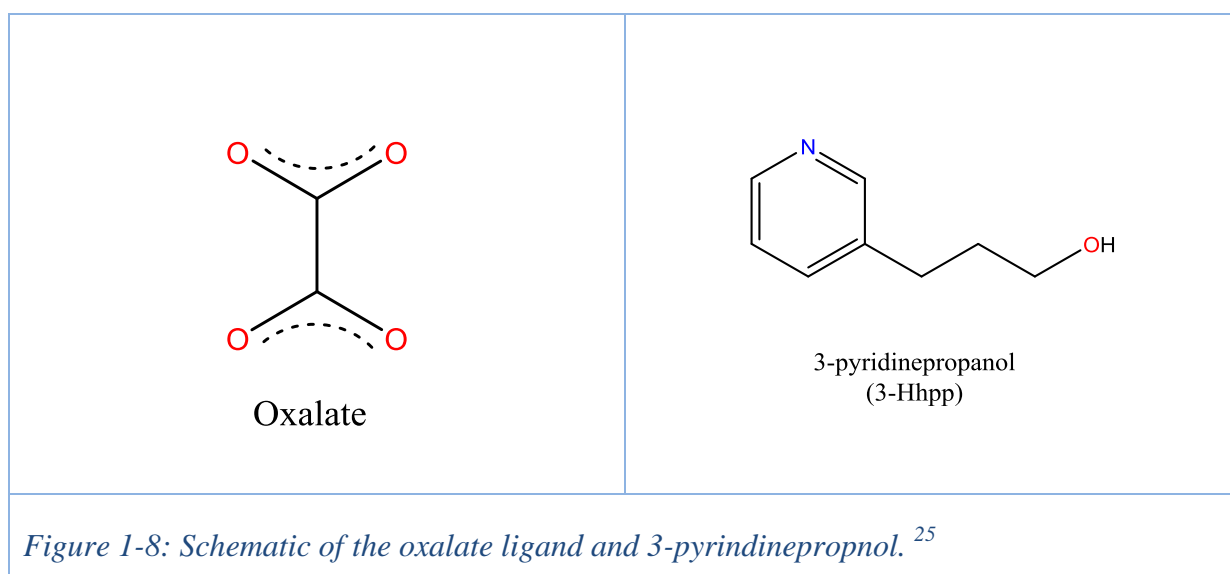


Figure 1-7: Molecular structure of solvothermal reaction in MeOH that produces Zn and Co complexes (top) and the reaction in deionized water that produces polymeric pentacoordinate Zn and Co complexes at room temperature (bottom).²³

In substituted benzoic acids, the substituents can be in *ortho*-, *meta*- and or *para*- position. The position of the substituent plays a huge role in the coordination mode of the metal centre in a complex. Their topologies are determined by the substituent on the benzoic acid in a way that the nearer the substituent to the carboxylate group, the greater is its effect. For example, the ligands oxalate (C_2O_4)²⁻ may be considered as two carboxylate ligands joined at the minimum separation. In such cases, chelating is expected and in addition, bridging is possible. The other ligand in the complex also has two functions (figure 1-8), a pyridine and alcohol group. In contrast, these have a *meta*- orientation on the ring and are quite remote. Chelating is impossible, yet they still may be bidentate in this case, by forming intermolecular bridges, forming a 2D- coordination polymer (figure 1-9 and 1-10). This array of closely-spaced copper ions was studied for its magnetic properties.²⁵



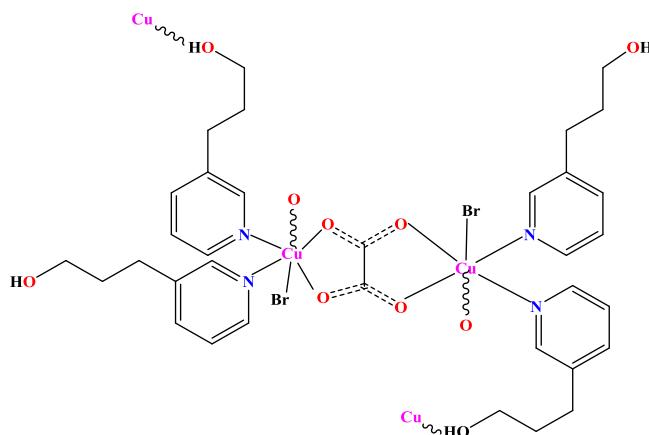


Figure 1-9: ChemSketch of the Cu(II) oxalate coordination polymer based on 3-pyridinepropanol bridging ligand.²⁵

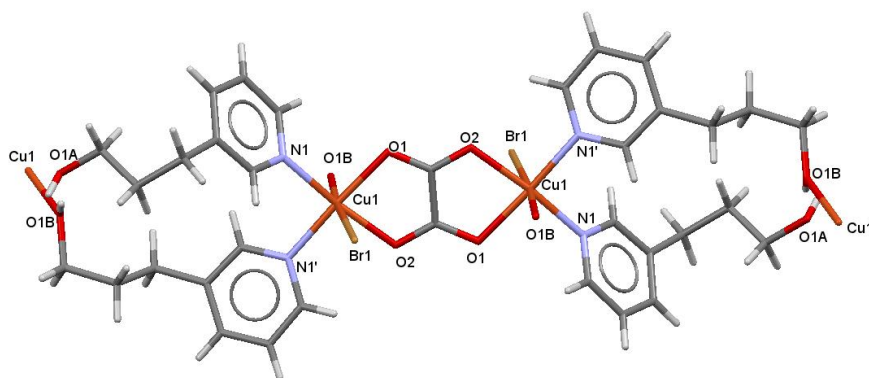


Figure 1-10: Molecular structure of the 2D Cu(II) oxalate coordination polymer based on 3-pyridinepropanol bridging ligand.²⁵

Oxalate acted as the bridging ligand that bridged the two metal centres in the structure of $[\text{Cu}_2(3\text{-Hhpp})_4\text{Br}_2(\text{ox})]_n$ as shown in figures 1-9 and 1-10.

Water is also an effective ligand for many d block metal ions.²² Water is cheap, abundant and the most friendly solvent because it is non-flammable and not toxic. It has a high heat capacity, it can act as a reliable donor or acceptor in the formation of coordination or H-bonding interactions, hence, it is the best and the ideal medium generally used in preparative chemistry.¹³

1.2. The Chemistry of 1st-row 3d Transition Metals

Transition metals are d-block elements in group 3 to 12 on the periodic table. Sometimes, group 12 (zinc, cadmium, and mercury) are not referred to as transition elements because they have completely filled d orbitals but they have similar properties as the transition metals, hence, they are always discussed along with the chemistry of transition metals. Transition metal atoms have a partially filled d subshell. They form one or more stable ions which have incompletely filled d-orbitals. They have a tendency to form complexes with a well-defined number of ligands and form coloured compounds. They are kinetically and thermodynamically stable.^{22, 26}

d block metals have nine valence atomic orbitals. Some of these orbitals are used to form bonds with ligands while the remaining orbitals are non-bonding.²²

The Aufbau principle is used to work out the electronic structure of the 1st-row 3d transition series (Sc to Zn) but this fails in chromium and copper as shown in table 1-1, due to the extra stability offered by maximizing the exchange energy, a quantum-mechanical term at its maximum for half-filled and fully filled shells.²²

Group	3	4	5	6	7	8	9	10	11	12
At. No.	21	22	23	24	25	26	27	28	29	30
Element	Sc	Ti	V	Cr	Mn	Fe	Co	Ni	Cu	Zn
Config.	$3d^14s^2$	$3d^24s^2$	$3d^34s^2$	$3d^54s^1$	$3d^54s^2$	$3d^64s^2$	$3d^74s^2$	$3d^84s^2$	$3d^{10}4s^1$	$3d^{10}4s^2$

Table 1-1: 1st-row 3d transition metals (Sc-Zn) and their electronic configurations.^{26, 27}

Previously, 1st-row 3d transition metal ions such as Cu(II), Zn(II), Co(II) and Ni(II) have been used to synthesize structure coordination polymer such as transition metal complexes which contained carboxylate based ligands and their metal-organic frameworks because they have a wide range of oxidation states (oxidation numbers) as shown in table 1-2.^{7, 28}

Metal	Oxidation States						
Sc			+3				
Ti	+1	+2	+3	+4			
V	+1	+2	+3	+4	+5		
Cr	+1	+2	+3	+4	+5	+6	
Mn	+1	+2	+3	+4	+5	+6	+7
Fe	+1	+2	+3	+4	+5	+6	
Co	+1	+2	+3	+4	+5		
Ni	+1	+2	+3	+4			
Cu	+1	+2	+3				
Zn	+1	+2					

Table 1-2: 1st-row 3d transition metals and their oxidation states.^{22, 26}
The oxidation states shaded in red accent colour are very rare oxidation states.

The d-electron count is used to describe the electron configuration of the valence electrons of a transition metal centre in a coordination complex. This gives an understanding of the geometry and reactivity of transition metal complexes in the form of crystal field theory and ligand field theory. It is obtained by subtracting the oxidation state from the sum of ‘said’ d electrons.²²

Metal ions such as Co(II), Cu(II), Zn(II), and Cd(II) have been used in making coordination polymers previously on the account of specific geometry and excellent chemical properties. In this study, transition metal ions such as Mn(II) and Ni(II) were used in addition to Cu(II), Co(II), and Zn(II) both in pure metal-ligand reactions and in bimetallic reactions.

Chemistry of 1st-row 3d transition metals in their +2 oxidation states

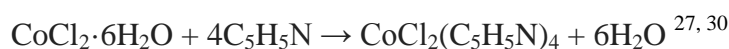
i. Chemistry of Mn(II)

Manganese occurs in all oxidation states between Mn(II) and Mn(VII) with Mn(II) being the most common and most stable. The electronic configuration of Mn(II) is $[Ar]4s^03d^5$. Examples of the compound in the +2 oxidation state are MnO, MnSO₄, MnCl₂, and MnCO₃. Mn(II) commonly exist with high spin, $S = \frac{5}{2}$ ground state because of its high pairing energy level. There are instances of low spin, $S = \frac{1}{2}$ but only with the strongest of crystal field splitting (see later). Also, there is no spin and orbitally-allowed d-d transition spin in Mn(II).^{27, 29}

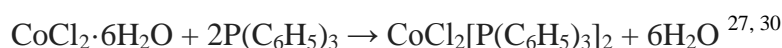
ii. Chemistry of Co(II)

Cobalt can show a variety of oxidation states between -1 to +4. Of all these states, Co(II) and Co(III) are common. Cobalt (II) is stable and forms a wide variety of stable complexes with ligands such as ammonia, chloride ion, and water, etc. The electron configuration of Co(II) is $[Ar]4s^03d^7$. An example of a Co(II) compound is CoCl₂ which is always supplied as hexahydrate, CoCl₂·6H₂O and it is the most common Co(II) source used in the lab.^{27, 30}

CoCl₂ and its hydrate are weak Lewis acids. When they react with a ligand, the geometric environment of Co is usually either octahedral or tetrahedral. For example, CoCl₂·6H₂O with pyridine (C₅H₅N) produced an octahedral complex.



While CoCl₂·6H₂O with triphenylphosphine [P(C₆H₅)₃] produced a tetrahedral complex.



iii. Chemistry of Ni(II)

The electronic configuration of Ni(II) is $[Ar]4s^03d^8$. Ni can show a variety of oxidation states between (0) to (IV). The most common oxidation state of Ni is Ni(II). Ni(I) complexes are

uncommon, but one example is the tetrahedral complex $\text{NiBr}(\text{PPh}_3)_3$. Ni(II) forms coordination compounds with all common anions such as sulfide, sulfate, carbonate, halides, hydroxide, and carboxylates. Common salts of Ni(II) are NiCl_2 or $\text{NiCl}_2 \cdot 6\text{H}_2\text{O}$, $\text{Ni}(\text{NO}_3)_2$, and NiSO_4 . Typically, Ni(II) complexes include $[\text{Ni}(\text{NH}_3)_6]^{2+}$, $[\text{Ni}(\text{C}_2\text{H}_4(\text{NH}_2)_2)]^{2+}$, $[\text{NiCl}_4]^{2-}$ and $[\text{Ni}(\text{H}_2\text{O})_6]^{2+}$.²⁷

Considering the geometric environment of Ni(II), some tetra-coordinate Ni(II) complex such as bis(triphenylphosphine)nickel dichloride exist as a tetrahedral (paramagnetic) and square planar (diamagnetic) complex.³¹ Some four-coordinate nickel complexes are tetrahedral [e.g. $(\text{NiCl}_4)^{2-}$] and some are square planar [e.g. $\text{Ni}(\text{Ph}_3\text{P})_2(\text{CN})_2$]. The stronger field ligand favour square geometry, while steric effects may overcome this preference. In some cases, both isomers, square planar and tetrahedral may be prepared [e.g. $(\text{Ph}_3\text{P})_2\text{NiCl}_2$].²⁷

iv. **Chemistry of Cu(II)**

The electronic configuration of Cu(II) is $[\text{Ar}]4s^03d^9$. Cu can show Cu(I), Cu(II) and Cu(III) oxidation states with Cu(II) being the most common.²⁶ Cu forms coordination compounds with ligands to produce complexes such as $[\text{Cu}(\text{NH}_3)_4(\text{H}_2\text{O})_2]^{2+}$. Salts of Cu(II) include $\text{Cu}(\text{CH}_3\text{COO})_2$, $\text{Cu}(\text{NO}_3)_2$, CuCO_3 and CuSO_4 anhydrous and $\text{CuSO}_4 \cdot 5\text{H}_2\text{O}$ hydrate. In solution, Cu(II) exists as $[\text{Cu}(\text{H}_2\text{O})_6]^{2+}$ and its pentahydrate.²⁷

v. **Chemistry of Zn(II)**

The electronic configuration of Zn(II) is $[\text{Ar}]4s^03d^{10}$. The oxidation state of Zn is +2. Zn can also exhibit +1 oxidation though it is very rare. An example is in $(\eta^5\text{C}_5\text{Me}_5)_2\text{Zn}$ which is the first known Zn compound in the +1 oxidation state. Zn is often not considered as a transition metal because unlike the rest of the d block metals, it has a completely filled d-shell. Zn is similar to magnesium for exhibiting one oxidation state, +2 and in its size. However, its chemistry is similar to that of Ni and Cu even though the d-shell of those elements is incompletely filled and its compounds are mostly diamagnetic while Cu(II) is always paramagnetic. Its complexes are always four (tetrahedral or square planar) or six (octahedral) coordinates while a five-coordinate complex is known. For example as in figure 1-7C.²³

While Cu(II) is always paramagnetic and Ni(II) is often so (when in tetrahedral, five-coordinate or octahedral complexes) Zn(II) is never paramagnetic. Its d-electron shell is always completely full because the d^{10} shell is equal in all directions, there is no strong preference for any given coordination geometry.

Zn(II) forms coordination compounds in a wide range of geometries, from tetrahedral (or square planar when imposed by the ligand) to five-coordinate (square pyramidal or trigonal bipyramidal) to six-coordinate (octahedral). In water, it forms $[\text{Zn}(\text{OH}_2)_6]^{2+}$. Salts of Zn include ZnCl_2 , $\text{Zn}(\text{NO}_3)_2$, $\text{Zn}(\text{ClO}_3)_2$, ZnSO_4 and $\text{Zn}_3(\text{PO}_4)_2$.²⁷

The number of coordinated ligand atoms governs the arrangement of ligands around the metal centre within a complex. In metal complexes, one, two (sp hybridization mode) and three (trigonal, sp^2 hybridization mode) coordinate complexes are few. Six coordinate (octahedral) is the most common coordination number for the d-block metal compounds followed by four coordinates (tetrahedral and square planar). The other coordination numbers include seven-coordinate: monocapped octahedron, pentagonal bipyramid, and tetragonally capped trigonal prism. Eight-coordinate: square antiprism, dodecahedron, and cube. Nine-coordinate: tricapped trigonal prism.^{22, 26, 32}

Metals with high oxidation states are usually bonded to oxygen or fluorine. The geometry environment of each transition metal depends on the oxidation state of the metal and the type of ligands the metal is reacting with. The oxidation number of all the 1st-row 3d transition metal under study is +2, and the possible geometric environments of each transition metal in this oxidation state are listed in table 1-3.

Transition metals in many instances generally form octahedral complexes depending on how many donor atoms can fit around the metal centre (coordination numbers). Coordination number and geometry are determined by the combination of metal ion size, electronic factors (electron configuration) and ligand type/size.

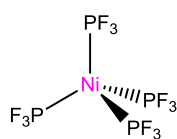
Often times, there are octahedral complexes in both high spin and low spin electron configuration. Taking d^6 as an example, in the octahedral high-spin complex, there are 4 unpaired electrons, they are paramagnetic and substitutionally labile while in the octahedral low-spin case, there are no unpaired electrons, and they are diamagnetic and substitutionally inert. In octahedral complexes, the metal ion functions as a Lewis acid towards six ions or molecules which are all Lewis bases.²⁶

S/No.	Metals	Most Preferred	Possible	Possible
1.	Cu^{2+}	Square planar	Octahedral	Tetrahedral
2.	Zn^{2+}	Tetrahedral	Square planar	Octahedral
3.	Co^{2+}	Octahedral	Trigonal bipyramidal or square pyramidal	Tetrahedral
4.	Ni^{2+}	Octahedral	Tetrahedral	Square planar
5.	Mn^{2+}	Octahedral	Tetrahedral	

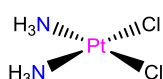
Table 1-3: Metals in +2 oxidation state, their most preferred and possible geometry.²⁶

Tetrahedral complexes can be described as using an sp^3 orbital hybridization. Square planar complexes use dsp^2 hybrids, while trigonal bipyramidal correspond to a dsp^3 hybridization using the dx^2-y^2 orbital. The same dsp^3 hybrids may be used to rationalize the bonding in square pyramidal geometries, except that dz^2 is used. Octahedrally coordinated complexes use d^2sp^3 hybrids.^{22, 32}

Four coordinate complexes

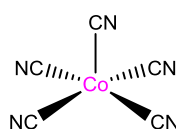


tetrahedral

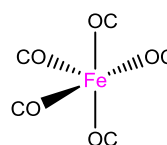


square planar

Five coordinate complexes

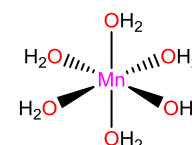


square-based pyramidal



trigonal bipyramidal

Six coordinate complex



octahedral

Figure 1-11: Examples of four-, five- and six-coordinate complexes.^{22, 26}

The Jahn-Teller effect is a geometric distortion of any non-linear molecular system. It is best known in octahedral complexes. When they exhibit distortion, their two axial bonds are shorter (compressed) or longer (elongated) than their equatorial bonds as a result of the

amount of overlap between the metal and the ligand orbitals. If the metal-ligand orbital interaction is strong, the chance that the Jahn-Teller effect will be observed is high. Jahn-Teller effect reduces the energy and symmetry of the complex. Examples of two common distortions seen in octahedral cases are shown in figure 1-12.²⁸

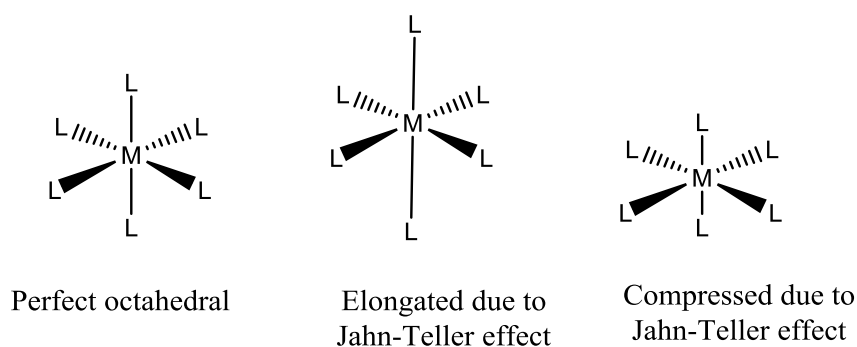


*Figure 1-12: Figures showing distortion in the octahedral coordination due to the Jahn-Teller effect.*²⁸

In the low spin and high spin complexes, d^3 , d^5 , d^8 , and d^{10} do not exhibit strong Jahn-Teller distortions but low-spin d^5 has an uneven occupation of the t_{2g} set orbitals that can lead to a so-called 2nd-order Jahn-Teller distortion.

The splitting of the d orbitals into different energy levels in transition metal complexes has essential consequences for their reactivity, their stability, and magnetic properties. The difference between the t_{2g} and e_g orbitals energies in an octahedral complex is represented by Δ_o . This splitting of the energy of the d orbitals is not minor as the magnitude of the splitting of t_{2g} and e_g orbitals alters from one octahedral complex to another. It depends on the identity of the metal ion, the charge on this ion, and the nature of the ligands coordinated to the metal ion. The d orbital energy diagram for an octahedral crystal field is shown in figure 1-13.^{26, 28, 32, 33}

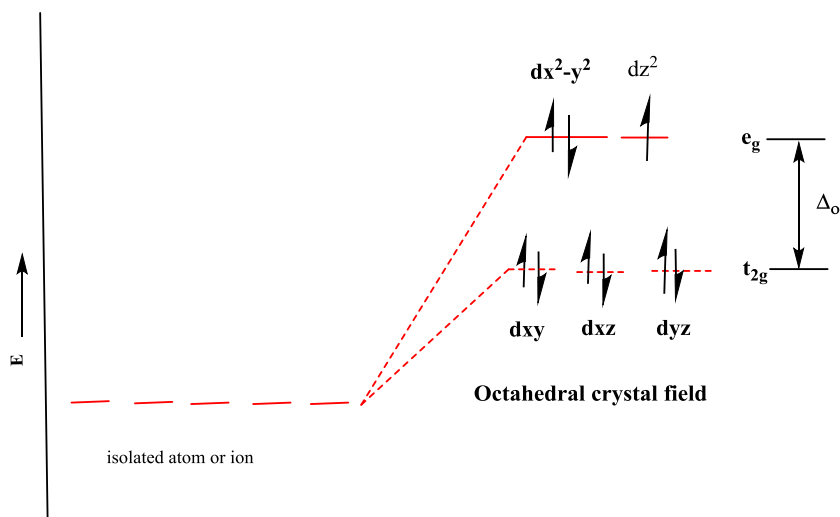


Figure 1-13: Octahedral crystal field of a d^9 system.^{28, 33}

In a tetrahedral crystal field, the splitting observed is the reverse of the splitting in an octahedral complex because a tetrahedral coordination complex has fewer ligands. The magnitude of the splitting is smaller as shown in figure 1-14. The differences between the t_2 and e orbitals energies in the tetrahedral complex (Δ_{tet}) are considerably less than half as large as the splitting in analogous octahedral complexes (Δ_{oct}).^{26, 28, 33}

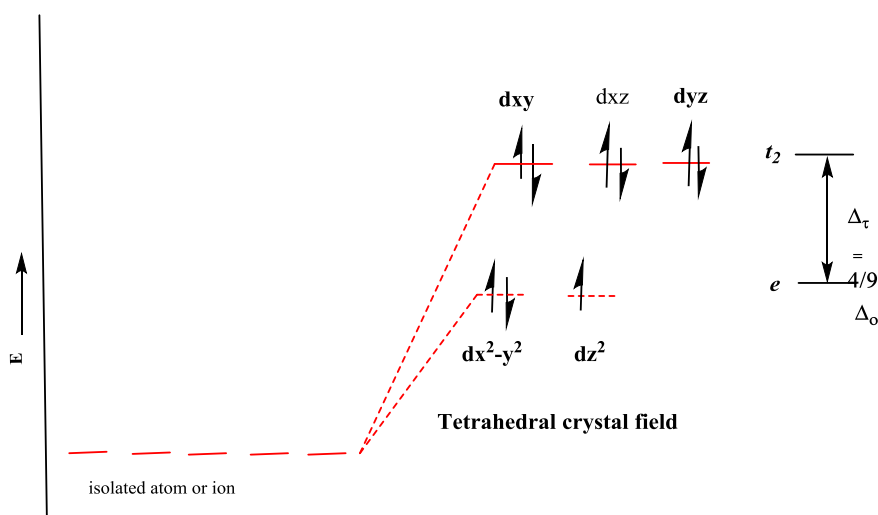


Figure 1-14: Tetrahedral crystal field of a d^9 system.^{28, 33}

The square planar coordination geometry around the metal centre is as a result of the removal of two ligands on the z -axis of an octahedron complex, leaving only the ligands in the x - y plane. As the z -ligands move away, the ligands in the square plane move a little closer to the metal. The orbital splitting diagram for square planar coordination can thus be derived from the octahedral diagram. The splitting diagram for square planar complexes is more complex than for octahedral and tetrahedral complexes with the relative energies of each orbital as shown figure 1-15.^{26, 28, 33}

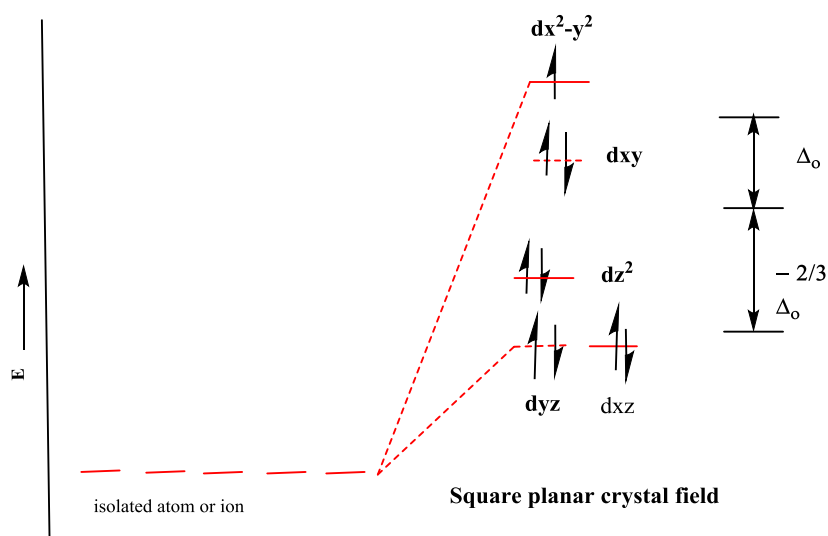


Figure 1-15: Square planar crystal field of a d^9 system.^{28, 33}

1.3. Coordination Polymers

A coordination polymer is a coordination compound with repeating coordination entities that extend into one- dimension, which may also show cross-links between two or more individual chains, loops, or Spiro-links, or a coordination compound that extends through repeating coordination entities in two- or three- dimensions.^{34, 35}

One-dimensional coordination polymers of metal complexes are studied intensely as materials with unusual properties. Their structure extends in a straight line along the x -axis as illustrated in figure 1-16. Their applications include molecular-based ferromagnetic, synthetic-metal conductors, non-linear optical (NLO) materials and ferroelectric materials. Many planar metal complexes also form one-dimensional stacked structures. These are mainly complexes of Ni, Pd or Pt with flat π conjugated ligands. In the structures of one-dimensional coordination polymers, there is usually a well-defined cooperative interaction between discrete molecules which provides a continuum between their fields.³⁶

A two-dimensional structure extends in a plane (two directions, x , and y -axes). 2D polymers can be isolated as multilayer crystals or an individual sheet and can be organized based on monomer interaction, as a single metal-organic, as covalently linked monomers, as coordination polymers and as supramolecular polymers.

A three-dimensional structure extends in three directions (x , y , and z -axes). Metal-Organic Frameworks are 3-dimensional, (figure 1-16). They are covered in detail in the following section.

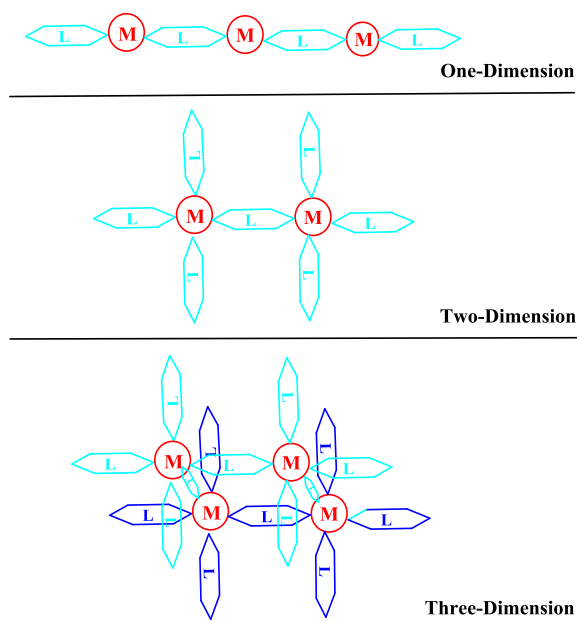


Figure 1-16: An illustration of 1-, 2-, and 3-dimensionality of Coordination Polymers.

Coordination Polymers are prepared by self-assembly. This involves the crystallization of an aqueous solution of a metal salt with an aqueous solution of the ligand in a reacting vessel at a preferred temperature and by using other crystallization methods such as solvent layering, slow diffusion, slow evaporation, slow cooling or hydro (solvo) thermal reaction. Their method of characterization is mainly Single Crystal X-ray Diffraction and Powder X-ray Diffraction. Coordination polymers are not totally soluble in most cases.⁴

Coordination compounds consist of mainly metal (usually transition metals and/or lanthanides in their halide, nitrate, hexafluorophosphate, triflate or tetrafluoroborate salts) and organic ligands. Though, sometimes, CPs do have guests and counterions with their most common binding sites being oxygen and nitrogen atoms. Sulfur and phosphorus can also act as the binding site sometimes.

Coordination networks are a subset of coordination polymers while metal-organic frameworks (MOFs) are a further subset of coordination networks as shown in figure 1-17.

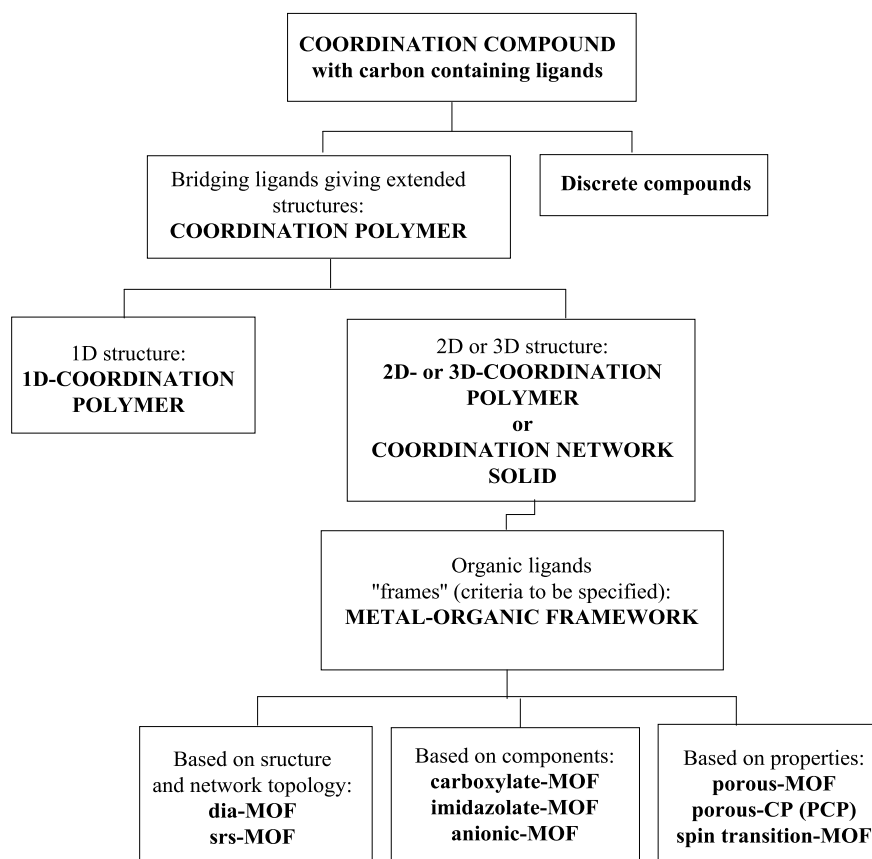


Figure 1-17: A tentative hierarchy of coordination polymers and metal-organic frameworks. The bottom descriptors are optional and not mutually exclusive. Three-letter topology codes according to O'Keeffe et al.³⁴

The main properties of coordination polymers are chirality,³⁷ porosity³⁸⁻⁴⁰ and chemical reactivity. Other properties include negative thermal expansion, magnetism,⁴¹ spin-transition behaviour, conductivity, redox activity, adsorption of hydrogen chloride gas, emission of sound during precipitation, a useful precursor for metal oxide materials, tendency to change colour whenever the solvent molecule changes, and they are multifunctional materials.⁴

1.4. Metal-Organic Frameworks

Metal-organic frameworks (MOFs) are extended crystalline structures whose metal cations or clusters of cations are connected by multi-topic organic strut or linker ions or molecules.⁴² MOFs are sponge-like materials, coordinated with organic molecules such as 1,4-benzene dicarboxylic acid to form two- or three-dimensional structures that can be porous. The pores in MOFs are without walls and they are less than 2nm in diameter. This allows substrate gases, and other molecules move in and out of the pores.^{13, 39}

MOFs are constructed from the mixture of metal ions such as transition metals or lanthanides, the counterions such as Na^+ in the case of NaCl, solvents such as MeOH, DMF and H_2O ,⁴³ azole, phosphonates, pyridine derivative and the bridging organic ligands such as the carboxylate based ligands which are the most commonly used.⁴⁴ Bidentate carboxylic based ligands such as oxalic acid, malonic acid, succinic acid, glutaric acid, phthalic acid, isophthalic acid, terephthalic acid are the major/common ligands used in making MOFs. For example, the use of carboxylate based ligand such as oxalate bridged with a rigid ligand should produce a layered network.⁴⁵ Other linkers include trimesic acid, citric acid, 1,2,3-triazole, pyrroldiazole, and squaric acid (figure 1-18).

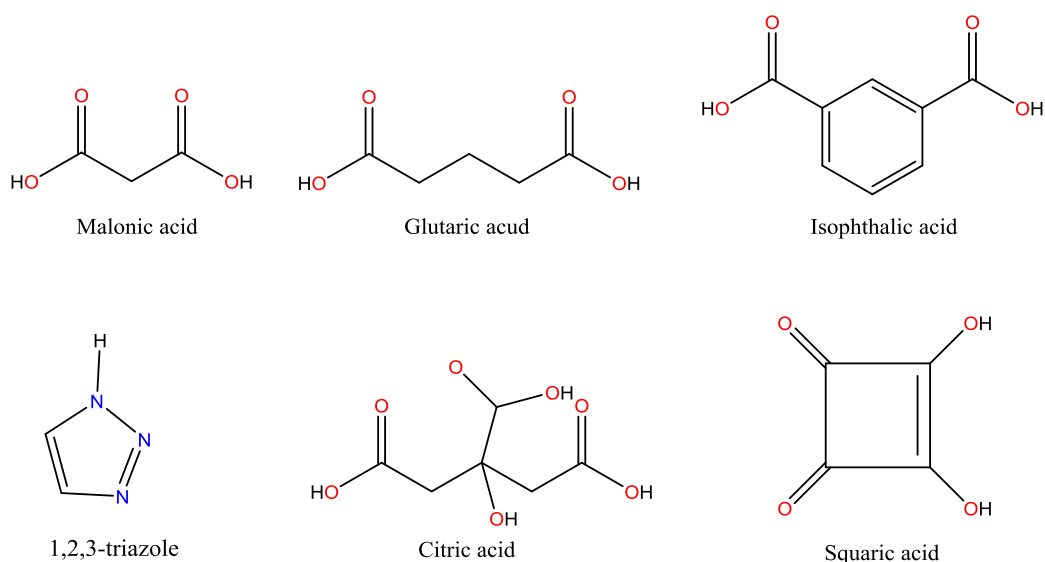


Figure 1-18: A range of ligands commonly employed in the formation of metal-organic frameworks.

MOFs may be prepared with more than one metal (as in bimetallic reactions) or more than one ligand (introduction of a guest molecule or auxiliary ligand), or more than one solvent in the solvent mixture such as in 50:50 MeOH /H₂O or functionalized after synthesis.^{43, 46}

MOFs display a wide range of luminescent behaviour due to the multifaceted nature of their structures. Their luminosity properties depend solely on the organic linkers, the coordinated metal ions, and guest molecules.⁴⁷ They are multifunctional porous materials because of their numerous applications⁴⁴ such as industrial applications.⁴⁸

MOFs are produced mainly by hydrothermal or solvothermal techniques where crystals are slowly grown from a hot solution, and less commonly by solution methods where crystals were left to self-assemble in solution at room temperature.⁷ Though solvothermal conditions are known to be inappropriate for thermally sensitive materials, hence, crystallization at room temperature is more sustainable. Metal binding solvents such as N-N-dimethylformamide (DMF) and water are often used for MOFs construction for the purpose of gas storage.⁴⁶

While there are some very recent examples of glassy MOFs,⁴⁹ the vast majority of MOFs grow in crystal form and they have a range of uses and potential applications especially when combined with nanoparticles for additional functionality such as for separations in gas-phase adsorptive separation and gas storage.^{39, 50} MOFs exhibit diverse coordination geometries as they can include light polytopic linkers⁵¹ and ancillary ligands.⁵² Their structures are amenable to expansion and incorporation of multiple functional groups within their interiors (flexibility).⁵³ They are known to have ultra-high porosity and high internal surface area.⁵⁴

MOFs are synthesized in order to obtain high-quality single crystals for structural characterization. The choice of metal, linker, solvent pH and the temperature has significant effects on the structure and properties.¹³ Their classes include heterocyclic azolate-based MOFs, metal-cyanide MOFs, covalent organic frameworks and carboxylate-based MOFs which are the most common. The bridging bidentate carboxylate groups favour a high degree of framework connectivity and strong metal-ligand bonds, necessary to maintain MOFs architecture under the conditions required to evacuate the solvent from the pores. The most common transition metals employed in carboxylate-based frameworks are Cu²⁺ or Zn²⁺ because they are strong Lewis acids.⁵⁵

MOFs and zeolites are advanced structures that are extremely ordered and have large internal surface areas, extensive porosity and a high degree of crystallinity in common. The porosity

of MOFs is the basis for their zeolitic behaviour.⁴ MOFs have thermal, hydrothermal and chemical stability compared to zeolite. The secondary building unit in MOFs is typically a polyatomic group, while it is typically a single atom in a zeolite. This imparts and enhances the stability of MOFs and makes them potentially useful for gas sequestration and storage.⁵⁶

MOFs are microporous materials with properties similar to those of activated carbons, zeolites, covalent organic frameworks, and microporous polymers. Their other properties include thermally robust structures, diversities in metal and the functional group, high mechanical and thermal stabilities, very low bulk volumes (most are free space) and selective uptake of small molecules. They resist decomposition at temperatures up to 300°C or higher, (above 500°C in a few cases) but the true strength of MOFs is not their thermal stability.³⁹

Magnetism occurs in MOFs with magnetic moment carriers which are paramagnetic such as in the 1st-row 3d transition metals (V, Cr, Mn, Fe, Co, Ni, and Cu) or open shell organic ligands or when both are present in the framework. If the framework remains non-magnetic, magnetism can then be introduced via a guest molecule for magnetic studies because magnetism is a cooperative phenomenon that requires some kind of exchange between the moment carriers.⁵⁵

MOFs are excellent candidates for catalysis.⁵⁶ They have an exceptionally high surface area and structural diversity.⁵⁷ They are used for carbon capture, gas storage or to separate gases or liquids from each other with greater performance and longevity than other existing methods.⁵⁸ They have been of great benefits in fuel production, luminescence,⁴⁷ imaging, in batteries and catalysis (heterogeneous catalysis), nonlinear optics,⁵⁹ as chemical sensors, ion exchange and gas sorption,^{50,60} as a solvent for water purification by removing heavy metal, oil or toxin, to purify gases and in pharmaceuticals. They protect biomolecules in harsh conditions, in electronic devices, for high carbon storage,⁶¹ and for gas separation.⁶² They are used in prototype development and systems testing and their application as a photocatalyst in the decomposition of organic contaminants.⁶³

As stated at the beginning of this chapter, the study of metal-organic frameworks (MOFs) and coordination polymers (CPs) are interwoven in a way that it is difficult to differentiate between the two. MOFs and CPs can only be differentiated on the basis that MOFs are based on strong (typically metal-oxide) linkages that yield robust frameworks but they are porous.⁴⁶ They can be represented as a special kind of graph called a period net such as in diamond

(dia) net. All MOFs are CPs but not all CPs are MOFs. CPs is the term used since the 1950s while MOFs is the term used since 1990s. CPs is always a 1D chain while MOFs can be 2D nets or 3D frameworks.¹³ The name MOFs are used for 3D network and it is inappropriate to use MOFs for a 1D chain. Inorganic Chemists uses the term CPs while Solid State Chemist uses the term MOFs.⁶⁴

1.5. Chemical Interactions in Crystal Structures and MOFs

Chemical bonding theory explains the attractions that hold atoms in molecules, crystals, and metals together which enable them to form different chemical compounds/structures and dictates the bulk properties of matter. These bonds may be as a result of the electrostatic force of attraction between ions with opposite charges, or by sharing of electrons as it is in covalent bonds. The negatively charged electrons that are orbiting the nucleus and the positively charged protons in the nucleus attract each other via simple electrostatic force. An electron positioned between two nuclei will be attracted to both and the nuclei will be attracted toward electrons in this position. The goal of all the different types of bonding is to achieve a lower energy state.⁶⁵⁻⁶⁶

A chemical bond may be a "strong bond" (when electrons are shared or transferred between the participating atoms) such as in covalent or ionic bonds or "weak bond" such as in dipole-dipole interaction, London dispersion force, and H-bonding. H-bonding results from intermolecular forces of attraction that bring different molecules together such as H-bonding to other atoms. Weaker non-covalent interactions just as in H-bonding or π - π stacking are important when it comes to the packing of the 1D chain, 2D nets, and 3D frameworks.⁴

The main structural bonding in MOFs is primarily the ionic bonding between the positively charged metal ions and the negatively charged heteroatoms of the organic linkers. Certain MOFs will also have contributions from other sorts of interactions. Bonding in MOFs is the same as in any other crystal structures. The different types of bonding in crystals according to their strength include covalent bonds, ionic bonds, metallic bonds, H-bonds, and Dipolar interactions, π – π stacking and Van der Waals interactions.⁶⁵

Aromatic-Aromatic, π - π stacking and C-H... π interactions are the important non-covalent intermolecular force which plays an important role in the assembling strategies of coordination polymer and in the connection process of their frameworks.⁷

The strong and attractive interactions in a π -system have been known to control phenomena such as packing of aromatic molecules in crystals. The geometries of π -interactions are controlled by electrostatic interaction while the major energetic contributions come from factors such as electron repulsion.⁶⁷

The weak numerous non-covalent interactions and poor directionality which involves the ligands and non-covalently bound anions, cations, solvent or guest molecules are the main reasons why the accurate prediction of the crystal structure cannot be possible.⁴

Covalent metal-ligand bonds (coordinative) in CPs and MOFs are stronger than H-bonds because metal-ligand has more directionality than the other weak interaction such as in π - π stacking.⁶⁸

H-bond is known to be a weak bond but it has always been recognized as a significant bond and as the strongest intermolecular interactions, the strongest of which is comparable with the weakest of the covalent bonds.⁶⁹

H-bond is a phenomenon in which hydrogen atom bridged two atoms X and A that are distinctively attracted to it, as shown in figure 1-19. This attraction is found commonly where X and A are electronegative. They are highly electrostatic.⁷⁰

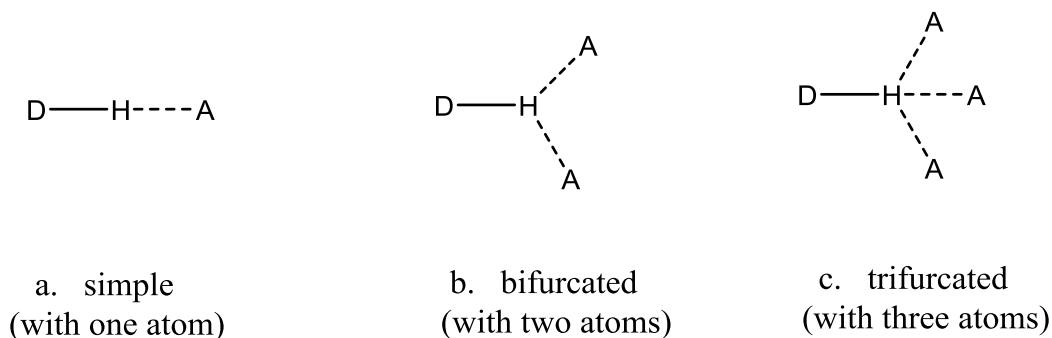


*Figure 1-19: Common H-bonding arrangements.*⁷¹

H-bond can be referred to as a synthetic ‘vector’ that controls the topology of a crystal and its other crucial physical phenomena such as crystal behaviour, mechanical strength, conductivity, solubility, optical properties, and thermal stability.⁷¹

H-bond may simply involve one donor and one acceptor. The acceptor always possesses a lone pair of electron. Example of H-bond donors are C – H, N – H and O–H while H-bonding acceptors are O, N or halogens such as F, Cl, and Br.⁷¹

Weak H-bonds or longer H-bonds are known to likely deviate from a linear arrangement as shown in figure 1-19b and c. Likewise, at the same distance, N–H...O bonds have a high tendency to deviate from the linear arrangement when compared to O–H...O bonds. Furthermore, short H–A bonds correlate with a long D–H bond.⁷⁰

Ligands such as triethanolamine (yeaH₃) are an interesting ligand with three ethanol arms and one fragment of amine and it is an excellent candidate for H-bond donation.⁷²

1.6. Studying the Formation of MOFs in Manchester

The inspiration for this study is derived from the studies of MOF-2. MOF-2 has been studied extensively in the past. A typical example of one of the MOF-2 is the [Zn-BDC] case, shown in figures 1-20 and 1-21. Out of the numerous samples of MOF-2 previously studied by different scientists, this example was synthesized from the direct precipitation of the aqueous solution of zinc acetate dihydrate and the linker terephthalic acid in deionized water and N.N-dimethylformamide at room temperature by N. Getachew *et al.* in 2014.⁴⁶ The method used in synthesizing Zn-BDC was crystallization in H₂O or DMF or MeOH at room temperature is the same method employed to synthesize the crystal structures obtained in these studies.

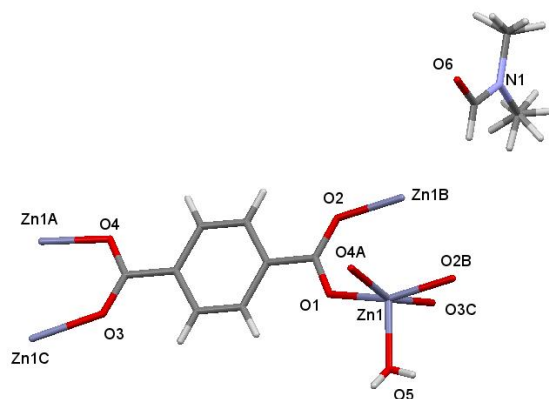


Figure 1-20: Molecular structure of MOF-2 [Zn-BDC].⁴⁶

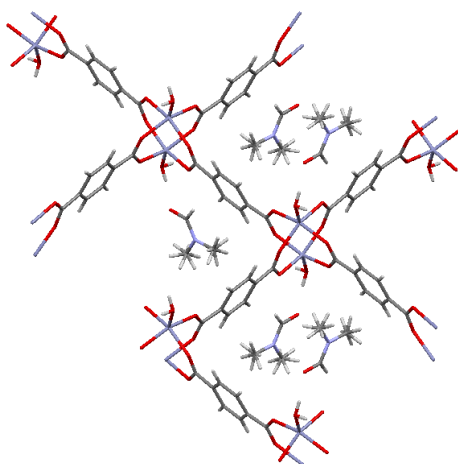


Figure 1-21: Polymeric expansion of Zn-BDC viewed down crystallographic a-axis.⁴⁶

Metal-Organic Frameworks (MOFs) were chosen for the initial experiment because their formation is not reliant on the solution becoming supersaturated i.e. the container containing the reacting solution can be sealed and left to stand at room temperature.

Also, some initial work had been carried out as part of a 4th year MChem project by William Reece, who crystallized a 2D net from cobalt(II)chloride and 2,5-dihydroxy terephthalic acid. However, these crystals were at the limit of detection of the in-house diffractometer and the resulting study was of poor quality.

Before discussing developments in its chemistry in chapter 3, a review of the methodology, crystal growth, and structure determination follow in chapter 2. Further studies on 2D coordination polymer networks using 2-amino-3-methylbenzoic acid with Zn, Co, Cu, and Ni is presented in chapter 4 while chapter 5 discussed a related work on manganese with unsubstituted benzoic acid. The thesis concludes with a summary and over-arching analysis of the outcomes of the research and suggested further works in chapter 7.

Chapter 2

The Theory and Practice of X-ray Single Crystal Diffraction

2.1. Introduction

Crystallography is the study of crystals, their structures, and properties. A crystal is a substance that is crystalline, periodic and contains a very high degree of long-range three-dimensional order of the component atoms, molecules or ions and they are bounded by plane faces, as shown in figure 2-1.⁷³

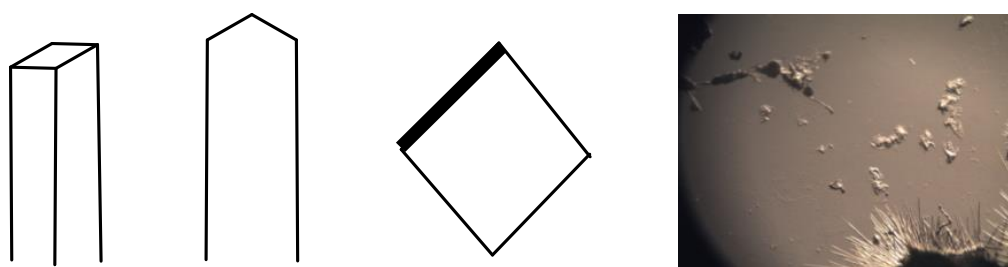


Figure 2-1: Different crystal shapes and the crystal obtained in Manchester.

A crystal structure can be described by the type, number and arrangement of atoms in the unit-cells and by the relative positions of the unit-cells as defined by the space lattice i.e. lattice convoluted with unit cell gives the macroscopic crystal. A crystal structure, simply put, can be described as how the internal structure of molecules connect and how they are packed together to form a solid crystalline material.⁷³

The primary aim of crystal structure analysis by X-ray diffraction is to obtain a detailed three-dimensional picture of the contents of the crystal at the atomic level. The position of individual atoms must be known precisely to be able to calculate interatomic distances, bond angles, the angles between the planes, the planarity of particular groups of atoms and conformation angles around the bonds. Crystal structure analysis is carried out because chemical and biological reactions occur in three-dimensions, not in two.⁷³⁻⁷⁴

2.2. The Crystallographic Concepts

Every crystal has a lattice as its geometrical basis. A lattice is defined as a regular, infinite arrangement of points in space in which every point has exactly the same environment as any other point. A crystal lattice is only the first level of classification of the structure. However, it is the basic network of points on which the repeating unit (the content of the unit cell) may be imagined to be laid down in order to obtain the regular repeating structure. This occurs equally in one-, two-, and three-dimensional space. According to Laue, Fredrich, and Knipping, a crystal is basically a three-dimensional diffraction grating.⁷³

2.2.1. Lattices and Unit Cells

A single crystal can be represented as a periodic geometrical assembly of spatial identical structural units called a Unit Cell. Size, geometry and atoms distribution within the unit cell depends on the specific material.⁷⁵

The unit cell is the basic building block of a crystal which consists of a single molecular entity (*Bergman, 1773, Hany, 1784, Burke, 1966*). As a building block, it must pack in three-dimensional space without any gaps. In a three-dimensional crystal structure, the unit cell can be defined by a parallelepiped with three cell axes (vectors) a , b , c , which are the length of the edges of the unit cell, and angles α , β , γ formed between the axes. It is a total representation of the content of the repeating unit of the crystal. The unit cell is a sufficient and representative portion of the lattice which is outlined by the vectors a , b , c ; an infinite number of such unit cells stacked side by side builds up the lattice (net two-dimensional space group).⁷⁴ It is the smallest repeating unit for which its delineating vectors are parallel to or coincide with important symmetry directions in the lattice. The asymmetric unit defines the molecular arrangement from which the unit cell can be constructed based on the given symmetry elements. The asymmetric unit can contain any arrangement of the molecule but if it contains more than one identical copy, it will be called non-crystallographic symmetry relating to the individual subunits.⁷⁶

Unit cells are classified into 7 crystal systems based on the minimum axes of symmetry and their molecular arrangements. The crystal systems are a set of reference axes, which have a direction as well as a magnitude and hence are vectors, as shown in figure 2-2.

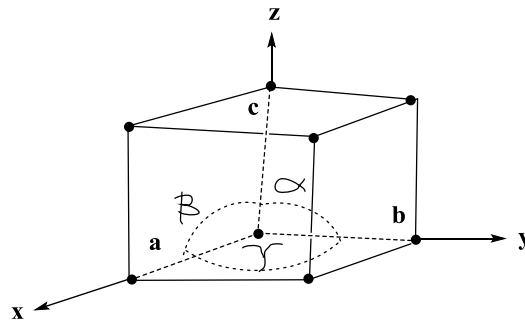


Figure 2-2: An example of a unit-cell with axes a , b , c and angles α , β , γ .⁷⁷

In its most general form, a crystal lattice can be defined as an infinite, one-, two-, or three-dimensional regular arrangement of points, each of which has identical surroundings. It is an end-to-end stacking of unit-cells in the directions of the cell axes.⁷⁷

1. One-dimensional crystal structure (Linear Lattice).
2. A two-dimensional crystal structure has two-dimensional translation repetition and can also be called a net because the images are formed in a regular manner. It exhibits two-fold rotational symmetry about each lattice point. In two-dimensional lattice systems, there are 5 Bravais lattices which are grouped into 4 crystal families namely oblique, rectangular, square and hexagonal.⁷³
3. A three-dimensional crystal structure (Bravais Lattice) has a three-dimensional translation repetition. It exhibits inversion symmetry about each lattice point. There are 7 three-dimensional lattice systems which are grouped into 6 crystal families. Their unit cells are specified according to the relative lengths of the cell edges (a , b , c) and the angles between them (α , β , γ) as listed in table 2-1.⁷⁸

Table 2-1 shows the applicable rotational symmetry of crystal systems, their allowed centering, the nature of unit-cell axes and angles, characteristic minimum symmetry axis and their Schoenflies notations.

Crystal System	Allowed Centering	Nature of unit-cell axes and angles	The characteristic minimum symmetry axis	Schoenflies notations
Triclinic or Anorthic	Primitive (P)	$a \neq b \neq c$ $\alpha \neq \beta \neq \gamma \neq 90^\circ$	None	C_i
Monoclinic	Primitive (P) Base-centred (C)	$a \neq b \neq c$ $\alpha = \gamma = 90^\circ \neq \beta$	2-fold	C_{2h}
Orthorhombic	Primitive (P) Base-centred (C) Body-centred (I) Face-centred (F)	$a \neq b \neq c$ $\alpha = \beta = \gamma = 90^\circ$	Three 2-fold at 90°	D_{2h}
Tetragonal	Primitive (P) Body-centred (I)	$a = b \neq c$ $\alpha = \beta = \gamma = 90^\circ$	4-fold	D_{4h}
Hexagonal	Primitive (P)	$a = b \neq c$ $\alpha = \beta = 90^\circ$ $\gamma = 120^\circ$	6-fold	D_{6h}
Rhombohedral or Trigonal	R - centered (R) P (R can be used if hexagonal axes are chosen)	$a = b = c$ $\alpha = \beta = \gamma \neq 90^\circ$	3-fold	D_{3d}
Cubic	Primitive (P) Body-centred (I) Face-centred (F)	$a = b = c$ $\alpha = \beta = \gamma = 90^\circ$	Four 3-fold at 109.47°	O_h

Table 2-1, The essential classified crystal system, their characteristic minimum symmetry axis, and Schoenflies notations.⁷⁹

Schoenflies notation is one of the two conventions commonly used to describe point groups. A point group in Schoenflies is adequate to describe the symmetry of a molecule. This is used mainly in spectroscopy.⁷⁷

The Hermann-mauguin notation is the second notation. This is also known as international notation used mainly in crystallography to describe the symmetry directions of the lattice point groups.⁷⁷

Crystal diffraction methods can be made to reveal the underlying three-dimensional structures within a crystal. Structures of macromolecules, such as proteins and viruses can be determined by visualizing them with an electron microscope though individual atoms cannot be distinguished.

2.2.2. Miller Indices

Miller indices are used to define crystal planes. They are represented by hkl , the allowed diffraction beams and corresponds to the inverse of the ratio of the intercepts on a , b , c axes of the unit cell. When hkl , the crystal face indices relative prime makes intercepts with the unit cell vectors a , b , c , we will have intercepts $\frac{a}{h}$, $\frac{b}{k}$, $\frac{c}{l}$ and the angles formed between them are α , β , γ as shown in figure 2-3.

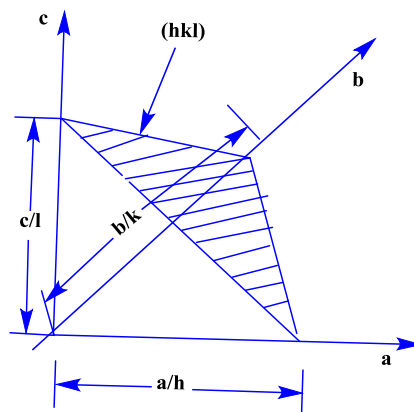


Figure 2-3: Figure showing the interception of miller planes with vectors a , b , c .⁷⁷

Miller indices are not only applicable to lattice plane as shown in figure 2-3, but they are also applicable to the external faces of crystals where the origin is conventionally taken to be at the centre of the crystal.⁸⁰

2.3. Symmetry and Space groups

2.3.1. Point Groups

A crystallographic point group is the collection of symmetry elements. Mathematically, it describes a group of symmetry operations which pass through a central point. They also describe the symmetry of a finite body. A lattice constitutes a mechanism for repetition to an infinite extent by translations parallel to three non-coplanar directions. It is the complete collection of all symmetry elements passing through a centre point, describing the symmetry of an individual object. One point of the symmetry operations must be left unchanged and the appearance of the object must be unaltered.⁷⁷

A point group that contains an inversion centre as one of its symmetry elements is centrosymmetric. For every point (x, y, z) in their unit cell, there is also an equivalent $(-x, -y, -z)$. They cannot display properties like the piezoelectric effect.

A point group that is lacking an inversion centre is termed to be non-centrosymmetric. They are divided into two types; polar and chiral (enantiomorphic).⁸¹

There are 32 crystallographic point groups and there are 4 symmetry operations of point groups which are⁷⁷

1. n - fold rotation axes: a rotation through $360^\circ/n$ which leaves the object unaltered. (n is an integer).
2. Mirror planes: This involves a reflection which takes place with respect to a mirror plane.
3. Inversions: This involves moving every point x, y, z to $-x, -y, -z$.
4. Improper rotation: This is a rotation followed by a reflection in a plane perpendicular to the axis of the rotation.

Other symmetry operations are:

5. Translations: This is a movement on a straight line in any direction in the crystal.
6. Screw axis (n_x): It is n-fold rotation of an object around an axis followed by a translation of x/n along that axis.
7. Glide plane: This is a reflection across a mirror plane followed by a translation of half of a unit parallel to the mirror plane. It is designated a, b, c depending on the direction

of the translation. Likewise, n-glide is possible when the translation is between the axes.

2.3.2. Space Groups

Space groups include the symmetry operations observed in point groups with the exception of 5 and 7-fold axes (which do not tessellate). They also include additional operations, which allow translation to occur but which, when repeated must produce translation by a whole number of unit cell dimension (a , b , c). The space group is the complete collection of all symmetry elements for an infinitely repeating pattern. It can be described as an infinite set of symmetry elements, its operation with respect to any of which brings the infinite array of points to which they refer into a state that is indistinguishable from that before the operation. A space group is a result of repeating a point-group pattern by the translations of a Bravais lattice. This produces an arrangement of atoms in a crystal. It is made up of two parts; a pattern motif and a repeat mechanism.⁷⁹

The symmetry created by the combination of 32 point groups and 14 Bravais lattices constitute the 230 space groups distinct combinations of three-dimensional crystals, with $P2_1/c$ as the most common of the 230 space groups. The numbers of space groups in each crystal systems are listed in table 2-2.⁸²

No.	Crystal Systems	Numbers of space groups
i.	Triclinic	2
ii.	Monoclinic	13
iii.	Trigonal	25
iv.	Hexagonal	27
v.	Cubic	36
vi.	Orthorhombic	59
vii.	Tetragonal	68
	Total	230

*Table 2-2: The numbers of space group in each of the crystal systems.*⁸²

2.4. Crystallization with particular reference to the techniques used in this study.

2.4.1. Crystal Growth

Generally, solution methods are used for growing crystals (crystals are grown in solution). Hydro (solvo) thermal synthesis has been proven to be an effective method in preparing functional coordination polymers and growing single crystal for structural studies. Other methods that can be used are cooling molten material or sublimation of material from a gas phase onto a surface. The crystallization process involves the formation of many new, stable noncovalent chemical bonds. The concepts governing crystal growth are solubility, stability, and reactivity. Crystallization consists of two major events, nucleation and crystal growth. Nucleation is the process of creating a new solid phase from a supersaturated homogenous mother phase or it is the rate at which new crystals are formed. It precedes crystallization and it is applicable to all types of crystallization techniques.⁸³

Crystal size and shapes are important. Crystals grown for single crystal diffraction must not necessarily be large. It could be around 0.1 mm to 0.3 mm but larger crystals are needed for neutron diffraction studies. Single crystal for characterization can be cut off with a scalpel or razor blade when crystals are grown in clumps. A crystal is termed good if it is well formed and has clear faces. A crazed crystal with a fibrous appearance will not be appropriate for single crystal characterization.⁸⁴

When growing crystals, solvent similar to the compound being crystallized in terms of polarity and functional groups may be used because like dissolves like. Anti-solvents that are not similar to the solvent may be used to reduce solubility. The mixture of similar solvent and solute allows manipulation of solubility.⁸⁵

The quality of crystals from which diffraction data are acquired determines the final quality of a crystal structure. Crystals should be grown slowly in the absence of dust and vibration. Vessels for growing crystal must be free of contamination. Old vessels must be avoided to prevent multiple nucleation points and growing a large number of small crystals. Likewise, if the inner surface of the container is too smooth, this may inhibit crystallization. The presence of dust and vibration may lead to the growth of too small or non-singular crystals. Crystals with defects such as impurities, dislocations, planar faults or internal strains are less precisely periodic in their atomic arrangement but they still have distinct diffraction peaks. Their diffraction peaks could be broadened, distorted and weakened.⁸⁶

Crystals are routinely cooled in a stream of cold, dry nitrogen gas to -150 K on modern diffractometers. The standard method of protecting the crystals while subjecting them to analysis under the microscope is to immerse the crystal in Fomblin oil. The oil freezes at -240 K so that it also acts as an adhesive. Efflorescent and deliquescent materials experience difficulties during crystal growth. This problem can be solved by placing the crystals in a sealed glass capillary tube or properly placed in a suitable atmospheric condition and cooled if necessary.

A single crystal with all the unit cells identical and aligned in the same orientation must be used as a sample for chemical crystallography. A suitable size must be chosen to reduce X-ray absorption. The absorption coefficient depends on the X-ray wavelength and on the chemical composition and can be very high when heavy elements are present.

Intensity usually has a standard uncertainty (S.U.) which can be calculated from the known statistical properties (parameters) of the X-ray generation and diffraction processes. The S.U. values are a measure of the precision or reliability of the measurement. The intensity of the diffracted X-ray beam is proportional to the square of the wave amplitude, which cannot be negative, but the weakest reflections from a diffractometer may be insignificantly above background.^{83, 86}

2.4.2. Characteristics of Crystals

The major external characteristic of crystals is that they usually have flat faces bounded by straight edges. Crystals may not be easy to grow and are often not visible to the naked eye. They can decompose when exposed to oxygen and effloresce or deliquesce as the relative humidity changes. Biological materials will only be stable when the relative humidity is extremely high.⁸³

2.4.3. Properties of Crystals

The properties of crystals are always direction dependent. Crystals are anisotropic. They grow and dissolve at different rates in different directions. Their refractive indices vary with direction and their thermal expansion coefficient and electrical conductivity are directionally dependent likewise their mechanical properties.

a. Optical properties:

When light interacts with molecules including transition metal complexes, we have the following possibilities:

- π - π^* transition in the ligands
- d-d transition in the metal
- d- π or π -d charge transfer transition between the metal and ligand.

Also, it is possible for molecules to rotate the plane of polarization of the light waves to exhibit optical activity. Because of the directional nature of these properties, the symmetry of the crystal plays an important role in determining the physical effects. These properties have important applications in different types of light modulator devices used in a variety of optical systems.

b. Non-linear optics:

Non-linear optics is a study that occurs as a result of the modification of the optical properties of a material system by the presence of light. Sometimes, most crystals were grown using the high-temperature flux method. This generally has high optical quality, a high damage threshold, chemical stability, and transparency far into the ultraviolet. Other crystals usually possess a wide wavelength range, good chemical stability, and high damage threshold.⁸⁷

c. Electrical properties:

A crystal can be an insulator, metallic conductor or semiconductor. Additionally, many crystals can be squeezed or pressed to create piezoelectricity. Piezoelectricity is the creation of an electrical potential by a crystal in response to applied mechanical stress or change in temperature.⁷⁷ It simply means the production of stress when an electric field is applied (*Curie and Curie, 1880*).

2.5. Crystallization Techniques commonly used for Small Molecules in the Chemical Laboratory

There are numerous crystallization techniques. Chemical properties such as air sensitivity, moisture sensitivity, bond formation, hygroscopic and reaction with certain solvents of the compound of interest mostly determine the crystallization techniques to choose. In every crystallization method, the solubility of the materials in the chosen solvent is very important because the aim of all the crystallization techniques is for the sample solution to attain saturation and supersaturation so they can grow good crystals.⁸⁸

The solution method is the most widely used due to its flexibility. It is suitable for use with molecular compounds that are the subject of most crystal structure determinations. When growing crystals using the solution method, the solution should not be allowed to dry out as this may cause the crystals to become encrusted and not remain single. Solution-based methods include slow evaporation of a solution, slow cooling and slow precipitation by vapour diffusion (evaporation), liquid-liquid diffusion such as solvent layering.

Crystals are obtained from solution by dissolving the required substance (solute) in a suitable solvent until it gets to its saturation point (under mild condition). Slow evaporation increases the concentration of the solute in the solution to give a saturated or supersaturated solution from which material separation occurs in the form of crystals.

During crystal growth, nucleation takes place when solute molecules meet with extraneous particles like dust or seeds in solution and form small aggregates.

Saturated solution → Super saturation → Nucleation → Crystal growth

One of the most common solution methods for chemical crystallography is vapour diffusion, also solvent layering is solution based.⁸⁵ There are other crystallization techniques which depend on the solution based method. These other techniques may be considered after using the solution method and no crystals were formed. In most cases, these techniques tend to change the nature of the sample been crystallized. The techniques include slow evaporation (sometimes by using NMR tube), crystallization from gels,⁸⁵ slow cooling and liquid diffusion,⁸⁴ thermal gradients, co-crystallization and clathrate, heavy atom and reactant diffusion.

2.6. Introduction to X-ray Crystallography

2.6.1. Bragg's Law and Diffraction

About 100 years ago, W.L Bragg derived an equation which explains how crystals are capable of diffracting X-rays. The equation is used to explain the diffraction geometry of X-rays by crystals. Bragg's law explains why the cleavage faces of crystals appear to reflect X-ray beams at certain angles of incidence. It is very useful for calculating the wavelengths and directions for which the diffraction condition is fulfilled by any given interplanar distance. Bragg derived the equation based on the work done by Freidrich, Knipping, and Laue. According to the Bragg's equation, crystals are said to be composed of a series of parallel planes of atoms separated by a small distance. The parallel planes are capable of reflecting the X-ray in a way that the angle of incidence equals the angle of reflection. Bragg's experiment demonstrated that X-rays could be diffracted by crystals.⁷⁵

2.6.2. Deriving Bragg's Law

Bragg's Law can be derived when we consider the conditions that are necessary to make the phases of the beams coincide when the incident angle equals the reflecting angle. The rays of the incident beam are always in phase and parallel up to the point at which the top beam strikes the top layer at atom z as shown in figure 2-4. The second beam continues to the next layer where it is scattered by atom **B** and must travel the extra distance **AB** + **BC** if the two beams continue to travel adjacent and parallel. The extra distance must be an integral (n) multiple of the wavelength for the phases of the two beams to be the same.

$$n\lambda = \mathbf{AB} + \mathbf{BC}$$

Equation (2-1)

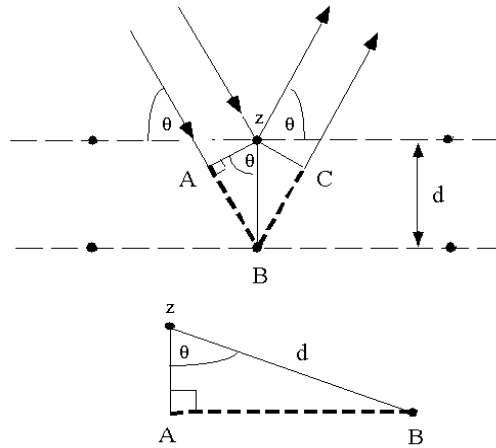


Figure 2-4: Deriving Bragg's Law by using reflection geometry and applying trigonometry.

<http://skuld.bmsc.washington.edu/~merritt/bc530/bragg/> Date accessed: 23/11/18

The lower beam should travel the extra distance (**AB + BC**) in order to continue traveling parallel and adjacent to the top beam. With **d** being the hypotenuse of the right triangle **ABz**, we will then use trigonometry to relate **d** to the distance (**AB + BC**). The distance **AB** is opposite the angle **θ**. Therefore,

$$AB = d \sin \theta \quad \text{Equation (2-2)}$$

Because **AB = BC**

$$n\lambda = 2AB \quad \text{Equation (2-3)}$$

When we substitute equation (2-2) into equation (2-3), we have the Bragg's equation,

$$n\lambda = 2 d \sin \theta \quad \text{Equation (2-4)}$$

Where

$\sin \theta$ is the angle of incidence of radiation.

λ is the wavelength

n is an integer (1, 2, 3, etc.).

d is the distance between atomic layers in a crystal.

2.7. Single Crystal Diffraction of X-rays

Single crystal diffraction of X-ray can be used to determine the molecular structure of a compound. Diffraction occurs when the light is scattered by a periodic array with long-range order, producing constructive interference at specific angles. The X-ray diffraction from a single crystal gives the amplitudes of the Fourier transform of the crystal structure. The phases of the diffracted waves (with respect to the unscattered beam) are lost so that the diffracting structure cannot be unambiguously reconstructed. The limitation of crystal diffraction is obtaining crystal samples with the highest regular long-range three-dimensional order characteristic of the ideal crystalline state.⁸⁹

X-rays are electromagnetic radiation of short wavelength. They are generated by the acceleration of electrons when they interact with an electromagnetic field. The most commonly used X-ray tube target materials are copper and molybdenum. They give characteristic X-ray wavelength of 1.5418\AA and 0.71073\AA respectively. The most commonly used source of X-rays in conventional crystallography laboratories is the sealed hot cathode tube, figure 2-5.

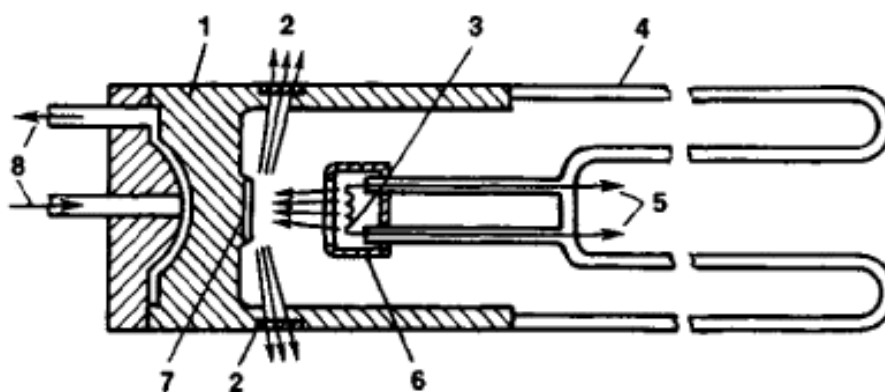


Figure 2-5: Schematic of an X-ray tube for X-ray diffraction analysis.

1. Metallic anode block (usually grounded). 2. Beryllium window for the exit of X-radiation. 3. Hot cathode. 4. Glass envelope insulating the anode part of the tube from the cathode part. 5. Cathode leads, to which the filament voltage and high voltage are supplied (with respect to the anode). 6. Electrostatic electron-focusing system. 7. Anode (antichode). 8. Inlet and outlet pipes for the flowing water that cools the anode block.

<https://encyclopedia2.thefreedictionary.com/Conventional+X-ray+generator> Date accessed: 23/11/2018

2.7.1. Production of X-rays

An X-ray tube is made of an evacuated enclosure of glass and metal construction that produces electrons by passing an electric current through a wire filament. The electrons are accelerated to a high velocity by an electrical potential of typically 40,000 - 60,000 volts across a few millimeters, then stop suddenly when they collide with the water-cooled metal block. At each collision, there will be a loss of energy ΔE . This energy loss ΔE gives rise to an X-ray photon of energy $\frac{hc}{\lambda}$ which has a wide range of values and likewise gives rise to a wide range of λ values. This is the origin of the continuous white or bremsstrahlung radiation and there will be a 'cut off' at a short wavelength called the short wavelength limit (swl).

$$\Delta E = eV = \frac{hc}{\lambda_{swl}} \quad \text{Equation (2-5)}$$

Where

V is a voltage of the X-ray tube

e is the charge on the electron

Bremsstrahlung is continuous and appears as a broad spectrum with a maximum intensity at $\frac{4}{3}\lambda_{swl}$. A series of sharp peaks are superimposed on the continuous radiation. These arise from electron transition between energy levels in the atom. The innermost shell (K-shell) has one energy level which is the lowest energy level, the L-shell has three and the M-shell has five such energy levels. When impinging electrons have sufficient energy equal to or greater than the work function, W_K , they will knock out an electron from the K-shell. In this situation, the incident electrons are strongly absorbed.

This ionized state of the atom is short lived and the atom returns to its ground state as a result of the electrons tumbling down from the outer to the innermost shell. Each transition is accompanied by the emission of an X-ray photon of energy and therefore wavelength characteristic of the difference between the energy levels. The spectra will take the following patterns:

- A Transition from L to K shell = K_{α} series
- A Transition from M to K shell = K_{β} series
- A Transition from M to L shell = L_{α} series

The most important in relation to X-ray diffraction is the K_{α} series. In L-shell, there are three closely separated energy levels K_{α_1} , K_{α_2} , and K_{α_3} . These three energy levels are not equally strong as K_{α_3} is very weak and K_{α_1} is about twice the intensity of K_{α_2} . K_{α_2} and K_{α_3} comprise K_{α} -doublet. K_{α_1} radiation is mostly used by making use of a crystal monochromator set to reflect only this particular wavelength and its sub-multiples.⁹⁰

$$\lambda K_{\alpha_1} = 2d \sin\theta$$

Equation (2-6)

2.7.2. X-ray Scattering from the Crystal

X-ray diffraction occurs when a crystal is oriented toward incoming X-ray waves of a suitable wavelength (λ) such that the waves interfere non-destructively between the ordered rows of electronic concentration in the crystal that are of a suitable separation.

Diffraction line shape analysis is an important method for studying crystal defects. The width of a diffraction peak is affected by the number of crystallographic planes contributing to the diffraction. Diffraction peaks will become sharper in theta angle as crystallites become larger.

Comparing light microscopy and X-ray diffraction, in light microscopy, the diffraction pattern is not recorded because the scattered light can be focused by the objective lenses to give a magnified image of the object in the study. With X-rays, a diffraction pattern is recorded photographically or electronically from crystals that give well-defined diffraction pattern.⁷⁴

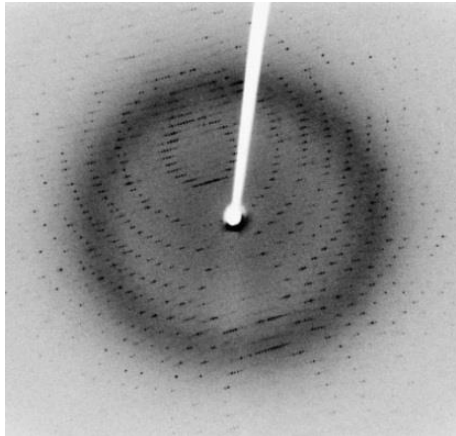


Figure 2-6: An example of a diffraction pattern formed from the constructive interference of X-ray passing through a crystal.

<https://en.wikipedia.org/wiki/Diffraction> Date accessed: 23/11/2018.

Scattering of X-rays by atoms produces a diffraction pattern. The pattern contains information about the atomic arrangement within the crystal. The X-ray diffraction pattern is given by the product of the scattering from the unit cell and the reciprocal lattice i.e. the scattering pattern of a single unit cell is observed only at the reciprocal lattice points. Many factors affect the intensity of X-rays in a diffraction pattern but the structure factor is only dependent upon the crystal structure and it can be expressed in terms of the contents of a single unit cell as

$$F(hkl) = \sum^N f_j [\cos 2\pi (hx_j + ky_j + lz_j) + i \sin 2\pi (hx_j + ky_j + lz_j)] \quad \text{Equation (2-7)}$$

Where

f_j is the Scattering factor - Scattering of X-rays by atom j

j^{th} atom position is given by the fractional coordinate as (x_j, y_j, z_j)

N is the atoms in the cell

Structure factors $F_{hkl} - F_{hkl}^2$ intensity of X-rays diffracted 'reflected' by plane h, k, l .

An image of the crystal structure can be calculated from the X-ray diffraction pattern. We see electrons in the image as electrons scatter the X-rays. An electron density map gives the value of electron density at every point in a single unit cell of the crystal. The units of density are the number of electrons per cubic Ångstrom unit measured in $e/\text{Å}^3$.

Ångstrom is used to measure the distance between atoms or ions in a crystal. $1 \text{ Ångstrom} = 10^{-10} \text{ m}$, $1 \text{ Å} = 100 \text{ pm} = 0.1 \text{ nm}$. The electron density can be expressed in term of structure factors as:

$$\rho(xyz) = \frac{1}{V} \sum_{h,k,l} |F(hkl)| \cdot \exp[i\phi(hkl)] \cdot \exp[-2\pi i(hx + ky + lz)] \quad \text{Equation (2-8)}$$

Where

ρ is the electron density.

V is the volume of the unit cell.

The summation is over all the structure factor $F(hkl)$.

Fourier transform links equations 2-7 and 2-8. Equation 2-7 transforms the electron density in the form of atomic scattering f_j to the structure factor $F(hkl)$ while equation 2-8 transforms the structure factor back to the electron density. A diffraction pattern is the Fourier transform of crystal structure corresponding to the pattern of waves scattered from an X-ray incident beam by a single crystal. Also, the crystal structure is the Fourier transform of the diffraction pattern and it is expressed in terms of the electron density distribution concentrated in atoms.⁹¹

2.7.3. Detection of X-rays

X-rays can be detected using three principles which are:

a. Photographic film: (Historical)

The photographic film made use of two types of film detection. The standard photographic film detection which is based on the chemical emulsion properties of the photographic film and the intensifying layer film, which was commercialized by Polaroid, and were commonly used in a large number of diffractometers because of their higher sensitivity and fast revealing process.⁷⁵

b. Fluorescent screen

Fluorescent screen system of detection is used mainly for the first calibration of equipment. It makes use of layers of zinc sulfide doped with nickel and produces X-ray fluorescence emission in the visible range, which can be detected by the human eye.⁷⁵

c. Area Detector

Photography has lost popularity as data is collected using four-circle instruments advanced because it is quicker to record the full data set than to obtain a complete photo set. An X-ray diffractometer is a conventional four-circle diffractometer in which the X-ray generator, crystals, and detector lie in the same horizontal plane. It measures intensity in automatic, computer-controlled processes. It has an electronic detector which in older machines is a Scintillation counter but on modern instruments is a Charge Coupled Device Area detector (CCD detector).

Area detectors are the electronic equivalent of a photographic film. They have many advantages over scintillation counters because many diffracted beam are recorded simultaneously. It can provide a high degree of redundancy of symmetry-related equivalent data.

A Charge Coupled Device (CCD detector) is a large area memory chip coated with an X-ray fluorescent material (cf digital camera). The light emitted is converted to electrons which are stored in a 2-dimensional array, which is formed on the chip. The electrons in each memory location can be read to produce a 2-dimensional image of the diffraction pattern.⁹²

2.8. Single Crystal X-ray Diffraction Practice

2.8.1. Measuring and Obtaining Single Crystal X-Ray Diffraction Data

The stages involved in measuring and obtaining single crystal X-ray diffraction data are⁹³

1. Grow Single Crystals.
2. Select a suitable crystal and mount it for X-ray study.
3. Centre the crystal on the diffractometer.
4. Determine the unit-cell geometry and preliminary symmetry information i.e. unit cell axes (vectors) a , b , c , angles α , β , γ , crystal system, space group and information about molecular symmetry.
5. Measure a full set of reflections i.e. intensity data like a list of hkl , I σ (I).
6. Data reduction; make various corrections applied to data like a list of hkl F σ (F) or hkl F^2 or (F^2).
7. Correct the data for instrumental effects.
8. Solve the structure by using Patterson methods or Direct methods and or other methods.
9. Complete the structure; find all the atoms.
10. Refine the structure with refinement package using least squares minimization.
11. Interpret the results i.e. molecular geometry, packaging arrangement, etc. (any given reflection gives a separation between a set of Miller plane).

2.8.2. X-ray Crystal Structure Determination

For diffraction, the experimental ways of determining molecular structure are:

1. Recording the X-ray scattering pattern.
2. Carrying out the combination subsequently by mathematics.

In obtaining crystals, a microscope with a polarizing attachment and with around x 40 magnification and a good depth of field and a strong light source are required. Crystals should be viewed in normal light to determine if they are well shaped, then curved and deformed crystals must be rejected. A set of polarized filters should be used because most crystals will transmit polarized light except tetragonal and hexagonal crystals when they are viewed in their unique *c*-axis and cubic crystals when they are viewed in any orientation. If a crystal transmits polarized light, the microscope stage must be turned until the crystal turns dark and light again. Extinction is the best optical indication of crystal quality because if a crystal does not extinguish completely it is not a single crystal and it must be rejected. Smaller crystals never extinguish. Lack of sharpness indicates a large mosaic spread within the crystal. In addition to their microscopic structure, large crystals are usually identifiable by their macroscopic geometrical shape, consisting of flat faces with specific, characteristic orientations.⁸¹

Once a suitable crystal has been obtained, crystal structure determination can begin. The stages involved include:

1. Measuring the intensities of Bragg reflections and taking note of the various geometrical symmetry and physical phenomena.
2. Using computer program and mathematical methods to imitate the behaviour of a microscope lens to solve the phase problems and produce an image of the atoms in a crystal from the diffraction pattern.
3. Refining the main structure in a way that there will be an agreement between the observed and the calculated structure factors.

Single crystal data are collected by mounting the crystal in the X-ray beam and randomly measuring the diffracted spots at a range of points in the reciprocal lattice. To collect an appropriate data set, the Bravais lattice is calculated. This information is used to determine the unit-cell dimensions and its orientation. As part of this process, the reflection Miller indices will also be determined.

2.8.3. Crystal Structure Analysis

- i. Collect intensity data:

In X-ray diffraction experiments, intensities of the reflections are to be measured but practically, their relative phases cannot be measured.

- ii. Solve the phase problem:

There are two main methods used in solving the small molecule crystallographic phase problem.

a. Patterson Synthesis:

Patterson method or Patterson synthesis is used in solving the crystallographic phase problem. It is widely used when one, or a small number of heavy atoms are present in the structure. The method was originated by A.L. Patterson as far back as 1934. He presented a synthesis, Patterson map which was obtained by performing a Fourier series on the square of the amplitude with all waves taken in phases. If there are N atoms in a unit cell, it means there are N^2 numbers of vector running between these atoms so a Patterson map appears where atoms are located relative to each other and not where they are located with respect to the unit cell origin.⁹⁴

b. Direct Methods:

Direct methods are used to solve phase problem when equal atoms are present in the structure i.e. structures that do not contain heavy atoms. The methods make use of the measured intensities because electron density within a crystal cannot be negative. This fact places restrictions on the possible phase angles between reflections. Fourier series are calculated using the measured intensities and the approximate phases. Direct methods are likewise described as a black box because the process is automatic and is performed by a computer.

An entirely different method is used to solve phase problems in macromolecular crystallography. Patterson synthesis methods cannot be used to solve the phase problem of macromolecule crystals because the heavy atom is not present. Also, direct methods cannot be used because the direct method requires a relatively low number of reflections for the

computations to be effective. The small protein contains a large number of atoms which would lead to an uninterpretable Patterson map. Therefore, Dual-space direct method can be used to solve small protein structures (up to approximately 1000 independent protein atoms) and other molecular structures with similar sizes provided that native data are available to a resolution which is usually 1.2 Å.⁹⁵

- iii. Compute electron density map.
- iv. Interpret the electron density map.
- v. Refine molecular structure.

As single crystal methods become more efficient and faster, it is now feasible to screen reaction mixtures by examining the solutions on an optical microscope and selecting crystals that conform to the standards for single crystal analysis. This saves much time in conventional synthesis, isolation and characterization methods. Effectively, it pushes XRD from the final stage of characterization to be the first stage.

2.9. Powder X-ray Diffraction (PXRD)

Diffraction is a powerful experimental technique that makes use of X-ray, neutron or electron diffraction on powder or microcrystalline samples to distinguish polycrystals from amorphous materials, detecting preferred orientation and grain size. It can even characterize the structure of unknown materials using computational methods that originate in single crystal studies.⁹⁶⁻⁹⁷

PXRD is a non-destructive experimental technique that has been used successfully for many decades. Its sample preparation is easy and fast. It has high accuracy for d-spacing measuring and calculations. It measures the average spacing between layers or rows of atoms, size, shapes and internal stress of small crystalline region. It can be done in-situ. The fundamental nature of the method is appreciated because each powder diffraction pattern represents a one-dimensional snapshot of the three-dimensional reciprocal lattice of a crystal.^{96, 98} Powder diffraction data usually lack the three-dimensionality of a single crystal diffraction image yet it is the only realistic experimental option for a reliable determination of the crystal structure of materials prepared in a polycrystalline form.^{97, 99} Each of the crystalline solid samples has their characteristic X-ray powder diffraction pattern which is mainly used as fingerprints for identifying them and determines their structure like sizes, shapes, how the atoms are packed together in their crystalline state and what are their interatomic distances and bond angles. The quality of a powder diffraction pattern depends on the physical and chemical conditions of the sample specimen. Also, the nature of energy radiation available and the resolution of the instrument is another determinant factor.¹⁰⁰

Powder diffraction is composed of multiple Bragg peaks which have different intensities in addition to varying position and shapes. In powder diffraction, when a solid material is crystalline, it scatters and diffracts but when a solid material is non-crystalline, it only scatters. The scattered intensity is customarily represented as a function of a single independent variable - Bragg angle - 2θ .^{96, 100-101}

Diffraction line-shape analysis is an important method for studying crystal defects. Crystals that have accurate periodicities over long distances have sharp and clear diffraction peaks while crystals with defects (such as impurities, dislocations, planar faults, internal strains, or small precipitates) have less accurate periodic atomic arrangements. Their diffraction peaks

are broadened, distorted, and weakened. Likewise, the lack of sharp diffraction peaks in diffraction experiments shows that the materials are amorphous.

Chapter 3

The Reaction of Substituted Benzoic Acids with a range of 1st-row Transition Metals and Investigation of the Products using Optical Microscopy and Single Crystal X-ray Diffraction

3.1. Introduction

Organic ligands are one of the most important materials in the preparation of CPs and MOFs because of their length, steric effects,¹⁰² and flexibility will lead to diverse structures of coordination polymers.⁵

Substituted benzoic acids have been previously studied extensively. The substituent can be in *ortho*-, *meta*- and *para*- position, but the closer the substituent is to the carboxyl group, the greater is its steric effect.¹⁰² Substituted benzoic acid can act as a monodentate or multidentate (bidentate or tridentate) coordinating ligands. An example of a monodentate ligand is benzoic acid which can bind to the metal centre at one of the carboxylate oxygen atoms or at both carboxylate oxygen atoms. Also, substituted benzoic acids such as aminobenzoic acid and nitrobenzoic acid can act as monodentate, bidentate or tridentate ligands binding to the metal centre at one or both of the carboxylate oxygen atoms and at the N atoms at the same time. Figure 3-1 shows the different coordination modes of the carboxylate based ligands used in this study.

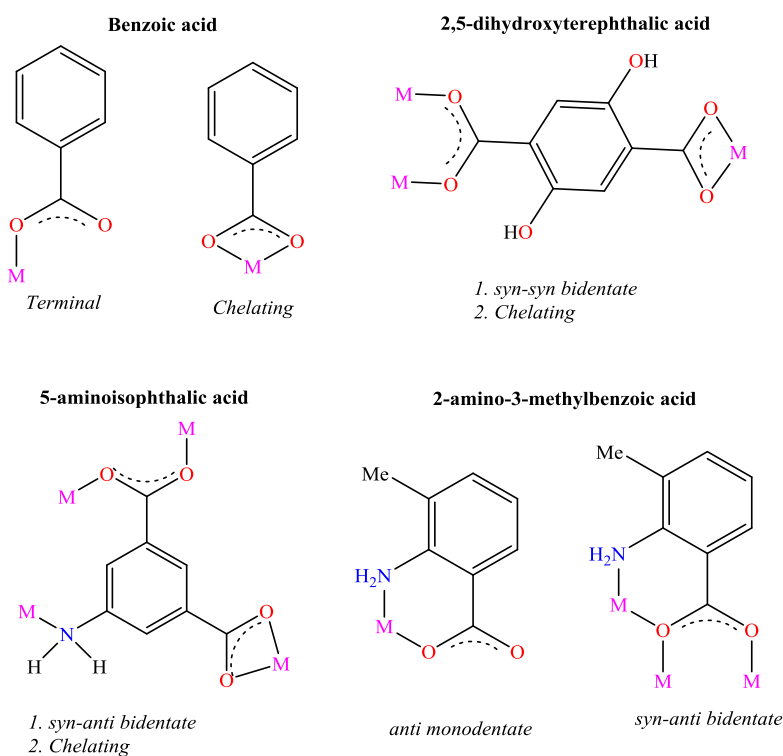


Figure 3-1: Coordination topology of benzoic acids, dicarboxylate ligands, and ortho N-substituted benzoic acid showing the chelating and bidentate coordination mode.

In 2,5-dihydroxyterephthalic acid, the hydroxyl groups act depending on their protonation or coordination states. 5-aminoisophthalic acid and AMB are multidentate.

The nature and position of the substituent groups on the aromatic ring may have an effect on the anti-inflammatory properties such as in the case of Cu complexes.¹⁰³ Length, rigidity, coordination modes, functional groups or the substituents on the organic ligands have consequences on the final structure of MOFs.¹⁶

It has been observed that interesting variation in the topology of the network of coordination polymers can be introduced by changing the alkyl/aryl group of the carboxylate. Kar *et al.* were able to synthesize different manganese complexes under ambient condition. These complexes are a 1D ladder, 2D sheet or 3D network as a result of introducing the nitro substituent in the *ortho*-, *meta*- or *para*- position of benzoate group.^{6, 16}

The introduction of methyl-substitution on the aromatic multicarboxylate ligand may impose influences on the assembling processes, the structure and even the properties of the coordination polymers due to their geometric and electronic effect.^{11, 104}

Often time, it is expected that the substituents on benzene rings result in the rotation of the carboxylate groups out of the plane that contains benzene ring to give a larger Θ . Hence, the critical parameters in the formation of paddle wheels units and their reticulated MOFs are a larger Θ and the size of the substituent.¹⁰⁵

Generally, N donors can act as a good candidate for the construction of metal-organic complexes. Carboxylate based ligands with NH_2 substituents are good candidates for the construction of metal-organic frameworks. The NH_2 group plays an important role in the formation of metal-organic complexes by either binding directly to the metal centre or behaving as an H-bonding donor (H-D) while NO_2 behaves as H-bonding acceptor (H-A).¹⁰⁶

Apart from carboxylate ligands, N-donor polyamine ligands are often used as auxiliary ligands which give rise to bridging and chelating linkers.¹⁶

It has been observed that interesting variation in the topologies of the networks can be introduced by changing the alkyl/aryl group of the carboxylate.⁶ Though in the crystallization reaction of 1st-row 3d transition metal and 2-amine-3-methylbenzoic acid (AMB) structures obtained in chapter 4 of this study, the methyl groups are not involved in

the coordination environment of the 1st-row 3d transition metals, the introduction of methyl groups and the *ortho*-, *meta*- or *para*- position of the substituent on the aromatic multicarboxylate may impose influences on the assembling processes, the structures and even the properties of coordination polymers due to their geometric and electronic effects.^{5, 104, 107-108}

In this study, different carboxylate based ligands ranging from monocarboxylate such as benzoic acid, dicarboxylic acid such terephthalic acid, amine substituted dicarboxylate group such as 5-aminoisophthalic acid, aminobenzoic acid, amine, and methyl substituted benzoic acid such as AMB were used to make coordination polymers. Hence, there are different intriguing architecture and topologies of the structures to be discussed in the following chapters.

3.2. Result and Discussion

3.2.1. Reactive Crystallization and Crystal Structure of $[\text{Zn}(\text{C}_8\text{H}_5\text{NO}_4)(\text{H}_2\text{O})]_n$

3.2.1.1. Introduction

Zinc Chloride is a metal halide. It is a white crystalline solid with molecular formula ZnCl_2 and molecular weight 136.315 g/mol. It is hygroscopic and very deliquescent. It is odourless and highly soluble in water. ZnCl_2 has some covalent character in the crystalline form. Zn adopts a tetrahedral coordination environment. ZnCl_2 contains closely packed anions with Zn occupying only 1 in 4 of all the tetrahedral sites. ZnCl_2 has four crystalline forms (polymorphs) which are; α with Tetragonal symmetry, β with Tetragonal symmetry, γ with monoclinic symmetry and δ with orthorhombic symmetry.¹⁰⁹⁻¹¹⁰

Aqueous solutions of ZnCl_2 are acidic. The acidity of its aqueous solution relative to the solutions of other Zn^{2+} salts is due to the formation of tetrahedral chloro-aqua complexes, where the reduction in coordination number from 6 to 4 reduces the strength of the O–H bonds in the coordinated water molecules. Zn^{2+} ions are tetrahedrally coordinated to four chloride ions. In dilute aqueous solution, octahedral $[\text{Zn}(\text{H}_2\text{O})_6]^{2+}$ is the predominant species.^{110, 111}

Single crystals of complex **1** were obtained from the reactive crystallization of 5-amino isophthalic acid and zinc chloride in deionized water at room temperature as shown in figure 3-2.

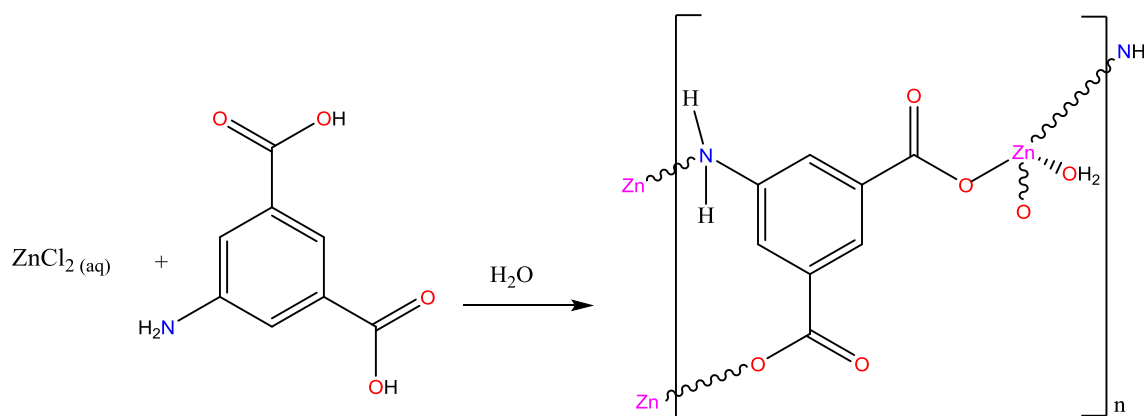


Figure 3-2: Schematic of the reaction that produced complex **1**.

3.2.1.2. Crystal Structure Determination of Complex 1

The measurement was carried out on an Agilent SuperNova Kappa geometry 4-circle diffractometer using the graphite monochromated Mo K α radiation, $\lambda = 0.71073 \text{ \AA}$ at 150 K. Complex **1** crystallizes in the monoclinic crystal system and P2₁/n space group.

Examination of the Cambridge Crystallographic Database Centre revealed that the structure had previously been studied to a high standard and published as **UFULEM**. However, complex **1** crystallizes at room temperature and was characterized at 150 K while **UFULEM** was synthesized hydrothermally and characterized at 293 K.¹¹²

A full list of crystal parameters and structure determination details, a view of the molecular structure of complex **1** and **UFULEM**, and tables of selected bond lengths and angles are presented below.

	1	UFULEM
Empirical formula	[Zn(C ₈ H ₅ NO ₄)(H ₂ O)] _n	Zn(C ₈ H ₅ NO ₄)(H ₂ O)] _n
Formula weight	247.52	262.52
Temperature (K)	150	293
Crystal system	Monoclinic	Monoclinic
Space group	P2 ₁ /n	P2 ₁ /n
<i>a</i> (Å)	8.999(2)	9.044(1)
<i>b</i> (Å)	8.2684(16)	8.264(1)
<i>c</i> (Å)	11.600(3)	11.646(1)
β (°)	101.59(2)	100.77(1)
Volume (Å ³)	845.5(4)	855.0(2)
Z	4	4
R factor (%)	9.88	4.22

Table 3-1: Crystal data collection of complex **1** and **UFULEM**.¹¹²

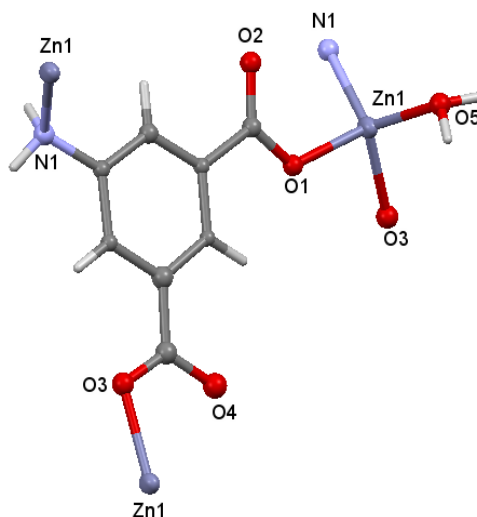


Figure 3-3: Molecular structure of complex 1 and UFULEM.¹¹²

The formula weight of complex **1** is smaller than that of **UFULEM** as shown in table 3-1. It is assumed that there may be a partial water molecule present in complex **1**.

The geometric environment of Zn^{2+} in the two Zn complexes is tetrahedral with one amine group, two *cis* carboxylate oxygen atoms and one coordinating water molecule, as shown in figure 3-3. When expanded, the network shows one Zn metal centre attached to three ligands via two of their carboxylate oxygen atoms and one via its amine group. The 2D sheet is generated by the rings forming nodes at the zinc atoms linking these nodes. However, it is not porous, because of void in one layer overly rings from the next layer. There is no linkage between the layers as shown in figure 3-4.

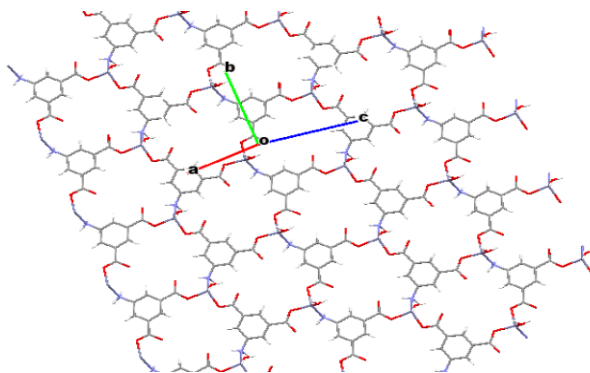


Figure 3-4: Expansion network of complex 1 and UFULEM.¹¹²

Zinc atoms in known complexes are often seen to be terminally bonded to a single O atom of the carboxylate group but never in chelating conformation. This is also the case of the coordination environment of Zn in **VOSSAX**.¹¹³

Complex **1** and **UFULEM** are identical but they were crystallized using different methods and characterized at a different temperature. This is responsible for the slightly higher values of the unit-cell obtained in **UFULEM** which is expected when the temperature is warm as shown in table 3-1. The selected bond distances and bond angles of the identical Zn complexes are listed in table 3-2.

1		UFULEM	
Distance	(Å)	Distance	(Å)
Zn1 – O1	1.955(9)	Zn1 – O2 ^{viii}	1.954(3)
Zn1 – O3 ¹	1.994(8)	Zn1 – O3	1.965(4)
Zn1 – O5	1.958(8)	Zn1 – O5 ^{ix}	1.973(3)
Zn1 – N1 ²	2.029(9)	Zn1 – N1	2.031(4)
Angle	(°)	Angle	(°)
O1 – Zn – O5	110.3(4)	O2 ^{viii} – Zn1 – O3	109.4(2)
O1 – Zn1 – O3 ¹	94.2(3)	O2 ^{viii} – Zn1 – O5 ^{ix}	94.9(1)
O5 – Zn1 – O3 ¹	109.7(3)	O3 – Zn1 – O5 ^{ix}	104(2)
O1 – Zn1 – N1 ²	104.7(4)	O2 ^{viii} – Zn1 – N1	105.1(2)
O5 – Zn1 – N1 ²	118.5(4)	O3 – Zn1 – N1	118.0(2)
O3 ¹ – Zn1 – N1 ²	116.3(4)	O5 ^{ix} – Zn1 – N1	116.1(2)
Symmetry code: ¹ -1/2+x, 1/2-y, 1/2+z; ² -1/2+x, 3/2-y, 1/2+z		Symmetry code: -1/2, -y+1/2, z+1/2; x, y-1, z	

*Table 3-2: Table of selected bond lengths and bond angles of complex **1** and **UFULEM**.¹¹²*

3.2.2. Reactive Crystallization and Crystal Structure of $(C_8H_6O_6).(Me_2NCHO)$

3.2.2.1. Introduction

Single crystals of complex **2** were obtained from the reactive crystallization of 2,5-dihydroxyterephthalic acid and zinc chloride in DMF, as shown in figure 3-5. It is suspected that the ligand failed to coordinate because no base was present to bring it into its coordinating conjugate base form. In the previous case, there was an amine on the ligand. Some portion of ligand, which was in excess, could have acted as a base. Nevertheless, crystals, suitable for single crystal analysis were obtained.

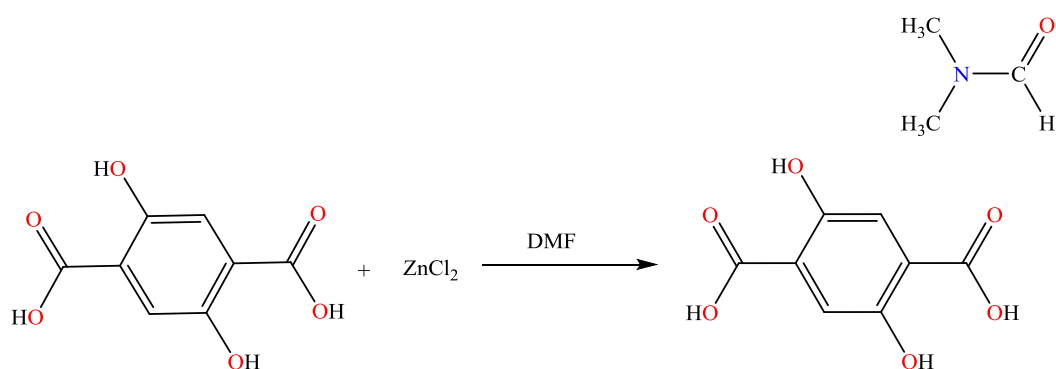


Figure 3-5: Schematic of the reaction that produced complex **2**.

3.2.2.2. Crystal Structure Determination of Complex **2**

The measurement was carried out on a Bruker Prospector diffractometer using $Cu\ K\alpha$ radiation, $\lambda = 1.54184\ \text{\AA}$ at 293 K. X-ray images were recorded on CCD detectors and stored for further processing. Complex **2** crystallizes in the monoclinic crystal system and $P2_1/a$ space group.

A full list of crystal parameters and structure determination details, a view of the molecular structure of complex **2**, and tables of selected bond lengths and angles are presented below.

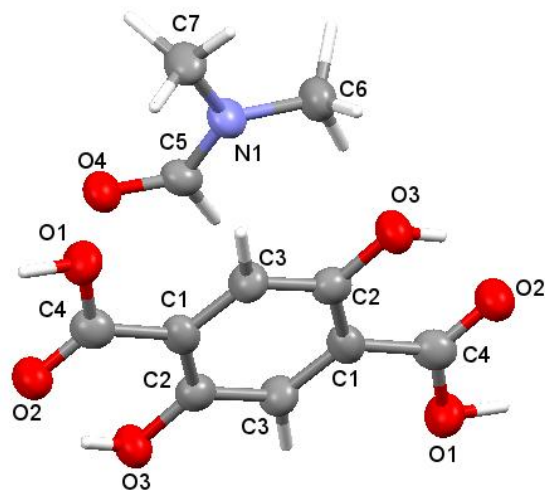


Figure 3-5: Molecular structure of complex 2.

Complex 2 consists of the carboxylate ligand, 2,5-dihydroxyterephthalic acid, and the solvent, dimethylformamide (DMF). The two formed a single crystal unit as shown in figure 3-5. The carboxylate based ligand, 2,5-dihydroxyterephthalic acid and the solvent, DMF are bonded to each other by an H-bond to form planar H-bonded adducts, then the adducts stack. The DMF has interrupted the H-bonded chain normally formed, resulting in discrete molecules in this case as shown in figure 3-6.

The H-bond between the adjacent aldehyde oxygen atom and carboxylate oxygen atom has a distance of $O2 \dots O3 = 2.642 \text{ \AA}$ while that of adjacent DMF oxygen atom and carboxylate oxygen atom has a distance of $O4 \dots O1 = 2.529 \text{ \AA}$, as shown in figure 3-6.

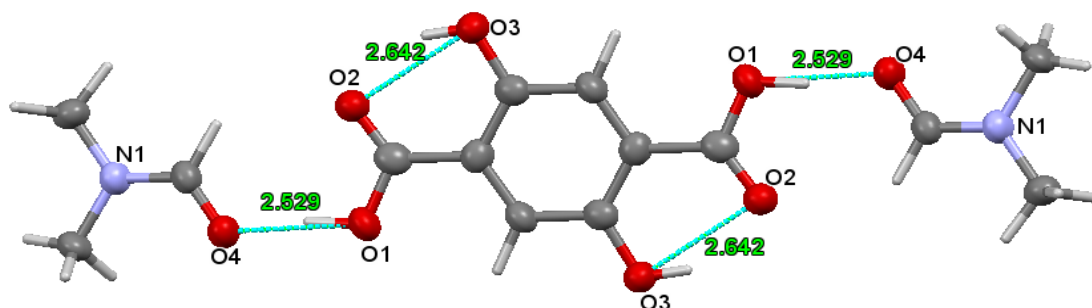


Figure 3-6: H-bonded $(C_8H_6O_6).(Me_2NCHO)$ adduct.

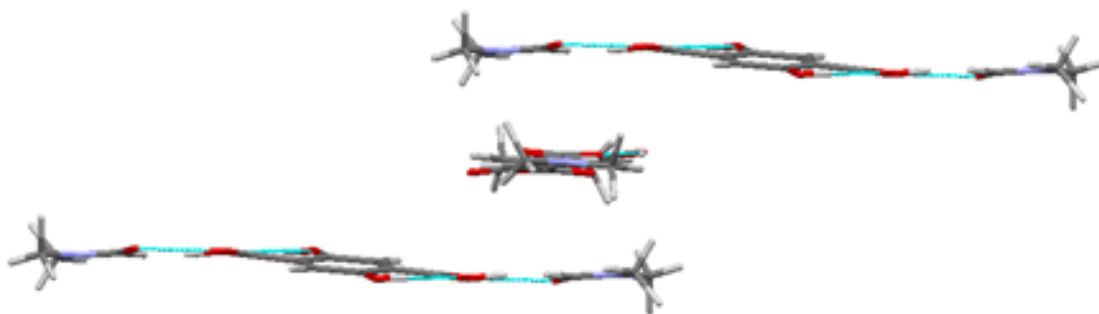


Figure 3-7: Side view showing stacking of the adducts in the crystal structure of complex 2.

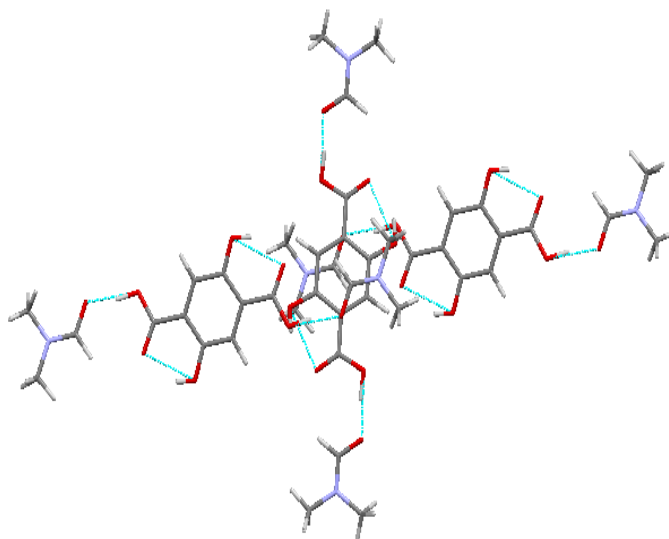
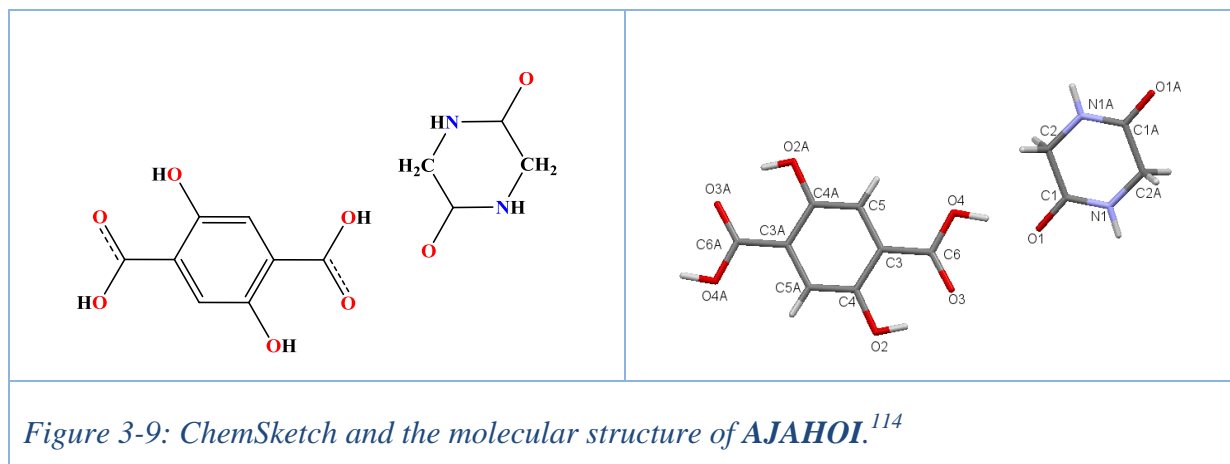
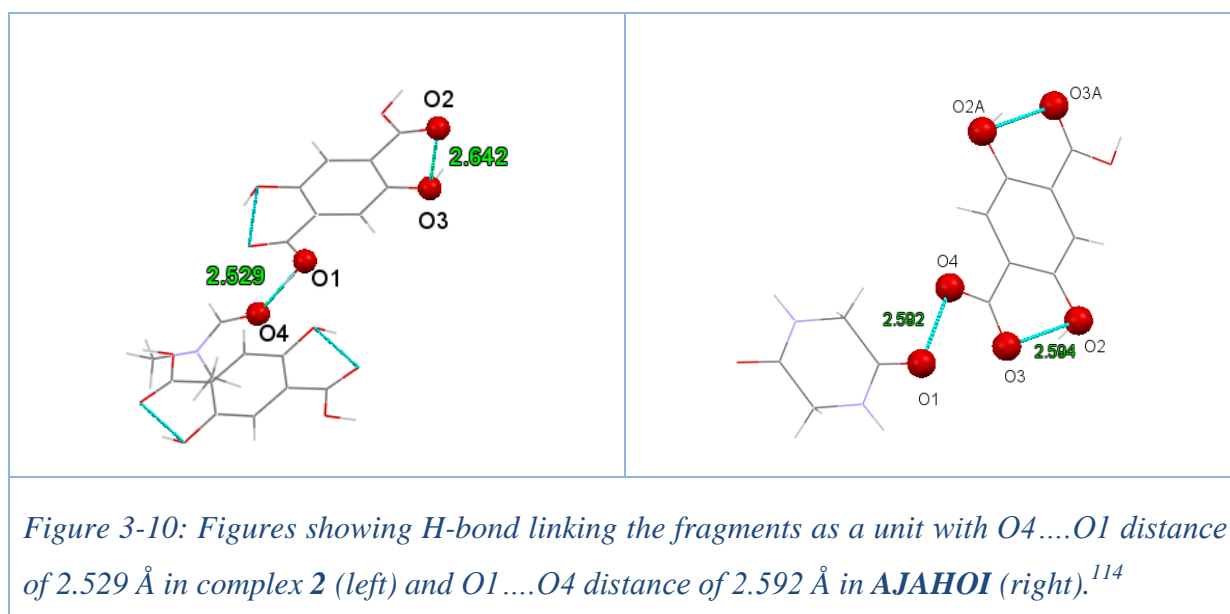


Figure 3-8: View of the stack perpendicular to the plane of the phenyl rings.

Complex **2** could not be matched to any known structure in the Cambridge Crystallographic Database but was compared with a structure deposited in the Cambridge Crystallographic Database as **AJAHOI**. In **AJAHOI**, the researcher examined the non-covalent interaction that occurs between the cyclic dipeptide of glycine and carboxylic acid guest (2,5-dihydroxyterephthalic acid) which is the free ligand in complex **2** (figure 3-9).¹¹⁴



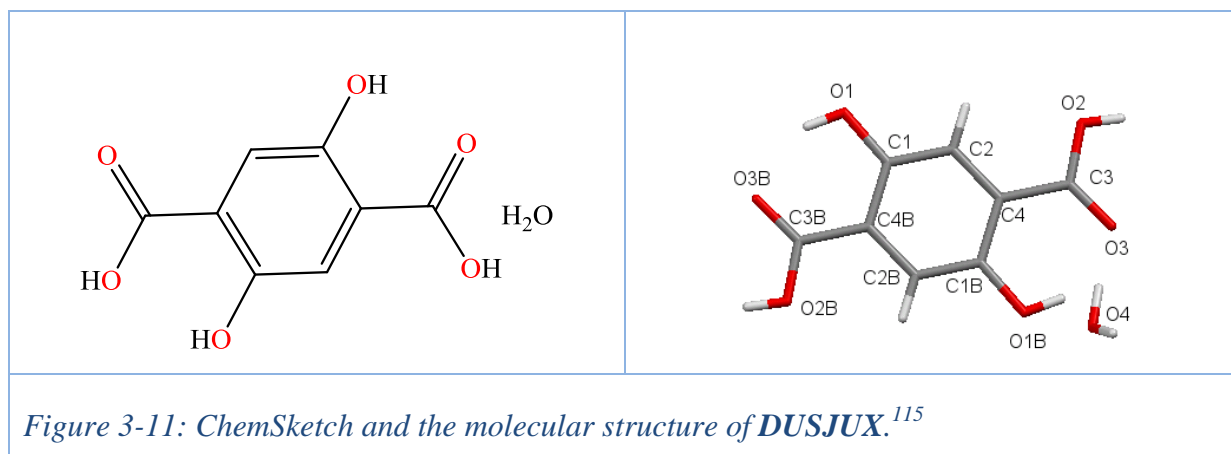
In complex **2**, like in AJAHOI, there is H-bond in the structure, linking the two fragments as a unit as shown in figure 3-10.



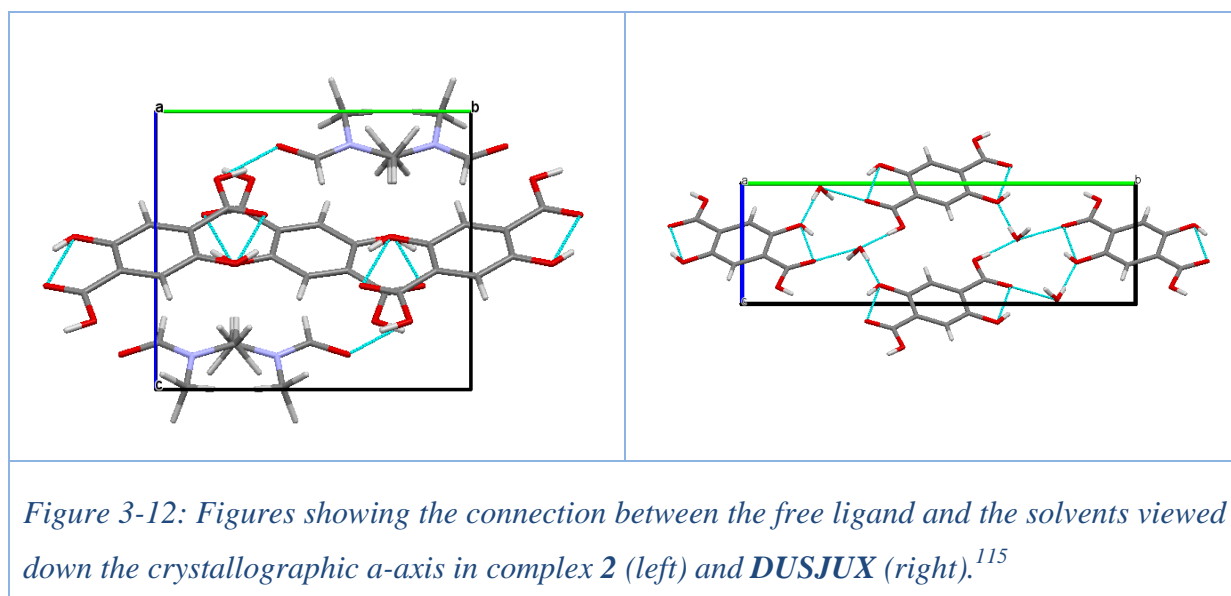
The distances between the carbon atoms in the free ligands of the two structures are in the same range of values which means the ligands were not affected by the crystallization reactions.

Complex **2** can also be compared with another structure deposited in the Cambridge Crystallographic Database as DUSJUX. This structure was obtained accidentally when the

researcher was trying to synthesize metal-organic coordination polymer by reacting LiOH with 2,5-dihydroxyterephthalic acid in H₂O under solvothermal conditions (heated at 363 K for 3 days). **DUSJUX** comprises of the free ligand in complex **2**, 2,5-dihydroxyterephthalic acid molecule located on a centre of inversion and one uncoordinated H₂O molecule that occupies a general position as shown in figure 3-11.¹¹⁵



In complex **2** and **DUSJUX**, the ligand, 2,5-dihydroxyterephthalic acid was connected to the solvent (DMF and H₂O respectively) via O-H...O bonding to form a layer in the *ab* plane as shown in figure 3-12.



Apart from the different starting materials used in synthesizing the two crystal structures, looking at the crystal data collection of both structures in table 3-3, their characterization temperature is different. Though the two structures crystallize in the monoclinic crystal system, their space groups translate in different planes. For complex **2**, P₂₁/a space group where **P** is Primitive unit cell 2-fold screw axis along *b*, a fold (translation along *a*-axis) in *ab* plane while for **DUSJUX**, P₂₁/c space group is where **P** is a Primitive lattice, 2-fold screw axis along *b*. *c* fold translation along *c* axis in *ac* plane.¹¹⁵

	2	DUSJUX
Empirical Formula	(C ₈ H ₆ O ₆). (Me ₂ NCHO)	C ₈ H ₆ O ₆ .2H ₂ O
Formula weight (g/mol.)	344.32	234.16
Temperature (K)	150	295
Crystal system	Monoclinic	Monoclinic
Space group	P ₂ ₁ /a	P ₂ ₁ /c
<i>a</i> (Å)	9.663(3)	5.1883(10)
<i>b</i> (Å)	9.8843(17)	17.545(4)
<i>c</i> (Å)	9.890(3)	5.4990(12)
β (°)	118.19(4)	103.03(1)
Volume (Å ³)	832.6(5)	487.68(17)
Z	2	2
D _x (Mg m ⁻³)	1.373	1.595 Mg m ⁻³
μ (mm ⁻¹)	0.973	0.15
F(000)	364	244
Crystal size (mm ³)	0.12 × 0.07 × 0.03	0.25 x 0.20 x 0.20
Crystal Shape	Plate, colourless	Tabular, light yellow
R factor (%)	7.44	0.061

Table 3-3: Crystal and refinement data collection of complex **2** and **DUSJUX**.¹¹⁵

The comparison of the bond distances and the bond angles of 2,5-dihydroxyterephthalic acid ligands in the two structures to observe what effect does the solvents, DMF in complex **2** and H₂O in **DUSJUX** had on the ligands are listed in table 3-4.

2		DUSJUX	
Distance	(Å)	Distance	(Å)
O1 – C4	1.339 (8)	O2 – C3	1.305 (3)
O2 – C4	1.232 (8)	O3 – C3	1.223 (4)
O3 – C2	1.369 (8)	O1 – C1	1.365 (4)
C3 – C1 ¹	1.389 (9)	C1 – C2	1.380 (4)
C1 – C2	1.417 (9)	C1 – C4 ⁱ	1.405 (4)
C1 – C3 ¹	1.389 (9)	C2 – C4	1.393 (4)
C1 – C4	1.484 (9)	C3 – C4	1.480 (4)
C2 – C3	1.404 (9)	C4 – C1 ⁱ	1.406 (4)
Angle	(°)	Angle	(°)
O3 – C2 – C3	117.6(6)	O2 – C3 – C4	114.3(3)
O2 – C4 – C1	123.7(6)	O3 – C3 – C4	122.3 (3)
O2 – C4 – O1	122.5(6)	O3 – C3 – O2	123.4 (3)
C2 – C1 – C4	118.7 (6)	C2 – C4 – C1 ⁱ	119.0 (3)
C3 ¹ – C1 – C2	120.4 (6)	C2 – C4 – C3	121.2 (3)
Symmetry code: ¹ 1-x,1-y,1-z		Symmetry code: (i) -x, -y+1, -z+2	

*Table 3-4: Selected bond lengths of the free ligands in complex **2** and **DUSJUX**.¹¹⁵*

The bond distances and bond angles of the free ligands in the two structures are not significantly different. Hence, the solvents and the force of interaction, H-bonding between the free ligand and the solvent in the crystal unit do not have any effect on the free ligands in the two structures.

3.2.3. Reactive Crystallization and Crystal Structure of $[\text{Co}(\text{C}_8\text{H}_4\text{O}_6)(\text{C}_3\text{H}_7\text{NO})_2(\text{H}_2\text{O})_2]_n$

3.2.3.1. Introduction

Cobalt(II)chloride is an inorganic compound of cobalt and chlorine with the formula CoCl_2 . Its hexahydrate, $\text{CoCl}_2 \cdot 6\text{H}_2\text{O}$, is one of the most commonly used cobalt compounds in the lab. It is odorless and has a deep purple colour (rose red crystals). Its molecular weight is 237.93 g/mol. In its solid state, $\text{CoCl}_2 \cdot 6\text{H}_2\text{O}$ consists of *trans*- $[\text{CoCl}_2(\text{H}_2\text{O})_4]$ and two molecules of water of crystallization. This dissolves readily in water and alcohol. $\text{CoCl}_2 \cdot 6\text{H}_2\text{O}$ is deliquescent and the anhydrous salt CoCl_2 is hygroscopic, readily converting to the hydrate. $\text{CoCl}_2 \cdot 6\text{H}_2\text{O}$ is a moderate Lewis acid. It reacts to give adducts with typically octahedral coordination geometry.^{109, 111}

Single crystals of complex **3** were obtained from the reactive crystallization of 2,5-dihydroxyterephthalic acid and cobalt(II)chloride hexahydrate in dimethylformamide at room temperature as shown in figure 3-13.

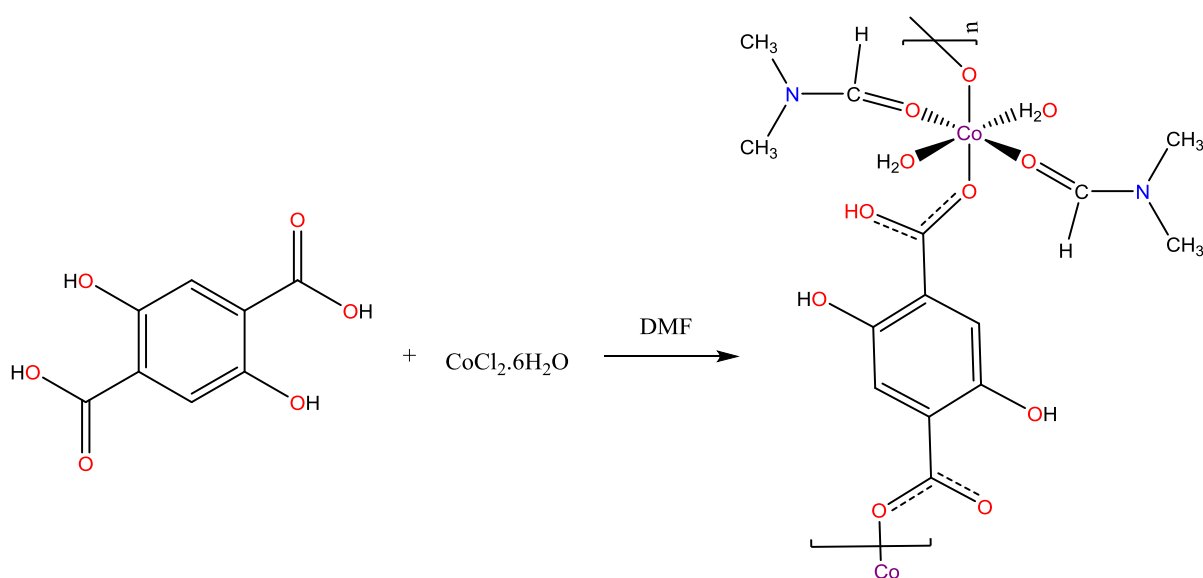
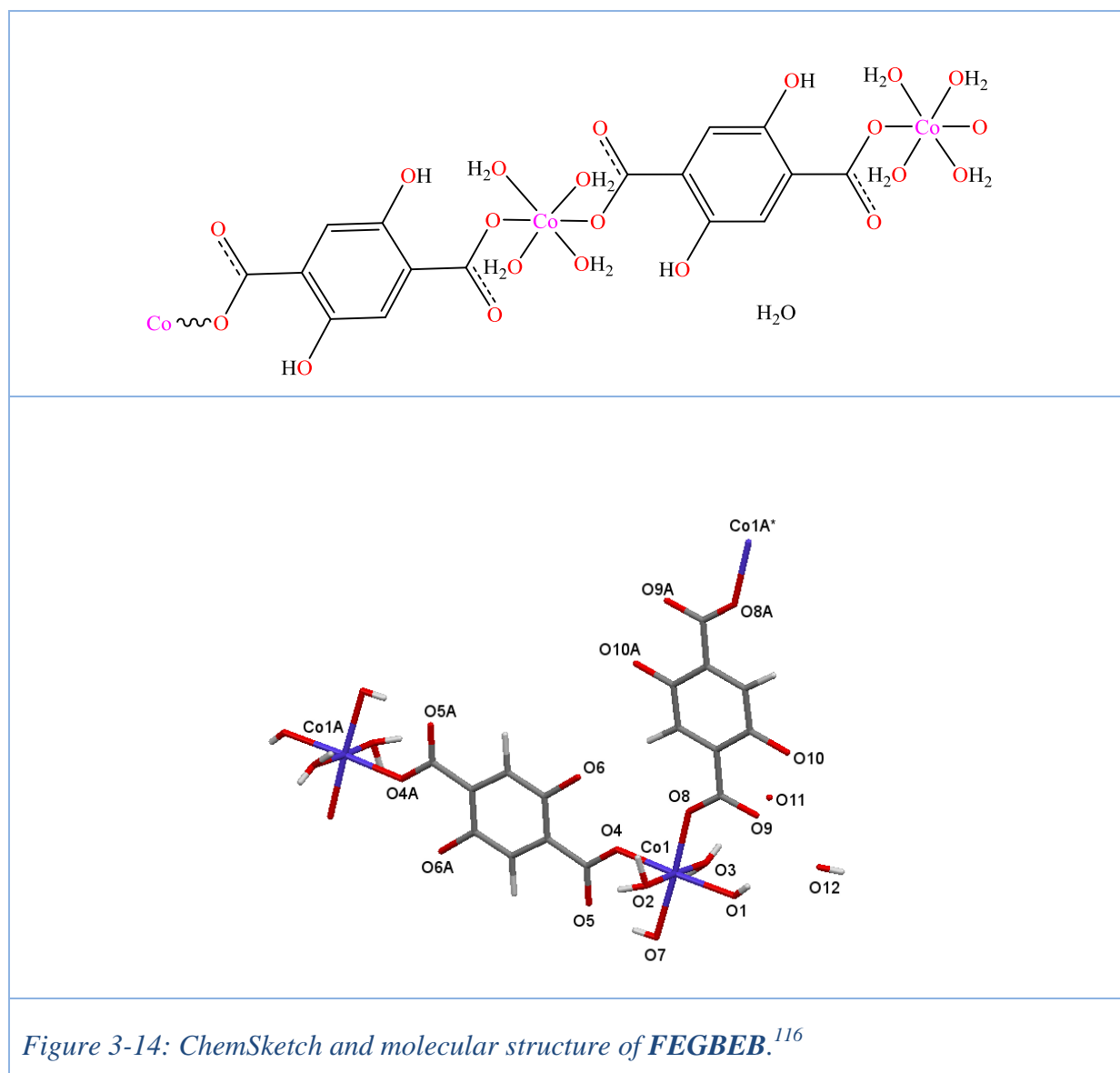


Figure 3-13: Schematic of the reaction that produced complex **3**.

A search of the Cambridge Crystallographic Database revealed that a six-coordinate cobalt complex prepared from the same ligand as complex **3** has been studied as *catena*[bis(μ -2,5-dihydroxybenzene-1,4-dicarboxylato)octaaqua-dicobalt(II)tetrahydrate] and deposited in the Cambridge Crystallographic Database as **FEGBEB** (figure 3-14).¹¹⁶



Unfortunately, the literature publication attached to this structure; Zhangliugen, *CSD Communication*, 2017 to study the preparation method was not found.

3.2.3.2. Crystal Structure Determination of Complex 3

The measurement was carried out on a Bruker Prospector diffractometer using Cu K α radiation, $\lambda = 1.54184 \text{ \AA}$ at 293 K. X-ray images were recorded on CCD detectors and stored for further processing. Complex **3** crystallizes in the monoclinic crystal system and P2₁/c space group.

A full list of crystal parameters and structure determination details, a view of the molecular structure of complex **3**, and tables of selected bond lengths and angles are presented below.

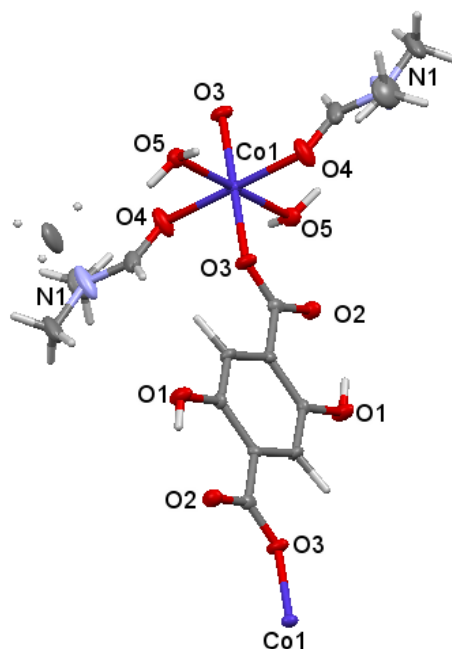


Figure 3-15: Molecular structure of complex 3.

Complex **3** is a 1D coordination polymer. The geometric environment of cobalt is octahedral with two *trans* carboxylate oxygen atoms, two *trans* oxygen atoms of DMF and two *trans* coordinating water atoms with cobalt sitting on the crystallographic inversion point, as shown in figure 3-15.

The carboxylate group acted as a monodentate ligand, binding to the metal centre at only one of its carboxylate oxygen atoms in *trans* position to form a 1D polymeric chain. All the coordinating water molecules are mutually in *trans* orientations.

When expanded, complex **3** shows a coordination polymer chain in which octahedral Co^{2+} coordinates to two molecules of 2,5-dihydroxyterephthalic acid and two DMF in *trans* orientation as shown in figure 3-16.

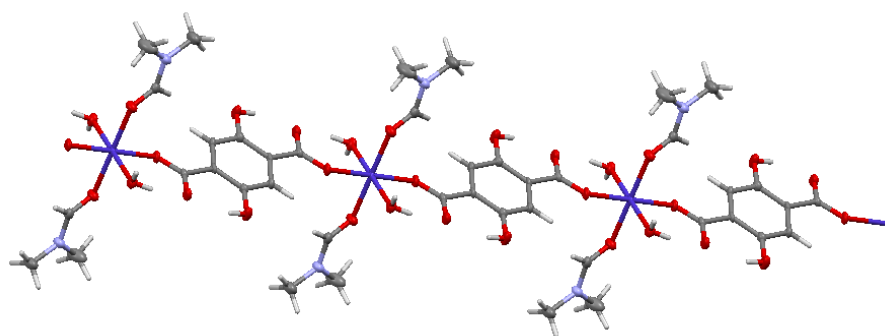


Figure 3-16: Polymeric chain of complex 3.

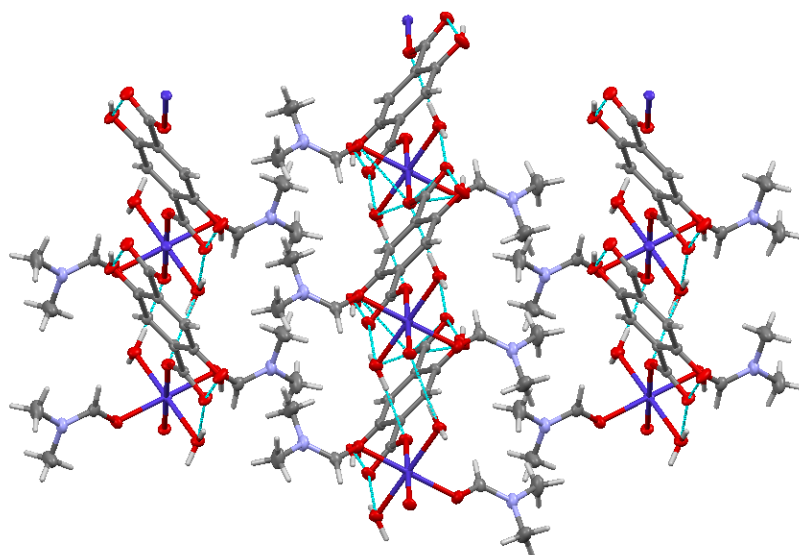


Figure 3-17: The layers in complex 3 generated through the interlinking of the 1D chains by H-bonding represented in turquoise dotted lines.

The chains are linked by H-bonds from coordinated water of one chain to a carboxylate oxygen atom of another chain.

Looking at the framework in figure 3-17 critically, it was assumed that if the crystallization reaction mixture was left for a longer period of time, the polymer chains may link as they link in the crystal structure shown in figure 3-18. Desolvation of the DMF bonding layer would promote bridging of ligands to further connect the layers. The ligands will bridge along and across to join the cobalt chain.

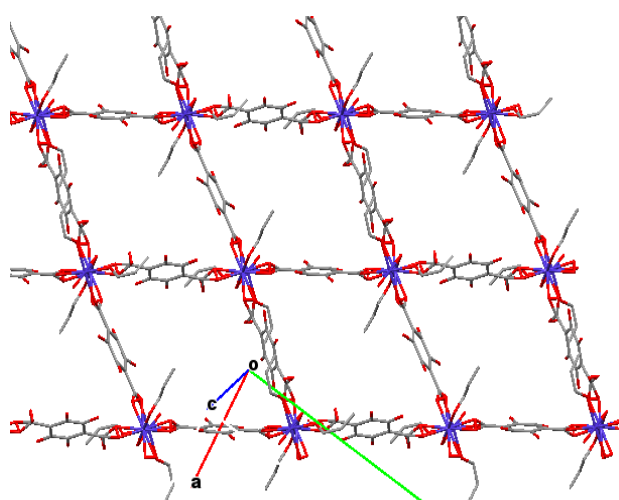


Figure 3-18: 3D framework obtained by William Reece.

The crystal structure in figure 3-18 was obtained from MOF-2 varying linker experiment by William Reece, a year 4 MCHM student. This was prepared by reacting CoCl_2 and 2,5-dihydroxyterephthalic acid in the molar ratio 1:2. Reece described the structure as a 2D layered structure which is possibly an intermediate in MOF formation. He also stated that there is some disorder present in the structure regarding the position of the coordinated DMF.

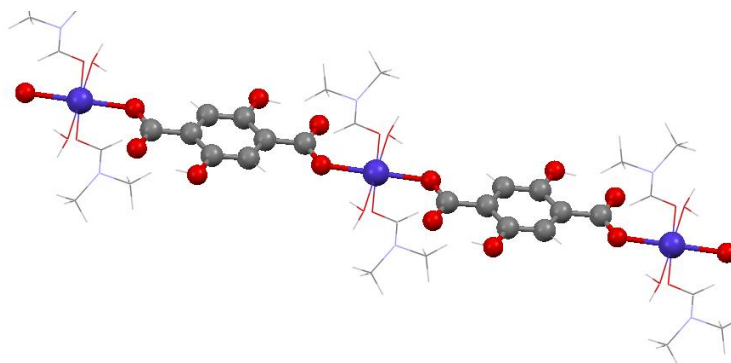


Figure 3-19: The polymer chain in the structure of complex 3.

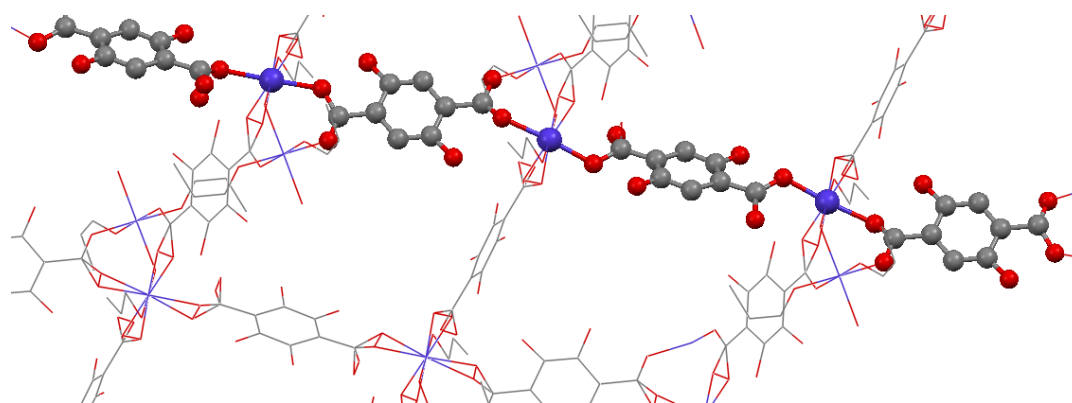


Figure 3-20: The polymer chain highlighted in the 2D structure of crystal obtained by William Reece.

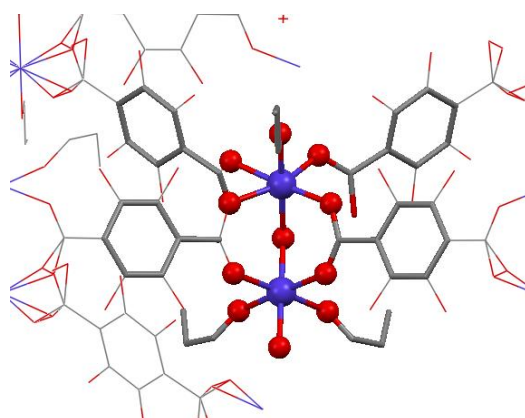
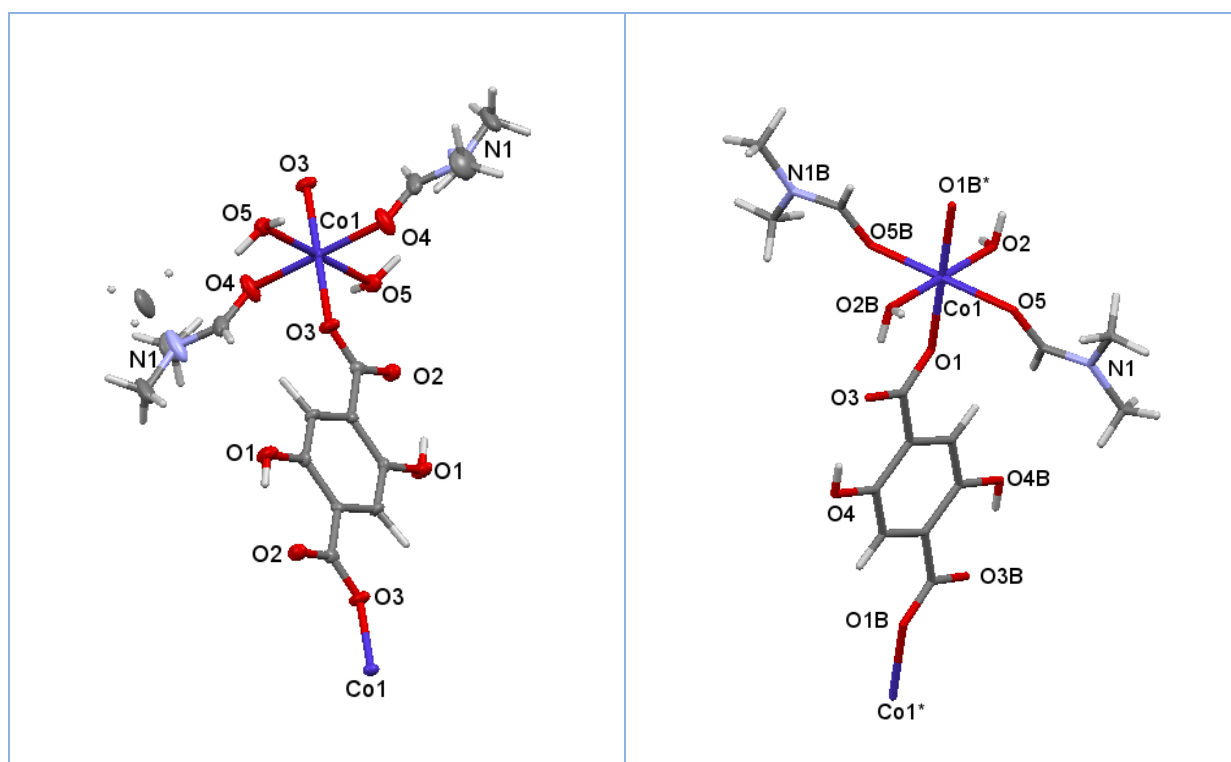


Figure 3-21: The links between polymer chains in the 2D structure obtained by William Reece.

Complex **3** was a novel compound at the time of its preparation but a recent paper has appeared which contain another determination of the structure. The determined structure was prepared from the slow diffusion of 2,5-dihydroxyterephthalic acid in DMF and an aqueous solution of cobalt acetate. Single crystals of $[\text{Co}(\text{DHT})(\text{DMF})_2(\text{H}_2\text{O})_2]$ were obtained after two weeks, characterized and deposited into the Cambridge Crystallographic database as **SEWXIE**.⁴⁴

Figure 3-22 shows that the molecular structure of complex **3** and **SEWXIE** are mirror images.



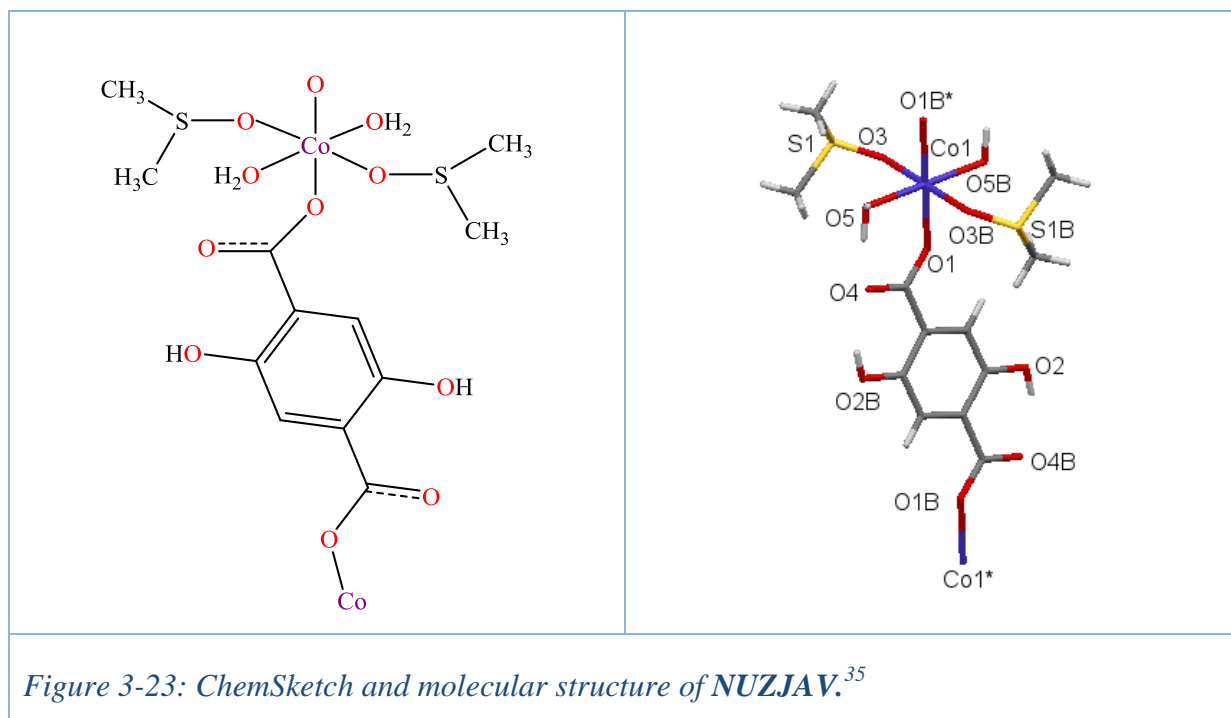
*Figure 3-22: Molecular structure of complex **3** (left) and **SEWXIE** (right) showing that the two cobalt complexes are mirror images.*⁴⁴

In the two complexes, Co^{2+} is sitting on the crystallography inversion. Like in complex **3**, the geometric environment of Co^{2+} in **SEWXIE** comprises of two carboxylate groups coordinated to Co^{2+} in the equatorial position and two coordinated water molecules in axial position. The octahedron geometric environment was completed with two DMF molecules in

the equatorial position.⁴⁴ In fact, while there were slight differences in the cell constants particularly in the values of *c* and in the angles, the two structures are identical. The differences are most likely the result of different data collection temperatures as shown in table 3-5.

Complex **3** can be compared to a known complex studied as catena-[trans-(μ-2,5-dihydroxyterephthalato)-bis(dimethylsulfoxide)-diaqua-cobalt(ii)] which had been studied to a high standard and deposited in the Cambridge Crystallographic database as **NUZJAV**.

NUZJAV was prepared from the liquid-liquid diffusion of 2,5-dihydroxyterephthalic acid and cobalt(II)nitrate hexahydrate in dimethyl sulfoxide over a period of six months. **NUZJAV** is similar to complex **3** save for the presence of dimethylsulfoxide (DMSO) in the place of dimethylformamide (DMF) in complex **3** as shown in figure 3-23.³⁵



Like in complex **3**, **NUZJAV** is a 1D coordination polymer (linear chain) with the general formula [trans-Co(DMSO)₂(H₂O)₂(L)]_n. Co²⁺ is located at the inversion centre. Its geometric environment like that of complex **3** is octahedral which comprises two coordinated water molecules, two dimethyl sulfoxide molecules and two ligands around the metal centre, as

shown in figure 3-23. Like in complex **3**, the ligand is coordinated to Co^{2+} in *trans* orientation.^{35, 44}

Complex **3** and **SEWXIE** are isostructural. They are a one-dimensional polymeric chain that crystallizes in the monoclinic crystal system and $P2_1/c$ space group. All the crystal data collection values are close for the two structures while **NUZJAV** also crystallizes in the monoclinic crystal system like the two Co^{2+} structures but at $P2_1/n$ space group. Also, data collection values for **NUZJAV** are slightly different, as listed in table 3-5.^{35, 44}

	3	SEWXIE	NUZJAV
Empirical Formula	$[\text{Co}(\text{C}_8\text{H}_4\text{O}_6)(\text{C}_3\text{H}_7\text{NO})_2(\text{H}_2\text{O})_2]_n$	$\text{C}_{14}\text{H}_{22}\text{CoN}_2\text{O}_{10}$	$\text{C}_{12}\text{H}_{20}\text{O}_{10}\text{S}_2\text{Co}$
Formula weight	437.26	437.27	447.33
Temperature (K)	293	293	150
Crystal system	Monoclinic	Monoclinic	Monoclinic
Space group	$P2_1/c$	$P2_1/c$	$P2_1/n$
a (Å)	10.0743(6)	10.0268(6)	10.071(5)
b (Å)	5.3585(3)	5.4025(3)	5.329(5)
c (Å)	17.2861(9)	17.5083(10)	16.094(5)
β (°)	95.352(5)	96.665(5)	99.047(5)
Volume (Å ³)	929.09(9)	942.01(9)	853.09(9)
d_{cal} (g cm ⁻³)	1.563	1.542	1.742
Z	2	2	2
μ (mm ⁻¹)	7.76	0.966 cm ⁻¹	1.301

Table 3-5: Crystal data collection of complex **3**, **SEWXIE** and **NUZJAV**.^{35,44}

In the three Co^{2+} complexes, the carboxylate groups are coordinated to Co^{2+} in *syn* monodentate conformation with $\text{Co1} - \text{O}_{\text{carb}}$ distances and bond angles similar in all the complexes, as listed in table 3-6.

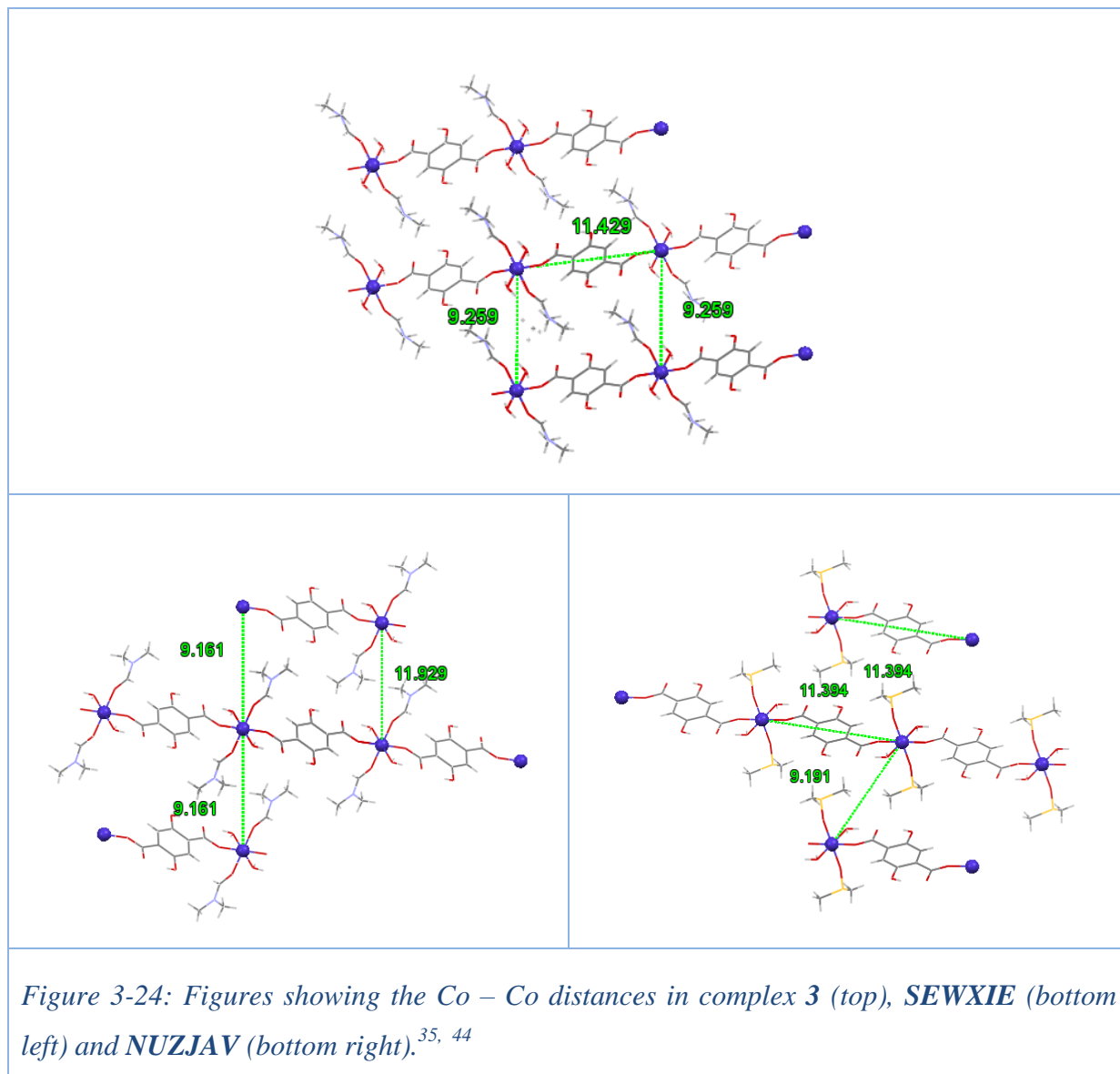
3		SEWXIE		NUZJAV	
Distance	(Å)	Distance	(Å)	Distance	(Å)
Co1 – O3	2.0739(18)	Co1 – O2 ⁱ	2.0660(17)	Co1 – O1	2.089(2)
Co1 – O4	2.071(2)	Co1 – O4 ⁱ	2.0734(19)	Co1 – O5	2.076(2)
Co1 – O5	2.128(2)	Co1 – O1	2.1270(18)	Co1 – O3	2.132(3)
O1 – C1	1.366(4)	O4 – C3	1.363(3)	O3 – C4	1.365(4)
O2 – C4	1.260(4)	O3 – C2	1.257(3)	O2 – C1	1.259(4)
O3 – C4	1.276(3)	O1 – C2	1.266(4)	O1 – C1	1.268(4)
O4 – C5	1.247(4)	O5 – C5	1.229(3)		
Angle	(°)	Angle	(°)	Angle	(°)
O3 – Co – O3 ¹	180.0	O2 ⁱ – Co1 – O2	180.0	O5 – Co1 – O5B	180.0
O3 ¹ – Co1 – O5 ¹	93.00(8)	O2 – Co1 – O4	92.08(8)	O1B – Co1 – O5B	91.91(10)
O4 ¹ – Co1 – O3	91.95(8)	O4 – Co1 – O1 ⁱ	88.93(8)	O1B – Co1 – O5	88.02(10)
O4 – Co1 – O5	89.10(9)	O2 – Co1 – O1 ⁱ	91.07(8)	O1 – Co1 – O3B	91.98(10)
O4 ¹ – Co1 – O3 ¹	88.05(8)	O2 ⁱ – Co1 – O1	93.21(7)	O3 – Co1 – O5B	93.83(10)
O5 ¹ – Co1 – O5	180.0	O1 – Co1 – O1 ⁱ	180.0	O3 – Co1 – O3B	180.0
Symmetry code: ¹ 1-x,-y,1-z; ² 2-x,1-y,1-z		Symmetry code: i = -x, -y, -z			

Table 3-6: Selected bond distances and bond angles in complex **3**, **SEWXIE** and **NUZJAV**.^{35, 44}

The carboxylate oxygen atoms coordinated to Co²⁺ are not significantly longer than the ones that do not take part in the geometric environment of Co²⁺. The C – O distances between the carbon atom on the phenyl ring and the hydroxyl groups is 1.364(4) Å in complex **3**, 1.363(3) Å in **SEWXIE** and 1.365(4) Å in **NUZJAV** while the C – O distances between the carbon atom and the oxygen atom in DMF is 1.247(4) Å in complex **3** and 1.229(3) Å in **SEWXIE**.^{35, 44}

The Co – Co distances in all the three Co²⁺ complexes are similar with distances 9.259 Å across and 11.429 Å along in complex **3**, distances 9.161 Å across and 11.929 Å along in **SEWXIE** and distances 9.191 Å across and 11.394 Å along **NUZJAV** as shown in figure 3-

24. These values may not favour magnetism. Hence, the magnetic study of complex **3** is recommended in further work.^{35, 44}



There are two similar H-bond types in the structure of the three Co^{2+} complexes. The first H-bond type is between the carboxylate oxygen atom and the hydroxyl group with the distance of $\text{O1} \dots \text{O2} = 2.574(4) \text{ \AA}$ in complex **3**, $\text{O3} \dots \text{O4} = 2.566(3) \text{ \AA}$ in **SEWXIE** and $\text{O2} \dots \text{O4B} = 2.553(3) \text{ \AA}$ in **NUSJAV**. The second H-bond type is between the carboxylate oxygen atom and the oxygen atom of the coordinating water molecule with the distance of $\text{O2} \dots \text{O5} =$

2.631(3) Å in complex **3**, O3...O2B = 2.663(3) Å in **SEWXIE** and 2.651(3) Å in **NUSJAV**, as shown in the figure 3-25.^{35, 44} This is the interaction that links the chains into layers.

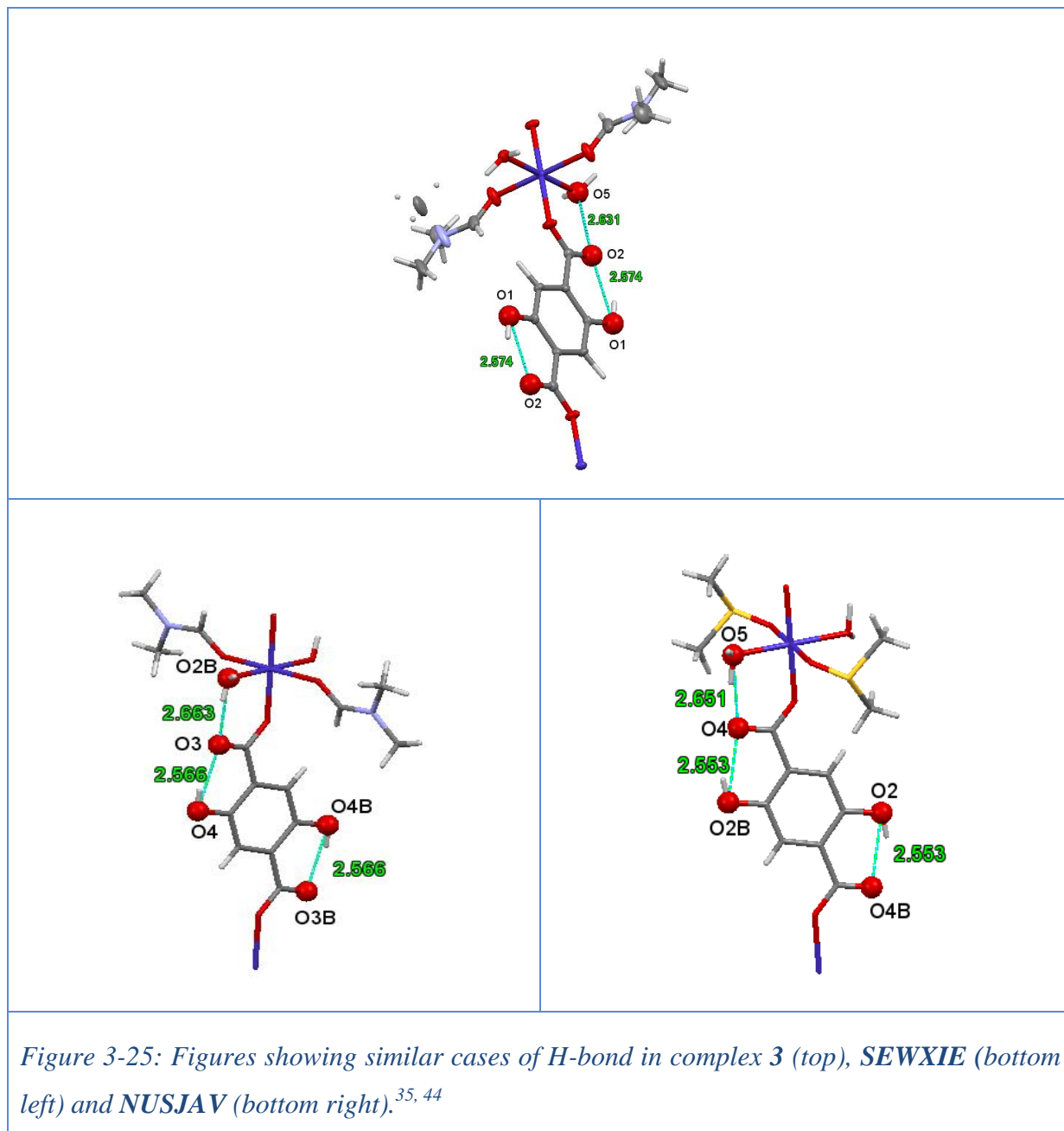
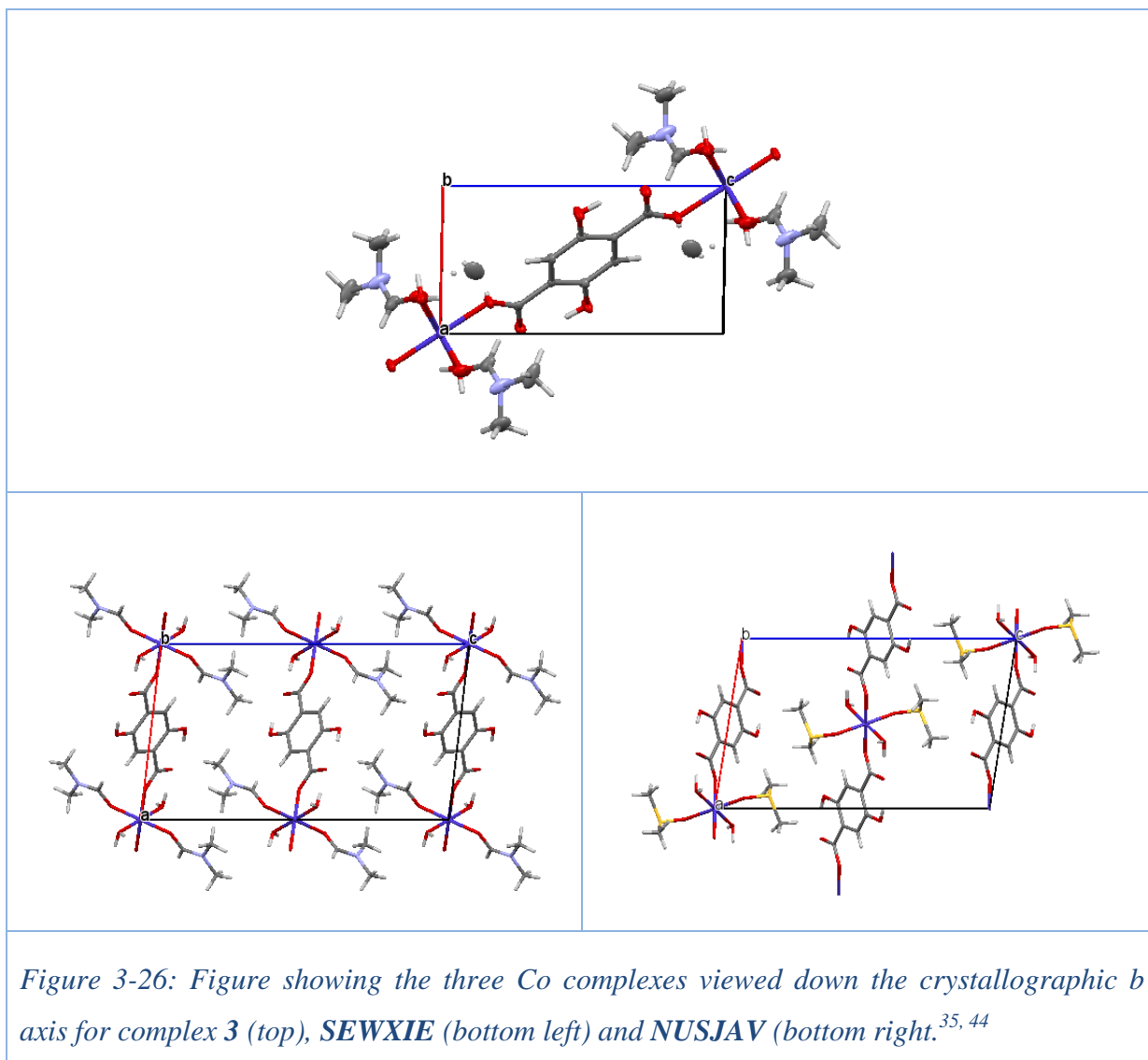


Figure 3-26 shows the packing diagram of the three Co²⁺ complexes viewed down the crystallographic *b* axis.



3.2.4. Reactive Crystallization and Crystal Structure of



3.2.4.1. Introduction

Single crystals of complex **4** were obtained from the reactive crystallization of 5-aminoisophthalic acid and vanadium(III)chloride in 50:50 MeOH/H₂O. This structure contained the alkali metal of the s block, Na¹⁺ instead of the intended d block transition metal V²⁺ cation as shown in figure 3.27.

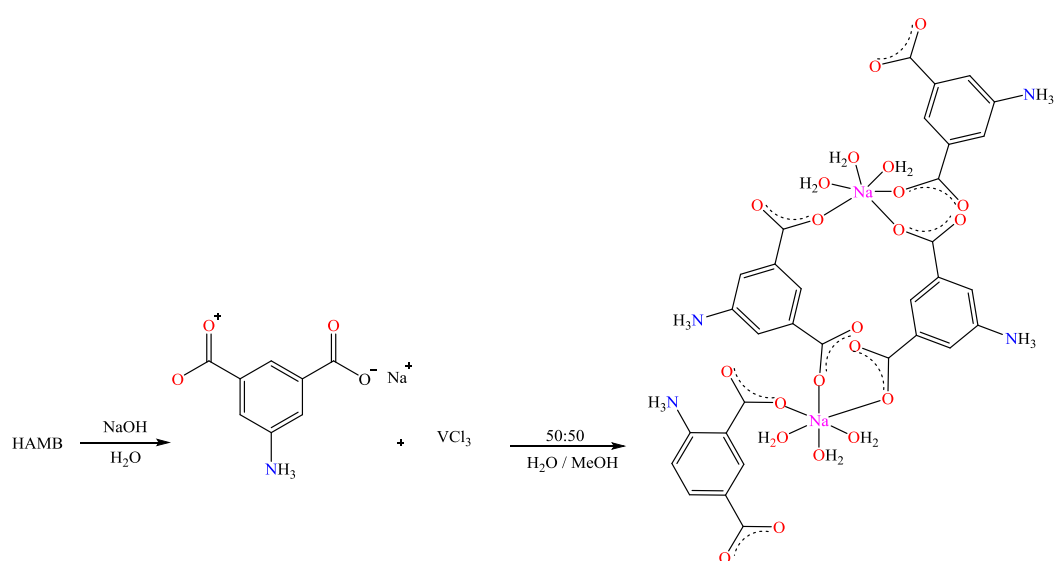


Figure 3-27: Schematic of the reaction that produced complex **4**.

3.2.4.2. Crystal Structure Determination of Complex **4**

The measurement was carried out on Oxford diffraction Xcalibur2 equipped with a Sapphire2 detector using Mo K α radiation, $\lambda = 0.71073 \text{ \AA}$ at 150 K. Complex **4** crystallizes in the triclinic crystal system and P-1 space group.

A search of the Cambridge Crystallographic Database Centre revealed that complex **4** had previously been studied at room temperature as bis(μ -3-amino-5-carboxybenzoato-k²O:O')bis[(5-aminoisophthalato)-triaquasodium(I)] and deposited in the Cambridge Crystallographic Database as **WIGWEP**.

The starting materials for the two Na complexes are different. **WIGWEP** was obtained from slow evaporation of the reaction of 5-aminoisophthalic acid and sodium hydroxide in a hot aqueous solution of pH 7.0 to 8.0 over 7 days. While complex **4** crystallizes from the reaction of 5-aminoisophthalic acid and NaOH with vanadium(III)chloride in deionized water at room temperature. **WIGWEP** was characterized at room temperature, 293 K while complex **4** was characterized at a lower temperature of 150 K.¹¹⁷

A full list of crystal parameters and structure determination details, a view of the molecular structure of complex **4** and **WIGWEP**, and a table of selected bond lengths and angles are presented below.

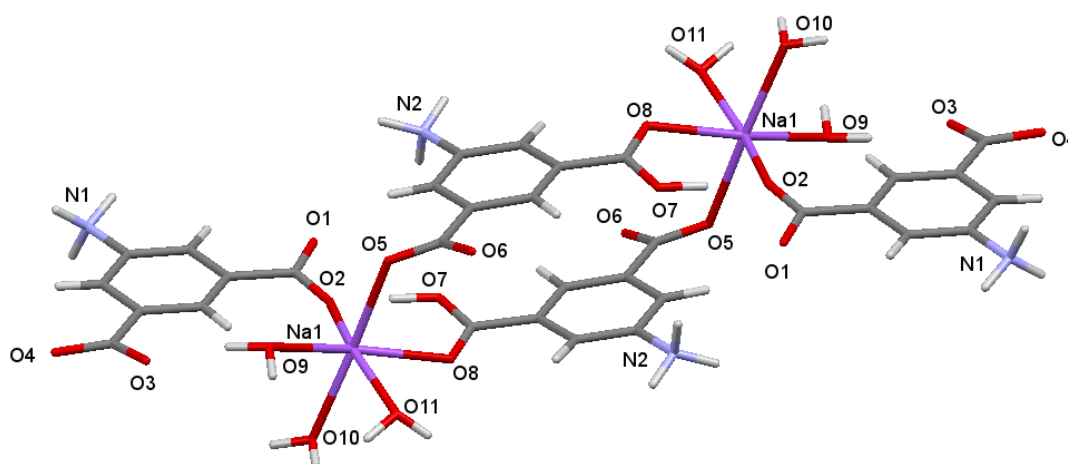


Figure 3-28: Molecular structure of complex **4** and **WIGWEP**.¹¹⁷

The two Na complexes are dinuclear centrosymmetric structures with two Na in distorted octahedron geometries. Each Na¹⁺ is coordinated to three carboxylate oxygen atoms O2, O5, and O8 from three different 5-aminoisophthalato ligands in *cis* position to one another and three H₂O molecules O9, O10, and O11 also in a *cis* position to one another as shown in figure 3-28.¹¹⁷

The two Na¹⁺ structures crystallize in the same crystal system and space group. The unit cells values listed in the crystal data collection in table 3-7 are similar.

	4	WIGWEP
Empirical Formula	Na ₂ (C ₈ H ₆ NO ₄) ₂ (C ₈ H ₇ NO ₄) ₂ (H ₂ O) ₆	[Na ₂ (C ₈ H ₆ NO ₄) ₂ (C ₈ H ₇ NO ₄) ₂ ·(H ₂ O) ₆]
Formula weight	876.64	876.64
Temperature (K)	150	293(2)
Crystal system	Triclinic	Triclinic
Space group	P-1	P-1
<i>a</i> (Å)	8.1801(5)	8.1889(3)
<i>b</i> (Å)	8.8600(6)	8.8821(3)
<i>c</i> (Å)	12.6052(9)	12.6381(5)
α (°)	95.675(6)	92.251(2)
β (°)	99.008(5)	98.649(2)
γ (°)	95.310(5)	95.200(2)
Volume (Å ³)	892.45(10)	899.86(6)
D _x (Mg m ⁻³)	1.631	1.618
Z	1	1
μ (mm ⁻¹)	0.159	0.16
F(000)	456.0	456
Crystal size (mm)	0.2 × 0.07 × 0.03	0.19 × 0.16 × 0.15
Crystal Shape	Needle, colourless	Block, colourless
R factor (%)	4.76	0.029

Table 3-7: Crystal and refinement data collection of complex **4** and **WIGWEP**.¹¹⁷

In the two Na¹⁺ complexes, all the ligands are monodentate, binding to Na¹⁺ with one of the carboxylate oxygen atoms in terminal conformation as either *syn* or *anti* with the distance of Na – O_{carb} shorter than the distances of Na – O_{water}. The bond distances and bond angles are within the same value range for both the crystal obtained at room temperature and at 150 K. However, bond distances tend to be shorter in complex **4** compared to that of **WIGWEP** as listed in table 3-8. This may be as a result of the warmer temperature.¹¹⁷

4		WIGWEP	
Length	(Å)	Length	(Å)
Na1 – O2	2.3489(18)	Na1 – O5	2.3520(14)
Na1 – O2	2.422(2)	Na1 – O2W	2.3535(16)
Na1 – O8 ⁱ	2.4035(19)	Na1 – O1	2.3922(14)
Na1 – O9	2.355 (2)	Na1 – O1W	2.4011(16)
Na1 – O10	2.395(2)	Na1 – O3W	2.4115(15)
Na1 – O11	2.409(2)	Na1 – O3 ⁱ	2.4347(15)
Angle	(°)	Angle	(°)
O2 – Na1 – O5	97.97(7)	O5 – Na1 – O1	82.66(5)
O2 – Na1 – O9	110.44(8)	O5 – Na1 – O2W	110.25(5)
O2 – Na1 – O10	86.92(7)	O5 – Na1 – O1W	87.51(5)
O2 – Na1 – O11	163.63(8)	O2W – Na1 – O1	166.86(6)
O8 ⁱ – Na1 – O5	89.92(7)	O2W – Na1 – O1W	87.97(6)
O8 ⁱ – Na1 – O11	83.28(7)	O1 – Na1 – O1W	95.25(6)
O9 – Na1 – O10	85.92(7)	O2W Na1 – O3W	84.43(5)
O9 – Na1 – O10	88.33(7)	O1 – Na1 – O3W	83.12(5)
O9 – Na1 – O11	84.22(8)	O1W – Na1 – O3W	85.74 (5)
O10 – Na1 – O8 ⁱ	95.01(7)	O5 – Na1 – O3 ⁱ	97.80(5)
O10 – Na1 – O11	86.25(8)	O2W – Na1 – O3 ⁱ	85.57(5)
O11 – Na1 – O5	90.10(7)	O1 – Na1 – O3 ⁱ	90.33(5)
O9 – Na1 – O8 ⁱ	166.81(8)	O5 – Na1 – O3W	163.62(6)
O10 – Na1 – O5	173.48(7)	O1W – Na1 – O3 ⁱ	172.76(6)
<i>Symmetry code: ^l-x,-y,-z</i>		<i>Symmetry code: (i) -x, -y, -z+2</i>	

Table 3-8: Selected bond distances and angles of complex 4 at 150 K and WIGWEP at 293 K.¹¹⁷

The distances between Na – O_{carb} and Na – O_{water} in complex **4** and **WIGWEP** can be compared with those in one of the structures studied as ‘sodium complexes of 3-phenyl-2-(3-phenyl-ureido)-propionic acid’ and deposited in the Cambridge Crystallographic Database as **POQTUL**. The starting materials used in preparing **POQTUL** are different from those used in preparing complex **4** and **WIGWEP**. **POQTUL** was prepared from the reaction of (phenylcarbamoyl) phenylalanine in MeOH / H₂O and NaOH while complex **4** was crystallized from the reaction of 5-aminoisophthalic acid and NaOH with vanadium(III)chloride in deionized water though, the proposed structure in the current study is a vanadium complex.¹¹⁸

Like in complex **4** and **WIGWEP**, **POQTUL** is a dinuclear complex that has the two Na¹⁺ sitting on the inversion centre. The geometric environment of each Na¹⁺ is distorted octahedron geometries that comprise of two bridging water molecules connecting the two Na¹⁺ centres, two coordinating water molecules in *trans* orientation and two carboxylate oxygen atoms of phenylcarbamoyl phenylalanine ligands as shown in figure 3-29.¹¹⁸

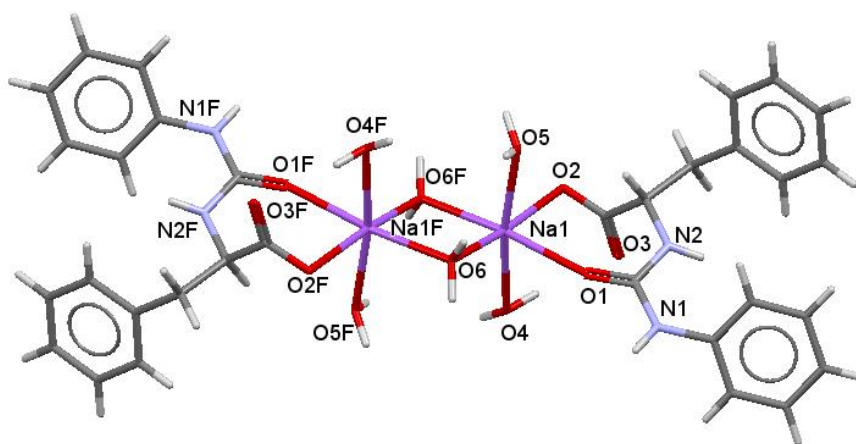


Figure 3-29: Molecular structure of **POQTUL**.¹¹⁸

The distances and angles of the atoms coordinating around the Na¹⁺ centre in **POQTUL** are listed in table 3-9.

Distance	(Å)	Angle	(°)
Na1 – O6	2.460	O4F – Na1F – O6F	107.07
Na1 – O6F	2.368	O6F – Na1F – O6	88.12
Na1 – O4	2.515	O6 – Na1F – O5F	93.17
Na1 – O5	2.447	O5F – Na1F – O2F	92.62
Na1 – O1	2.276	O2F – Na1F – O1F	83.74
Na1 – O2	2.782	O1 – Na1F – O4F	76.74

Table 3-9: Selected bond distance and bond angles in POQTUL.¹¹⁸

These values are in the same range as those in complex **4** except for distance Na1 – O2 which is longer than those in complex **4**.

The bond angles are similar. The *trans* angles are 168.06 °, 169.39 ° and 174.96 °.¹¹⁸ Just like in complex **4**, none of the *trans* angles is 180 ° as expected of perfect octahedral coordination.

The coordination modes of carboxylate groups to Na¹⁺ are similar to those in complex **4** and **WIGWEP**.

Also, there is intramolecular H-bond between the oxygen atom of the carboxylate group and the oxygen atom of the hydroxyl group in the three Na¹⁺ complexes.

3.3. Summary

As a result of the reactive crystallization of different *ortho*-, *meta*- and *para*- substituted benzoic acids with different 1st-row 3d transition metals, four complexes were obtained. Complexes **1**, **3** and **4** have been previously reported while complex **2** is novel.

X-ray single crystal method for screening of crystal structures worked correctly and accurate data were collected. It is feasible to monitor crystallization reaction using optical microscopy and single crystal diffraction as opposed to the more tradition powder X-ray diffraction method.

The characterization is quick because the material is known, the unit cell dimension is sufficient for identification and these were determined as fast as in 10 minutes from a crystal of 0.1 x 0.1 x 0.1 mm. Full structure determination of novel compounds was carried out in a few hours.

It is relatively straightforward to build up a unit-cell dimension so that a comprehensive study can be carried out of the progress of a reaction which involves multiple crystallization processes. Pure metal and bimetallic reactive crystallization of 1st-row 3d transition metals and 2-amine-3-methylbenzoic acid (AMB) were carried out in the next chapter.

Complex **1** crystallizes in the monoclinic crystal system and $P2_1/n$ space group where **P** is a Primitive lattice, 2_1 is a rotation by 180° around *b* axis and a translation by $b/2$ and *n* is *n*-glide which consists of a reflection in the *ac* plane and a translation by $a/2 + c/2$.

Complex **2** crystallizes in the monoclinic crystal system and $P2_1/a$ space group where **P** is a Primitive lattice, 2_1 is a rotation by 180° around *b* axis and a translation by *a*-axis in *ab* plane.

Complex **3** crystallizes in the monoclinic crystal system and $P2_1/c$ space group where **P** is a Primitive lattice, 2_+ is a rotation by 180° around *b* axis and a translation by $b/2$ and *c* is a *c*-glide which consists of a reflection in a mirror parallel to the *ac* plane and a translation by $c/2$.

Complex **4** crystallizes in the triclinic crystal system and **P-1** space group where **P** is a Primitive unit cell which contains only one symmetry operation namely, an inversion centre.

Chapter 4

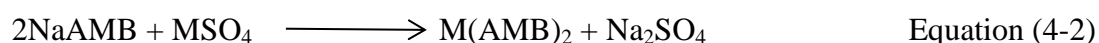
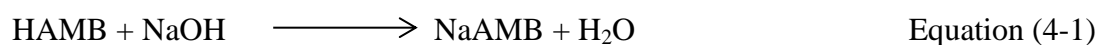
**The Small-scale Crystallization of MSO_4 , where $\text{M} = \text{Cu, Co, Zn,}$
and Ni Hydrates with NaAMB from Aqueous Solution in order to
screen for Mixed Metal Compounds, Polymorphs, and Solvates**

4.1. Introduction

2-amino-3-methyl benzoic acid (AMB) can be reacted with metals to make a range of coordination products including monomers, dimers, and polymers. AMB could act as a monodentate, bidentate or tridentate ligand.

2-amino-3-methyl benzoic acid (AMB) has been studied previously as a free ligand ¹¹⁹ and has formed complexes with post-transition metals such as Bismuth ^{120, 121} and Thallium, ¹²² 3rd-row transition metals such as Rhenium ¹²³ and with 1st-row 3d transition metals such as copper and zinc. The diffusion of an aqueous solution of copper nitrate [Cu(NO₃)₂] and sodium 2-amino-3-methyl benzoate [NaAMB] over ten days forms CuAMB. ¹⁰³ Likewise, the diffusion of aqueous solutions of zinc nitrate and sodium 2-amino-3-methyl benzoate in a ratio of 1:2 over a period of six weeks forms ZnAMB. ¹¹³

In this study, the metal salts used are the 1st-row 3d transition metal sulfates ranging from Mn(II) to Zn(II). This reaction involves neutralizing the carboxylic acid with NaOH before reacting with the 3d metal sulfate in water. For example,



Where M is a divalent 1st-row 3d transition metal M(AMB)₂.

This chapter examines the different metal to ligand ratio, bimetallic reaction, different concentration, and various metals in small-scale crystallization using an optical microscope to monitor the reaction and single crystal diffractometer to characterize the product obtained.

The crystal structures obtained from the small-scale crystallization of MSO₄, where M = Cu, Co, Zn, and Ni hydrates with NaAMB from aqueous solution revealed that 1st-row 3d transition metals can be incorporated into the layered structure by themselves. The bimetallic reaction did not work as expected but crystals suitable for single crystal analysis were obtained and characterized.

In the bimetallic crystallization reaction series, various crystals were obtained. Sample bottles were selected for single crystal analysis based on the morphological changes and dichroic colour changes of the single crystals obtained.

It was observed that as the volume of ZnSO_4 added increases in the series, there were changes in the morphology and dichroic colour change of the crystals formed. With the lesser volume of ZnSO_4 , the crystals obtained are dark green clustered needle crystals. This turned light green as the volume of the aqueous solution of ZnSO_4 increases and there was a change in the crystal habit, the needle crystals change to cubic single crystals in the series.

The clear green solution of NaAMB and CuSO_4 formed dark green powder at the bottom of the vial sample bottle. Under the polarised microscope, the dark green powder was seen to consist of a cluster of dark green needles and colourless crystals. On closer examination of the crystals obtained in the NaAMB with $\text{CuSO}_4 / \text{ZnSO}_4$ crystallization reaction series, the dark green needle clusters were seen to join together to form a fan or star shape. This gave one of the three identical determinations of anhydrous CuAMB complex **5b**.

The remaining two identical determinations of anhydrous CuAMB complexes **5a** and **5c** were obtained from a different set of crystallization reaction, as a mono metal-ligand reaction and as bimetallic crystallization reaction respectively.

The bimetallic crystallization that contained NaAMB with $\text{CuSO}_4 / \text{ZnSO}_4$ and $\text{CuSO}_4 / \text{NiSO}_4$ produced the hydrate CuAMB complexes **6**, **7** and **8**.

4.2. Results and Discussion

4.2.1. Reactive Crystallization and Crystal Structure of $[\text{Cu}(\text{C}_8\text{H}_8\text{NO}_2)_2]_n$

4.2.1.1. Introduction

In the mono metal and bimetallic crystallization reaction set up, sample bottles for single crystal analysis were selected based on the morphological changes of the crystals obtained. In this reaction set up, three different determinations of anhydrous CuAMB complexes **5a**, **5b**, and **5c** were obtained and characterized.

Single crystals of complex **5a** were obtained from the reactive crystallization of the aqueous solution of NaAMB and CuSO_4 in the molar ratio 1:2.

Single crystals of complex **5b** were obtained from the bimetallic crystallization reaction of the aqueous solution of NaAMB with CuSO_4 and ZnSO_4 in the molar ratio 1:2.

Single crystals of complex **5c** were obtained from the bimetallic crystallization reaction of the aqueous solution of NaAMB with CuSO_4 and CoSO_4 in the molar ratio 1:2.

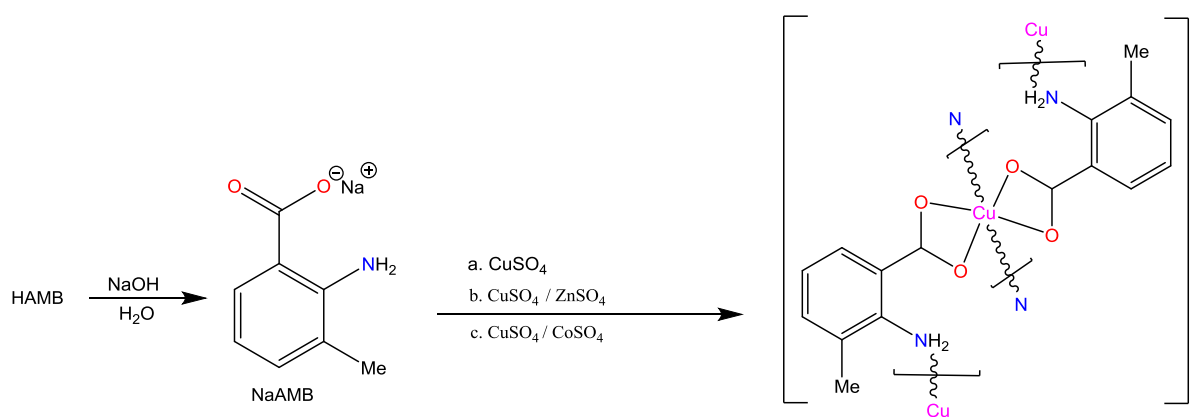


Figure 4-1: Schematic of the reaction that produced complexes **5a**, **5b**, and **5c**.

A search of the Cambridge Crystallographic Database revealed that a structure identical to these three determinations of anhydrous CuAMB structures has been studied to a high standard as copper 3-methylanthranilate [bis(2-amino-3-methylbenzoato)copper(II)] and

deposited as **DUKTIM** in the Cambridge Crystallographic Database. **DUKTIM** was prepared by the diffusion of aqueous solutions of $[\text{Cu}(\text{NO}_3)_2]$ and NaAMB over ten days.¹⁰³

4.2.1.2. Crystal Structure Determination of Complexes **5a**, **5b**, **5c** and, **DUKTIM**

The measurement for the three determinations of anhydrous CuAMB structures was carried out on a Bruker Prospector diffractometer equipped with Cu $K\alpha$ radiation, $\lambda = 1.54184 \text{ \AA}$ at 150 K. They crystallize in the orthorhombic crystal system with Pbcu space group.

A full list of crystal parameters and structure determination details, a view of the molecular structure of the three determinations of CuAMB, complexes **5a**, **5b**, **5c** and, **DUKTIM**, and tables of the selected bond lengths and angles are presented below.

	5a	5b	5c	DUKTIM
Form. Weight	363.85	363.85	363.85	363.90
Temperature (K)	150	150	150	293(1)
Crystal System	Orthorhombic	Orthorhombic	Orthorhombic	Orthorhombic
Space group	Pbcu	Pbcu	Pbcu	Pbcu
<i>a</i> (Å)	9.6401(17)	9.6379(4)	9.6229(5)	9.580(2)
<i>b</i> (Å)	7.1641(14)	7.1595(3)	7.1737(3)	7.213(1)
<i>c</i> (Å)	21.592(4)	21.5441(12)	21.6571(13)	21.867(3)
Volume (Å ³)	1491.2(5)	1486.59(12)	1495.03(13)	1511.1(6)
Z	4	4	4	4
ρ_{calc} (g cm ⁻³)	1.621	1.626	1.617	1.67
μ (mm ⁻¹)	1.487	1.492	1.483	15.3 cm ⁻¹
F(000)	748	748	748	748
R factor (%)	8.57	4.26	4.93	0.055

Table 4-1: Crystal data collection of complexes **5a**, **5b**, **5c** and, **DUKTIM**.¹⁰³

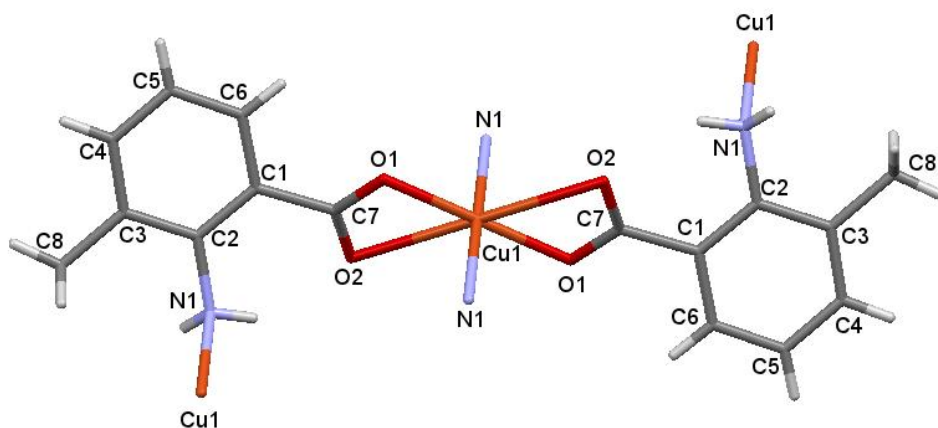


Figure 4-2: Molecular structure of complexes *5a*, *5b*, *5c* and *DUKTIM*.¹⁰³

The coordination environment of Cu^{2+} in the anhydrous CuAMB structures is distorted octahedral due to the Jahn-Teller effect. Cu^{2+} is coordinated to four methyl-amino-benzoate ligands acting as bridging bidentate ligands. Each of the Cu^{2+} centres is bonded to two carboxylate oxygen atoms of two different ligands in *cis* position to one another and contained two axial N atoms of the NH_2 group from two different ligands in *trans* orientation, each ligands bridging two Cu^{2+} centres, as shown in figure 4-2.

The bridging ligands lead to a two-dimensional polymeric network, as shown in figure 4-3. This is strengthened further by H-bonding between adjacent molecules. It is composed of puckered rings of 24 atoms.

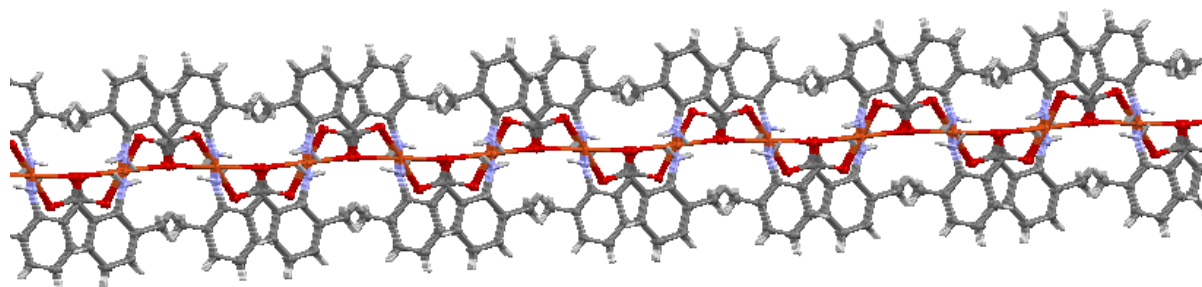


Figure 4-3: A two-dimensional polymeric network of the anhydrous CuAMB complex.

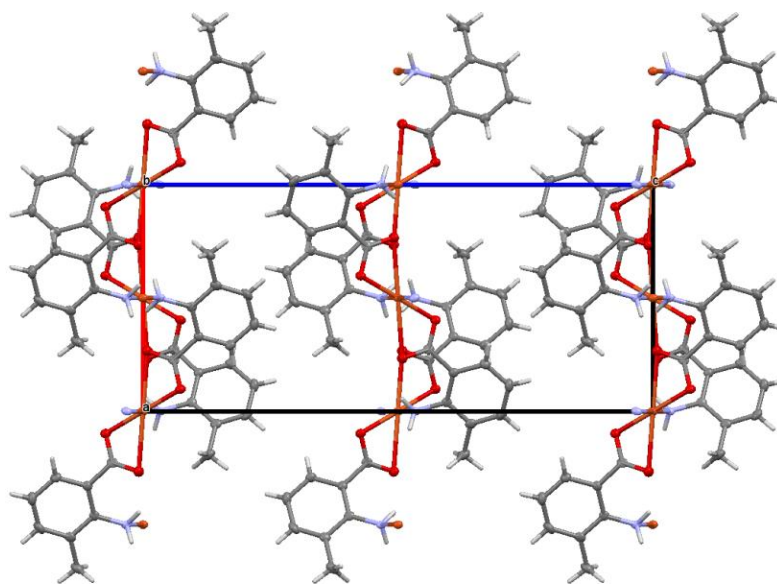


Figure 4-4: A packing figure of the anhydrous CuAMB viewed down crystallographic *b* axis.

In anhydrous CuAMB, the carboxylate oxygen atoms are coordinated to the Cu^{2+} centre in chelating bridging coordination mode.

The bond distances of the symmetric atoms coordinating around Cu^{2+} in all the three determinations of anhydrous CuAMB structures are not significantly different. Their Cu–O and Cu – N distances are in the same range as those of **DUKTIM**. The distance of Cu1 – O2 are significantly longer than Cu1 – O1 in the CuAMB structures, as listed in table 4-2.

Their C – O distances are not significantly different. But each pair of C – O distances of the carboxylate group are longer than each other. It is observed that when the C–O distances are longer, the Cu – O distances tend to be shorter. Hence, longer Cu – O distances appear to correlate with short C – O distances and *vice-versa*.¹²⁴

	5a	5b	5c	DUKTIM
Distance	(Å)	(Å)	(Å)	(Å)
Cu1 – O1	1.955(5)	1.950(2)	1.955(2)	1.954(3)
Cu1 – O2	2.557(3)	2.572(2)	2.565(2)	2.572(3)
Cu1 – N1 ²	2.050(5)	2.054(3)	2.053(3)	2.054(3)
O1 – C1	1.273(8)	1.277(4)	1.283(4)	1.273(5)
O2 – C1	1.258(9)	1.263(4)	1.258(4)	1.249(5)
Angle	(°)	(°)	(°)	(°)
O1 – Cu1 – O1	180.0	180.0	180.0	180.0
O1 ¹ – Cu1 – N1 ²	91.5(2)	91.90(10)	91.88(11)	92.82(4)
O1 – Cu1 – N1	88.5(2)	88.10(10)	88.12(11)	88.0(4)
N1 ² – Cu1 – N1 ³	180.0	180.00(16)	180.00(17)	180.0

*Table 4-2: Bond distances and bond angles of atoms coordinating around Cu²⁺ in complexes **5a**, **5b**, **5c** and **DUKTIM**.¹⁰³*

In line with the bond distances and bond angles listed in table 4-2, despite the different starting materials, different crystallization methods, varying metal compositions using the bimetallic solutions of Cu/Zn and Cu/Co for the crystallization reaction that produced complexes **5b** and **5c**, and different characterization temperature, it is established that the three different determinations of anhydrous CuAMB complexes **5a**, **5b**, and **5c** are the identical structure of **DUKTIM**. They all crystallize in the orthorhombic crystal system and Pbc_a space group.

The unit cell dimensions in **DUKTIM** appeared higher because the structure was characterized at room temperature whereas complexes **5a**, **5b**, and **5c** were characterized at a lower temperature of 150 K. Though there are no significant changes in cooling, the unit cell differences are expected when the temperature is warmer. When compared side by side, the geometry around the Cu²⁺ centre, the bond distances, and bond angles of the atoms coordinating around Cu²⁺ centre in the anhydrous CuAMB structures are the same.¹⁰³

4.2.2. Reactive Crystallization and Crystal Structures of Novel Hydrated CuAMB Complexes $[\text{Cu}(\text{C}_8\text{H}_8\text{NO}_2)\cdot\text{H}_2\text{O}]_2$, $\{[\text{Cu}(\text{C}_8\text{H}_8\text{NO}_2)_2]_2\cdot 8/3\text{H}_2\text{O}\}_n$ and $\{[\text{Cu}(\text{C}_8\text{H}_8\text{NO}_2)_2]_2\cdot 13/5\text{H}_2\text{O}\}_n$

In the mono and bimetallic crystallization reaction of aqueous NaAMB and 1st-row 3d transition metals that produced the three identical determinations of anhydrous CuAMB complexes **5a**, **5b** and **5c**, three different novel hydrated CuAMB complexes **6**, **7** and **8** were also obtained. Complex **6** is a dimer while complexes **7** and **8** are extended coordination polymers that have a common basic structure. They are both layered coordination polymers with lattice water.

In the course of this study, the three types of novel hydrated CuAMB complexes obtained in the bimetallic reaction will be compared thoroughly because their difference extends right down to their atomic level.

4.2.2.1. Structural Characterization of $[\text{Cu}(\text{C}_8\text{H}_8\text{NO}_2)\cdot\text{H}_2\text{O}]_2$

4.2.2.2. Introduction

Single crystals of complex **6** were obtained from the reactive crystallization of aqueous solution of NaAMB and CuSO_4 . A few drops of the solution were placed in a Petri Dish and were allowed to slowly evaporate to dryness overnight, as shown in figure 4-5.

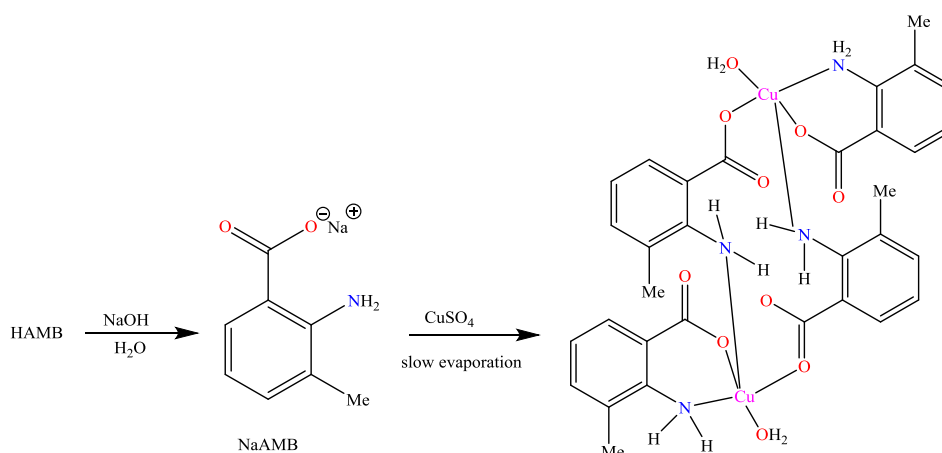


Figure 4-5: Schematic of the reaction that produced complex **6**.

4.2.2.3. Crystal Structure Determination of Complex **6**

The measurement was carried out on an Agilent SuperNova Kappa geometry 4-circle diffractometer using the graphite monochromated Mo K α radiation, $\lambda = 0.71073 \text{ \AA}$ at 150 K. Complex **6** crystallizes in the monoclinic crystal system with P2 $_1$ /c space group.

A full list of crystal parameters and structure determination details, a view of the molecular structure of complex **6**, a table of selected bond lengths and angles are presented below.

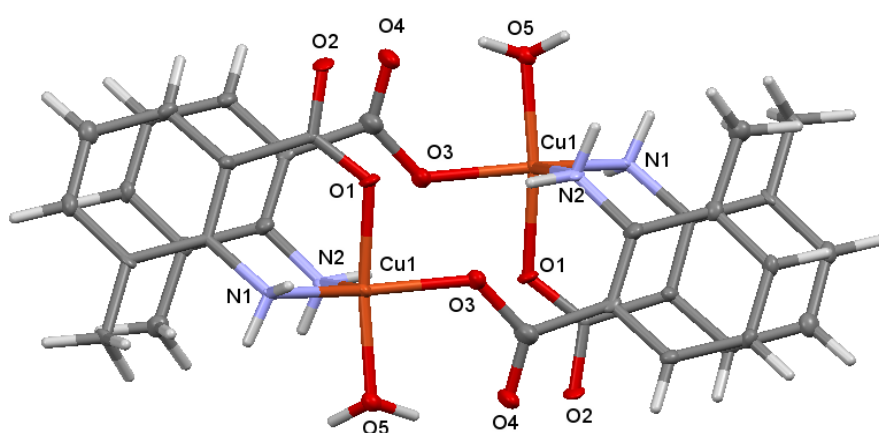


Figure 4-6: Molecular structure of complex **6**.

Complex **6** is a dimer (it has two metal centres). The geometry environment of Cu $^{2+}$ is square based pyramidal with five atoms coordinating around Cu $^{2+}$. These consist of two carboxylate oxygen atoms, two NH $_2$ groups, and one water molecule coordinating to Cu $^{2+}$ centre. Each of the monomers is attached to Cu centre via one bridging NH $_2$ group and two carboxylate oxygen atoms from different ligands leaving each Cu centre to see three ligands. The carboxylate oxygen atoms are coordinated to each Cu centre in a *syn* monodentate coordination mode, as shown in figure 4-6.

When expanded, it built different sets of individual units of the compound (dimers), as shown in figure 4-7.

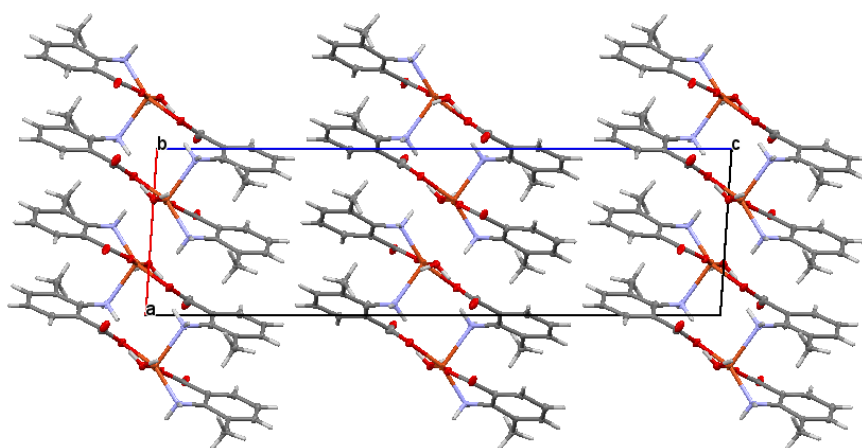


Figure 4-7: The packing diagram of complex **6** viewed down crystallographic *b* axis flipped by 90° around the *z*-axis, showing lack of intermolecular interaction.

This forms a centrosymmetric dimer, linked together by Cu – N coordination bonds and intramolecular H-bonds as shown in figure 4-8.

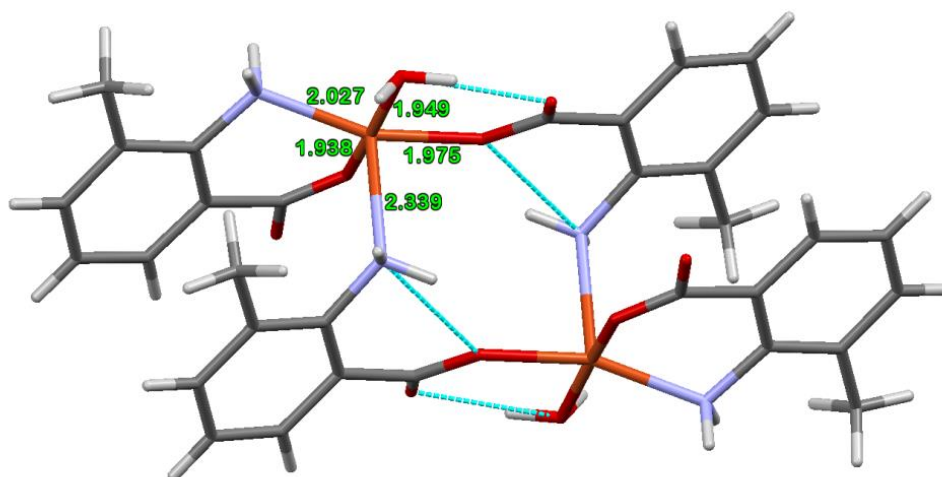


Figure 4-8: $\text{CuL}_2\text{H}_2\text{O}$ forms a centrosymmetric dimer linked together by Cu – N coordination bonds. Intramolecular H-bonds, shown in turquoise, are a feature of each monomer.

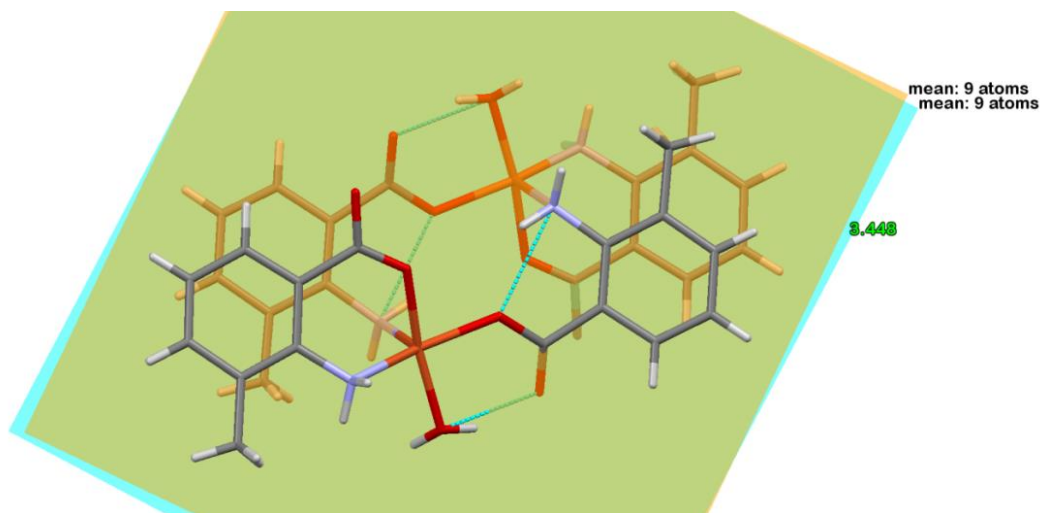


Figure 4-9: The coordination bonds holding the dimer together are assisted by π - π stacking with interplanar separations of 3.45 Å.

The H-bond within each asymmetric unit is between the amine group and the adjacent carboxylate oxygen atom of the same phenyl ring with the distance of $N2 \dots O3 = 2.790(1)$ Å. There is also H-bond between $O-H \dots O$ in the unit represented by a turquoise dotted line as shown in figure 4-10, with a distance of $O4 \dots O5 = 2.573$ Å.

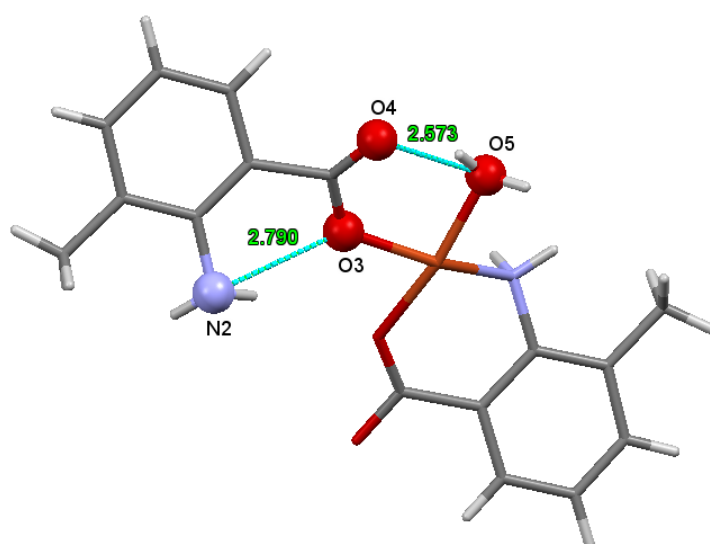


Figure 4-10: H-bonding between $N \dots O$ is $2.790(1)$ Å and $O \dots O = 2.573(1)$ Å in complex 6.

The adjacent dimers were linked by intermolecular H-bonds with the distance N...O = 2.790(1) Å. There is also $\pi - \pi$ stacking of distance 3.59 Å which forms a column along the crystallographic direction. This value is well within the range of VdW suggested by C. Janiak of 3.3 – 3.8 Å.⁶⁷⁻⁶⁸ These values were also supported by S. Alvarez.¹²⁵

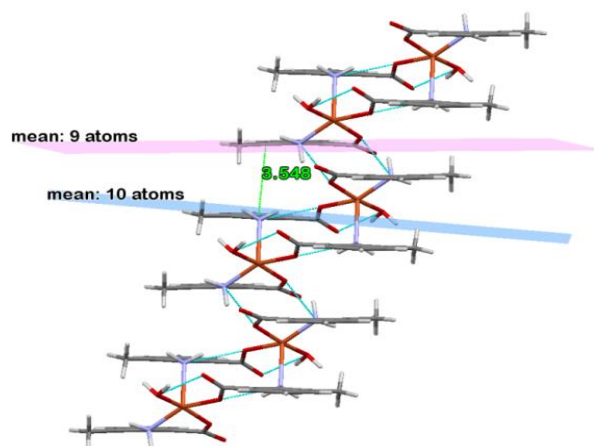


Figure 4-11: Adjacent dimers are linked by intermolecular H-bonds and further π - π stacking to form columns along the crystallographic *a* direction.

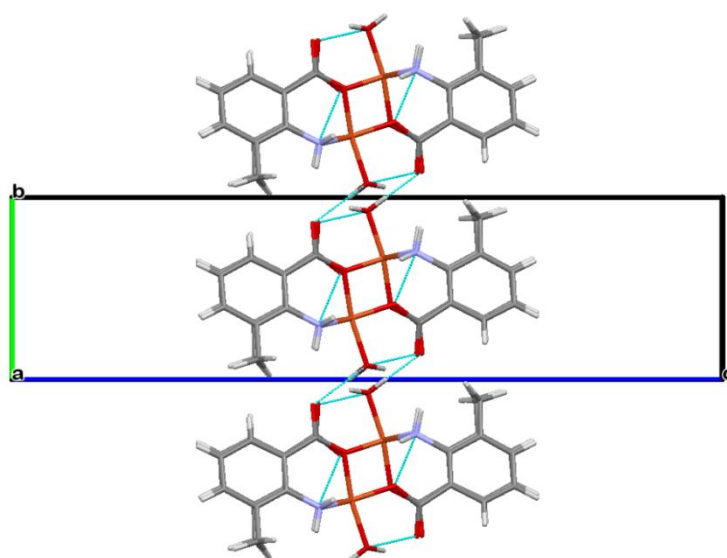


Figure 4-12: Adjacent columns are linked together via H-bonds to form a wall parallel to the crystallographic *ab* plane.

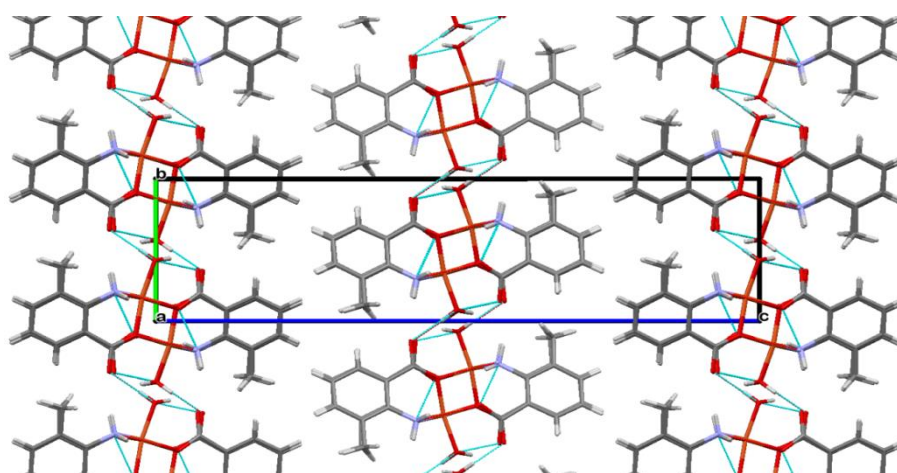


Figure 4-13: The walls associate in the crystallographic c direction via dispersion forces to form the 3D crystal structure.

The C – O distances in the carboxylate group case one is 1.240(2) Å and 1.248(1) Å. These values are close and there is no significant difference in their geometry, they are a mirror image and they carry a negative charge, they are identical within the experimental error unlike the C – O distances in the carboxylate group case two which are 1.370(2) Å and 1.156(2) Å. The difference between the distances is significant. The difference is seven times the standard deviation. This is an indication that the π delocalization between these bonds is not equal as a consequence of the bonding configuration. This reflects the different bonding environment of the two carboxylic groups. In the one case, the carboxylate oxygen atom is involved in the two H-bonds, the NH₂ group in an adjacent dimer and the oxygen atom of the coordinated water molecule. Another carboxylate oxygen atom is involved in an adjacent dimer.

The longer carboxylate oxygen atom distance is involved with the NH₂ group of the same AMB. The second carboxylate oxygen atom distance is involved with the coordinated water molecule in the same asymmetric unit.

Complex **6** can be compared to a five-coordinate Cu complex, copper quinaldinate monohydrate [aquabis(2-quinolinecarboxylato)copper(II)]; pentacoordinate copper which has been studied extensively and deposited in the Cambridge Crystallographic Database as **DICHAY**. This crystal was grown by reactive diffusion between a methanol solution of copper(II) acetate monohydrate and an ethanol solution of quinaldinic acid, in a 1:4 ratio.¹²⁶

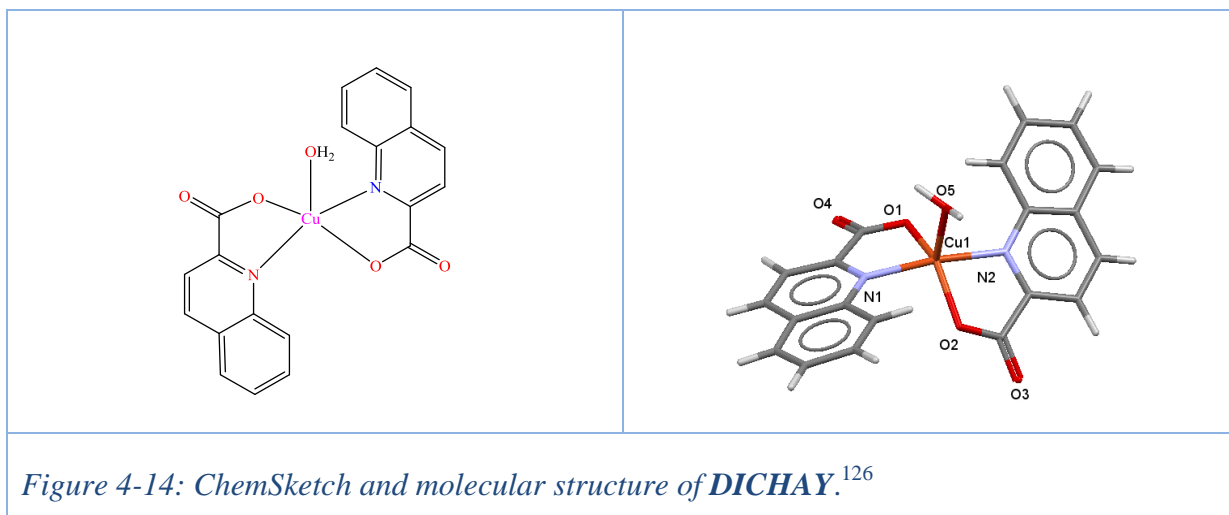
Despite the starting materials, metal-ligand and the solvents used are different, the two hydrated Cu complexes crystallize in the monoclinic crystal system and P2₁/c space group, as listed in table 4-3.

	6	DICHAY
Emp. Formulae	[Cu(C ₈ H ₈ NO ₂) ₂ H ₂ O] ₂	[Cu(C ₁₀ H ₆ NO ₂) ₂ (H ₂ O)]
Form. Weight	381.86	425.9
Temperature (K)	150	293
Crystal System	Monoclinic	Monoclinic
Space group	P2 ₁ /c	P2 ₁ /c
<i>a</i> (Å)	7.7428(11)	7.756(1)
<i>b</i> (Å)	7.1438(10)	7.628(2)
<i>c</i> (Å)	26.666(4)	29.573(5)
γ (°)	93.847(12)°	95.31(1)
Volume (Å ³)	1471.7(4)	1742.2
Z	4	4
D _{calc} (g cm ⁻³)	1.724	1.60
μ (mm ⁻¹)	1.516	13.4
F(000)	788.0	868
R factor (%)	10.41	0.050

*Table 4-3: Crystal data collection of complex 6 and DICHAY.*¹²⁶

Though complex **6** is a dimer, the two Cu²⁺ complexes have similar geometric coordination environment around their Cu²⁺ centre as five-coordinate, as shown in figure 4-14.

Like in complex **6**, **DICHAY** has a Penta-coordinated Cu atom with the quinaldinate ligand acting as bidentate and forming a five-membered chelate ring with the Cu centre. The coordinated water molecule made up the fifth coordination site.



The bond distance of the atoms coordinating around Cu centre in both copper Penta-coordinated complexes vary slightly but C – O distances are significantly different, as listed in table 4-4.

6		DICHAY	
Distance	(Å)	Distance	(Å)
Cu1 – O1	1.938(7)	Cu – O1	1.954(3)
Cu1 – O3	1.975(7)	Cu – O2	1.962(3)
Cu1 – O5	1.949(7)	Cu – O5	2.143(3)
Cu1 – N1	2.027(7)	Cu – N1	2.014(3)
Cu1 – N2 ¹	2.339(8)	Cu – N1	2.012(3)
O1 – C1	1.245(11)	O1 – C1	1.248(5)
O2 – C1	1.264(12)	O4 – C1	1.221(5)
O3 – C9	1.320(13)	O2 – C11	1.286(5)
O4 – C9	1.201(13)	O3 – C11	1.233(5)

Symmetry code: 1/2-x, 1-y, 1-z

Table 4-4: Bond distances of atoms coordinating around Cu^{2+} and C – O bonds in complex **6** and *DICHAY*.¹²⁶

The Cu – Cu distance between the dimer in complex **6** is 5.400(2) Å while the Cu – Cu distance between the two sets of dimers is 4.019(2) Å. These values will be more favourable for magnetic studies when compared to that of **DICHAY** that has its Cu – Cu distances to be 8.776 Å and 10.879 Å. These distances are longer than those in complex **6**, as shown in figure 4-15.

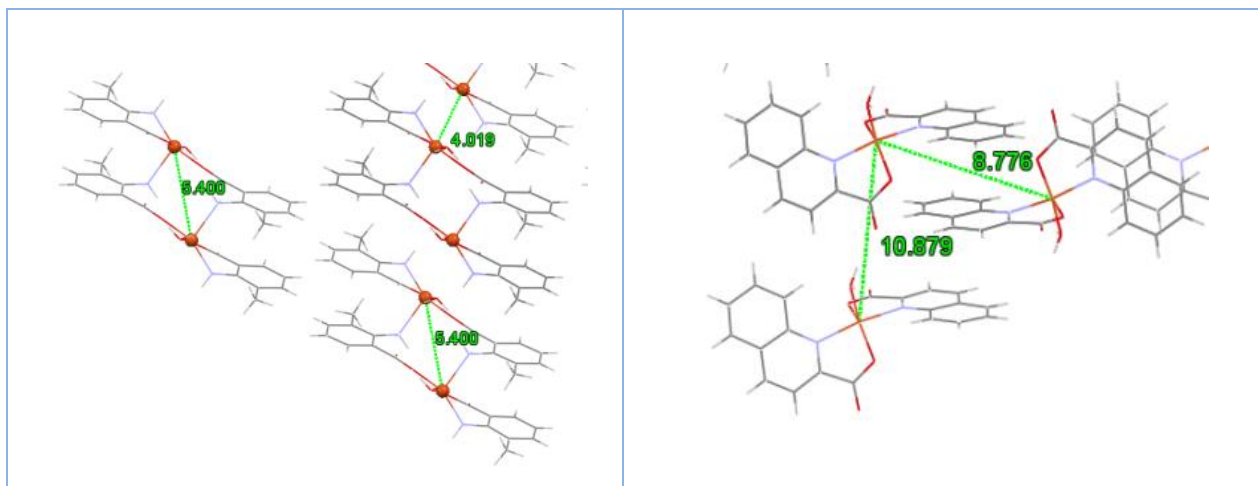


Figure 4-15: Figure showing the Cu – Cu distances in complex **6** (left) and **DICHAY** (right).¹²⁶

In complex **6**, the bond angles of the atoms coordinating around Cu²⁺ simply explains the square based pyramidal geometric environment of Cu²⁺ centres. These bond angles are compared to that of **DICHAY** and are listed in table 4-5.

6		DICHAY	
Angle	(°)	Angle	(°)
O1 – Cu1 – O3	84.2(3)	O1 – Cu – O5	106.0(1)
O5 – Cu1 – O3	91.3(3)	O2 – Cu – O5	113.7(1)
O1 – Cu1 – O5	169.1(3)	O1 – Cu – O2	140.3(1)
O1 – Cu1 – N1	88.4(3)	O1 – Cu – N1	82.1(1)
O3 – Cu1 – N1	156.5(3)	O5 – Cu – N1	97.9(1)
N1 – Cu – N2 ⁱ	111.6(3)	N1 – Cu – N2	168.2(1)
O1 – C1 – O2	120.5(11)	O2 – C11 – O3	123.5(4)
O4 – C9 – O3	128.2(16)	O1 – C1 – O4	128.4(4)

Symmetry code: (i) -x, -y+1, -z+1.

Table 4-5: Selected Bond angles in complex 6 and DICHAY.¹²⁶

4.2.3. Structural Characterization of $\{[\text{Cu}(\text{C}_8\text{H}_8\text{NO}_2)_2]_2 \cdot 8/3\text{H}_2\text{O}\}_n$

4.2.3.1. Introduction

Single crystals of complex **7** were obtained in solution from the bimetallic reaction solution which contains aqueous solutions of NaAMB with CuSO_4 and ZnSO_4 as shown in figure 4-16.

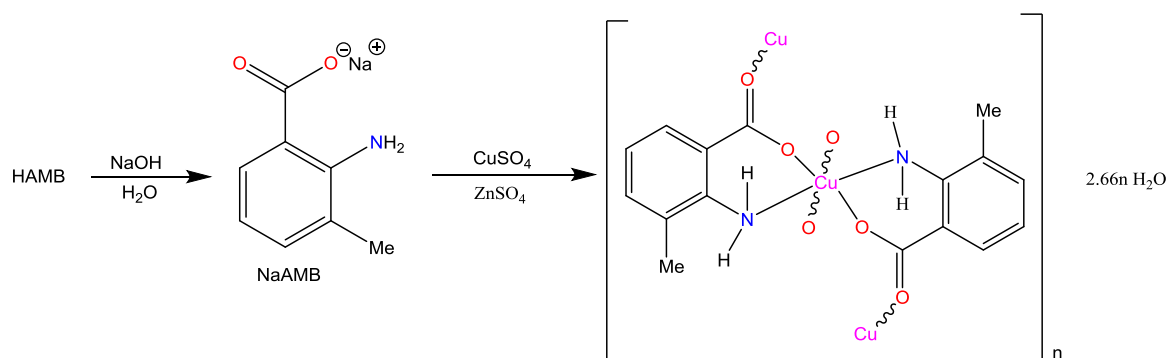


Figure 4-16: Schematic of reaction that produced complex **7**.

4.2.3.2. Crystal Structure Determination of Complex **7**

The measurement was carried out on an Agilent SuperNova Kappa geometry 4-circle diffractometer using the graphite monochromated Mo K α radiation, $\lambda = 0.71073 \text{ \AA}$ at 150 K. Complex **7** crystallizes in the monoclinic crystal system with $P2_1/n$ space group.

A full list of crystal parameters and structure determination details, a view of the molecular structure of complex **7**, and tables of selected bond lengths and angles are presented below.

The asymmetric unit of complex **7** comprises of two crystallographically independent Cu centres with each Cu seeing two ligands, each ligand binding to the Cu atoms at one of the carboxylate oxygen atom and at the NH₂ groups with four molecules of lattice water around the structure, as shown in figure 4-17.

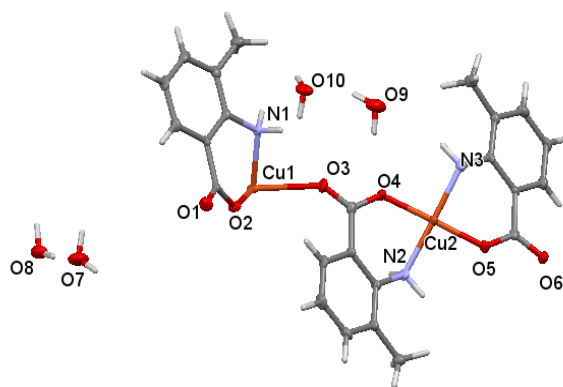


Figure 4-17: An asymmetric unit of complex 7.

The molecular structure of complex **7** comprises of two crystallographically independent Cu centres. Each Cu centre is coordinated to two bidentate amino-carboxylates. In each case, the *anti*-coordinated oxygen atom of the carboxylate group forms a bridge to another Cu centre, forming a chain. Since each of the carboxylate oxygen atoms does this, they form links in two-dimension, so that 2D sheets are formed. These linkers complete the octahedral environment around each Cu centre. The structure also has four molecules of lattice water, as shown in figures 4-18.

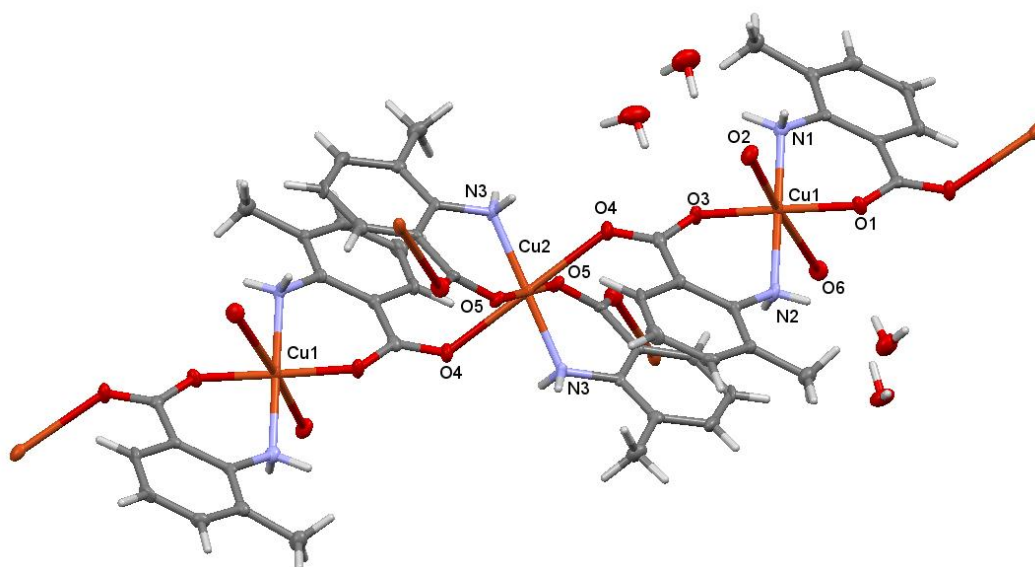


Figure 4-18: Molecular structure of complex 7.

In complex **7**, one of the two crystallographically independent Cu^{2+} sits in a general position and the second Cu^{2+} sits on a crystallographic inversion point tetragonally distorted octahedral. The coordination environment of each of the two Cu^{2+} centres consists of four equatorial carboxylate oxygen atoms and two axial NH_2 groups.

When expanded, the two-dimensional coordination polymer formed a layered structure that has octahedral Cu^{2+} coordinated to an AMB with lattice water molecules around the structure, as shown in figure 4-19. Figures 4-20 and 4-21 presented the water channel between the layers.

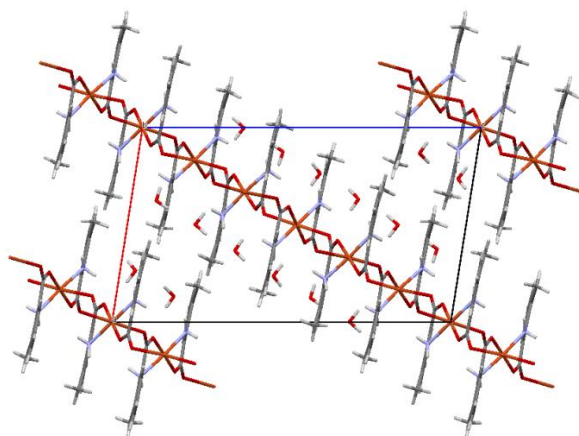


Figure 4-19: Packing diagram of complex 7 viewed down crystallographic b axis, showing the presence of water between the layers.

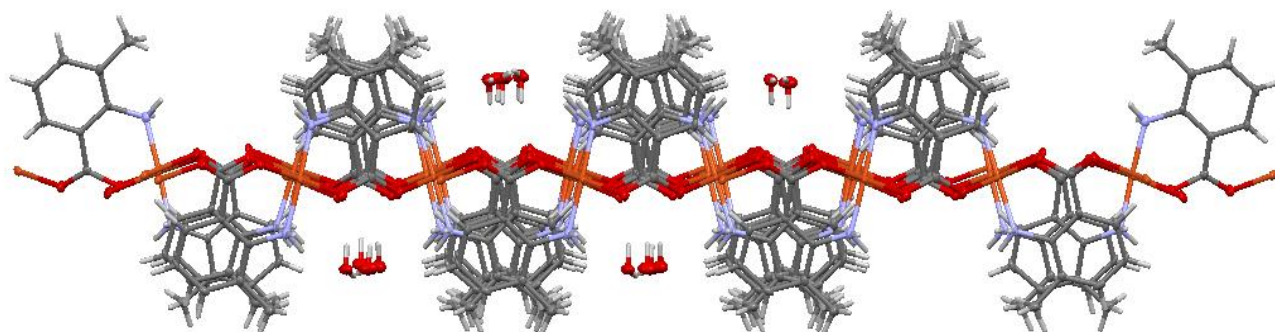


Figure 4-20: Figure of complex 7 viewed down one layer, showing water filling the channels in the zigzag layer.

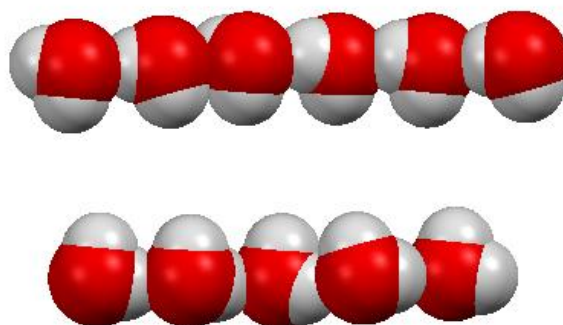


Figure 4-21: Figure showing the waters in the channel highlighted.

Empirical Formulae	$\{[\text{Cu}(\text{C}_8\text{H}_8\text{NO}_2)_2]_2 \cdot \frac{8}{3}\text{H}_2\text{O}\}_n$
Form. Weight	617.83
Temperature (K)	150
Crystal System	Monoclinic
Space group	$P2_1/n$
a (Å)	11.8753(9)
b (Å)	10.3363(7)
c (Å)	20.4429(16)
β (°)	$98.928(7)^\circ$
Volume (Å ³)	2478.9(3)
Z	4
D_x (Mg m ⁻³)	1.655
μ mm ⁻¹	1.363
F(000)	1282.0
Crystal size (mm)	$0.33 \times 0.25 \times 0.02$
Crystal Shape	Plate, Blue
R factor (%)	6.08

Table 4-6: Crystal data collection of complex 7.

The carboxylate oxygen atom is coordinated to the Cu^{2+} centres in *anti-anti* bidentate coordination mode. The C – O distances in the pairs of carbonyl groups are significantly

different. In case one, the distances of $C1 - O1 = 1.245(11) \text{ \AA}$ and $C1 - O2 = 1.264(12) \text{ \AA}$, there is no significant difference in these distances. The $C - O$ bond, in this case, is a mirror image and they carry a negative charge. They are identical within experimental error. In case two, the distances of $C9 - O3 = 1.320(13) \text{ \AA}$ and $C9 - O4 = 1.201(13) \text{ \AA}$ are significantly different. They are seven times the standard deviation. This reflects the different bonding mode of the two carboxylate groups to the metal centre.

The longer carboxylate oxygen atom is involved in H-bonding with the NH_2 group of the same AMB ligand. The shorter carboxylate oxygen atom is involved in H-bonding with O_{water} in the same asymmetric unit. The carboxylate oxygen atoms are involved in the two H-bonds, the O_{water} is involved with the NH_2 group in an adjacent dimer and another O_{carb} is involved in an adjacent dimer. This shows that the π delocalization between these two bonds is not equal. This may be the effect of the bonding configuration, in that, the longest $C - O$ distance is the O atom that makes the shortest $Cu - O$ bond.

In complex **7**, the atoms coordinating around $Cu1$ centre are not symmetrical while the atoms coordinating around $Cu2$ centre are symmetrical, as shown in figure 4-22 and listed in table 4-7.

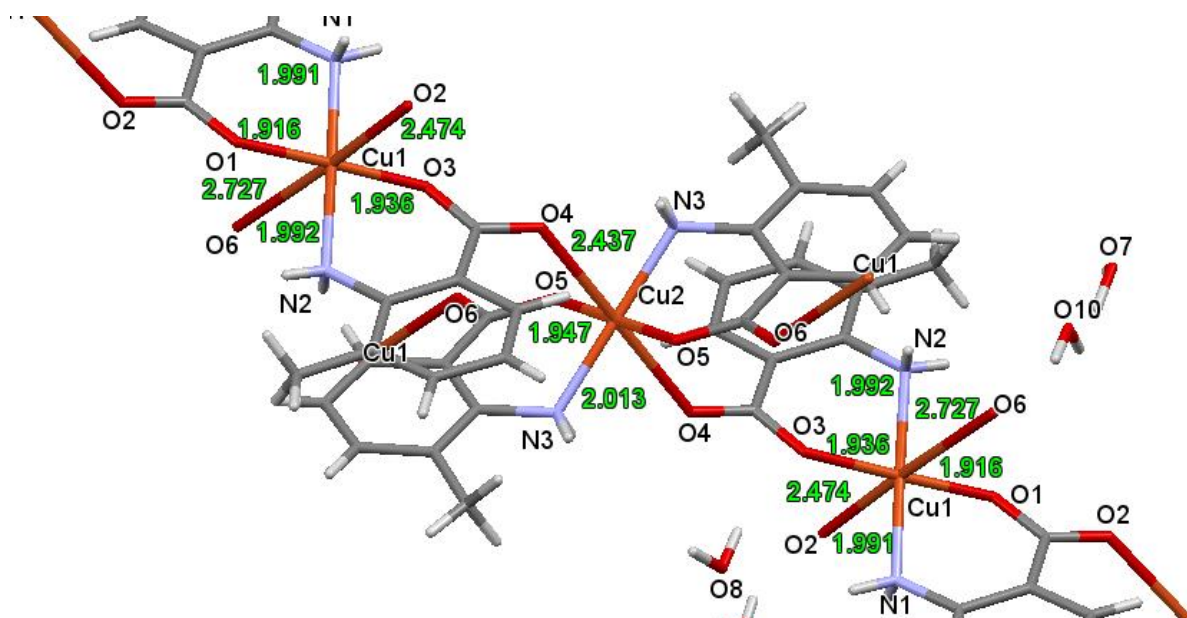


Figure 4-22: Bond distances of atoms coordinating around the Cu^{2+} centres in complex **7**.

Distance	(Å)	Distance	(Å)
Cu1 – O1	1.916(3)	Cu2 – O4	2.437(3)
Cu1 – O2	2.474(3)	Cu2 – O4 ¹	2.437(3)
Cu1 – O3	1.937(3)	Cu2 – O5	1.947(2)
Cu1 – O6	2.727(3)	Cu2 – O5 ¹	1.947(2)
Cu1 – N1	1.992(4)	Cu2 – N3	2.014(4)
Cu1 – N2	1.993(4)	Cu2 – N3 ¹	2.014(4)
C7 – O1	1.290(4)	C15 – O3	1.286(5)
C7 – O2	1.240(4)	C15 – O4	1.236(5)

Symmetric code: ¹1-x, 1-y, 1-z

Table 4-7: Selected bond distances of the atoms coordinating around Cu²⁺ centres in complex 7.

In complex 7, the distance between Cu1 – Cu2 = 6.160 Å while the distance between Cu1 – Cu1 = 6.274 Å as shown in figure 4-23.

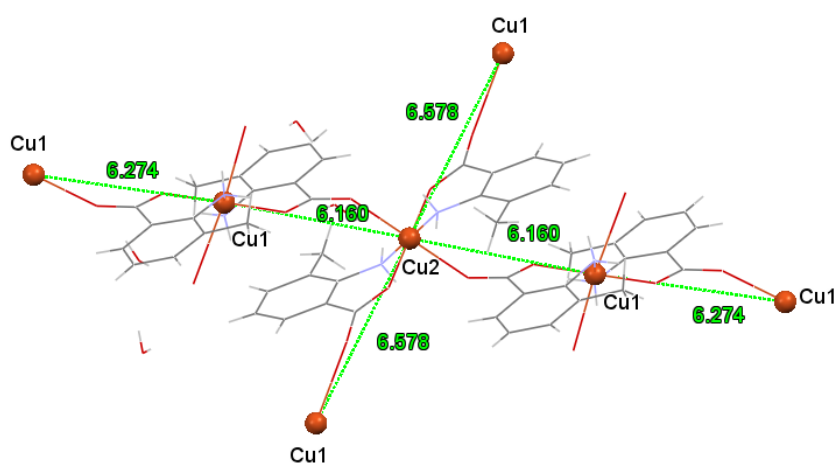


Figure 4-23: Figure showing Cu – Cu distances in complex 7.

This Cu – Cu distances can be compared to those obtained in the structure and magnetic studies of a two-dimensional sheet-like Cu(II) complex with bridging pyridine-4-carboxylate and trans-oxamidate ligands. This structure was made with bridging carboxylate ligand and has been studied to a high standard and deposited into the Cambridge Crystallographic Database as **PONLEJ**. In this structure, the magnetic coupling was measured and strong antiferromagnetic coupling was found at Cu – Cu distances of 5.2 Å and 6.9 Å. The Cu – Cu distances of 6.160 Å and 6.274 Å in complex **7** are not likely to be more weakly coupled.¹⁸

In complex **7**, the *trans* angles of N3 – Cu2 – N3ⁱ = 180.0 ° and O4 – Cu2 – O4ⁱ = 180.0° in Cu2 centre while In Cu1 centre, angles N1 – Cu1 – N2 = 174.85(17) ° and O1 – Cu1 – O3 = 178.86(12)°, as listed in table 4-8. This shows that there is a slight distortion in the octahedral geometry environment of Cu1 centre in complex **7**.

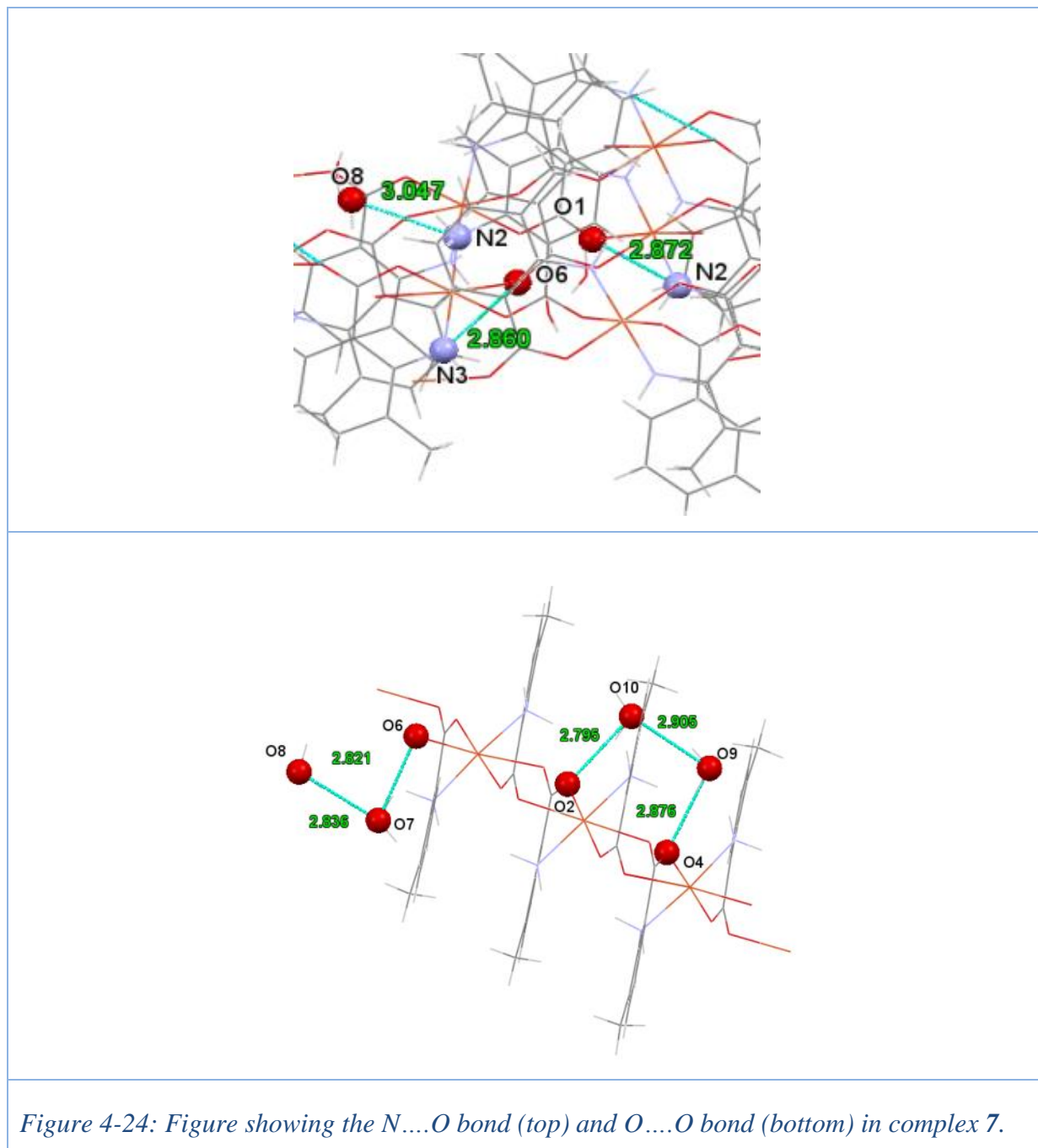
Angle	(°)	Angle	(°)
O1 – Cu1 – N1	88.01(14)	N3 – Cu2 – O4 ⁱ	77.19(13)
O1 – Cu – N2	93.15(14)	N3 – Cu2 – O4	102.81(13)
O3 – Cu1 – N2	85.86(14)	O5 ⁱ – Cu2 – N3	92.38(13)
N1 – Cu1 – N2	174.85(17)	N3 – Cu2 – N3 ⁱ	180.0
O1 – Cu1 – O3	178.86(12)	O4 – Cu2 – O4 ⁱ	180.0
O3 – Cu1 – N1	92.92(14)	O5 ⁱ – Cu2 – N3 ⁱ	87.62(13)
		O5 – Cu2 – O4 ⁱ	94.34(10)

Symmetry code: ⁱ1-x,1-y,1-y

Table 4-8: Selected bond angles of atoms coordinating around Cu²⁺ centre in complex **7**.

There are three types of H-bond in complex **7**. The first H-bond type is between the NH₂ group and the oxygen atom of the lattice water with the distance of N2....O8 = 3.047(5) Å, N1....O2 = 2.872(5) Å, and N3....O6 = 2.860(6) Å. The second type of H-bond is between the carboxylate oxygen atom and the oxygen atom of the lattice water with the distance of O6....O7 = 2.821(5) Å, O4....O9 = 2.876(5) Å, and O2....O10 = 2.796(5) Å. The third type

of H-bond is between the two lattice water molecules with the distance of O7...O8 = 2.836(5) Å and O9...O10 = 2.905(5) Å, as shown in figures 4-24.



4.2.3.3. Structural Characterization of $\{[\text{Cu}(\text{C}_8\text{H}_8\text{NO}_2)_2]_2 \cdot 13/5\text{H}_2\text{O}\}_n$

4.2.3.4. Introduction

As it was observed that increase in the volume of ZnSO_4 in the bimetallic reaction gives rise to morphology changes and crystal behaviour of the crystals obtained in the first part of this experiment, the addition of NiSO_4 also affected the morphology of the crystals obtained.

In the bimetallic crystallization reaction of the aqueous solutions of NaAMB with CuSO_4 and NiSO_4 , a clear green solution of NaAMB_z and Cu_xNi_y gave two different shapes of crystals; needle-shaped crystals and plate-shaped crystals. The plate shape crystal was thin and brown but not a good crystal because there was no diffraction when mounted on the single crystal diffractometer. The needle crystals were thick and had a light greenish blue colour. This produced complex **8**.

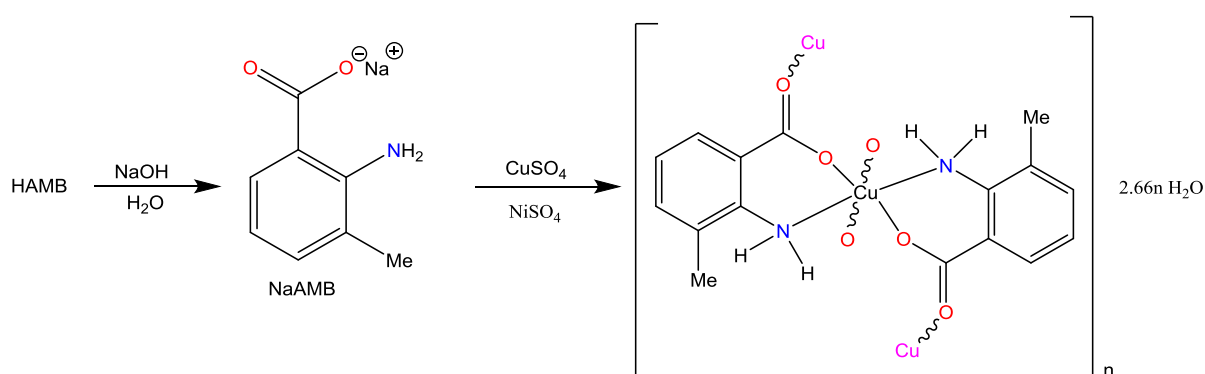


Figure 4-25: Schematic of the reaction that produced complex 8.

When a single crystal of complex **8** was mounted on the diffractometer, the crystal gave some weak diffraction peaks. When processed, the crystal structure obtained is sub-cell and it is three times smaller because the diffraction peaks are weak, sub-cell is great for the carboxylate group and copper because they are not disordered but not good for water which is disordered.

4.2.4.2. Crystal Structure Determination of Complex **8**

The measurement was carried out on an Agilent Supernova Kappa geometry 4-circle diffractometer using the Mo K α radiation, $\lambda = 0.71073 \text{ \AA}$ at 150 K. Complex **8** crystallizes in the monoclinic crystal system with P2₁ space group.

A full list of crystal parameters and structure determination details, a view of the molecular structure of complex **8**, and tables of selected bond lengths and angles are presented below.

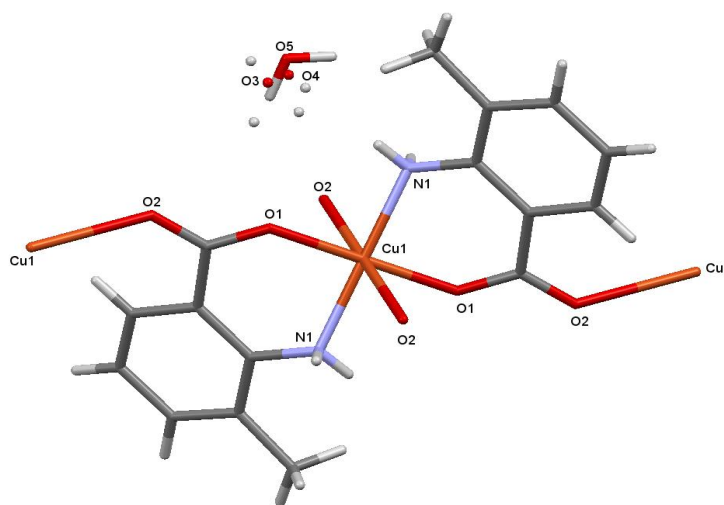
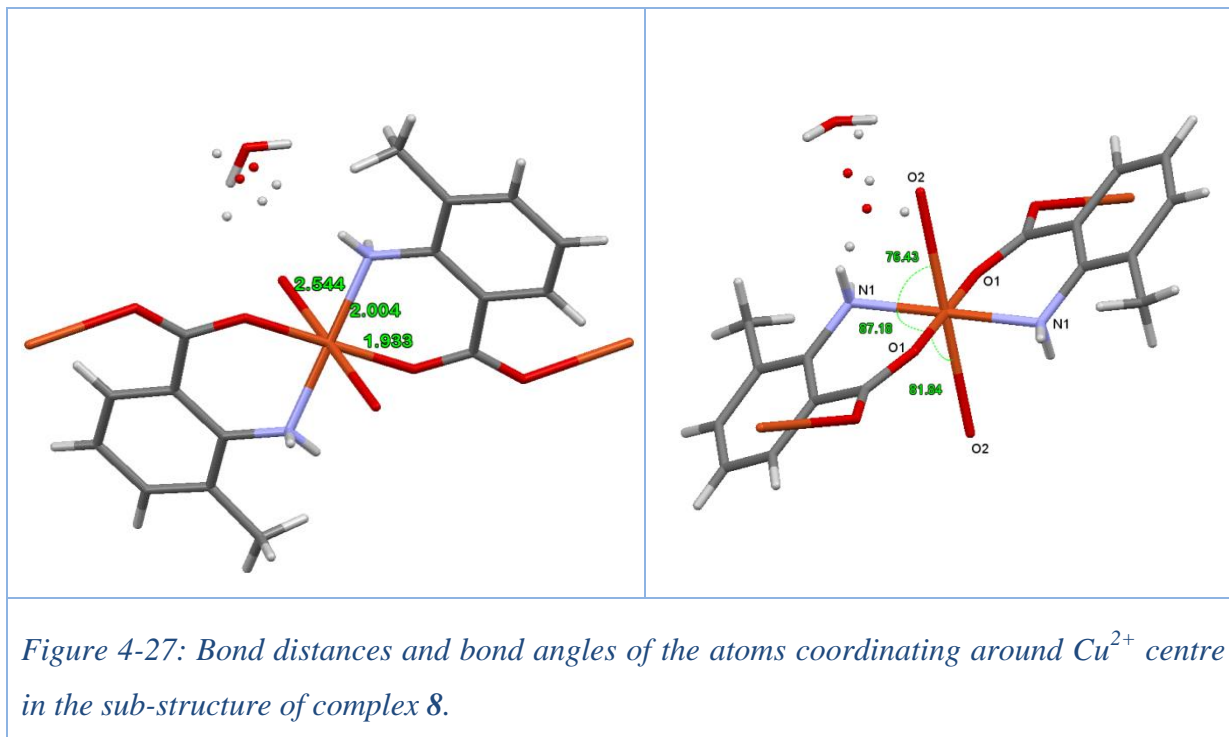


*Figure 4-26: Sub-structure of complex **8** showing the disordered lattice water.*

The sub-structure contains one metal centre bonded to two carboxylate based ligands at the O_{carb} and NH₂ binding site. Also, there is disordered lattice water around the structure, as shown in figure 4-26.

In the sub-structure, the geometric environment of Cu²⁺ centre is octahedral with two equatorial NH₂ groups, two equatorial carboxylate oxygen atoms and two axial carboxylate oxygen atoms with Cu²⁺ sitting on a crystallographic inversion and the atoms coordinating around Cu²⁺ are symmetrical with the distances of Cu1 – O1 = 1.933(8) Å, Cu1 – O2 = 2.544(8) Å and Cu1 – N1 = 2.004(8) Å.

The selected bond distances and angles of the atoms coordinating around Cu^{2+} are shown in figure 4-27 and listed in table 4-9.



Distance	(Å)	Angle	(°)
Cu1 – O1	1.933(8)	O1 ⁱ – Cu1 – N1 ⁱ	87.18(3)
Cu1 – O1 ⁱ	1.933(8)	O1 – Cu1 – N1 ⁱ	92.82(3)
Cu1 – N1	2.004(9)	O1 – Cu1 – O1 ⁱ	180.0
Cu1 – N1 ⁱ	2.004(9)	N1 ⁱ – Cu1 – N1	180.0

Table 4-9: Selected bond distances and angles of atoms coordinating around Cu^{2+} centre in the sub-structure of complex **8**.

It is possible to choose a small cell ($Z = 2$) if the water position is modeled as disordered. Choice of a larger cell ($Z = 10$) allows the non-disordered model to be refined, as shown in figure 4-28. This revealed the real structure of complex **8**.

The full structure of complex **8** contains five crystallographically independent Cu centres, Cu1 to Cu5 with three bidentate ligands binding to each metal centres at the carboxylate oxygen atom and NH₂ binding sites on each ring.

Like the two other hydrate CuAMB complexes **6** and **7** and the three determinations of anhydrous CuAMB complexes obtained in the reaction series, complex **8** is a layered structure in which octahedral Cu²⁺ coordinates to an AMB surrounded with thirteen lattice water molecules, as shown in figure 4-28.

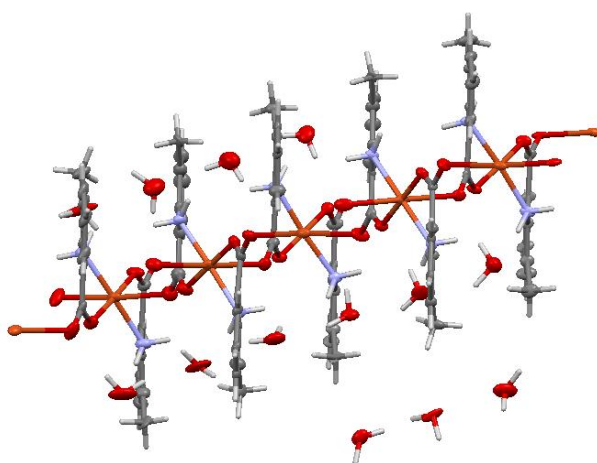


Figure 4-28: Full structure of complex 8 showing that the lattice water is not disordered.

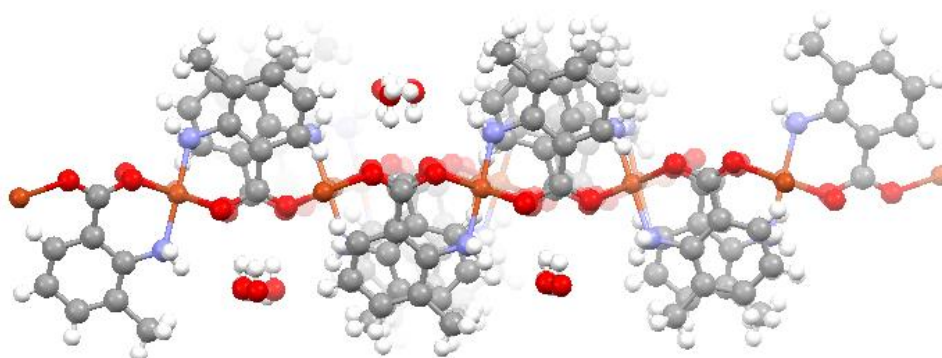


Figure 4-29: Expansion network of complex 8 showing the water filling channels in the zigzag layer.

When expanded, it built a 2D network of CuAMB with molecules of water appearing in the structure in the form of a channel, as shown in figures 4-30 and 4-31.

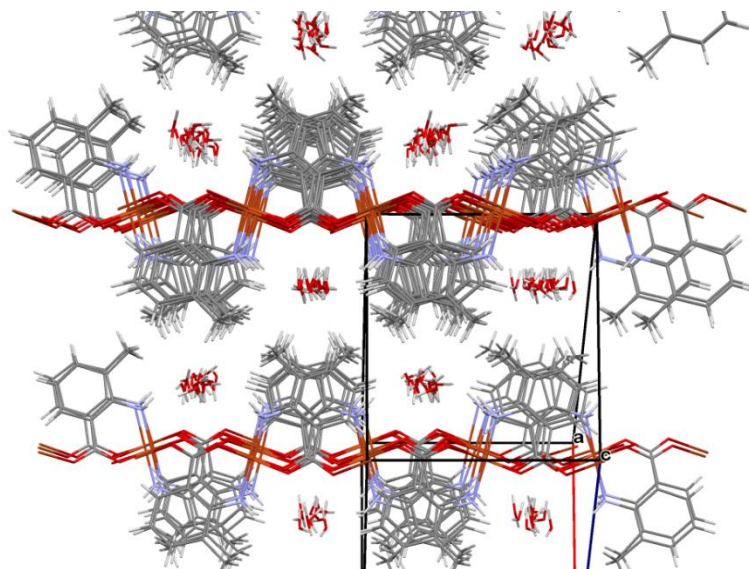


Figure 4-30: View of complex 8 looking parallel to the planes and the H-bonded lattice water chains.

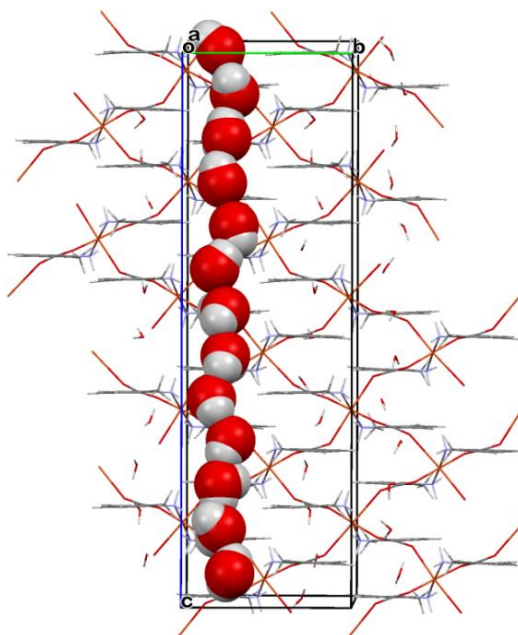


Figure 4-31: View of a single layer of complex 8, with lattice water in one channel highlighted.

Empirical Formula	$\{[\text{Cu}(\text{C}_8\text{H}_8\text{NO}_2)_2]_2 \cdot \frac{13}{5} \text{H}_2\text{O}\}_n$
Formula Weight	2053.44
Temperature (K)	150
Crystal System	Monoclinic
Space group	$P2_1$
a (Å)	11.8279(17)
b (Å)	10.3620(14)
c (Å)	33.691(4)
β (°)	93.305(12)
Volume (Å ³)	4122.4(10)
Z	2
D_x (Mg m ⁻³)	1.654
μ (mm ⁻¹)	1.366
F(000)	2130.0
Crystal size (mm)	0.18 × 0.06 × 0.04
Crystal Shape	Block, blue
R factor (%)	8.38

Table 4-10: Crystal data collection of the full structure of complex 8.

Complex **8** consists of five crystallographically independent Cu centres with the octahedral geometric environment. For example, the Cu – N bond distances in the five metal centres are different. Distances Cu1 – N1 = 1.994(3) Å and Cu1 – N2 = 1.983(3) Å, likewise distances Cu2 – N3 = 1.989(2) Å and Cu2 – N4 = 2.017(3) Å. Their differences in four out of the five metal centres are significant by an experimental error while their distances in Cu3 centre is close with the distances of Cu3 – N5 = 2.002(3) Å and Cu3 – N6 = 2.003(3) Å.

The bond distances of the atoms coordinating around the five Cu centres in complex **8** are listed in table 4-11.

Distance	(Å)	Distance	(Å)
Cu1 – N1	1.994(3)	Cu4 – N7	2.025(3)
Cu1 – N2	1.984(3)	Cu4 – N8	1.984(3)
Cu1 – O1	1.949(2)	Cu4 – O13	1.899(3)
Cu2 – N3	1.989(2)	Cu4 – O15	1.947(3)
Cu2 – N4	2.017(3)	Cu5 – N9	2.010(3)
Cu2 – O2	2.438(2)	Cu5 – N10	2.037(3)
Cu2 – O5	1.935(2)	Cu5 – O16	2.412(3)
Cu2 – O7	1.942(2)	Cu5 – O17	1.950(3)
Cu3 – N5	2.001(3)	Cu5 – O19	1.944(3)
Cu3 – N6	2.003(3)		
Cu3 – O9	1.912(2)		
Cu3 – O11	1.938(2)		

Table 4-11: Selected bond distances of atoms coordinating around Cu²⁺ centres in complex 8.

The carboxylate oxygen atoms are coordinated to each of the Cu centres in *anti-anti* bidentate coordination mode which give rise to the 2D grid of 16-membered rings. In most of the cases, the bond distances of the Cu centre with the axial carboxylate oxygen atoms is longer than that of the equatorial carboxylate oxygen atoms, as listed in table 4-11. This causes slight distortion in the octahedral geometric environment of the Cu centre due to Jahn-Teller effect and results to the significant difference between the C – O bonds of the carboxylate group in a way that when Cu – O bond is short, the C – O bonds are longer and vice versa. Therefore, the long Cu – O bond correlates with the short C – O bond, as shown in figure 4-32 and listed in table 4-12.

Distance	(Å)	Distance	(Å)
O1 – C7	1.277(4)	O11 – C47	1.313(4)
O2 – C7	1.219(4)	O12 – C47	1.244(5)
O3 – C15	1.292(4)	O13 – C55	1.260(5)
O4 – C15	1.227(4)	O14 – C55	1.238(5)
O5 – C23	1.302(4)	O15 – C63	1.297(5)
O6 – C23	1.213(4)	O16 – C63	1.241(5)
O7 – C31	1.285(4)	O17 – C71	1.279(5)
O8 – C31	1.242(4)	O18 – C71	1.225(5)
O9 – C39	1.271(4)	O19 – C79	1.292(5)
O10 – C39	1.248(8)	O20 – C79	1.233(5)

Table 4-12: C – O bond distances in complex 8.

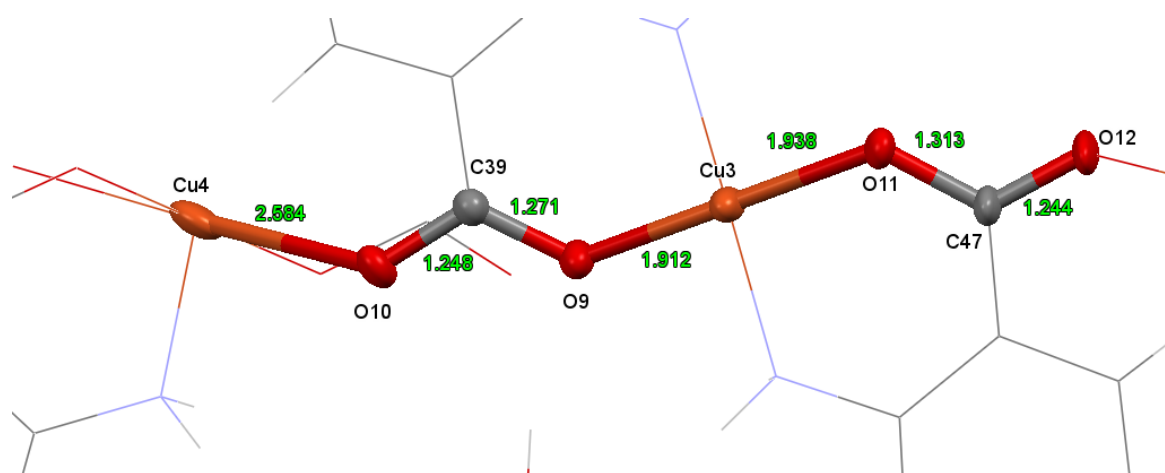


Figure 4-32: Figure supporting that short Cu – O bonds correlates with long C – O bonds in complex 8.

The Cu – Cu distances in the full structure are different along and across the structure in a way that the distances of Cu1 – Cu2 = 6.569(1) Å, Cu2 – Cu3 = 6.172(1) Å, Cu3 – Cu4 = 6.224(1) Å, Cu4 – Cu5 = 6.177(1) Å, Cu5 – Cu5 = 6.366(1) Å and Cu1 – Cu1 = 6.286(9) Å, as shown in figure 4-33.

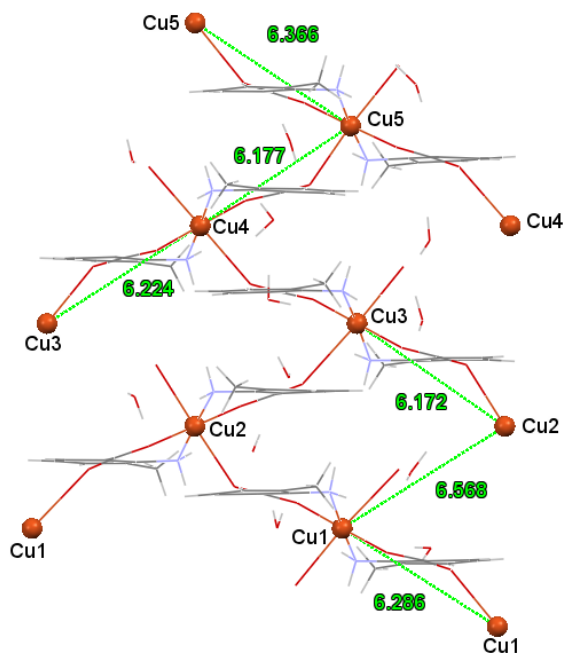


Figure 4-33: Figure showing Cu – Cu distances in complex **8**.

All the Cu – Cu values were compared with those of the published 2D structure deposited in the database as **PONLEJ** in which the magnetic coupling was measured and strong antiferromagnetic coupling was found at Cu – Cu distances of 5.2 Å and 6.9 Å while in complex **8**, Cu – Cu distances range from 6.172(1) Å to 6.569(1) Å. This is not likely to be more weakly coupled.¹⁸

The bond angle shows that there is slight distortion in the octahedral environment of Cu²⁺ in a way that bond angle O – Cu – O are different in each of the Cu centres. At Cu1 centre, angle O3 – Cu1 – O6 = 77.50(8) °, at Cu2 centre, angle O2 – Cu2 – O7 = 84.85(8) °, at Cu3 centre, angle O9 – Cu3 – O8 = 78.97(9) °, at Cu4 centre, angle O10 – Cu4 – O15 = 81.37(9) ° and at the Cu5 centre, angle O19 – Cu5 – O18 = 79.17(9) °. The *trans* angles in all the five Cu centres are in the ranges of 174.86(11) ° and 179.67(10) °, as listed in table 4-13.

Angle	(°)	Angle	(°)
O3 – Cu1 – O6	77.50(8)	O9 – Cu3 – O8	78.97(9)
O6 – Cu1 – N1	74.19(9)	O8 – Cu3 – N6	72.91(9)
N1 – Cu1 – O1	85.2(1)	N5 – Cu3 – N6	174.86(11)
O1 – Cu1 – O4	83.65(8)	O9 – Cu3 – O11	179.67(10)
O4 – Cu1 – N2	78.15(9)	O10 – Cu4 – O15	81.37(9)
N2 – Cu1 – O3	88.7(1)	O15 – Cu4 – N8	87.0(1)
N2 – Cu1 – N1	175.62(11)	N8 – Cu4 – O20	73.64(9)
O3 – Cu1 – O1	178.17(9)	O20 – Cu4 – O13	80.89(9)
O2 – Cu2 – O7	84.85(8)	O13 – Cu4 – N7	87.0(1)
O7 – Cu2 – N4	86.4(1)	N7 – Cu4 – O10	76.86(9)
N4 – Cu2 – O12	77.3(1)	N8 – Cu4 – N7	177.98(12)
O12 – Cu2 – O5	86.30(9)	O13 – Cu4 – O15	179.34(11)
O5 – Cu2 – N3	88.22(9)	N10 – Cu5 – O19	87.1(1)
N3 – Cu2 – O2	76.28(9)	O19 – Cu5 – O18	79.17(9)
N3 – Cu2 – N4	178.04(13)	O18 – Cu5 – N9	73.1(1)
N4 – Cu2 – O2	102.63(10)	N9 – Cu5 – O17	87.5(1)
N6 – Cu3 – O11	86.4(1)	O17 – Cu5 – O16	86.0(1)
O11 – Cu3 – O14	83.14(9)	O16 – Cu5 – N10	77.1(1)
O14 – Cu3 – N5	78.7(1)	N9 – Cu5 – N10	176.69(13)
N5 – Cu3 – O9	88.1(1)	N9 – Cu5 – O16	105.98(10)

Table 4-13: Selected bond angles of atom coordinating around the Cu²⁺ centres in complex 8.

In complex **8**, there is H-bonds between NH₂ groups and O_{water} (lattice water molecule). These H-bonds are represented with turquoise dotted lines with distances N8....O29 = 3.048(4) Å and N9....O30 = 3.053(4) Å respectively, as shown in figure 4-34.

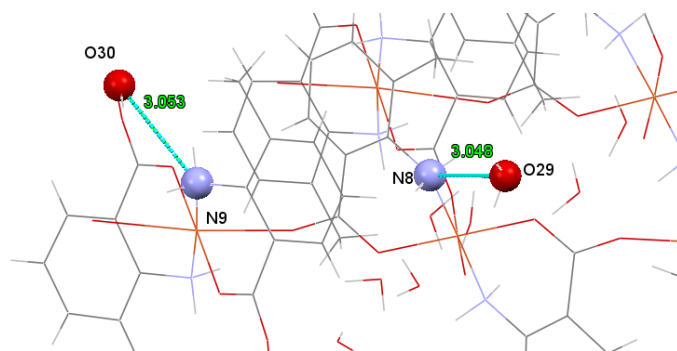


Figure 4-34: The H-bond between N...O is 3.053 Å and 3.048 Å in complex **8**.

The full structure of complex **8** is composed of a 16-membered rings unit. Four Cu centres are bridged by four carboxylate groups in a way that each Cu is a node of the 2-dimensional grid which has a zigzag conformation, as shown in figure 4-35.

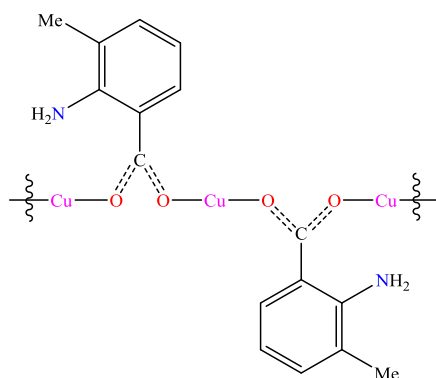


Figure 4-35: Fragment of the coordination of ligands to metal showing the zigzag conformation in complex **8**.

The three different types of hydrate CuAMB complexes **6**, **7** and **8** were obtained by either slow evaporation of the aqueous solution NaAMB with Cu or the bimetallic solution of NaAMB with Cu/Zn or Cu/Co or in solution respectively. Their data were collected at a lower temperature of 150 K. The three hydrates CuAMB complexes crystallize in the monoclinic crystal system with space groups $P2_1/c$, $P2_1/n$, and $P2_1$ respectively, as shown in table 4-14.

	6	7	8
Emp. Formulae	$[\text{Cu}(\text{C}_8\text{H}_8\text{NO}_2)_2\text{H}_2\text{O}]_2$	$\{[\text{Cu}(\text{C}_8\text{H}_8\text{NO}_2)_2]_2 \cdot \frac{8}{3}\text{H}_2\text{O}\}_n$	$\{[\text{Cu}(\text{C}_8\text{H}_8\text{NO}_2)_2]_2 \cdot \frac{13}{5}\text{H}_2\text{O}\}_n$
Form. Weight	381.86	1235.67	2053.44
Temperature (K)	150	150	150
Crystal System	Monoclinic	Monoclinic	Monoclinic
Space group	$P2_1/c$	$P2_1/n$	$P2_1$
a (Å)	7.7416(9)	11.8753(9)	11.8279(17)
b (Å)	7.141(1)	10.3363(7)	10.3620(14)
c (Å)	26.662(3)	20.4429(16)	33.691(4)
β (°)	93.904(10)	98.928(7)	93.305(12)
Volume (Å ³)	1470.5(3)	2478.9(3)	4122.4(10)
Z	4	2	2
D_x (Mg m ⁻³)	1.725	1.655	1.654
μ (mm ⁻¹)	1.52	1.36	1.37
F(000)	788.0	1282	2130
Crystal size (mm)	0.14 × 0.03 × 0.03	0.33 × 0.25 × 0.02	0.18 × 0.06 × 0.04
Crystal Shape	Needle, Blue	Plate, Blue	Block, Blue
R factor (%)	10.41	6.08	8.38

Table 4-14: Table comparing the crystal data collection of the hydrated CuAMB complexes 6, 7 and 8.

The volume of complex **7** is almost twice of the volume of complex **6** and the full structure of complex **8** is approximately twice that of complex **7** and the unit cell is five times bigger and contains ten $\text{Cu}(\text{AMB})_2$. The cell in complex **7** is three times the volume of the complex **8** subcells and contains six $\text{Cu}(\text{AMB})_2$ units. The main crystallographic differences are caused by the different amounts of lattice water molecules filling the channels in the zigzag layers.

These experiments were carried out to study the effect of varying the Cu/Zn ratios and to understand the Cu/Zn or Cu/Co ratios which gave us the anhydrous layered structures, the hydrated layered structures, and the dimer. No incorporation of Zn would disrupt 2D lattice because Zn is a weaker Lewis acid than Cu, so, Cu is preferred. Therefore, the conditions needed to form the novel lamellar coordination polymer, complex **8** in which the narrow

channels that span the crystal lattice single file H-bonded chains of lattice water shown in figures 4-30 and 4-31 was identified in this session.¹²⁷

The coordination environment of Cu^{2+} in the two hydrated CuAMB complexes **7** and **8** can be compared with those in the structure of bis(ortho-aminobenzoato)copper(II), $\text{Cu}(\text{H}_2\text{NC}_6\text{H}_4\text{COO})_2$ which has been studied to a high standard and deposited in the Cambridge Crystallographic Database as **OABZCU**.

Though their starting materials are different, they crystallize in the same crystal system. **OABZCU** was prepared from the diffusion of the aqueous solution of copper sulfate and the sodium salt of *ortho*-aminobenzoic acid over two months while complexes **7** and **8** were prepared from the bimetallic crystallization reaction of aqueous NaAMB with $\text{CuSO}_4 / \text{ZnSO}_4$ for complex **7** and NaAMB with $\text{CuSO}_4 / \text{NiSO}_4$ for complex **8**.¹²⁸

The coordination environment of Cu^{2+} is distorted octahedral in all the structures. In **OABZCU**, the distorted octahedron environment of Cu^{2+} comprises of four equatorial positions occupied by two nitrogen atoms and two carboxylate oxygen atoms from different ligands, in *trans* orientation. This is completed by two axial carboxylate oxygen atoms in *trans* orientation, as shown in figure 4-36. The same geometric coordination mode found in complexes **7** and **8** save for the coordinated and uncoordinated water molecules in the hydrate structures and the absence of the methyl group in **OABZCU**.¹²⁸

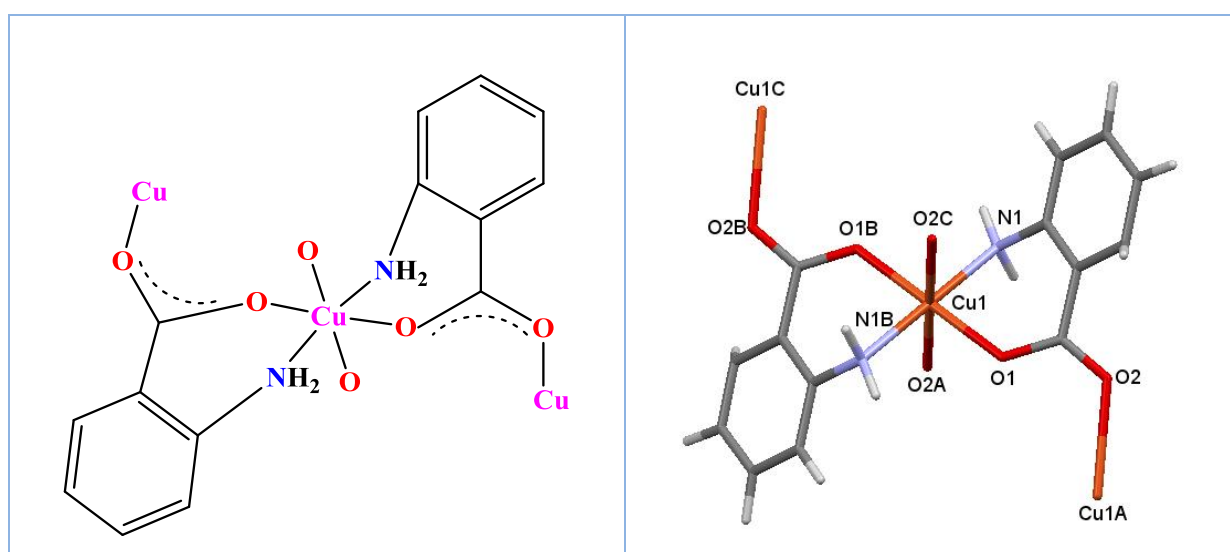


Figure 4-36: ChemSketch and molecular structure of **OABZCU**.¹²⁸

In **OABZCU**, the ligands are related by symmetry at the Cu centre. Each *ortho*-aminobenzoate group acted as a tridentate ligand binding to different Cu centres. The amino nitrogen atom of the NH₂ group, N1 and the carboxylate oxygen atom, O1 coordinate to Cu centre equatorially in the *cis* orientation while the distorted octahedron geometric of the Cu centre was completed with two axial carboxylate oxygen atoms, O2 from a different *ortho*-aminobenzoate ligand. Four *ortho*-aminobenzoate ligands attached to each of the Cu atoms making each Cu²⁺ attached to the other four Cu atoms through a carboxylate bridge to give a two-dimensional polymeric sheet. In this structure, H-bonding occurs between the amino nitrogen, N1, and the carbonyl oxygen, O2 in an adjacent molecule.¹²⁸

In **OABZCU**, the bond distances of Cu – O1 = 1.973(5) Å, Cu – O2 = 2.415(5) Å and Cu – N1 = 2.024(7) Å and bond angles listed in table 4-15 are similar to those that coordinated around Cu centre in complexes **7** and **8**.

Distance	(Å)	Angle	(°)
Cu – O1	1.973(5)	O1 – Cu – N1	87.1(2)
Cu...O2b	2.415(5)	O1 – Cu...O2b	89.4(2)
Cu – N1	2.024(7)	O2 – Cu – N1	93.8(2)
C1 – O1	1.276(8)	O1 – C1 – O2	123.1(7)
C1 – O2	1.244(8)		

Table 4-15: Bond distances and angles of atoms coordination around Cu²⁺ centre and the C – O distances in **OABZCU**.¹¹⁹

In complex **8**, there are two types of intramolecular H-bonds. The first type of H-bond is between N atom of the NH₂ group and the carboxylate oxygen atom. The second type of H-bond is between the N atom of the NH₂ group and the O atom of the lattice water while in **OABZCU**; there are intermolecular H-bonds between the N atom of the NH₂ group and the O atom of the carboxylate group attached to the same metal centre.

4.2.5. Reactive Crystallization of Anhydrous ZnAMB $[\text{Zn}(\text{C}_8\text{H}_8\text{NO}_2)_2]_n$

4.2.5.1. Introduction

Like the crystallization reaction that produced CuAMB complexes, previous studies have shown that single crystals of ZnAMB were prepared by diffusion of aqueous solutions of zinc nitrate and sodium 2-amino-3-methyl benzoate in ratio 1:2 over a period of six weeks. The expected bis complex was not formed instead the structure of $[\text{Zn}(\text{OH})\text{C}_8\text{H}_8\text{NO}_2]$ was obtained and was deposited in the Cambridge Crystallographic Database as VOSSAX.¹¹³

In this study, one ZnAMB complex $[\text{Zn}(\text{C}_8\text{H}_8\text{NO}_2)_2]_n$ and an identical structure of VOSSAX was obtained.

4.2.5.2. Structural Characterization of Anhydrous ZnAMB $[\text{Zn}(\text{C}_8\text{H}_8\text{NO}_2)_2]_n$

4.2.5.3. Introduction

In the aqueous solution of the reactive crystallization of Zn and NaAMB in the molar ratio 1:2 as shown in figure 4-37, single crystals of complex **9** were seen floating on the surface after five days.

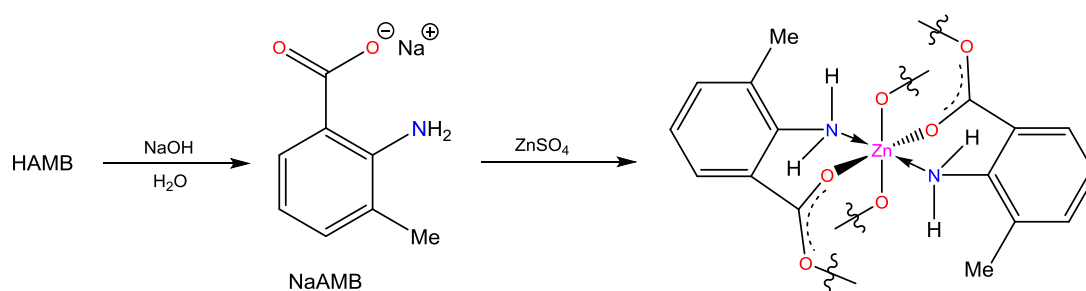


Figure 4-37: Schematic of the reaction that produced complex **9**.

4.2.5.4. Crystal Structure Determination of Complex **9**

The measurement was carried out on an Oxford diffraction Xcalibur2 equipped with a Sapphire2 detector using Mo K α radiation, $\lambda = 0.71073 \text{ \AA}$ at 150 K. Complex **9** crystallizes in the monoclinic crystal system and P2₁/c space group.

A full list of crystal parameters and structure determination details, a view of the molecular structures, tables of selected bond lengths and angles of complex **9** are presented below.

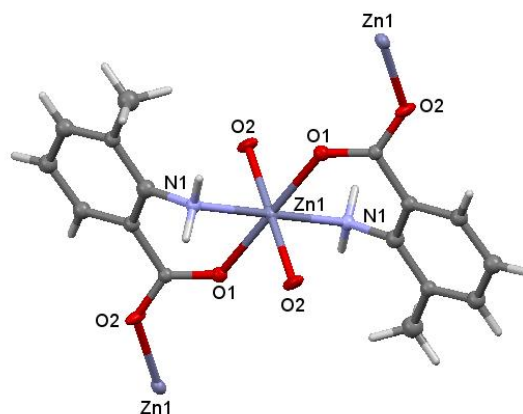


Figure 4-38: Molecular structure of complex 9.

The coordination environment of Zn^{2+} in complex **9** is octahedral. Each ligand coordinates to a Zn in a bidentate fashion via NH_2 , and a carboxylate oxygen atom. The second carboxylate oxygen atom coordinates to another Zn, forming a bridge, as shown in figure 4-38.

When expanded, like the anhydrous $[\text{CuAMB}]_n$ structures, it forms a layered structure in a way that the octahedral Zn^{2+} coordinates to an AMB, as shown in figure 4-39.

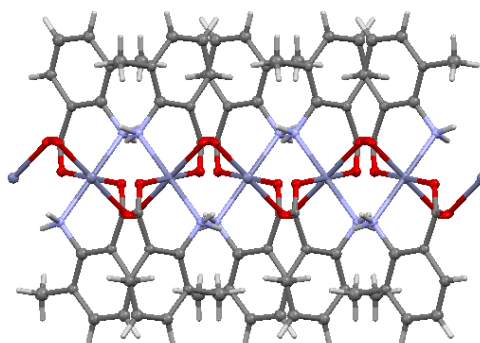


Figure 4-39: Polymeric expansion of complex 9 viewed down the crystallographic c axis and flipped by 90 ° around the axis.

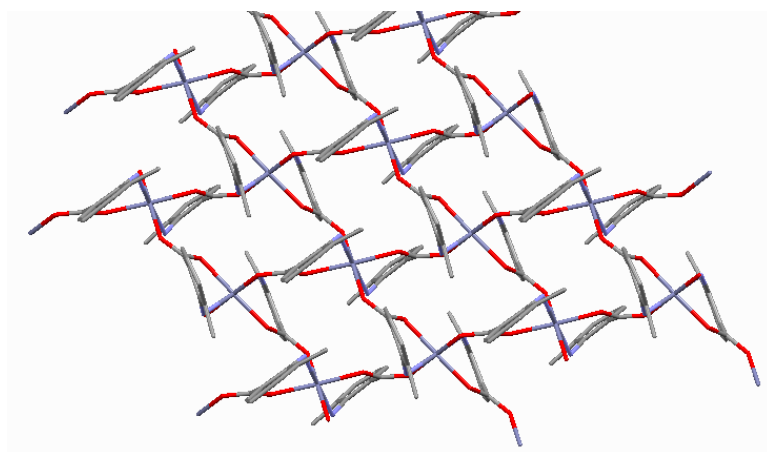
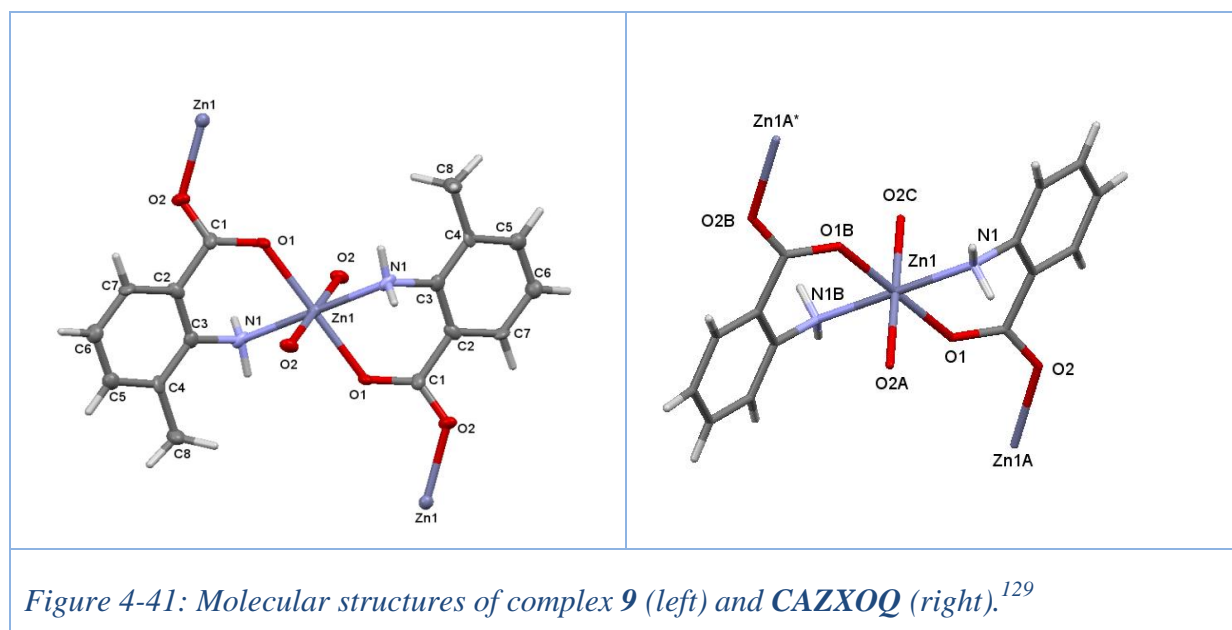


Figure 4-40: Figure showing the mode of association in complex **9**.

Complex **9** is a novel structure of high quality and could not be matched with any known structure in the Cambridge Crystallographic Database. However, the un-methylated analogue, bis(*ortho*-aminobenzoato)zinc(II) has been reported previously and deposited into the Cambridge Crystallographic Database as **CAZXOQ**. The two Zn^{2+} complexes were prepared using different starting materials and different crystallization methods. Single crystals of **CAZXOQ** were prepared by reactive diffusion between solutions of zinc acetate and sodium anthranilate while single crystals of complex **9** were prepared by reactive crystallization of aqueous solution of zinc sulfate and sodium 2-amino-3-methyl benzoic acid.¹²⁹

Comparing the two Zn^{2+} complexes side by side, the coordination environment of Zn^{2+} in the two complexes is octahedral. In **CAZXOQ**, Zn^{2+} occupies an octahedral site with bidentate anthranilate binding via one of its carboxylate oxygen atoms and NH_2 . Those are mutually *trans*. The remaining two *trans* coordination sites are filled by inter-molecular coordination bonds via the other carboxylate oxygen atom, as shown in figure 4-41. In these features, the structures of complex **9**, **CAZXOQ** and complexes **7** and **8** are identical. They differ, however in the details of crystal packing.

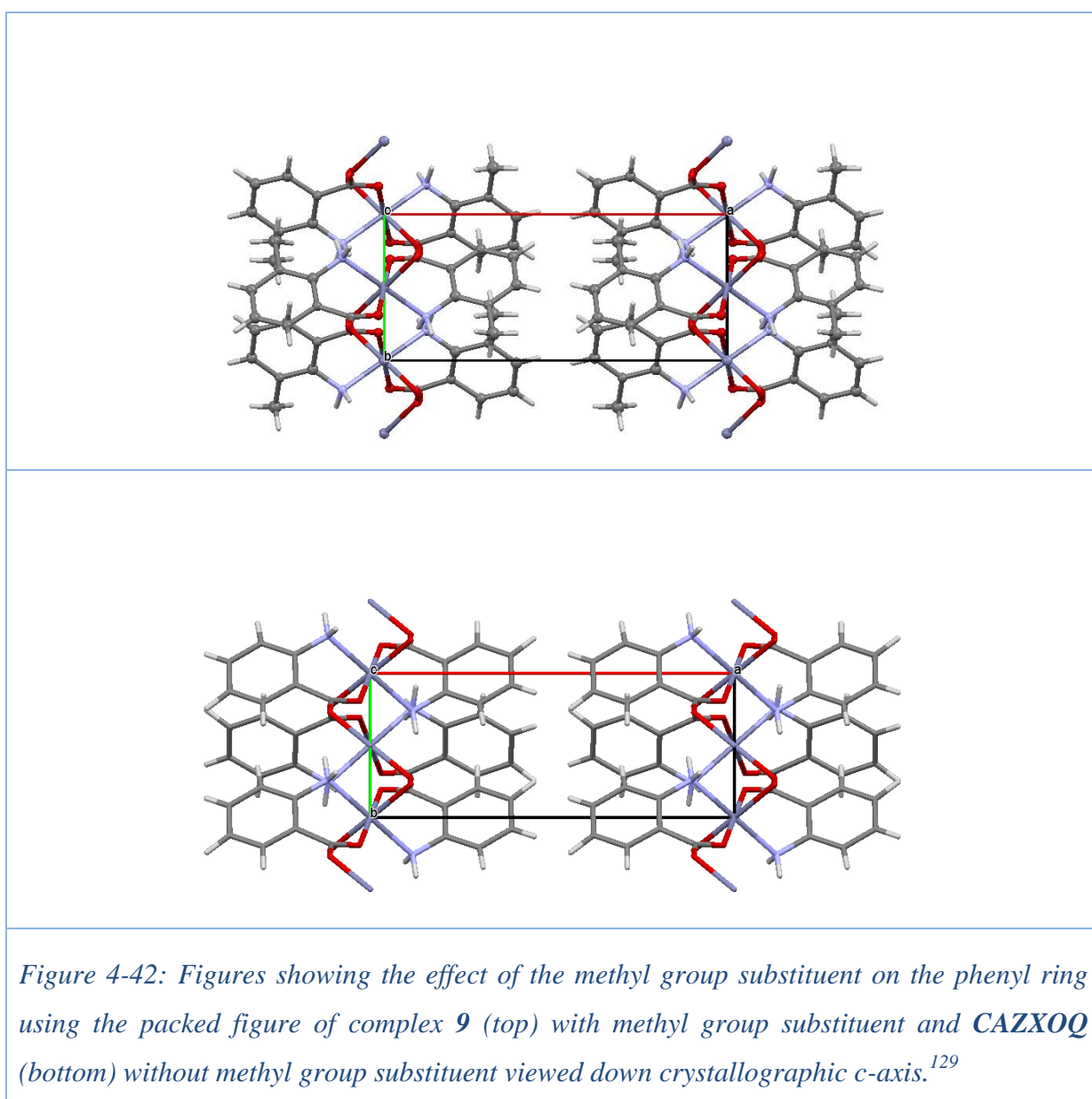


	9	CAZXOQ
Emp. Form.	[Zn(C ₈ H ₈ NO ₂) ₂] _n	[Zn(C ₁₄ H ₁₂ N ₂ O ₄)]
Form. weight	365.68	337.6
Temperature (K)	150	150
Crystal System	Monoclinic	Monoclinic
Space group	P2 ₁ /c	P2 ₁ /c
<i>a</i> (Å)	14.032(3)	13.938(2)
<i>b</i> (Å)	5.6455(14)	5.207(1)
<i>c</i> (Å)	9.580(2)	9.346(1)
β (°)	109.36(3)	108.37(1)
Volume (Å ³)	716.0(3)	643.7(2)
Z	2	2
D _x (Mg m ⁻³)	1.696	1.74
μ (mm ⁻¹)	1.74	19.8 cm ⁻¹
F(000)	376	344
Crystal size (mm)	0.2 x 0.06 x 0.02	0.45 x 0.50 x 0.04
Crystal Shape	Trapezoid, colourless	Flat parallelepipeds, light tan
R factor (%)	0.153	0.047

Table 4-16: Crystal and refinement data collection of the two Zn²⁺ complexes.¹²⁹

The two Zn^{2+} complexes are essentially isostructural and isomorphous save for the presence of an additional methyl group in complex **9** which affects the packing in complex **9** as shown in figure 4-42. The two Zn^{2+} complexes crystallize in the monoclinic crystal system and $P2_1/c$ space group. Also, their data were collected at 150 K, as listed in table 4-16.

As shown in figure 4-42 and table 4-17, the presence of the methyl group in complex **9** causes an expansion of the cell along b from 5.2 Å to 5.6 Å. A slightly smaller expansion along c (from 9.3 Å to 9.6 Å) was also found, while a dimension is essentially unchanged.



In the two complexes, Zn^{2+} sits on a crystallographic inversion centre, as their pairs of bonds are related by symmetry. In complex **9**, the distances of $Zn1 - O1 = 2.135(4)$ Å, $Zn1 - O2 = 2.113(5)$ Å and $Zn1 - N1 = 2.128(6)$ Å. These values are well within the ranges of $Zn - O = (1.97 \text{ Å} - 2.26 \text{ Å})$ and $Zn - N = (1.99 \text{ Å} - 2.15 \text{ Å})$ in previous studies.¹²⁹

Looking critically at the geometry around Zn^{2+} in both Zn^{2+} complexes, there is a very slight distortion in their geometric environment which is not due to the Jahn-Teller effect.

In the two Zn^{2+} complexes, the carboxylate groups are coordinated to Zn centres in *syn-anti* coordination mode in a way that the short C – O distance correlates with the long Zn – O distance and *vice versa*.

Pairs of angles in the two structures are related by symmetry as Zn^{2+} sits on a crystallographic inversion centre. In complex **9**, angles $N1 - Zn1 - O1 = 82.69(1)^\circ$, $O2 - Zn1 - O1 = 86.6(2)^\circ$ and $N1 - Zn1 - O2 = 91.6(2)^\circ$ as compared to that of **CAZXOQ** as listed in table 4-17.

	9	CAZXOQ
Distance	(Å)	(Å)
Zn – O1	2.135(4)	2.066(3)
Zn – O2	2.113(5)	2.145(4)
Zn – N1	2.128(6)	2.166(4)
O1 – C7	1.256(8)	1.262(9)
N1 – C3	1.447(9)	1.447(9)
Angle	(°)	(°)
O1 – Zn – N1	82.7(2)	84.3(2)
O2 – Zn – N1	91.6(2)	89.3(2)
O1 – Zn – O2	93.44(18)	90.0(1)
O1 – Zn \cdots O2	176(2)	

Table 4-17: Selected bond distances and angles of atoms coordinating around Zn^{2+} in the two Zn^{2+} complexes.¹²⁹

The structure of complex **9** is similar to one of the hydrated CuAMB complex **8** if the water channel is absent. They have the same basic square grid, as shown in figure 4-43 however, the detailed supramolecular arrangement differs.

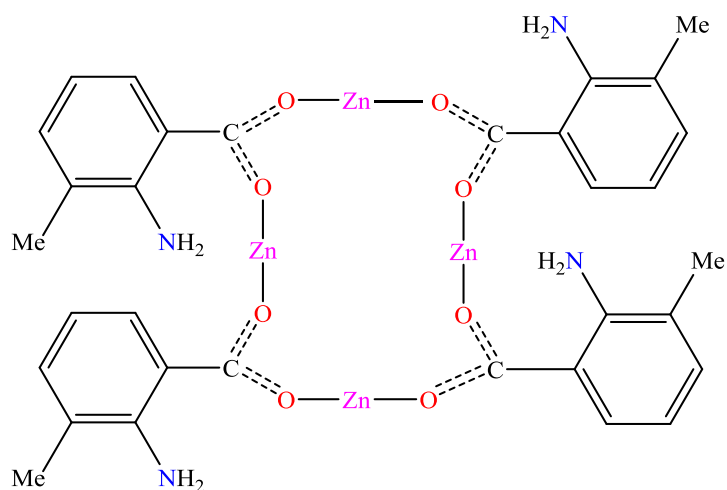


*Figure 4-43: Figure showing the square grid conformation in the hydrate CuAMB complex **8** and ZnAMB complex **9**.*

Also, complex **9** was compared with the three determinations of anhydrous CuAMB obtained in this study. Despite the identical stoichiometry save for the identity of the metal, the structures of the anhydrous $[\text{Zn}(\text{AMB})_2]_n$ and $[\text{Cu}(\text{AMB})_2]_n$ are different in detail. The Zn case more closely resembles the 2D packing arrangement in the hydrate CuAMB complex **8**. Cu was down – down – up – up (channels) while Zn was up – down – up – down (even penetration), as shown in figure 4-44.

In the case of anhydrous $[\text{Zn}(\text{AMB})_2]_n$, complex **9** and the three determinations of $[\text{Cu}(\text{AMB})_2]_n$, complexes **5a**, **5b**, and **5c**, there is a much smaller range of metal-oxygen distances than in the hydrated CuAMB complex **8**.

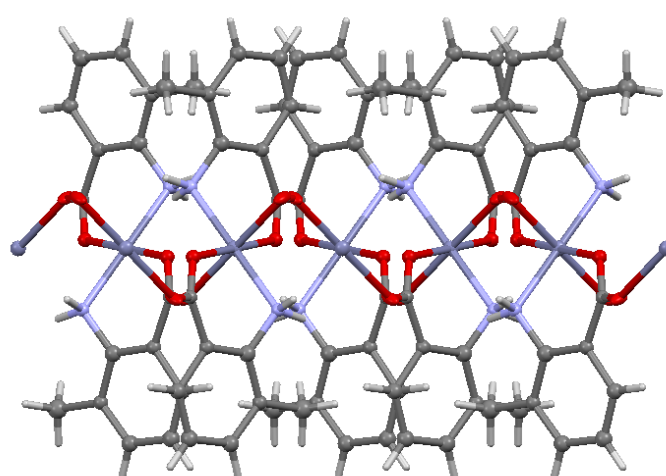
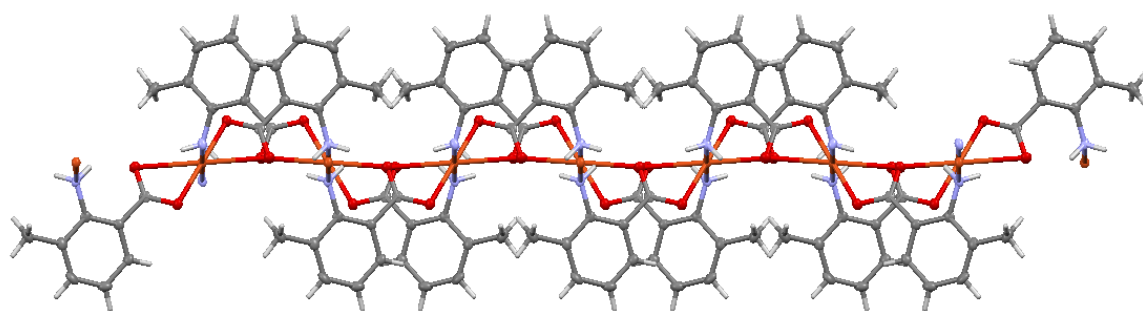


Figure 4-44: Figures showing the similarity between hydrated CuAMB complex **8** (top) and the anhydrous ZnAMB complex **9** (bottom).

There are similar cases of H-bonding in complex **9** and **CAZXOQ**. H-bond occurs between the amine group, N1 and two adjacent *trans* carboxylate oxygen atoms, O1 and O2. These H-bondings provides additional crosslinking in the molecule, making the structure more stable.

In complex **9**, the distances of N1...O1 = 2.897(1) Å and N1...O2 = 3.046(1) Å with the angle of N1 – H1B – O1 = 145.98 °. While in **CAZXOQ**, the distances of N1...O1 = 2.953 Å and N1B...O2 = 3.066 Å with angle N1B – H2B – O1B = 146.39 °, as represented by a turquoise dotted line in figures 4-45.

These bond distances fall within the normal range found for H-bonding formed between the N atom of the amine groups and O_{carb} in previous works which ranges between 2.57 Å – 3.22 Å as suggested by C. Janiak⁶⁸ and support by S. Alvarez.¹²⁵

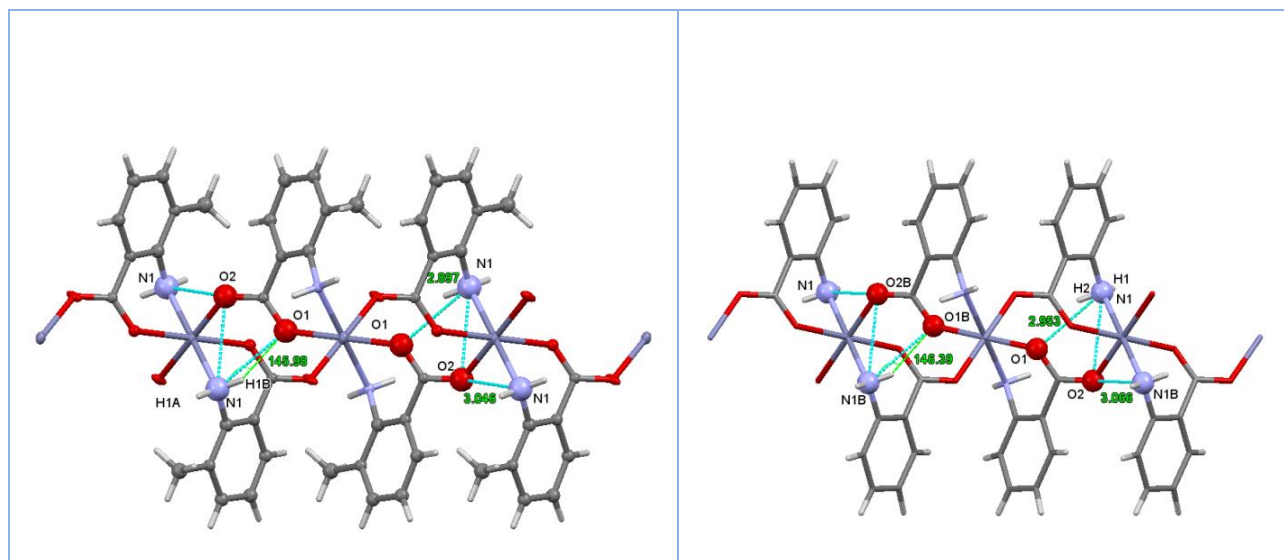
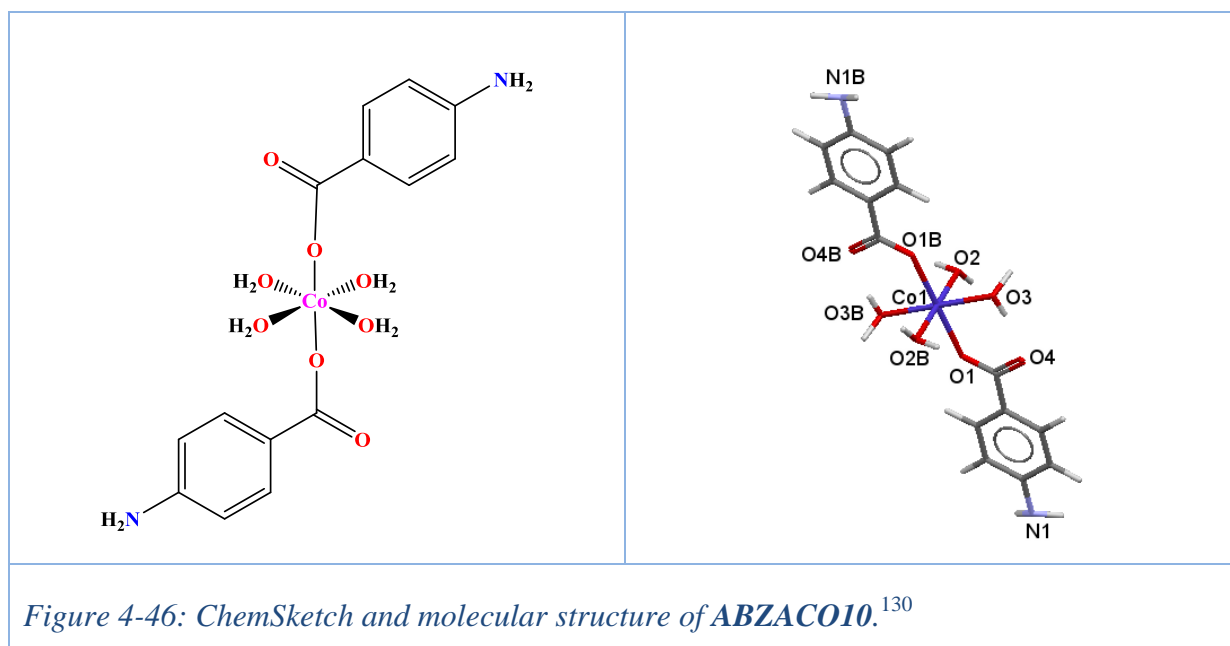


Figure 4-45: Figure showing N...O distances in complex **9** (left) and **CAZXOQ** (right).¹²⁹

4.2.6. Reactive Crystallization and Crystal Structure of Novel Anhydrous and Hydrated CoAMB $[\text{Co}(\text{C}_8\text{H}_8\text{NO}_2)_2]_n$ and $\{[\text{Co}(\text{C}_8\text{H}_8\text{NO}_2)_2]\cdot\text{H}_2\text{O}\}_n$

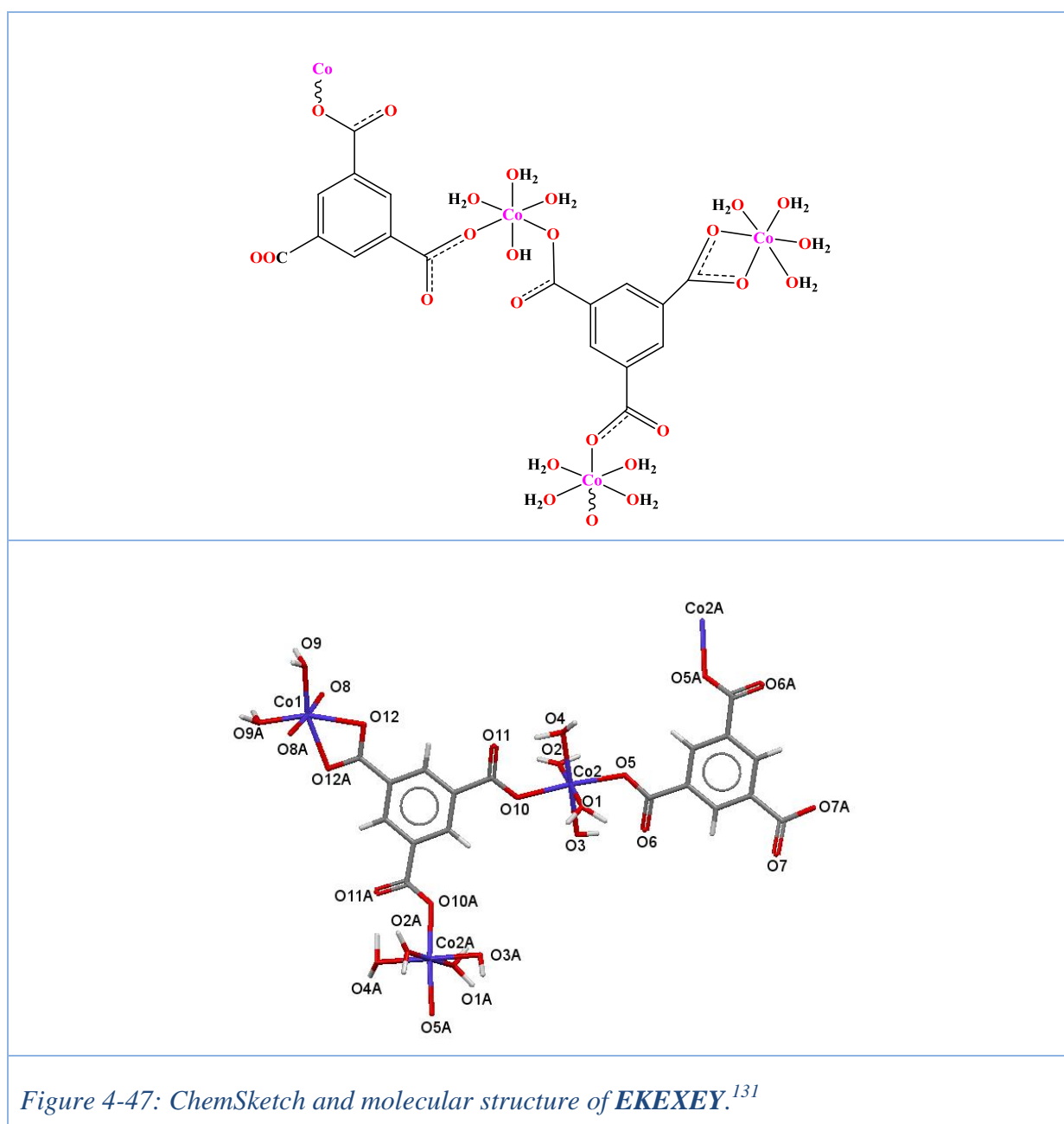
4.2.6.1. Introduction

The search of the Cambridge Crystallographic database revealed that about 4000 cobalt complexes made with carboxylate based ligands have been studied in the past of which about 290 six-coordinate cobalt complexes are made from mono-, di-, tri- and tetra-carboxylate ligands. Also, in the majority of the known hydrate cobalt complexes in the database, Co^{2+} centres are coordinated to four aqua oxygen atoms. A typical example of the cobalt complex obtained from a mono-carboxylate ligand is $[\text{Co}(\text{H}_2\text{NC}_6\text{H}_4\text{CO}_2)_2\cdot 4\text{H}_2\text{O}]$. This complex was obtained from the reaction of aqueous cobalt(II) sulfate with sodium *p*-aminobenzoate in a ratio of 1:2 in H_2O at boiling point. Light brown crystals obtained were characterized as tetraqua-bis[*p*-aminobenzoate cobalt(II)] and deposited in the Cambridge Crystallographic Database as **ABZACO10**.¹³⁰



The geometric environment of Co^{2+} is octahedral with four aqua oxygen atoms occupying the equatorial positions and two carboxylate oxygen atoms occupying the axial positions coordinating to Co^{2+} in *anti-anti* monodentate coordination mode. The amine groups in the ligand are in *para* position hence, it does not coordinate to cobalt as shown in figure 4-46.

Also, a typical example of the cobalt complex obtained from a tetra-carboxylate ligand is $\text{C}_9\text{H}_{14}\text{Co}_{1.50}\text{O}_{12}$. This complex was obtained from the hydrothermal reaction of the 1,3,5-benzene tricarboxylic acid (H_3btc) and LiOH with $\text{CoCl}_2 \cdot 6\text{H}_2\text{O}$ in H_2O at 220°C . A light pink crystal obtained was characterized to be a six-coordinate cobalt complex in which the three carboxylate groups of H_3btc coordinates to the two crystallographic independent Co^{2+} in chelating tetradentate coordination mode and four aqua oxygen atoms in the equatorial position, as shown in figure 4-47. This complex was studied and deposited in the Cambridge Crystallographic Database as **EKEXEY**.¹³¹



The previous studies and search of the Cambridge Crystallographic Database revealed that complexes made from the reactive crystallization of Co^{2+} and NaAMB had not been previously studied, unlike in the case of Cu^{2+} and Zn^{2+} in which the aqueous diffusion of Cu^{2+} and NaAMB produced the anhydrous CuAMB complex ¹⁰³ and the aqueous diffusion of Zn^{2+} and NaAMB produced ZnAMB complex ¹¹³ respectively in the previous studies. Hence, the reaction of an aqueous solution of Co^{2+} and NaAMB was carried out in this study.

Hydrated CoAMB $\{[\text{Co}(\text{AMB})_2]_2 \cdot \text{H}_2\text{O}\}_n$ complex **10** and anhydrous CoAMB $[\text{Co}(\text{AMB})_2]_n$ complex **11** were obtained from the reactive crystallization of NaAMB with an aqueous solution of Co^{2+} at the molar ratio 1:2.

The two CoAMB complexes **10** and **11** are novel with features similar to the three determinations of anhydrous CuAMB complexes **5a**, **5b** and **5c**, hydrated CuAMB complex **8** and anhydrous ZnAMB complex **9** obtained in this study.

4.2.6.2. Structural Characterization of Hydrated CoAMB Structure



4.2.6.3. Introduction

Light pink crystals of complex **10** were obtained from the reactive crystallization of aqueous solutions of Co^{2+} and NaAMB in the molar ratio 1:2 as shown in figure 4-48.

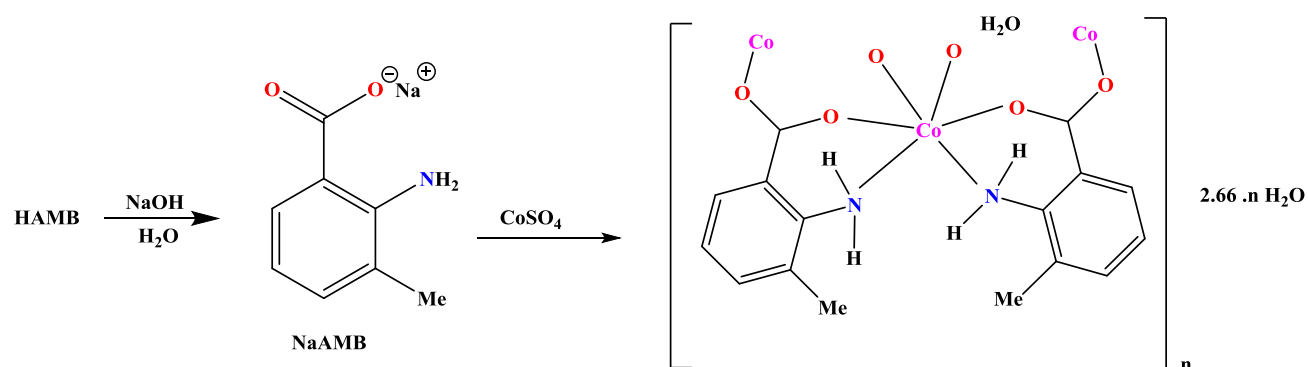


Figure 4-48: Schematic of the reaction that produced complex **10**.

Complex **10** is an odd structure which has a large apparent void in the middle of the unit cell that is big enough to hold another layer and is probably an extremely disordered layer. It has lattice water. This structure is similar to the structure of hydrated CuAMB complex **8** obtained in this studies except for the arrangement of the atoms coordinating around Co^{2+} which is *cis* for the two NH_2 groups and the bridging carboxylate oxygen atoms (non-crystallographic C_2) as opposed to all *trans* for the Cu^{2+} in complex **8** (crystallographic inversion symmetry).

4.2.6.4. Crystal Structure Determination of Complex **10**

The measurement was carried out on an Oxford diffraction Xcalibur2 equipped with a Sapphire2 detector using Mo $\text{K}\alpha$ radiation, $\lambda = 0.71073 \text{ \AA}$ at 293 K. Complex **10** crystallizes in the monoclinic crystal system and P2_1 space group.

A full list of crystal parameters and structure determination details, a view of the molecular structure of complex **10**, tables of selected bond lengths and angles are presented below.

Empirical Formulae	$\{[\text{Co}(\text{C}_8\text{H}_8\text{NO}_2)_2\cdot\text{H}_2\text{O}]\}_n$
Formulae weight	375.24
Temperature (K)	293
Crystal System	Monoclinic
Space group	P2_1
a (\AA)	7.2618(11)
b (\AA)	7.6774(13)
c (\AA)	26.629(5)
β ($^\circ$)	92.788(14)
Volume (\AA^3)	1482.8(5)
Z	2
D_x (Mg m^{-3})	0.840
μ (mm^{-1})	0.59
F(000)	386

Table 4-18: Crystal data collection of complex **10**.

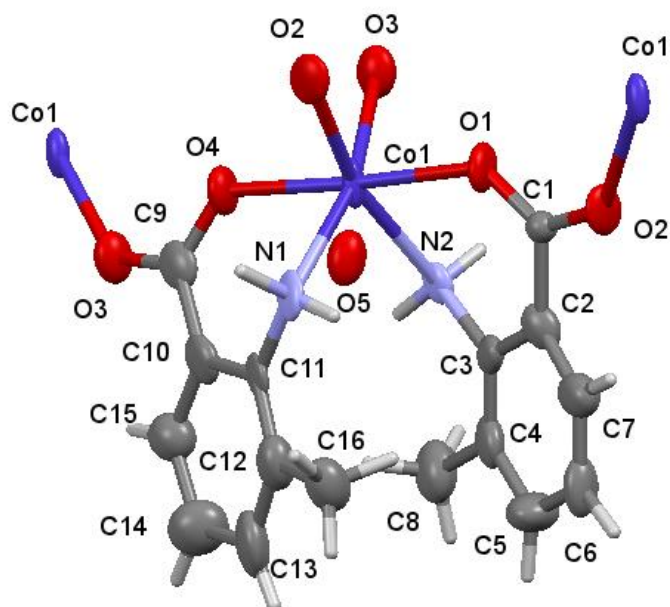


Figure 4-49: Molecular structure of complex **10**.

The coordination environment of Co^{2+} is distorted octahedral. This consists of two bidentate ligands attached to the Co centre at their carboxylate oxygen atoms and at two amine groups, NH_2 at *cis* orientation with one lattice water molecule as shown in figure 4-49. The distortion in the geometric environment of Co^{2+} is caused by each ligand acting as bidentate binding to one metal centre at the carboxylate oxygen atom and NH_2 group.

When expanded, the network built is lamellar with the lattice water molecules sitting in the channel in between the *cis* NH_2 groups, as shown in figures 4-50 and 4-51. This differs from the coordination environment of the metal centres in the CuAMB and ZnAMB complexes which shared both O and N groups of the two binding amino-carboxylates to be mutually *trans*, whereas, in complex **10**, the only carboxylate O atom is in *trans* orientation while the two N groups are in *cis* orientation. This enforces catenation to occur via the remaining two *cis* positions.

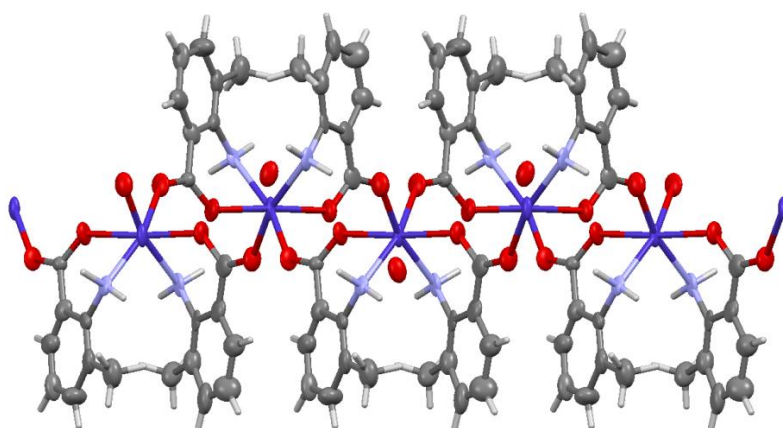


Figure 4-50: The lamellar structure of complex 10 showing the lattice water molecules sitting in-between two cis NH₂ groups.

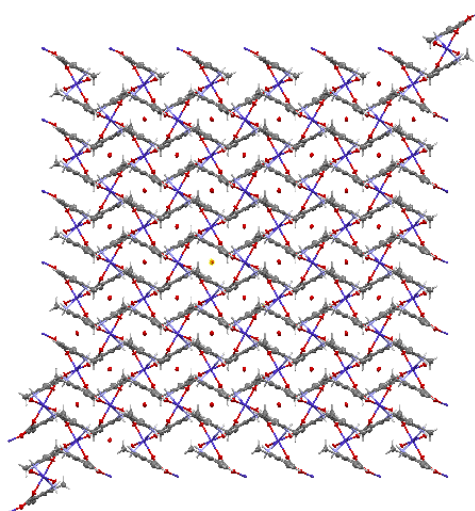


Figure 4-51: Lamellar structure of complex 10 viewed down crystallographic c axis showing water lattice in each unit.

When packed, there is a gap between the coordination polymer layers. This is a very large apparent void in between that is big enough to house another layer as shown in figure 4-52. It is thought likely that in fact, this “void” is filled by a highly disordered layer similar to the ordered layer characterized. The absence of this layer in the model leads to a non-plausible density.

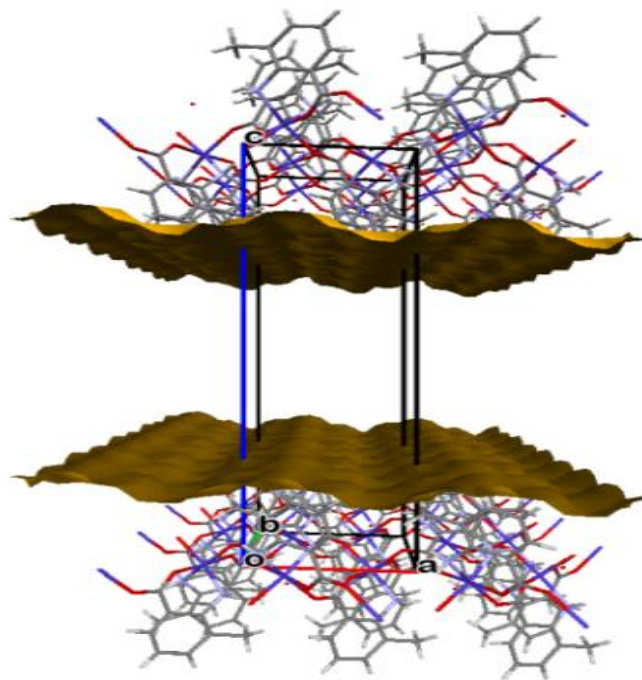


Figure 4-52: A packed figure of complex **10** showing the large apparent void in the structure.

Save for the presence of lattice water in complex **10**, the geometry environment of Co^{2+} in this complex can be compared to that of a structure studied as poly[bis(μ_2 -4-pyridinecarboxylato- $\kappa^3\text{N}: \text{O}, \text{O}'$)cobalt(II)], a triply interpenetrated structure with diamondoid topology. This structure was deposited in the Cambridge Crystallographic Database as **YIGGEB**. This complex was obtained unexpectedly from the hydrothermal reaction of bimetallic solutions of $\text{Co}(\text{NO}_3)_2 \cdot 6\text{H}_2\text{O}$ and $\text{Gd}(\text{NO}_3)_3 \cdot 6\text{H}_2\text{O}$ with a 4-pyridinecarboxylic acid solution in ethanol-water solution at 160°C .¹³²

The structure obtained, is a three-dimensional coordination network with Co^{2+} located on a 2-fold axis, coordinated to four O atoms derived from two chelating carboxylate ligands and two pyridine N atoms that define a distorted octahedral geometry within a *cis* N_2O_4 donor set. The distortion from the ideal octahedral geometry is caused by the chelating coordination mode of the carboxylate group in which two carboxylate oxygen atoms of the same carbonyl group is bonded to the same metal centre with an acute angle of $60.43(7)^\circ$ for $\text{O1} - \text{Co} - \text{O2}$ with distances of $\text{C} - \text{O} = 1.250(3) \text{ \AA}$ and $1.252(3) \text{ \AA}$.¹³²

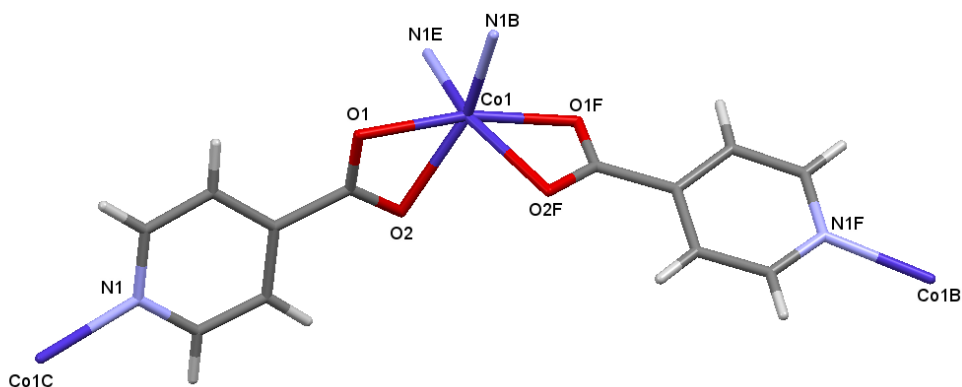


Figure 4-53: Molecular structure of **YIGGEB**.¹³²

The metal-ligand used as the starting materials for the two Co^{2+} complexes are different but they both had a distorted octahedral geometry environment in which Co^{2+} is coordinated to four carboxylate oxygen atoms in both Co^{2+} complexes and two N atoms of the amine groups in complex **10** and two pyridine N atoms in **YIGGEB**. Complex **10** crystallizes in the monoclinic crystal system and $P2_1$ space group while **YIGGEB** crystallizes in tetragonal crystal system and $P4_32_12$ space group.¹³²

In **YIGGEB**, the carboxylate oxygen atoms chelate, binding to one Co centre as shown in figure 4-53 while in complex **10**, the carboxylate oxygen atoms are coordinated to the Co^{2+} centre in *syn-anti* bidentate bridging coordination mode in which the two rings sit on the plane with distances that appear longer in one case than in the second case. This may be as a result of Co^{2+} centre pulling the carboxylate oxygen atoms closer. The difference in the bridging modes of carboxylate oxygen atoms seems to be responsible for the short interatomic Co – Co distance of 5.346(2) Å across the structure of complex **10** against the Co – Co distance in **YIGGEB** which is 8.800 Å. It is believed that short interatomic metal-metal distances promote the magnetic strength of metal in a complex. Hence, the magnetic study of complex **10** is recommended in further work.¹³²

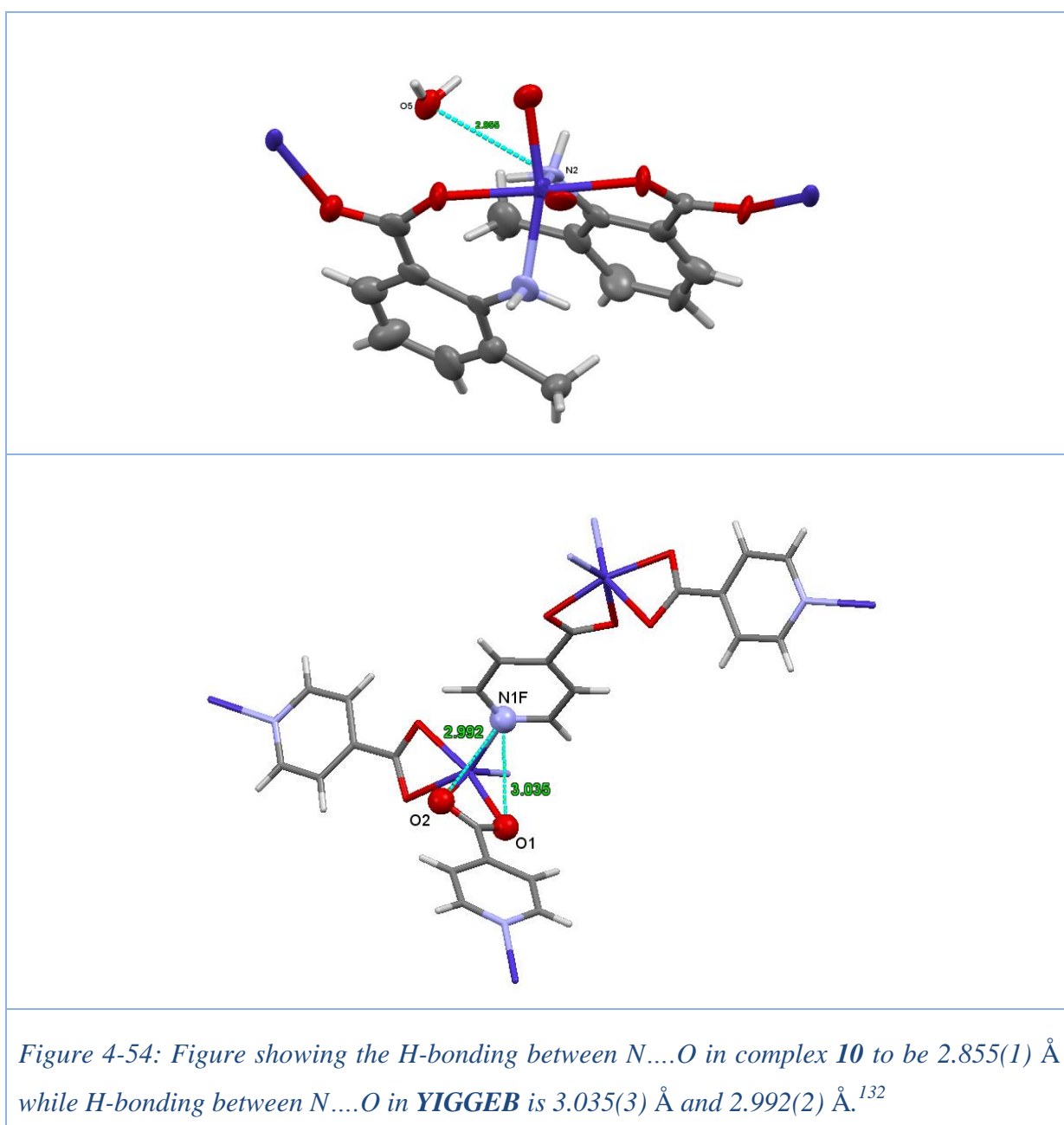
In complex **10**, the atoms coordinating around Co^{2+} are not symmetrical, hence, x, y, z is not equal to $-x, -y, -z$ while in **YIGGEB**, there are two symmetric N atoms of pyridine and two sets of carboxylate oxygen atoms. Hence, the bond distances of the atom coordinating around Co^{2+} in the two Co^{2+} complexes are significantly different, likewise the carboxylate groups.

Also, the distorted coordination environment of Co^{2+} in the two complexes is significantly different as listed in table 4-19.¹³²

10		YIGGEB	
Distance	(Å)	Distance	(Å)
Co1 – O1	2.018(8)	Co1 – O1	2.1104 (16)
Co1 – O2	2.051(9)	Co1 – O1 ⁱⁱⁱ	2.1104 (16)
Co1 – O3	2.028(9)	Co1 – O2	2.2279 (16)
Co1 – O4	2.028(8)	Co1 – O2 ⁱⁱⁱ	2.2279 (16)
Co1 – N1	2.105(11)	Co1 – N1 ⁱ	2.0723 (16)
Co1 – N2	2.138(10)	Co1 – N1 ⁱⁱ	2.0723 (16)
O1 – C1	1.235(14)	O1 – C6	1.253 (3)
O2 – C1 ¹	1.242(14)	O2 – C6	1.250 (3)
O3 – C9	1.286(17)		
O3 – C9 ²	1.279(16)		
Angle	(°)	Angle	(°)
O1 – Co1 – O2	84.5(4)	O1 – Co1 – O2	60.43(7)
O4 – Co1 – O2	92.9(4)	O1 ⁱⁱⁱ – Co1 – O2	109.99(7)
O4 – Co1 – N1	79.6(4)	N1 ⁱ – Co1 – O1 ⁱⁱⁱ	94.63(7)
O3 – Co1 – N2	95.3(3)	N1 ⁱⁱ – Co1 – O2 ⁱⁱⁱ	88.08(6)
O2 – Co1 – N1	94.0(3)	N1 ⁱⁱ – Co1 – O1	94.67(7)
O4 – Co1 – N2	103.7(4)	N1 ⁱⁱ – Co1 – O2	153.36(7)
O1 – Co1 – O4	176.5(4)	O1 ⁱⁱⁱ – Co1 – O1	167.50(11)
O2 – Co1 – N2	163.3(4)	N1 ⁱ – Co1 – N1 ⁱⁱⁱ	103.65(10)
Symmetry code: ¹ 1-x,1/2+y,-z; ² -x,1/2+y,-z;		Symmetry code: (i) x-1/2, -y+1/2, -z-3/4; (ii) -y+1/2, x-1/2, z+3/4; (iii) y, x, -z;	

Table 4-19: Bond distances and angles of atoms coordinating around Co^{2+} centre and C – O distances in the two Co^{2+} complexes.¹³²

In complex **10**, H-bonding occurred between the NH₂ group and the oxygen atom of the lattice water molecule with a distance of N2...O5 = 2.855(1) Å. This bond distance is well within the range found for H-bonds formed between amine groups and oxygen in previous works which are in the ranges N...O = 2.57 Å – 3.22 Å.⁶ While in **YIGGEB**, there are two similar types of H-bonding. These occurred between the N atom of the pyridine and the two carboxylate oxygen atoms attached to an adjacent Co²⁺ centre with the distances of N1...O1F = 3.035(3) Å and N1...O2F = 2.992(2) Å. The H-bonding are represented in teal dotted lines as shown in figure 4-54.¹³²



4.2.7. Structural Characterization of Anhydrous CoAMB $[\text{Co}(\text{C}_8\text{H}_8\text{NO}_2)_2]_n$

4.2.7.1. Introduction

In solution, light and reddish pink single crystals of complex **11** were obtained from the reactive crystallization of aqueous solutions of Co and NaAMB in the molar ratio 1:2 as shown in figure 4-55.

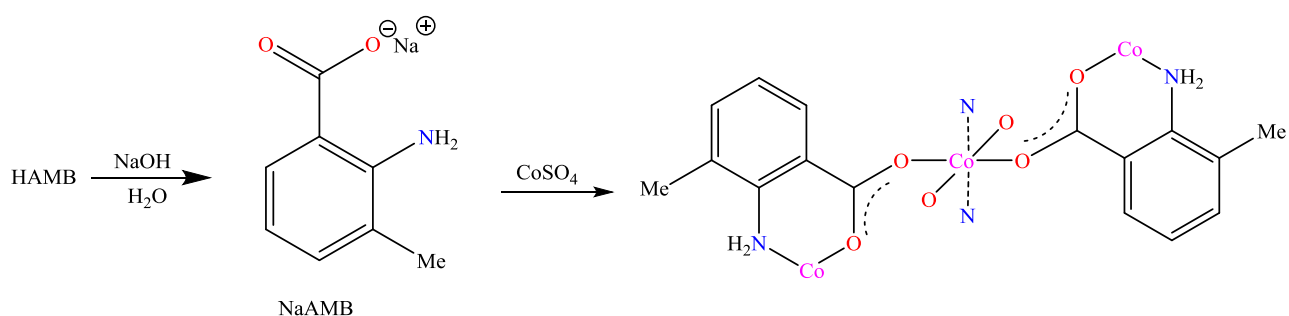


Figure 4-55: Schematic of the reaction that produced complex **11**.

4.2.7.2. Crystal Structure Determination of Complex **11**

The measurement was carried out on an Oxford diffraction Xcalibur2 equipped with a Sapphire2 detector using Mo K α radiation, $\lambda = 0.71073 \text{ \AA}$ at 100 K. Complex **11** crystallizes in the monoclinic crystal system and P2₁/c space group.

The structure of complex **11** has the same topology as the hydrated CuAMB complex **8** and ZnAMB complex **9** structures obtained in this study. The structure of complex **11** is also similar to the structure of the hydrate CoAMB complex **10** except for the *trans* arrangement of all the atoms coordinating around Co²⁺, there is no lattice water and there is no apparent void in complex **11**. This is an excellent structure and could not be matched to any known structure in the Cambridge Crystallographic Database.

A full list of crystal parameters and structure determination details, a view of the molecular structure of complex **11**, and tables of selected bond lengths and angles are presented below.

Empirical Formula	$[\text{Co}(\text{C}_8\text{H}_8\text{NO}_2)_2]_n$
Formulae weight	359.24
Temperature (K)	100
Crystal System	Monoclinic
Space group	$P2_1/c$
a (Å)	13.9353(18)
b (Å)	5.6414(5)
c (Å)	9.5115(9)
β (°)	107.840(12)
Volume (Å ³)	711.79(14)
Z	2
D_x (Mg m ⁻³)	1.676
μ (mm ⁻¹)	1.23
F(000)	370.0
Crystal size (mm)	0.22 × 0.2 × 0.01
Crystal Shape	Plate, light pink
R factor (%)	6.38

Table 4-20: Crystal data collection of complex **11**.

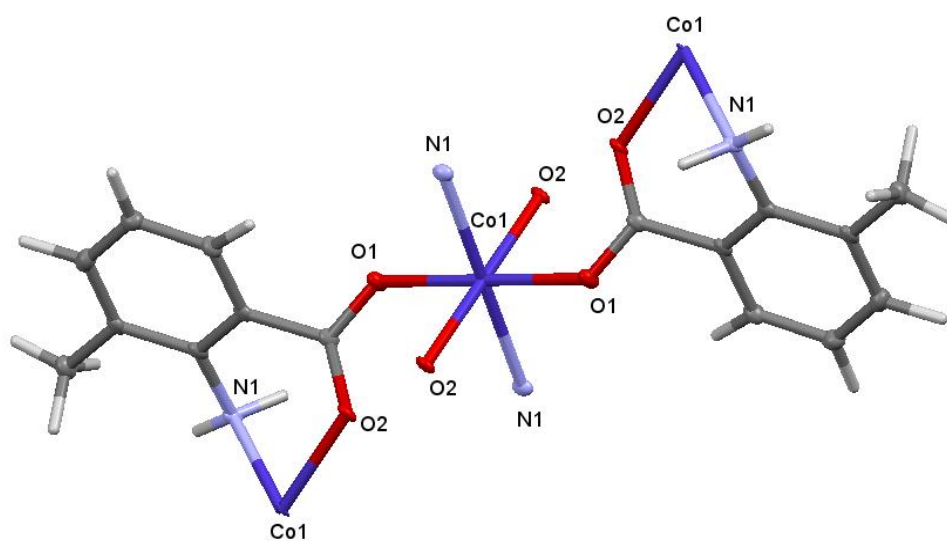


Figure 4-56: Molecular structure of complex **11**.

The geometry environment of Co^{2+} is octahedral. This consists of four equatorial carboxylate oxygen atoms and two axial NH_2 with no lattice water. The ligand acted as bidentate binding to Co^{2+} at O_{carb} and at NH_2 , as shown in figure 4-56.

When expanded, like the structures of anhydrous CuAMB and ZnAMB obtained in this study, the polymeric network built is a layered structure, as shown in figure 4-57.

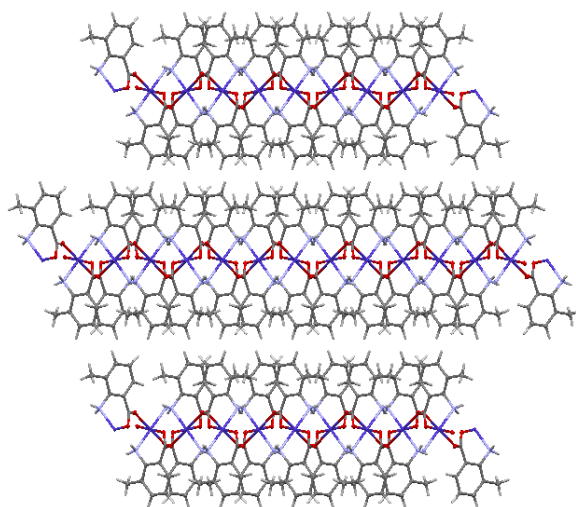


Figure 4-57: Expanded network showing the layers in the structure of complex 11.

When packed and viewed down crystallographic b axis, there are no gaps between the coordination polymer layers of complex **11** as shown in figure 4-58 unlike in the structure of hydrate CoAMB complex **10** which had a very large apparent void in between the layers large enough to accommodate another layer.

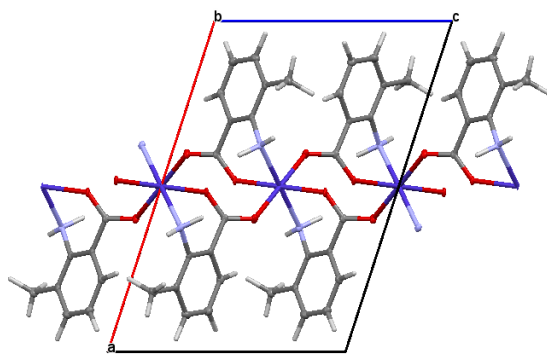


Figure 4-58: A packing figure showing that there is no apparent void in complex **11**.

The geometric environment of Co^{2+} in the anhydrous CoAMB complex **11** can be compared to that of a structure of hydrated Co^{2+} complex which is one of the structures studied as ‘two novels Co(II)-based coordination polymers with hms and pcu nets: syntheses, structures, and properties’. This complex was obtained from the hydrothermal reaction of the mixture of the solution of the primary ligand, 5-(4-carboxyphenoxy)methyl)benzene-1,3-dioic acid (H_3L) and the auxiliary ligand, 4,4'-bipyridine (bpy) with cobalt(II)acetate tetrahydrate in H_2O at $130\text{ }^\circ\text{C}$ for three days. The complex obtained was deposited in the Cambridge Crystallographic Database as **DEJXUO**.¹³³

The two Co^{2+} complexes crystallize in the monoclinic crystal system and $\text{P2}_1/\text{c}$ space group despite the differing crystallization methods, solution method vs hydrothermal reaction. Furthermore, the starting materials (both metal salt and ligand) used in preparing the two Co^{2+} complexes are different. Also, Co^{2+} centres in both complexes are coordinated to four carboxylate oxygen atoms in an equatorial position and two N atoms of the amine groups in the axial position in complex **11** while the distorted octahedral geometric environment of Co^{2+} in **DEJXUO** comprises four carboxylate oxygen atoms and two pyridine N atoms, as shown in figure 4-59.¹³³

In **DEJXUO**, two adjacent Co(II) ions are connected by HL^{2-} to obtain the Co_2 unit. This connection yielded a 2D layer. One part of the carboxylate group is coordinated to the metal centre in *syn-syn* bidentate coordination mode while the second part is chelating, as shown in figure 4-59.¹³³

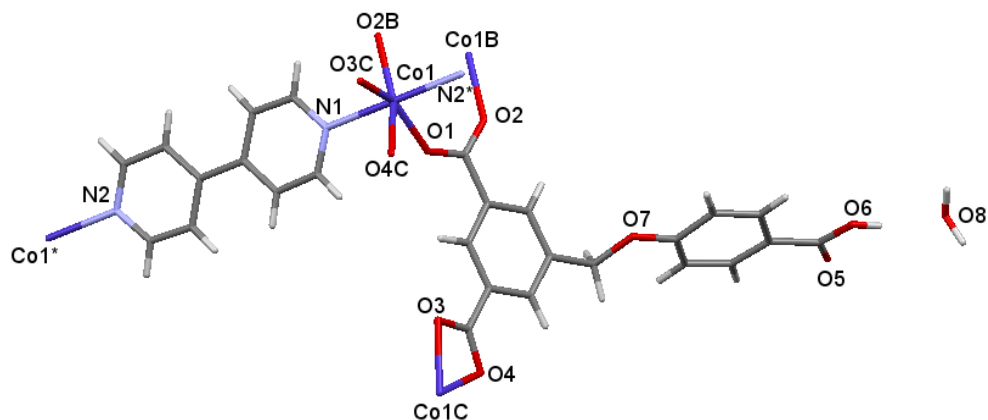


Figure 4-59: Molecular structure of **DEJXUO**.¹³³

The distortion from the ideal octahedral geometry in **DEJXUO** occurred at the *syn-syn* bidentate coordination mode of the carboxylate group to the metal centre in which the distance of *trans* Co1 – O2B = 1.992(3) Å and Co1 – O4C = 2.255(3) Å in one case and the distance of *trans* Co1 – O1 = 1.994(3) Å and Co1 – O3C = 2.135(3) Å in the second case while in complex **11**, the carboxylate oxygen atoms are coordinated to Co²⁺ in *syn-anti* bidentate bridging coordination mode in which the two rings sit on the plane with distances that appear longer in one case than in the second case. This may be as a result of the Co centre pulling the carboxylate oxygen atoms closer. The difference in the bridging modes of carboxylate group seems to be responsible for the short interatomic Co – Co distance of 5.529 Å across the structure of complex **11**. This distance is shorter when compared to 8.161(1) Å which is the Co – Co distance in **DEJXUO**. It is believed that a short interatomic metal-metal distance promotes the magnetic coupling of metal centres in a complex. Hence, the magnetic study of this structure is recommended in further work.¹³³

In complex **11**, there are two symmetrical carboxylate oxygen atoms and two NH₂ groups coordinating around Co with distances of Co1 – O1 = 2.078(4) Å, Co1 – O2² = 2.108(4) Å and Co1 – N1² = 2.168(5) Å.

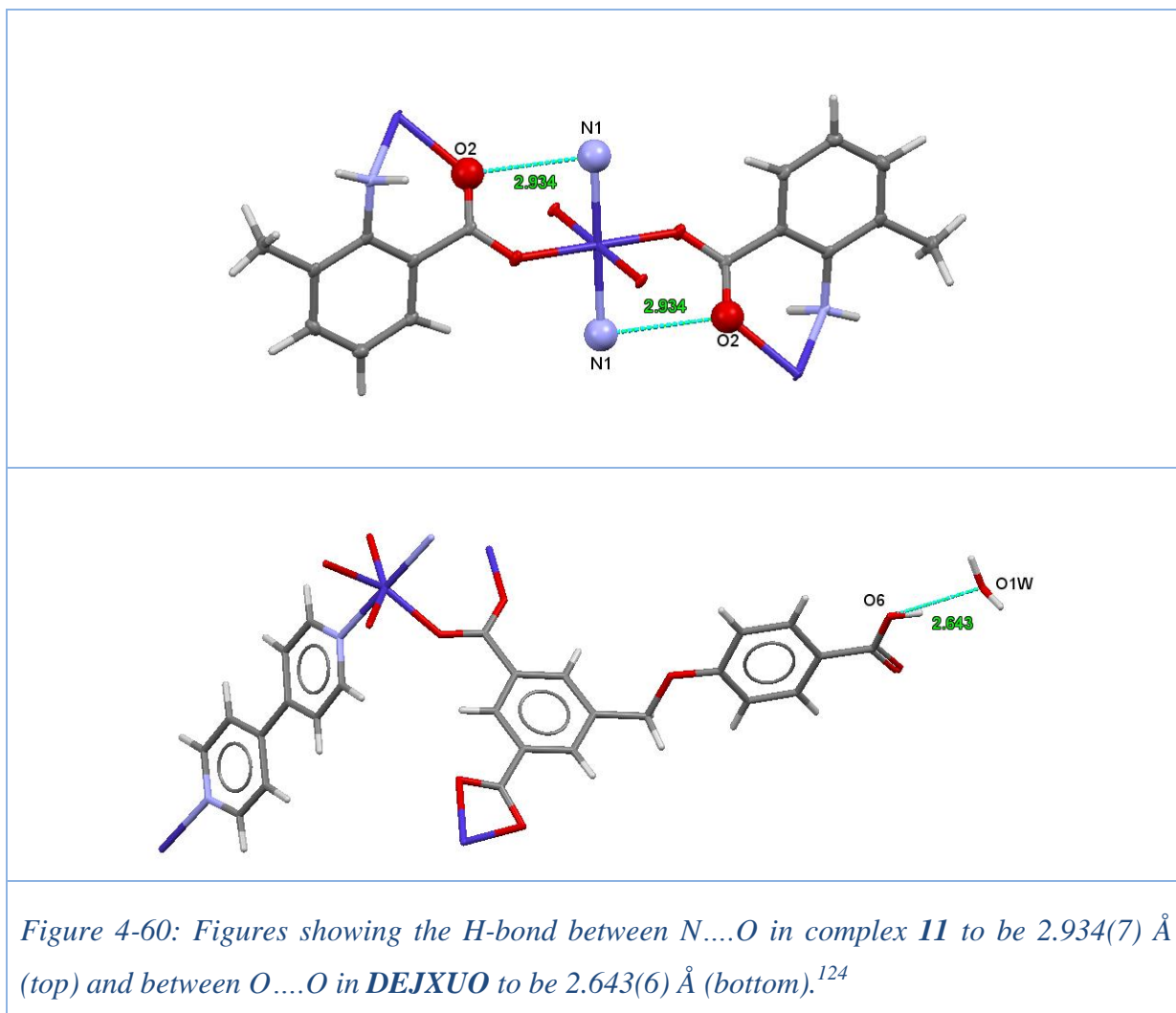
The bond distances and angles of the atom coordinating around Co²⁺ in the two complexes are significantly different likewise the carboxylate groups as listed in table 4-21.

11		DEJXUO	
Atoms	(Å)	Atoms	(Å)
Co1 – O1	2.078(4)	Co1 – O2B	1.992(3)
		Co1 – O3C	2.135(3)
Co1 – O2	2.108(4)	Co1 – O1	1.994(3)
		Co1 – O4C	2.255(3)
Co1 – N1	2.168(5)	Co1 – N1	2.153(4)
		Co1 – N1*	2.165(4)
O1 – C1	1.267(7)	O1 – C6	1.253 (3)
O2 – C1	1.278(7)	O2 – C6	1.250 (3)
Angle	(°)	Angle	(°)
O1 – Co1 – N1 ²	91.57(17)	O2 ^{#1} – Co1 – N1	87.42(14)
O2 ³ – Co1 – N1 ²	97.14(17)	O3 ^{#2} – Co1 – N1	94.00(14)
O1 ¹ – Co1 – O2 ²	87.15(15)	O2 ^{#1} – Co1 – O1	119.47(14)
O1 – Co1 – O1 ¹	180.0	O1 – Co1 – O3 ^{#2}	148.85(14)
N1 ² – Co1 – N1 ³	180.0(3)	N1 – Co1 – N2 ^{#3}	178.83(14)
Symmetry code: (i) -x+1, -y, -z+1; (ii) x, -y+1/2, z-1/2; (iii) -x+1, y-1/2, -z+3/2.		Symmetry code: ^{#1} -x, -y, -z+1; ^{#2} x, -y+1/2, z+1/2; ^{#3} x-1, y, z.	

Table 4-21: Selected bond distances and angles of atoms coordinating around Co²⁺ and the C – O distances in complex 11 and DEJXUO.¹³³

The lower symmetry in **DEJXUO** masks the fact that similar distances are to be found in this pair of complexes. Hence, the mean for the pair of the distance of atoms coordinating around Co centre in **DEJXUO** for Co – O is 2.063(3) Å and 2.124(3) Å and for Co – N is 2.159(4) Å respectively, as listed in table 4-21. These values are well within the range for those in complex **11**.

In complex **11**, H-bonding occurred between NH₂ and the opposite carboxylate oxygen atom with a distance of N1...O2 = 2.934(7) Å. In **DEJXUO**, H-bonding occurs between the carboxylate oxygen atom and the lattice water with the shorter distance of O6...O1W = 2.643(6) Å. H-bonds are represented in teal dotted lines, as shown in figures 4-60.



The reactive crystallization condition of Co^{2+} and NaAMB that produced the hydrated and anhydrous CoAMB complexes **10** and **11** are the same. The two structures crystallize in the monoclinic crystal system and $P2_1/c$ space group but data for the anhydrous CoAMB complex **11** was collected at a lower temperature of 100 K while that of the hydrate CoAMB complex **10** was collected at 150 K.

In complex **10**, the two NH_2 groups occupy the *cis* orientation with the uncoordinated water molecule sitting between the *cis* NH_2 groups while the NH_2 groups are in *trans* orientation in the anhydrous CoAMB complex **11**.

4.2.8. Reactive Crystallization of Novel Hydrated NiAMB $\text{Ni}(\text{C}_8\text{H}_8\text{NO}_2)(\text{H}_2\text{O})_2 \cdot 2\text{H}_2\text{O}$

4.2.8.1. Introduction

Numerous Ni complexes made from carboxylate based ligands have been previously characterized and studied to a high standard. Ni^{2+} has been shown to form layered structures and coordination polymers with carboxylate based ligands such as *para*-aminobenzoic acid (PAA) ¹³⁴ and the 2-methylamine benzoic acid ¹³⁵ in previous studies like other 1st-row 3d transition metals.

In this study, the crystallization reaction of NaAMB with an aqueous solution of Ni^{2+} (1st experiment) and NaAMB with the bimetallic solution of Ni/Cu (2nd experiment) was carried out. In the two reactions, two identical sets of hydrate NiAMB structures were obtained.

4.2.8.2. Structural Characterization of Complex **12**

In solution, light green and colourless single crystals of complex **12** were obtained from the bimetallic crystallization reaction of aqueous solutions of NaAMB, with CuSO_4 and NiSO_4 in the molar ratio 1:2, as shown in figure 4-61.

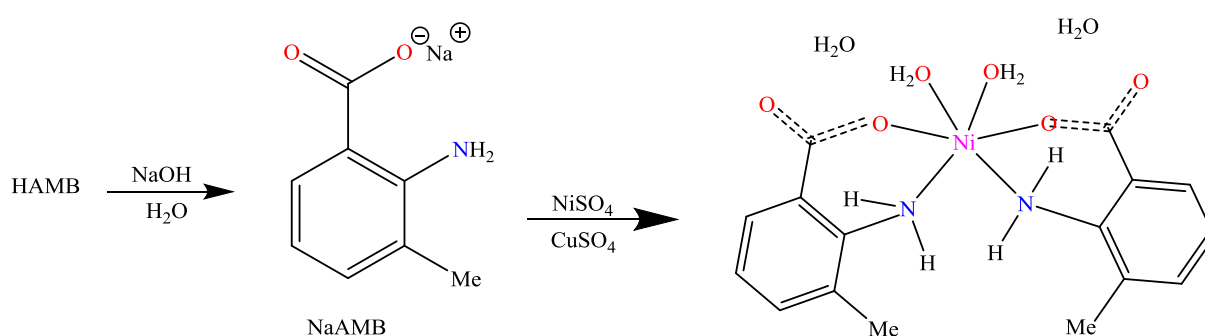


Figure 4-61: Schematic of the reaction that produced complex **12**.

Complex **12** is novel and could not be matched to any known structure in the Cambridge Crystallographic Database.

4.2.8.3. Crystal Structure Determination of Complex **12**

The measurement was carried out on an Oxford diffraction Xcalibur2 equipped with a Sapphire2 detector using Mo K α radiation, $\lambda = 0.71073 \text{ \AA}$ at 100 K. Complex **12** crystallizes in the monoclinic crystal system and P2₁/c space group.

A full list of crystal parameters and structure determination details, a view of the molecular structure of complex **12**, and tables of selected bond lengths and angles are presented below.

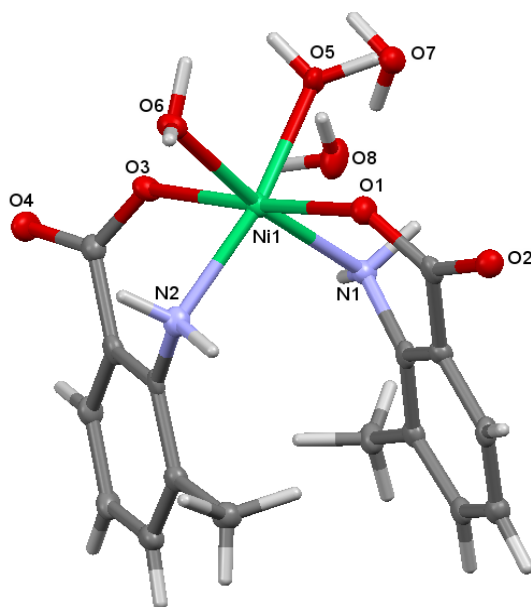


Figure 4-62: Molecular structure of complex **12**.

The geometric environment of complex **12** is distorted octahedral, not due to the Jahn-Teller effect. AMB acts as a bidentate ligand terminally coordinating via a single carboxylate oxygen atom and the amino nitrogen. Two of such ligands are attached in such a way that the O atoms are in *trans* orientation while the N atoms are in *cis* orientation. Two terminal coordinated water molecules in *cis* orientation complete the octahedral environment and a further two lattice water molecules fill voids in the structure. A diagram showing such a monomer is presented as figure 4-62.

When the structure of complex **12** was expanded, its expansion is nine monomer units of the compound linked together with the H-bonding networks represented with turquoise dotted lines as shown in figure 4-63.

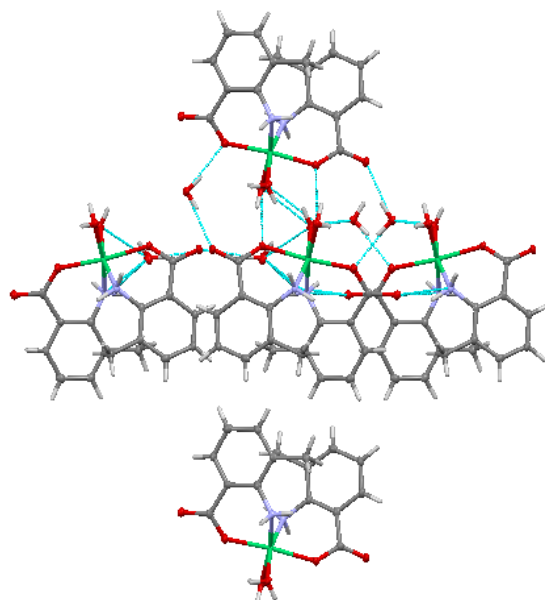


Figure 4-63: The expansion of complex 12 showing the H-bonding network linking the monomers.

The two coordinating O_{water} bonds deviated from regular octahedral geometry, moving towards each other to form an angle of 89.15° with Ni^{2+} . This may be the effect of the NH_2 group and the O_{carb} on the Ni atom crowding the water molecules.

The coordinating atoms and the Ni centre are not sitting perfectly on the plane. Ni^{2+} deviates from the plane by 0.040 \AA , N2 deviates from the plane by 0.012 \AA , O3 deviates from the plane by 0.034 \AA , O5 deviates from the plane by 0.013 \AA and O1 deviates from the plane by 0.032 \AA , as shown in figure 4-64.

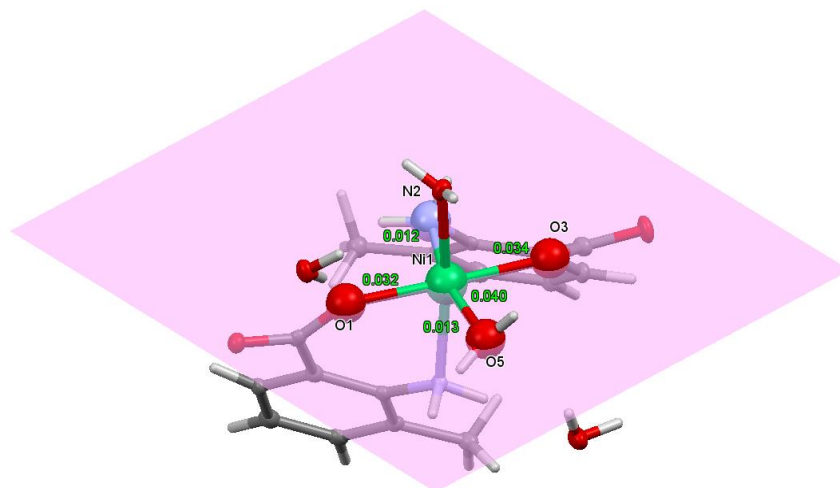
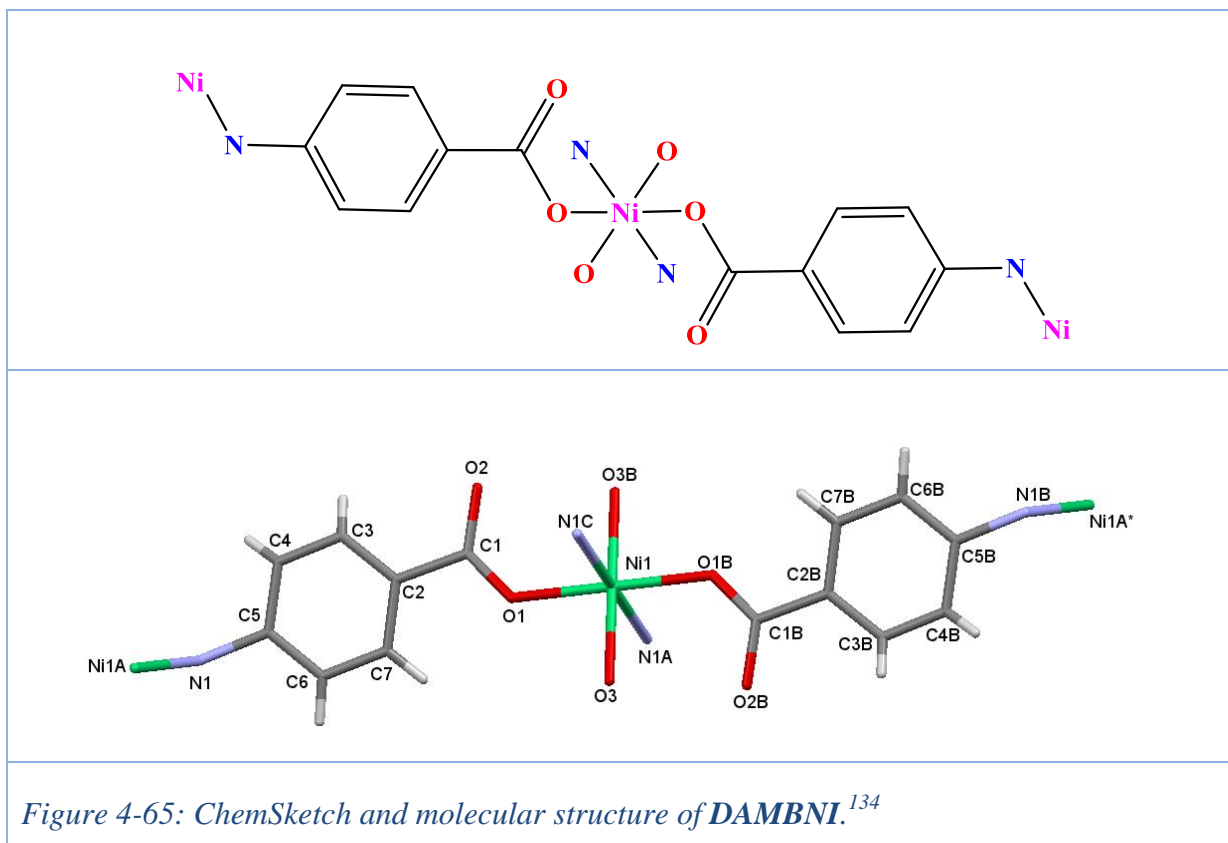


Figure 4-64: Figure showing that Ni and its coordinating atoms are not perfectly sitting on the plane in complex **12**.

Complex **12** can be compared with the structure of bis-(*p*-aminobenzoato)diaquonickel(II) which had been studied previously and deposited in the Cambridge Crystallographic Database as **DAMBNI**. This structure was prepared with different starting materials but has a coordination environment for Ni centre, similar to that of complex **12**.

DAMBNI was obtained by adding a solution of sodium *p*-amino benzoate to a solution of NiSO₄ slowly. In **DAMBNI**, just as in complex **12**, *para*-aminobenzoic acid (PAA) acted as a bidentate ligand, coordinating to Ni²⁺ at the amine and carboxyl groups of the ligand with Ni sitting on crystallographic inversion and all the coordinated atoms are symmetrical. However, the carbonyl oxygen atom, O and amino N bridged different metals, forming a coordination polymer, the octahedral geometry was completed with two coordinated water molecules, O3 and O3B, as shown in figure 4-65¹³⁴ while in complex **12**, the ligands are chelating, leading to isolated molecules. This different assembly mode is as a result of the *para* position of the substituent on the ligand in **DAMBNI** whereas, in complex **12**, the substituent is in the *ortho* position on the ligand.



Complex **12** and **DAMBNI** crystallizes in the monoclinic crystal system but in a different space group. Complex **12** is a coordination polymer network, layered in H-bond to water of crystallization while **DAMBNI** is a molecular 2D coordination metal polymer.

Complex **12** can also be compared with the structure of tetraaquabis[4-(methylamino)benzoato- κ O] nickel(II) which has been previously studied and deposited in the Cambridge Crystallographic Database as **NUNRUK**. Green single crystals of **NUNRUK** were prepared by the reaction of nickel(II)sulfate hexahydrate and sodium 4-(methylamino)benzoate in water. The mixture was filtered and left to grow crystals at ambient temperature for one week. Like in complex **12**, the coordination environment of Ni in **NUNRUK** is slightly distorted octahedron with Ni sitting on crystallographic inversion with two 4-(methylamino)benzoate (PMAB) anion and four coordinated water molecules as shown in figure 4-66.¹³⁵

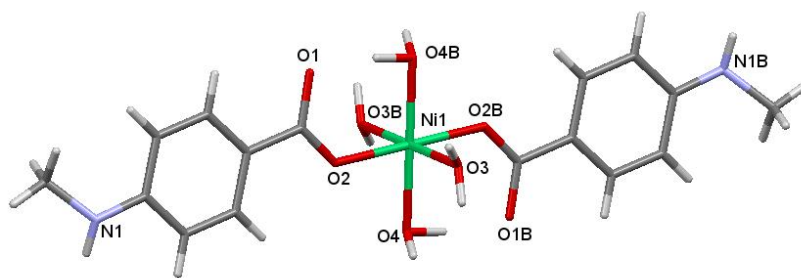
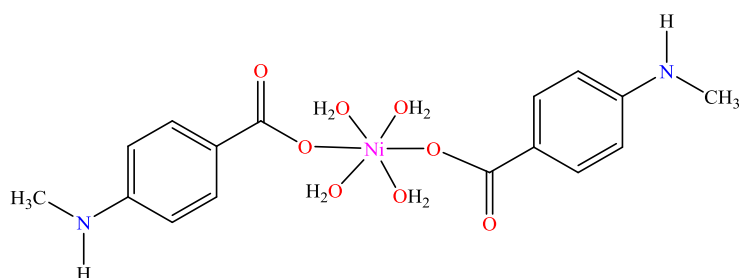


Figure 4-66: ChemSketch and molecular structure of **NUNRUK**.¹³⁵

In **NUNRUK**, the H-bond types O – H...O, O – H...N, N – H...O and C – H...O link the molecules into a three-dimensional network while in complex **12**, O – H...O and N – H...O H-bonds link the polymer to a two-dimensional network.

In **NUNRUK**, Ni²⁺ was displaced out of the least square of the carbonyl group O1/C1/O2 by 0.0728(1) Å, in contrast, O1, O2, N1, and C1 atoms are away from the plane of the benzene ring (C1 – C7) by 0.0061(11) Å, 0.0549(10) Å, -0.0636(13) Å respectively just like in complex **12**.

The two aminomethylbenzoate ligands in complex **12** are crystallographically independent but chemically similar. The distances of the two O_{carb} bonded to Ni are Ni1 – O1 = 2.008(2) Å and Ni1 – O3 = 2.050(2) Å, for NH₂ distances Ni1 – N1 = 2.092(3) Å and Ni – N2 = 2.085(8) Å and for the coordinating O_{water}, distance Ni1 – O5 = 2.123(3) Å and Ni1 – O6 = 2.089(3) Å. The bond distance of one of the coordinating O_{water} is longer. This is one aspect of the distortion in the geometric environment of Ni.

In **DAMBNI**, unlike in complex **12**, the six-coordinate Ni complex is situated at a centre of inversion and it is surrounded by two symmetry-related nitrogen atoms with distances

2.166(9) Å, two carboxylate oxygen atoms with distances 2.025(7) Å and two oxygen atom of coordinating water molecules with distances 2.041(8) Å. All atoms are mutually in *trans* orientation, as required of the inversion symmetry element.

Also in **NUNRUK**, Ni is sitting on a crystallographic inversion centre with four coordinating water molecules and two carboxylate oxygen atoms with their distances listed in table 4-22.

12		DAMBNI		NUNRUK	
Distance	(Å)	Distance	(Å)	Distance	(Å)
Ni1 – O1	2.008(2)	Ni1 – O1	2.025(7)	Ni1 – O2	2.0537(10)
Ni1 – O3	2.050(2)	Ni1 – O1B	2.025(7)	Ni1 – O2B	2.0537(10)
Ni1 – O5	2.123(3)	Ni1 – O3	2.041(8)	Ni1 – O3	2.0662(10)
Ni1 – O6	2.090(3)	Ni1 – O3B	2.041(8)	Ni1 – O3B	2.0662(10)
Ni1 – N1	2.092(3)	Ni1 – N1A	2.166(9)	Ni1 – O2	2.0772(10)
Ni1 – N2	2.085(8)	Ni1 – N1C	2.166(9)	Ni1 – O2B	2.0772(10)
O1 – C7	1.280(4)	O1 – C1	1.256(15)	O1 – C1	1.276(2)
O2 – C7	1.242(4)	O2 – C1	1.282(14)	O1B – C1B	1.276(2)
O3 – C15	1.280(4)	O1B – C1B	1.256(15)	O2 – C1	1.256(2)
O4 – C15	1.240(4)	O2B – C1B	1.282(14)	O2B – C1B	1.256(2)

Table 4-22: Bond distances of the atoms coordinating around Ni²⁺ and C – O distances in complex **12**, **DAMBNI** and **NUNRUK**.^{134, 135}

The carboxylate oxygen atom coordinated to Ni in **DAMBNI** and **NUNRUK** is in terminal (*syn*) conformation while in complex **12**, the carboxylate groups exhibit the terminal (*anti*) conformation in a way that the two O_{carb} are chemically equivalent even though they are not crystallographically related. The distance between the two *trans* O_{carb} bonded to Ni are C7 – O1 = 1.280(4) Å and C15 – O3 = 1.280(4) Å. Also, the distances of the O_{carb} that are not coordinated to Ni centre are C7 – O2 = 1.242(4) Å and C15 – O4 = 1.240(4) Å. The O_{carb} coordinated to Ni²⁺ is longer than the O_{carb} that is not coordinated to Ni²⁺ due to the Ni²⁺

pulling the O_{carb} while the reverse is the case in **DAMBNI** and **NUNRUK** as listed in table 4-22.¹³⁴⁻¹³⁵

The C–O bonds in the carboxylate groups in complex **12** were compared with the corresponding distances in the other centrosymmetric Ni complexes made from carboxylate based ligands such as in the structure of [Ni(C₈H₇O₃)₂(C₆H₆N₂O)₂(H₂O)]₂(H₂O)₂, with C – O distances of 1.2681(15) Å and 1.2644(16) Å,¹³⁶ C – O distances of 1.263(4) Å and 1.249(4) Å in the structure of [Ni(C₈O₅O₃)₂(C₁₀H₁₄N₂O)₂(H₂O)₂],¹³⁷ C – O distances of 1.258(3) Å and 1.267(3) Å in the structure [Ni(C₇H₄ClO₂)₂(C₆H₆N₂O)₂-(H₂O)₂],¹³⁸ and C – O distances of 1.2678(17) Å and 1.2654(17) Å in the structure of [Ni(C₈H₇O₂)₂(C₆H₆N₂O)₂(H₂O)₂].¹³⁹ These distances are in the same range as those in complex **12** but it was observed that in each pair of the C – O bonds, the distances are in close range values unlike the C – O distance in the non-centrosymmetric Ni²⁺ in complex **12** which has longer C – O distances in the carboxylate oxygen atom coordinated to the Ni²⁺ centre.

In complex **12**, each of the atoms coordinating around Ni²⁺ is in *cis* orientation. There is a deviation from the octahedral geometric environment of Ni²⁺ which results from packing effects. Therefore, their angles deviate from 90°. In **DAMBNI** and **NUNRUK**, the atoms are coordinated to Ni²⁺ in *trans* orientation and the geometric environment of Ni²⁺ is a near perfect octahedron.

Selected bond angles in the three Ni complexes are listed in table 4-23.

12		DAMBNI		NUNRUK	
Angle	(°)	Angle	(°)	Angle	(°)
O1 – Ni1 – O5	92.83(10)	O1 – Ni1 – O3	91.2(3)	O2 ⁱ – Ni1 – O3	91.62(4)
N1 – Ni1 – O5	85.94(11)	O1 – Ni1 – N ⁷	93.6(3)	O2 – Ni1 – O3	88.38(4)
O3 – Ni1 – N1	100.93(10)	O3 – Ni1 – N ⁷	92.7(3)	O2 – Ni1 – O4	85.84(4)
N2 – Ni1 – N1	97.49(12)	O1B – Ni1 – N1A	86.41(3)	O2 ⁱ – Ni1 – O4	94.17(4)
O1 – Ni1 – O3	175.17(9)	O1B – Ni1 – O1	180.0	O2 – Ni1 – O2 ⁱ	180.00(2)

Table 4-23: Selected bond angles of the atoms coordinating around Ni²⁺ in the three Ni complexes.¹³⁴⁻¹³⁵

Torsion angle measurement was considered because of the geometric environment of Ni²⁺ centre in complex **12** in which the rings are not flat but are folded. Also, the examination of the effect of the coordination around the metal centre is of interest as the carboxylate oxygen atoms and the NH₂ group of each of the ligands are attached to the metal centre in *cis* orientation, in a way that the metal centre is pulling the NH₂ away from the ring. These measurements were compared to that of the ring of the free ligand which has been studied extensively and deposited in the Cambridge Crystallography Database as **AMEBAC**.¹¹⁹

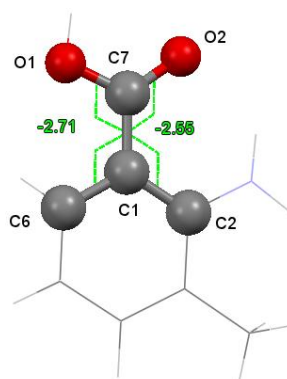
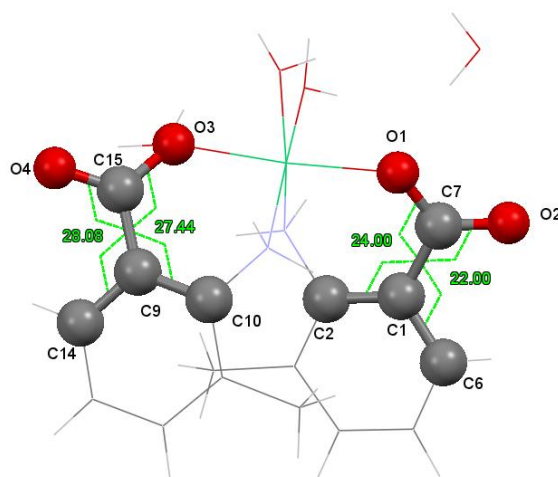


Figure 4-67: Figures showing the torsion angles in rings A and B in complex **12** (top) and in the free ligand: **AMEBAC** (bottom).¹¹⁹

The free ligand, 2-amino-3-methylbenzoic acid (AMB) has a low torsion value of -2.77° and -2.55° but in complex **12**, the rotation of the atoms around the bond increased as the AMB ligands coordinated to the metal centre at the carboxylate oxygen and the nitrogen atoms binding site. This increased the torsion value of the ring to 28.08° and 27.44° on ring **A** and 24.00° and 22.00° on ring **B** of complex **12**, as shown in figures 4-67.¹¹⁹

The C – C distances in the phenyl rings of each Ni^{2+} complexes and in the free ligand was considered and was found to be within $1.362 \text{ \AA} - 1.420 \text{ \AA}$. These values are within the normal range values for C – C in a phenyl ring.⁶⁷

In **DAMBNI**, the H-bonding comes from the uncoordinated carboxylate oxygen atom with the distance of $\text{C1} - \text{O2} \dots \text{O3B} = 2.709 \text{ \AA}$ while in complex **12**, H-bonding comes from the coordinated carboxylate oxygen atom with a distance of $\text{C7} - \text{O1} \dots \text{O7} = 2.664(3) \text{ \AA}$. Both are strong H-bonds.¹³⁴

In **NUNRUK**, there is H-bonding between the carboxylate oxygen atom and the oxygen atom of the coordinated water molecule with the distance of $\text{O4} - \text{H4A} \dots \text{O1} = 2.6240(14) \text{ \AA}$.¹³⁵

In complex **12**, there are three types of H-bonds. The first H-bond is between the coordinated N atom of the amine group and O_{water} (lattice water) with a distance of $\text{N1} \dots \text{O8} = 2.991(4) \text{ \AA}$. The second type of H-bond is between O_{water} (lattice water) and the uncoordinated water molecule with a distance of $\text{O8} \dots \text{O5} = 3.304(4) \text{ \AA}$. The third type of H-bond is between the coordinated carboxylate oxygen atom and the second O_{water} (lattice water) with a distance of $\text{O1} \dots \text{O7} = 2.664(3) \text{ \AA}$. These H-bonds are the network linkers, linking monomers in complex **12**, represented by turquoise dotted lines as shown in figure 4-68.

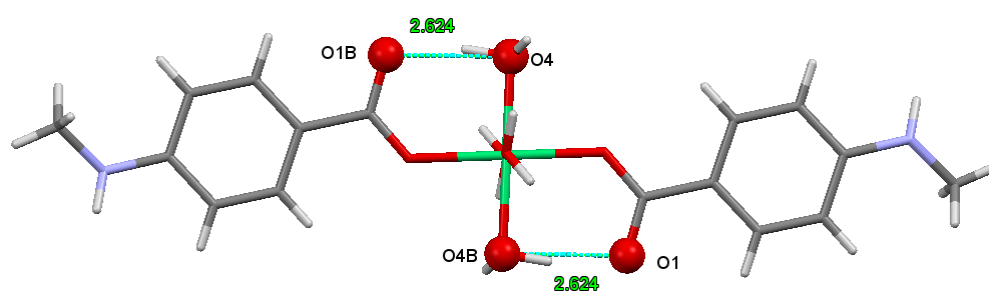
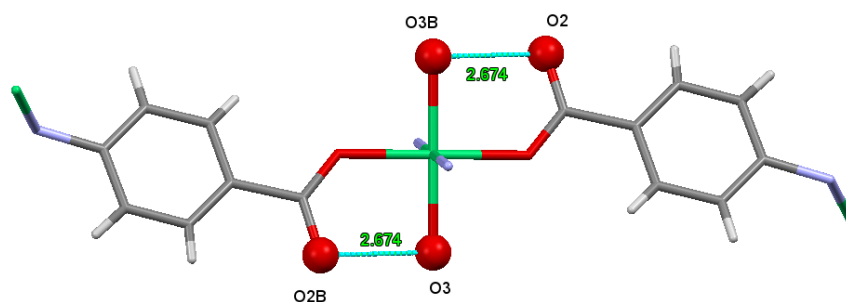
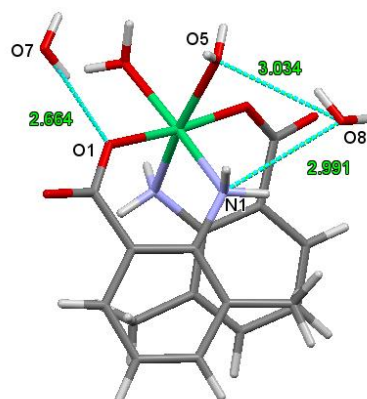


Figure 4-68: Figures showing H-bonding in complex **12** (top), **DAMBNI** (middle) and **NUNRUK** (bottom).^{134, 135}

In complex **12**, the distance between the two ring centroids is 4.582 Å. This is as a result of the coordination around the Ni²⁺ centre especially the *cis* position of the two NH₂ groups

which occupies the *ortho* position to the carboxylate groups on two different rings and were coordinated to the metal centre in *cis* orientation. This made the rings become folded as the Ni centre was pulling the two NH₂ group to itself away from the rings. Also, there is a relatively close $\pi - \pi$ contact of distance 4.583 Å, as shown in figure 4-69, but the distance is too long to be reviewed as a structure-directing influence.⁶⁷

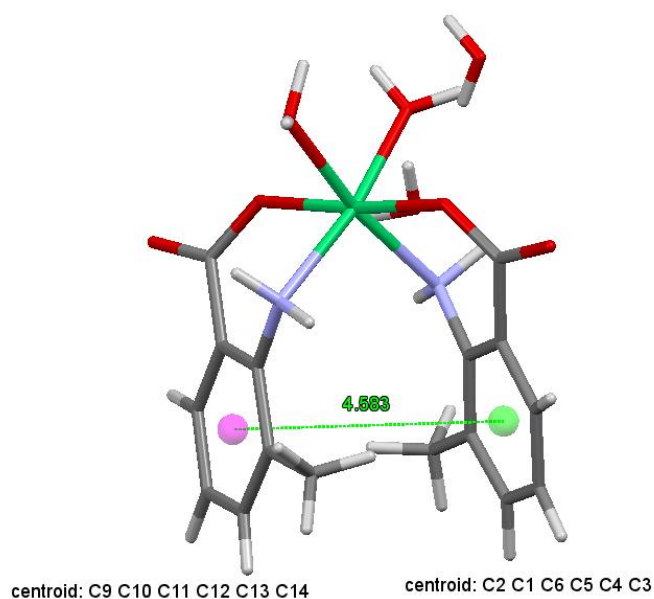


Figure 4-69: The distance between the two ring centroids is 4.582 Å in complex 12.

	12	DAMBNI	NUNRUK
Emp. Form.	Ni(C ₈ H ₈ NO ₂)(H ₂ O) ₂ .2H ₂ O	[Ni(H ₂ NC ₆ H ₄ COO) ₂ .2H ₂ O]	[Ni(C ₈ H ₈ NO ₂) ₂ (H ₂ O) ₄]
Formulae weight	431.08	734.1	431.06
Temperature (K)	100	100	100
Crystal System	Monoclinic	Monoclinic	Monoclinic
Space group	P2 ₁ /c	P2 ₁ /a	P2 ₁ /n
<i>a</i> (Å)	17.1962(9)	11.721(12)	7.5466(2)
<i>b</i> (Å)	14.4447(6)	7.643(6)	6.1811(2)
<i>c</i> (Å)	7.1416(3)	8.590(9)	19.4802(3)
β (°)	97.741(5)	109.74(8)	98.628(3)
Volume (Å ³)	1757.76(14)	724.24	898.40(4)
Z	4	2	2
D _x (Mg m ⁻³)	1.629	1.68 g / cm ⁻³	1.59
Crystal Shape	Plate, Green	Green	Block, Green
R factor (%)	4.12	8.3	0.023

Table 4-24: Crystal data collection of complex 12, DAMBNI and NUNRUK.^{134, 135}

4.3. Summary

The work described in this chapter is an attempt to discover if different 1st-row 3d transition metals can be incorporated into layered structures either by themselves or as bimetallic compounds. 1st-row 3d transition metal complexes $M(\text{AMB})_n$ where $M^{2+} = \text{Cu}^{2+}, \text{Zn}^{2+}, \text{Co}^{2+}$ and Ni^{2+} , no bimetallic crystallization reactions produced bimetallic complexes, but the presence of other metal affected the identity of the deposited crystalline phases, affecting the crystal habit and the extent of hydration.

In the reaction series, AMB acted as monodentate, bidentate or tridentate ligand binding to the metal centre either through the amine groups (NH_2), and one or both of its carboxylate oxygen atoms (COO^-). All the CuAMB crystals studied in this chapter, both anhydrous and hydrate are two-dimensional layered coordination polymers structured in a way that a molecule extends across the whole layer.

The reactive crystallization of the aqueous solutions of NaAMB and NiSO_4 produced two identical hydrated NiAMB complexes. This was compared to two Ni complexes which had been studied previously and deposited in Cambridge Crystallographic Database as **DAMBNI** and **NUNRUK**.

Also, the reactive crystallization of the aqueous solutions of NaAMB and CoSO_4 produced novel hydrated and anhydrous CoAMB complexes **10** and **11**. They crystallize in the monoclinic crystal system and $P2_1/c$ space group but there is apparent void in the structure of the hydrated CoAMB complex **10**.

There is a significant and uniform H-bonding pattern which occurs mainly between N atom of the amine group and O_{carb} in the anhydrous and hydrated novel $M(\text{AMB})_n$ structures under study.

The three determinations of anhydrous CuAMB complexes **5a**, **5b**, and **5c** crystallizes in the orthorhombic crystal system and $Pbca$ space group where **P** is Primitive unit cell (1 lattice point), *b* glide (translation along *b* axis) in *bc* plane, *c* glide (translation along *c* axis) in *ac* plane and *a* glide (translation along *a* axis) in *ab* plane while the three novel hydrated CuAMB complexes crystallize in the monoclinic crystal system and at a different Primitive lattice.

Complexes **6**, **9**, **10** and **11** crystallizes in the monoclinic crystal system and $P2_1/c$ space group where **P** is a Primitive unit cell (1 lattice point), 2_1 is a rotation by 180° around b axis (2-fold screw axis along b : the unique axis) and a translation by $b/2$ and c is a c -glide which consists of reflection in a mirror parallel to the ac plane and a translation by $c/2$.

Complex **7** crystallizes in the monocline crystal system and $P2_1/n$ space group where **P** is a Primitive lattice, 2_1 is a rotation by 180° around b axis and a translation by $b/2$ and b is n -glide which consists of a reflection in the ac plane and a translation by $a/2 + c/2$.

Complex **8** crystallizes in the monoclinic crystal and $P2_1$ space group where **P** is a Primitive unit cell, 2_1 is a rotation by 180° around b axis and a translation by $b/2$.

Complex **12** crystallizes in the monoclinic crystal system and $P2_1/a$ space group where **P** is a Primitive unit cell, 2_1 is a rotation by 180° around b axis and a translation by a -axis in the ab plane.

In the metal-AMB complexes, there seems to be a uniform pattern observed in the connection network of metal-ligand in the complexes under study. The ligands chelate, and bind with metal centre at one of its carboxylate oxygen atom and at the NH_2 such as in the hydrated CuAMB structures complexes **7** and **8**, in the CoAMB structures complexes **10** and **11**, and NiAMB structure complex **12**. This connection occurs in the hydrated CuAMB complexes **7** (figures 4-72 and 4-73) and **8** (figure 4-75), in the anhydrous ZnAMB complex **9** (figure 4-81), in the anhydrous and hydrated CoAMB complexes **10** and **11** (figures 4-82 and 4-84 respectively), and in the NiAMB complex **12** (figure 4-79). But not in the three determinations of anhydrous CuAMB complexes **5a**, **5b**, and **5c** in which the two carboxylate oxygen atoms chelate (attached to one metal centre) while the NH_2 on the same ligand bind to another metal centre in the coordination polymer, as shown in figures 4-70 and 4-71. Save for the carboxylate group acting as bidentate chelating in the three determinations of anhydrous CuAMB complexes **5a**, **5b**, and **5c**, they are topographically related to the hydrated CuAMB complexes **7** and **8** because they are all composed of 2D networks of rings containing four Cu^{2+} and four AMB. The three determinations of anhydrous CuAMB complexes **5a**, **5b**, **5c** and complexes **7** and **8** are all composed of 16-membered rings. Also, the presence of water in the channel in complexes **7** (figure 4-74) and **8** (figure 4-76) is the main difference between the anhydrous and hydrated complexes.

The absence of water in the supramolecular anhydrous CuAMB gave a conformation in which the carboxylate oxygen atoms chelates, binding to one metal centre while the NH₂ group binds to another metal centre in a coordination polymer complex, as shown in figures 4-70 and 4-71.

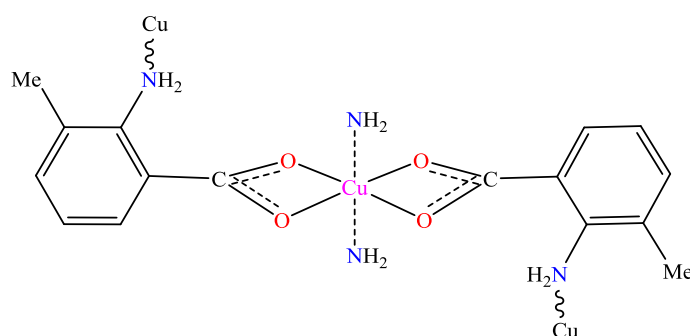


Figure 4-70: Figure showing the coordination environment of the three determinations of anhydrous CuAMB under study: complexes **5a**, **5b**, **5c**, and **DUKTIM**.

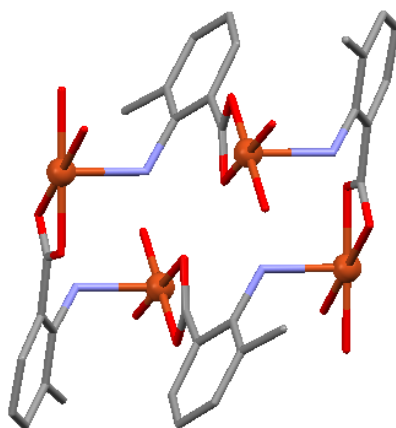


Figure 4-71: Figure showing the interaction of the coordination around Cu²⁺ in the three determinations of anhydrous CuAMB complexes **5a**, **5b**, **5c**, and **DUKTIM**.

When water was introduced and acted as a guest to the host in the supramolecular anhydrous CuAMB structure, it can be said that the guest water molecules are directing the precise mode of assembly of the CuAMB complexes which leads to a change in the coordination around

Cu^{2+} . The carboxylate groups changed from chelating *syn-anti* bridging for complexes **7** and **8**, as shown in figures 4-72 and 4-73. Instead of chelating carboxylate 4-membered rings, each ligand chelates a Cu^{2+} centre in a 6-membered ring via N and O. Assembly of monomers containing two of such chelate rings is achieved by bridges from the non-chelating carboxylate oxygen atom of one monomer to a Cu^{2+} centre in the next. These contacts are much longer (mean 2.51875 Å for complex **7** and mean 2.5505 Å for complex **8**) compared to the intra-chelate distances (mean 1.9365 Å for complex **7** and mean 1.9338 Å for complex **8**).

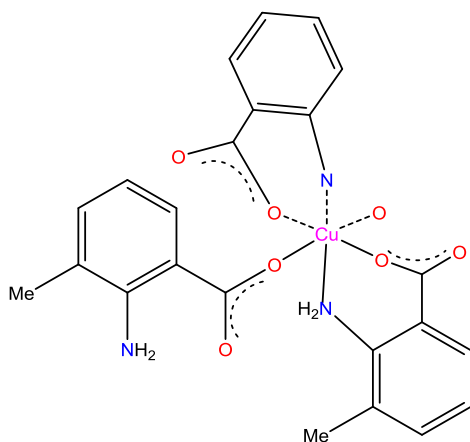


Figure 4-72: Figure showing the coordination environment of Cu^{2+} in complexes **7** and **8** which is as a result of the guest water molecules.

Water in the channel promotes changes in the structure. There is a phase change accompanying partial filling of the channel. Figure 4-73 is a view of one of the layers from the top showing clearly how the 2D net is formed in complex **7**. 16-membered rings with Cu^{2+} at the nodes form the secondary building unit. Cu – O distances alternate long and short, showing the effect of Jahn-Teller distortion (*vide infra*).

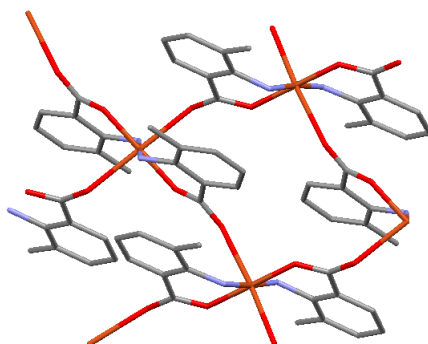


Figure 4-73: Figure of one layer from the top viewed down showing the connection that leads to the 2D net in complex 7.

The lattice water molecules in complex 7 are ordered, as shown in figure 4-74 when compared with those in complex 8.

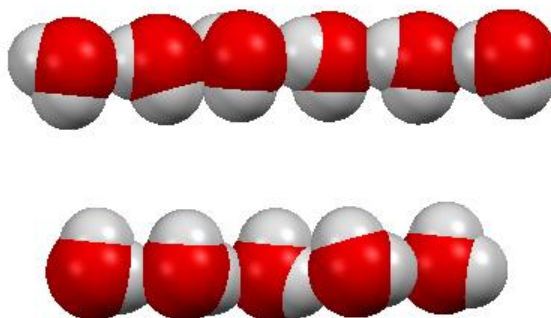
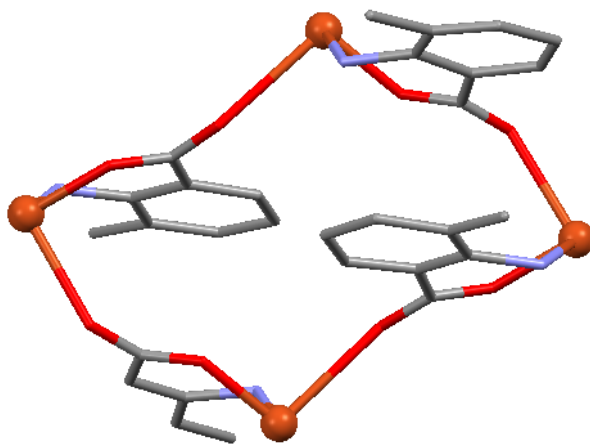


Figure 4-74: Figure showing 1D H-bonded water molecules in the channel in complex 7.

It might be assumed that the addition of Ni^{2+} salts to the Cu^{2+} solution in the preparation of complex 8 leads to the fact that complex 8 (figure 4-75) differs from the three determinations of anhydrous CuAMB complexes 5a, 5b, and 5c but in fact complex 8 is almost identical to complex 7 which was crystallized in the absence of Ni^{2+} ; it differs only to the extent of filling of the water channel. However, one factor that is shared by complexes 7, 8, and 12 (the nickel complex, *vide infra*) is the coordination mode of the AMB, which is O, N chelated, whereas the three determinations of anhydrous CuAMB complexes 5a, 5b and 5c have the COO^-

chelated, with the NH₂ group forming bridges to another Cu centre, a role that it exchanges with the second carboxylate oxygen atom in complexes **7**, **8** and **12**.



*Figure 4-75: Figure showing the connection between the geometric environments of Cu²⁺ in complex **8**.*

In complex **8**, the H-bonded water chain is disordered. The geometry of each of the water molecules is not uniform (facing the opposite direction to each other), as shown in figure 4-76. This is due to the fact that the overall quality of the data obtained is not sufficient to analyze in detail.

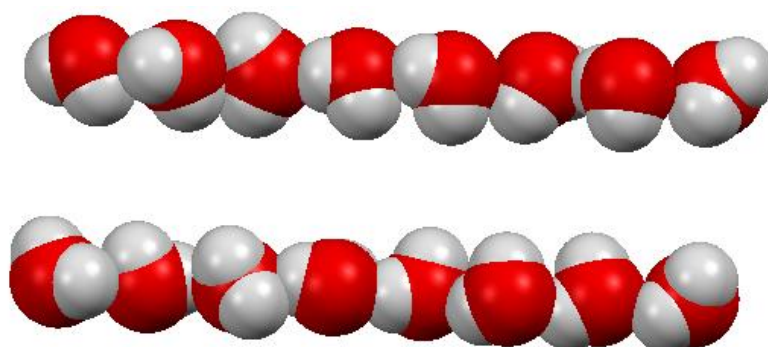


*Figure 4-76: Figure showing 1D H-bonded water molecules in the channel in complex **8**.*

H-bonded 1D water chain is of great interest in chemistry world of recent time because water is the world's most important molecule and for the important role played in water transport and other functions such as in proton translocation through membranes.¹⁴⁰⁻¹⁴² H-bonding interactions and their fluctuations are the major determinants of the properties of water molecules. Understanding and describing the interactions between water molecules is difficult.¹⁴³ Also, water plays a space filling role where there are cavities of a suitable size which result from close packing of the organic molecules.¹⁴⁴ Recently, a single crystal analysis of a compound revealed the emergence and the stabilization of 1D water chains of lattice water trapped inside the hydrophilic channels of a 2D H-bonded network from *S*-alkylation (*o*-aminothiophenol and *p*-xylene dibromide) and Schiff base condensation (4-pyridinecarboxaldehyde) in acetonitrile at room temperature. The solvent was left to evaporate and the crude product was purified by re-crystallization in chloroform-methanol. The single crystal obtained was characterized and deposited in the Cambridge Crystallographic Database as **GIHFOV**.¹⁴¹

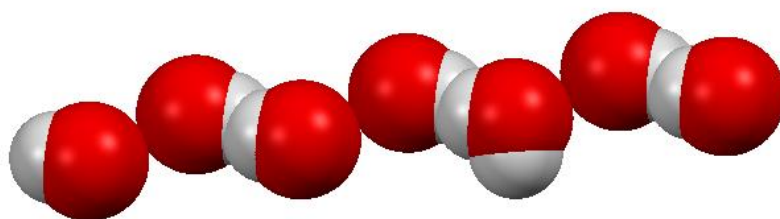


*Figure 4-77: A view of H-bonded 1D water strand in GIHFOV.*¹⁴¹

It is a known fact that 1D water chains can be stabilized by strong H-bonding between neighboring water molecules and donor-acceptor groups associated with the channels.¹⁴² The structure and dynamics of 1D water chains that were stabilized using imidazole have been studied and deposited in the Cambridge Crystallographic Database as **BEHBOG**. In the structure, the uncoordinated water molecules are trigonally distorted and form strong H-bonds with symmetry-related molecules and with the nitrogen atoms of imidazole which are directed towards the channels, as shown in figure 4-78.¹⁴²

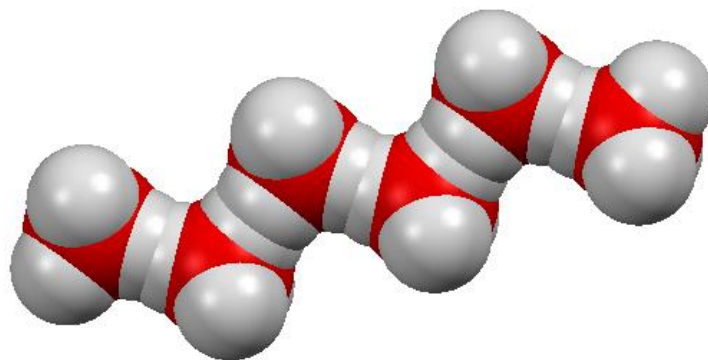


Figure 4-78: A view of trigonally distorted 1D water chain in **BEHBOG**.¹⁴²

Chemically, complexes **7** and **8** are the same but they are crystallographically different because of different occupancy of the water channel. The geometric isomers around Cu centre are the same in the hydrated complexes. Complex **7** has ordered lattice water more than complex **8**.

Complex **7** crystallizes from a solution which does not contain Ni²⁺ salt solution while complex **8** has a small amount of Ni²⁺ salt solution.

Complex **12** has the same O, N chelated form of AMB as in complexes **7** and **8** but while in complexes **7** and **8**, these were mutually *trans*, in complex **12**, the N atoms are *cis* while the O atoms are *trans* (figure 4-79). This leads to a much different pattern of association. Because complex **12** also contains two coordinated water molecules, it is not able to form a coordination network. Hence, there is nothing in complex **12** which offers a clear rationale for the presence of the water channel in complex **8**.

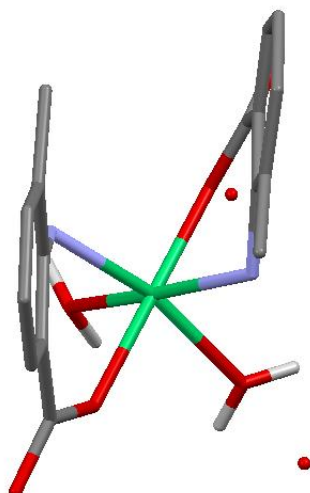


Figure 4-79: Figure showing the interaction of the coordination around Ni^{2+} in NiAMB: complex 12.

A further structure showing common features as other CuAMB complexes were characterized and analyzed as complex **6**. Like the other CuAMB complexes obtained in this study, complex **6** has coordinated water molecules. It possesses two different coordination modes, the chelating O, N as in the hydrated CuAMB complexes **7** and **8** and the bridging O, N as in the three determinations of anhydrous CuAMB complexes **5a**, **5b**, and **5c**, as shown in figure 4-80. The COO^- in the three determinations of CuAMB complexes **5a**, **5b** and **5c** are chelating bidentate while they are monodentate in complex **6**.

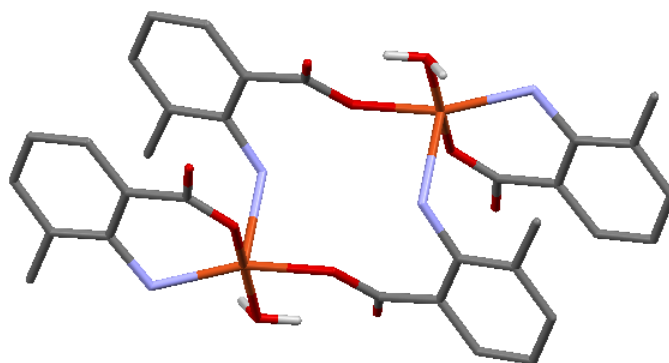


Figure 4-80: Figure showing the interaction of the coordination around Cu^{2+} in the CuAMB dimer: complex 6.

The closest intermolecular contact in complex **6** is 3.226(2) Å. The chelating O, N distance is equatorial with the closest distance of 2.02(2) Å while the bridging O, N is axial with a longer distance of 2.64(2) Å.

The connection network of the coordination around Zn²⁺ in ZnAMB is similar to those in complexes **7** and **8**, as shown in figure 4-81.

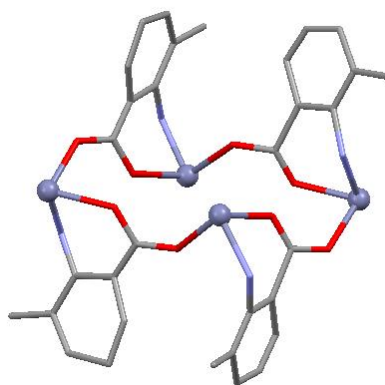


Figure 4-81: Figure showing the interaction of the coordination around Zn²⁺ in ZnAMB: complex **9**.

That is to say, 16-membered rings are formed by four monomers via *syn-anti* bridging carboxylates which formed a 2D net via metal nodes. The amines coordinate mutually *trans* completing the octahedral coordination around the metal. It differs, however in details. In complexes **7** and **8**, the phenyl rings were paired, up-up, down-down, with respect to the 16-membered ring plane. In complex **9**, the rings alternate, up-down, up-down. This results in the absence of the water-containing channels in complex **9**, which is present in complexes **7** and **8**. In the case of anhydrous [Zn(AMB)₂]_n, there is a much smaller range of metal-oxygen distances than in the three determinations of anhydrous CuAMB complexes **5a**, **5b**, and **5c** or hydrated CuAMB complexes **7** and **8**.

The ligands in the anhydrous and the hydrated CoAMB complexes acted similarly, chelating, binding to Co centre at one of the carboxylate oxygen atom and at the NH₂. The coordination environment of Co²⁺ is similar in the two Co²⁺ complexes under study save for the fact that

the NH₂ groups are in *cis* orientation in the hydrated CoAMB complex **10** but are in *trans* orientation in the anhydrous CoAMB complex **11**, as shown in figures 4-82 and 4-84.

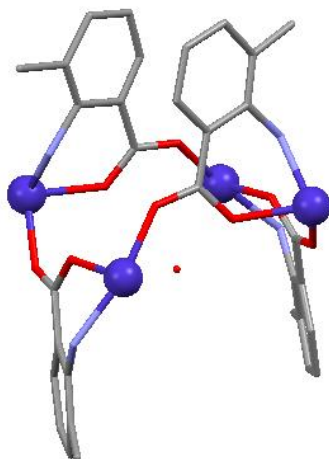


Figure 4-82: Figure showing the interaction of the coordination around Co²⁺ in the hydrated CoAMB complex **10**.

This gave 16-membered puckered rings which look more compressed. There is $\pi - \pi$ stacking in the structure between rings C10 – C15 and C2 – C7, their ring centroids are separated by a distance of 3.558 Å, as shown in figure 4-83. This distance can be compared with a distance of 3.6 Å found by Lightfoot *et al.* in a π -stacked aromatic amide.¹⁴⁵ The other two aryls are separated by a centroid-centroid distance of 4.498 Å. This larger distance allows accommodation of water of crystallization in the void.

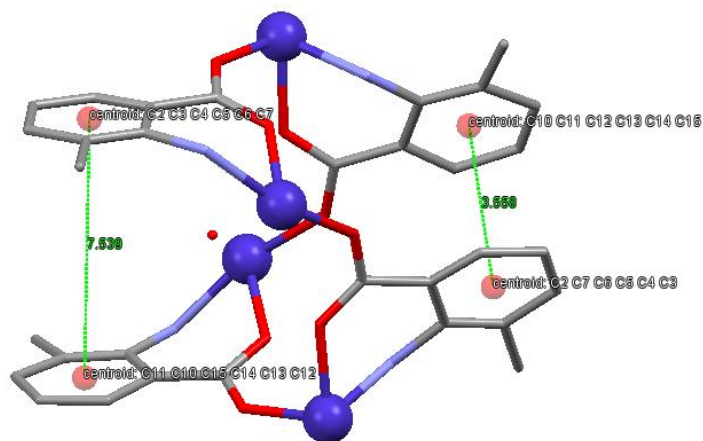


Figure 4-83: Figure showing the $\pi - \pi$ stacking distance between the two rings as 3.558 Å in the structure of complex **10**.

The rings are slightly closed up-down, up-down. The complex has a different topology 2D sheet though it is an octahedral complex with 16-membered rings like the anhydrous CoAMB complex **11**.

In complex **11**, the NH_2 groups are in *trans* orientation in the anhydrous CoAMB complex **11** as shown in figure 4-84. The rings are not compressed and there is no $\pi - \pi$ stacking in the structure of complex **11** as the distance between the two rings is 11.238 Å.

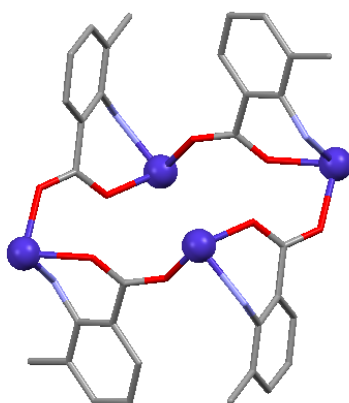


Figure 4-84: Figure showing the interaction of the coordination around Co^{2+} in the anhydrous CoAMB complex **11**.

In the complexes under study, there is distortion in the octahedral geometric environment of Cu^{2+} in complexes **7** and **8** due to the Jahn-Teller effect in the form of tetragonal elongation. This is as a result of the unequal electron occupancy of the d orbitals in $\text{Cu}(\text{II})$ that comprises the formal set of e_g of the undistorted precursor.^{146, 147}

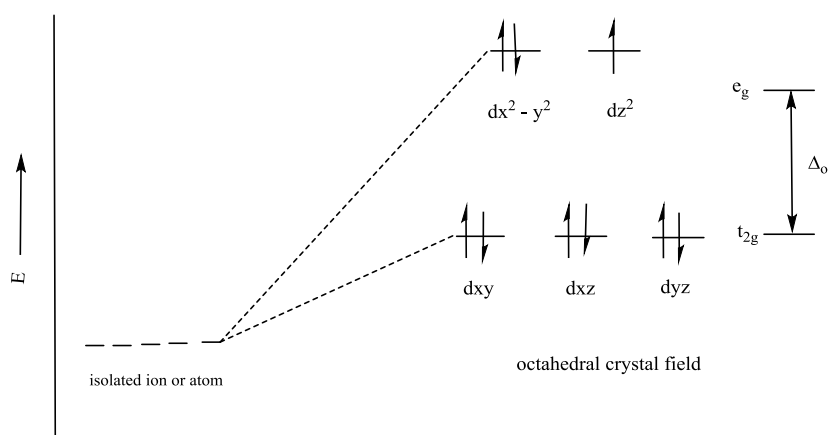


Figure 4-85: Configuration with significant Jahn-Teller distortion in d^9 [Cu^{2+}].

Though d^8 and d^{10} complexes do not exhibit Jahn-Teller distortion, considerable distortion may be observed in low spin d^7 complexes because Jahn-Teller distortion is usually significant for asymmetrically occupied e_g orbitals since they are directed towards the ligands (figures 4-86 and 4-87).

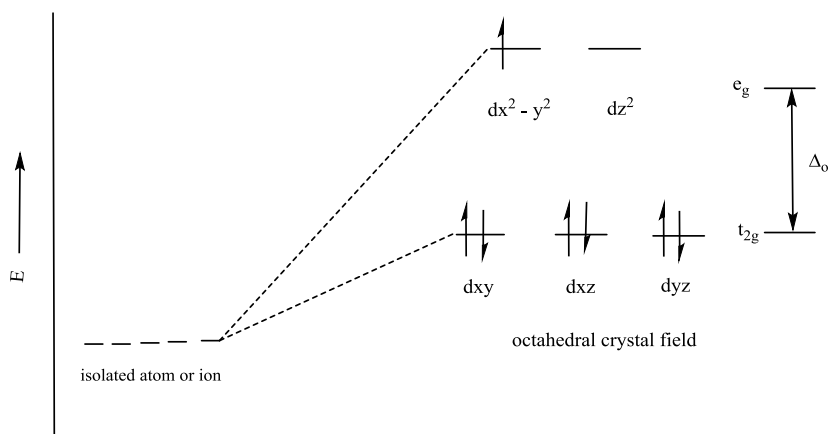


Figure 4-86: Configuration with significant Jahn-Teller distortion in low spin d^7 [Co^{2+}].

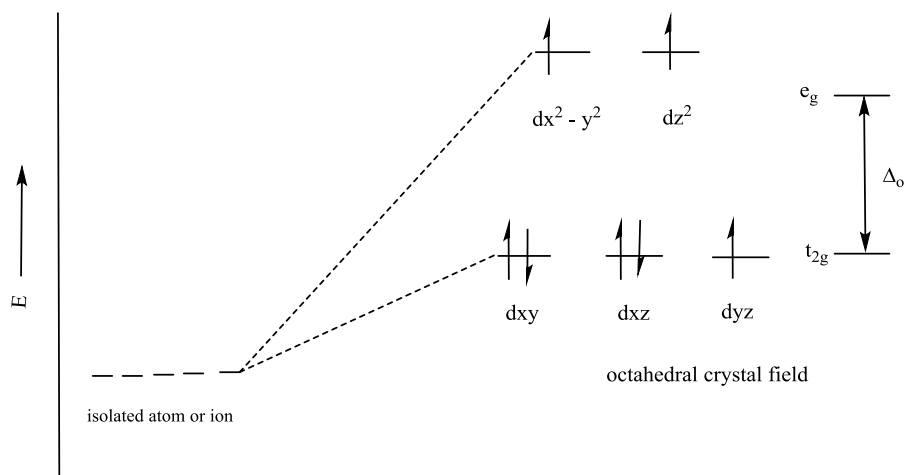


Figure 4-87: Configuration with less significant Jahn-Teller distortion in high spin d^7 [Co^{2+}].

Though the methyl group attached to the AMB ligand does not take part in the coordination environment of the transition metal complexes, it radically affected packing in the $[\text{M}(\text{AMB})_n]$ structures as shown in figure 4-88. This is a feature which led, directly, to the channels in complexes **7** and **8** being filled by 1D H-bonded water molecules.

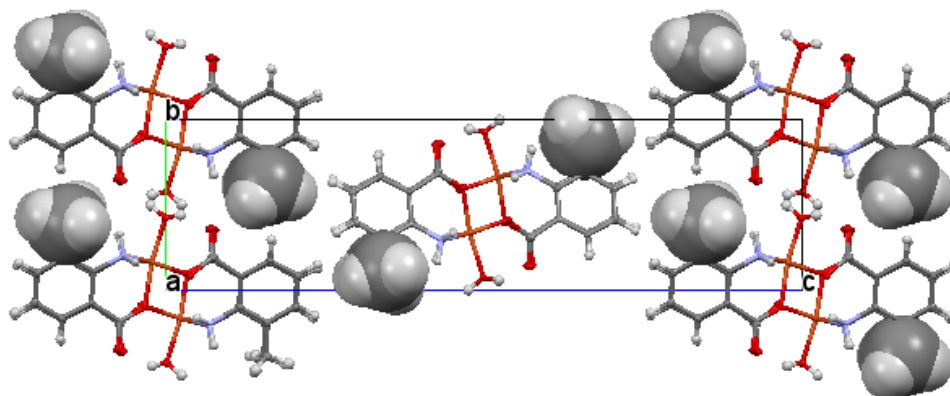


Figure 4-88: Figure of the dimer CuAMB complex showing the effect of the methyl group (highlighted) when packed.

Chapter 5

Small-scale Crystallization of MgSO_4 and MnCO_3 Hydrates with Benzoic Acid from Aqueous Solution in order to screen for Polymorphs and Solvates

5.1. Introduction

Manganese complexes have potential application as molecular magnets when constructed with short bridging ligands such as O^{2-} , $(OH)^-$, N_3^- $(CN)^-$ and $(SCN)^-$ to link Mn cations as it is proven that a short Mn – Mn distance benefits the magnetic exchange between adjacent metal atoms. They also have the ability to function as nodes for constructing metal-organic frameworks, which have important uses for the interchange of gases.¹⁴

A search of the Cambridge Crystallographic Database for carboxylate based manganese complexes as illustrated in figure 5-1 shows that 1099 carboxylate based manganese complexes have been previously studied.

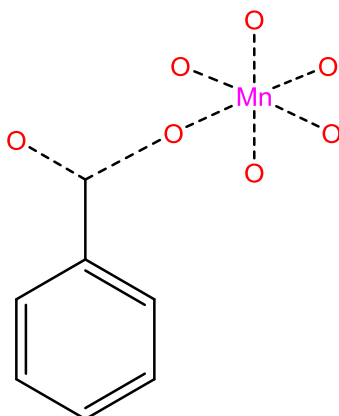


Figure 5-1: Query built for the statistics of manganese carboxylate based complexes studied and deposited in the Cambridge Crystallographic Database.

A typical example found in the database is $Mn(H_2O)_2(4,4'-bipy)(HBTC)_2 \cdot [H_4,4'bpy]_2$ i.e. catena-[bis(4,4'-bipyridin-1-ium) (μ_2 -4,4'-bipyridine-N,N')-diaqua-bis(1-carboxybenzene-2,4-dicarboxylato-O)-manganese(ii)]; which was one of the complexes studied as part of research on the 'synthesis, structures and magnetic properties of three metal-organic frameworks containing manganese' and was deposited into the Cambridge Crystallographic Database as **NAFGEI**. Single crystals of **NAFGEI** were obtained by the evaporation of the mother liquor of a standard hydrothermal reaction of the mixture of H_3BTC and $MnC_4H_6O_4 \cdot 4H_2O$ and 4,4'-bipyridine in ratio 1:1:1/2 in distilled water at 140 °C for 72 hours.¹⁴

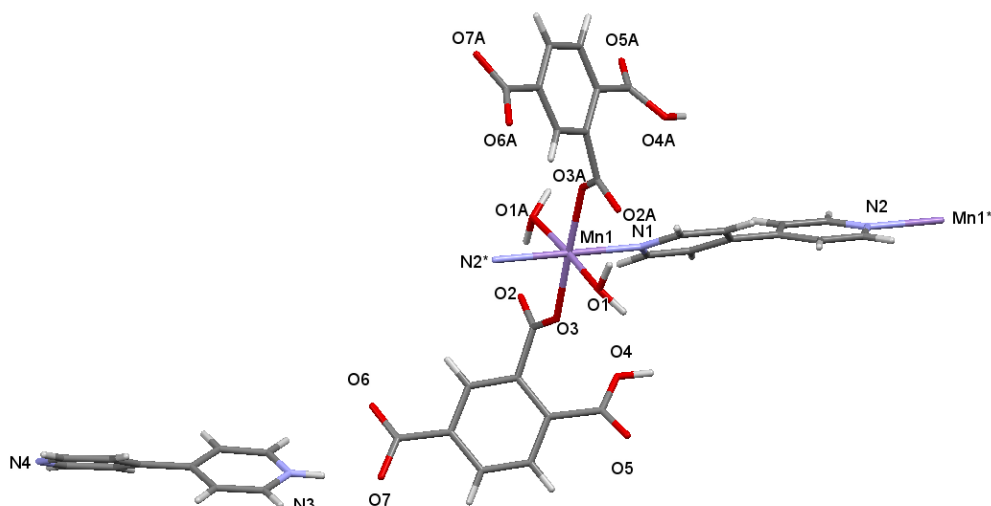


Figure 5-2: Molecular structure of **NAFGEL**.¹⁴

NAFGEL crystallizes in the monoclinic system and displays C_2 symmetry with a two-fold crystallographic axis running along the axis defined by the two nitrogen donors N1 and N2 from the 4,4'-bpy ligands with Mn – N distances of 2.273 Å and 2.304 Å and two symmetrical Mn – O_{water} distances of 2.188 Å. The distorted octahedral geometry is completed by two symmetrical Mn – O_{carb} distances of 2.167 Å to the H₂BTC ligands, as shown in figure 5-2.¹⁴

An example of a manganese complex without N donor atoms but in which the carboxylate groups are deprotonated appeared in a report on the ‘crystal structures, topological analyses and magnetic properties of manganese-dihydroxyterephthalate complexes’ and was deposited in the Cambridge Crystallographic Database as **QUJJUB01**. This was obtained from the solvothermal reaction of Mn(OAc)₂ and H₄dhtp in mixed ethanol and water in the ratio 1:1 at a temperature of 110 °C in 4 days.¹⁴⁸

QUJJUB01 consists of 1D carboxylate-bridged Mn(II) chains, which are further connected by H₂dhtp ligands to form a 3D network. It crystallizes in the monoclinic crystal system and $P2_1/c$ space group. The octahedral environment of Mn²⁺ has C_2 crystallographic symmetry and comprises of four symmetrical carboxylate oxygen atoms from individual ligands with Mn – O_{carb} distances of 2.125 Å and 2.173 Å. The distorted octahedron motif is completed by two symmetrical water molecules in a *cis* orientation to each other with Mn – O_{water} distances of 2.197 Å. The carboxylate groups in the ligand adopt a *syn-anti* bidentate coordination

mode in which each of the four carboxylate oxygen atoms coordinates to a metal centre as shown in figure 5-3.¹⁴⁸

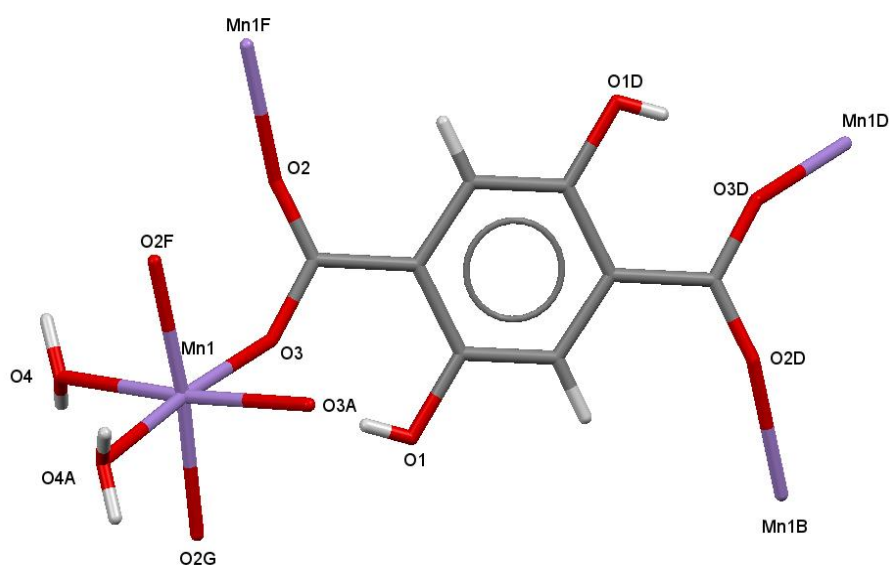


Figure 5-3: Molecular structure of QUJJUB01.¹⁴⁸

Comparing with the previous chapter in the current study, manganese does not form layered structures when reacted with NaAMB at different concentrations in the same way the other 1st-row 3d transition metals do, *c.f.* Cu²⁺, Co²⁺, Ni²⁺ and Zn²⁺.

A search of the Cambridge Crystallographic Database revealed that approximately 80 structures containing manganese with only benzoate ligands had previously studied. These are mainly large clusters of the types used for single molecule magnets, but there are some extended structures, including six coordination polymer chains. However, no 2D structures of the type encountered in the current study were reported. Hence, as part of this study, two sets of manganese benzoate reactive crystallization reactions were carried out in an effort to develop our understanding of binary 1D and 2D manganese benzoate structures.

Colourless needle-shaped crystals of complex **13** were obtained from experiment 1 and subjected to single crystal analysis. Three sets of crystals with different habits, as shown in figure 5-4, were obtained from experiment 2 and subjected to single crystal analysis.

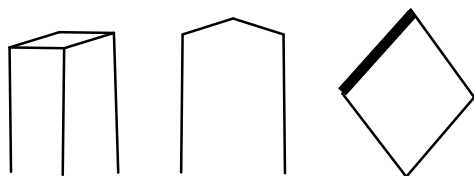


Figure 5-4: Shape of the crystals obtained from experiment 2.

These three crystals were subjected to single crystal analysis at 150 K and 293 K. Single crystal analysis revealed that two of the three crystals are the same as complex **13**, obtained in experiments 1, but the third crystal shape had a different crystal system and space group compared to complex **13** and was shown to be a new structure, complex **14**.

5.2. Results and Discussion

5.2.1. Structural Characterization of $[\text{Mn}_2(\text{C}_6\text{H}_5\text{CO}_2)_4(\text{H}_2\text{O})_6]\cdot(\text{H}_2\text{O})_2$

5.2.1.1. Introduction

Colourless needle-shaped crystals of complex **13** were obtained by the reactive crystallization of manganese(II)sulfate monohydrate and sodium benzoate in deionized water at room temperature, as shown in figure 5-5.

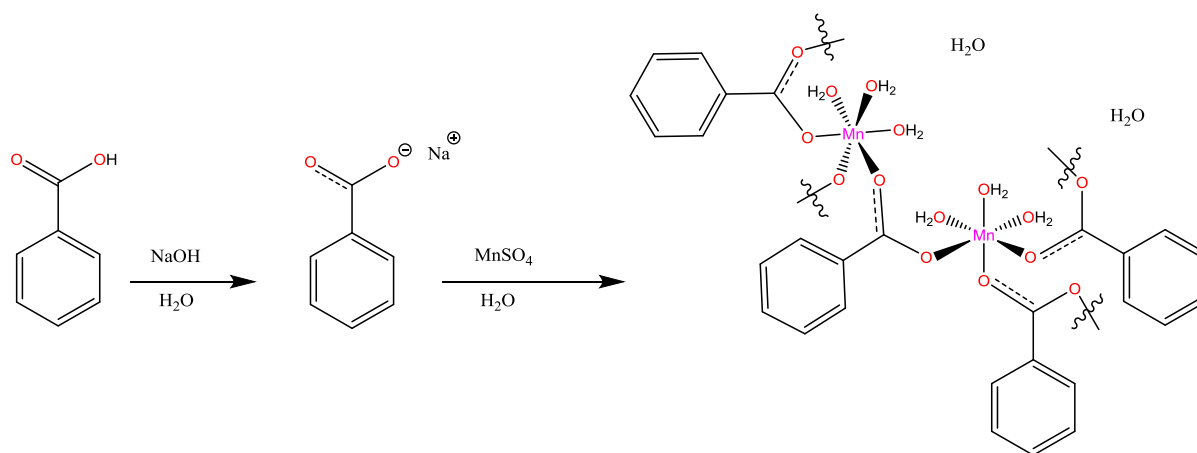


Figure 5-5: Schematic of the reaction that produced complex **13**.

A single crystal of complex **13** was subjected to single crystal analysis at 150 K. The structure obtained could not be matched to any structure in the Cambridge Crystallographic Database.

5.2.1.2. Crystal Structure Determination of Complex **13**

The measurement was carried out on an XtaLAB AFC11 (RINC): Kappa single diffractometer using Mo K α radiation, $\lambda = 0.71073 \text{ \AA}$ at 150 K. Complex **13** crystallizes in the monoclinic crystal system and P2₁/n space group.

A full list of crystal parameters and structure determination details, a view of the molecular structure of complex **13**, and tables of selected bond lengths and angles are presented below.

	13
Empirical formula	$[\text{Mn}_2(\text{C}_6\text{H}_5\text{CO}_2)_4(\text{H}_2\text{O})_6] \cdot (\text{H}_2\text{O})_2$
Formula weight	738.45
Temperature (K)	150
Crystal system	Monoclinic
Space group	$P2_1/n$
a (Å)	8.9041(4)
b (Å)	10.5638(4)
c (Å)	35.2830(16)
β (°)	96.521(4)
Volume (Å ³)	3297.3(2)
Z	4
D_x (Mg m ⁻³)	1.488
μ (mm ⁻¹)	0.84
$F(000)$	1528
R factor (%)	7.93

Table 5-1: Crystal data collection of complex 13.

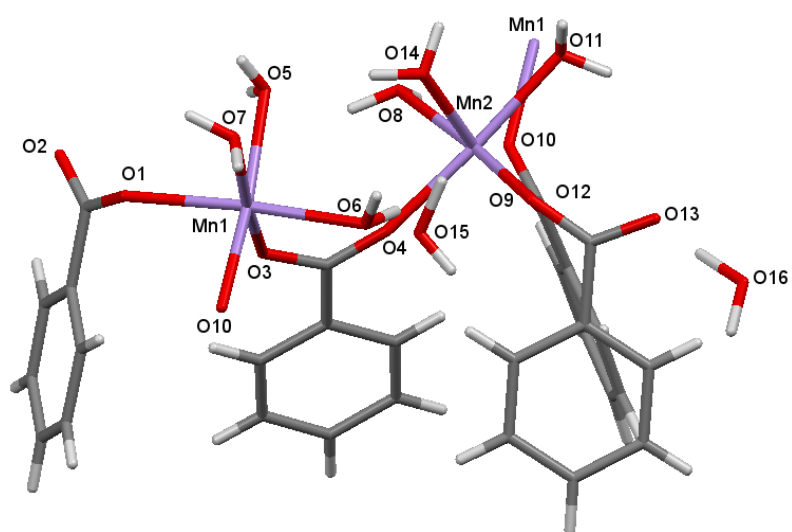
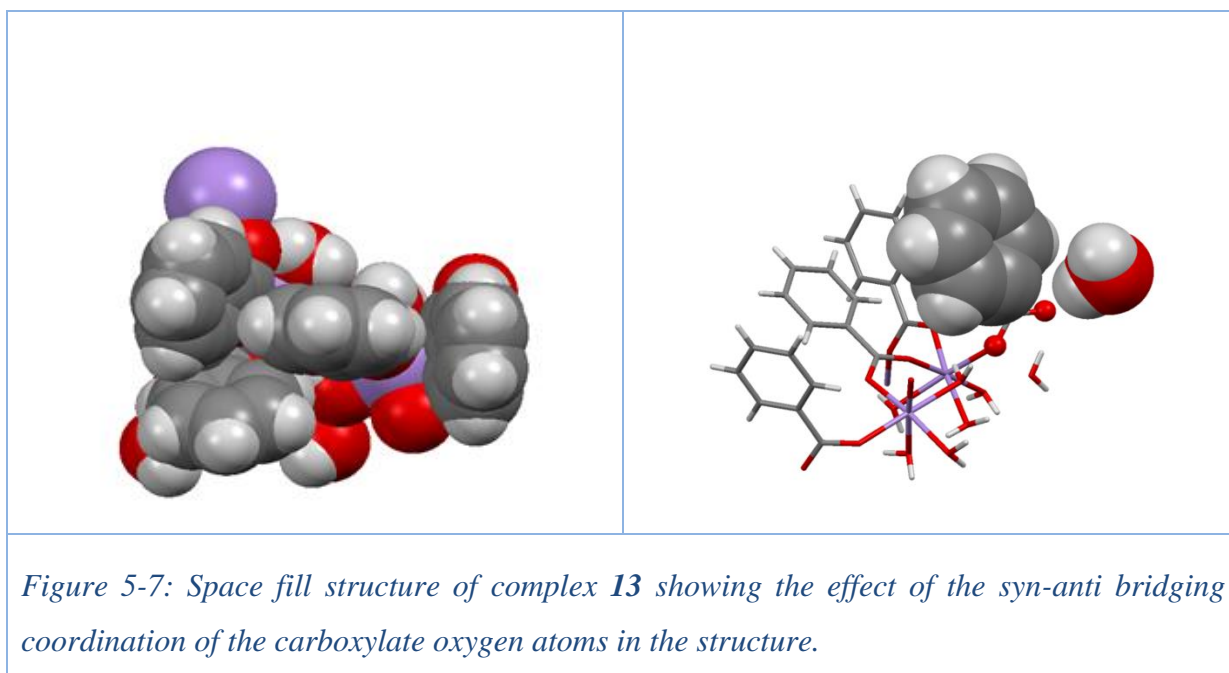


Figure 5-6: Molecular structure of complex 13.

The structure is very nearly **C** centered and can be refined in a **C** centered space group by omitting all the weak reflections to give a good R factor of 0.079. However, in this space group, the lattice water is disordered over 2 semi-populated sites. When the symmetry is reduced to **P** the number of atoms in the asymmetric unit doubles and the disordered water is replaced by ordered molecules, which is the preferred representation of complex **13**.

Complex **13** contains two crystallographically independent (non-symmetric) metal centres, Mn1 and Mn2. Both Mn²⁺ centres adopt a distorted octahedral geometry, which involves three *cis* aqua oxygen atoms and three *cis* oxygen atoms of bridging carboxylate groups; with two water lattices as shown in figure 5-6.

The carboxylate oxygen atoms for two of the benzoates are coordinated to the metal centres in *syn-anti* bridging coordination mode, in which one ring sits in the plane and the second ring faces the side of the first ring because there is no space for the ring to sit in the plane. The third benzoate is attached to the metal centre in a *syn* orientation with its second oxygen in a non-coordinating position, as shown in figure 5-7b.



The C – O distances are significantly different. The shorter C – O bond distances are 1.239(2) Å and 1.246(2) Å, which are for O_{carb} that do not bond to any Mn centre, but they are close to the lattice water in the structure.

Complex **13** is a one-dimensional polymer chain that has water filling gaps around it. When expanded, the uncoordinated water molecules fill gaps in between the polymeric chains leading to a distinctly lamellar arrangement, as shown in figure 5-8.

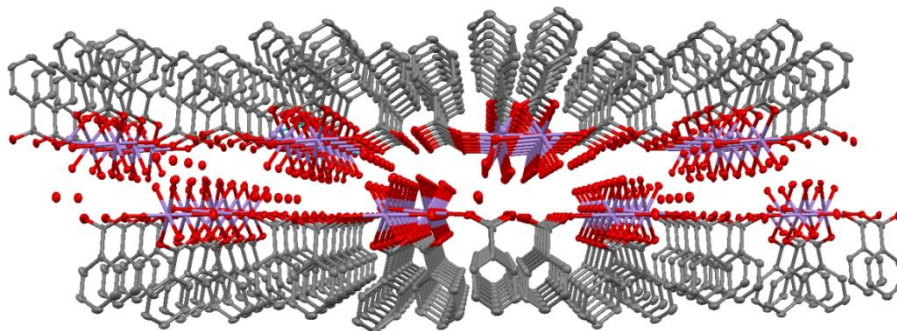


*Figure 5-8: Layered structure of complex **13** showing the coordinated and uncoordinated water molecules in-between the chain. Hydrogen atoms have been omitted.*

The difference in the bridging modes of carboxylate group seems to be responsible for the shorter interatomic Mn – Mn distance of 4.867(4) Å. This value appears favourable to magnetism, hence, the magnetic study for complex **13** is recommended in further work.

When packed, the water fills the spaces between the molecules, connecting them via H-bonds, as shown in figure 5-9.

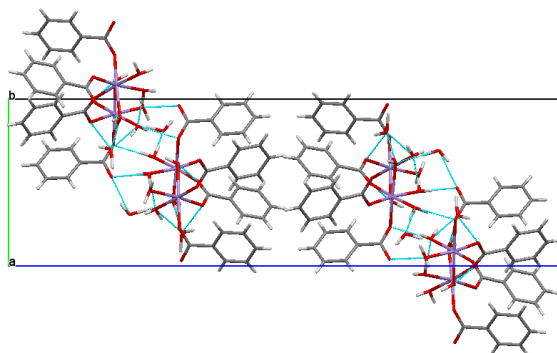


*Figure 5-9: Structure of complex **13** viewed down *b* crystallographic packing view showing the H-bond connection in turquoise dotted lines.*

The geometric environment of complex **13** can be compared with that of a structure which had been previously studied as the crystal structure of bis(4-nitrobenzoate) tetraaquamanganese(II) dehydrate, $[\text{Mn}(p\text{-NO}_2\text{C}_6\text{H}_4\text{COO})_2(\text{H}_2\text{O})_4]\cdot 2\text{H}_2\text{O}$ and deposited in the Cambridge Crystallographic Database as **QIHQUT**.

QIHQUT was prepared by the reaction of a mixture of $\text{Mn}(\text{NO}_3)_2$ and $\text{NH}_4\text{C}_7\text{H}_4\text{NO}_4$, a para-substituted benzoic acid, in boiling water, while complex **13** was prepared from $\text{MnSO}_4\cdot\text{H}_2\text{O}$ and $\text{NaC}_7\text{H}_5\text{O}_2$, a monocarboxylic acid, in H_2O at room temperature.¹⁴⁹

Complex **13** crystallizes in the monoclinic crystal system and $\text{P}2_1/\text{n}$ space group, while **QIHQUT** crystallizes in the triclinic crystal system and $\text{P}-1$ space group. Complex **13** contains two crystallographically independent Mn centres while **QIHQUT** has one Mn centre. Hence, the coordination environment of the only Mn centre in **QIHQUT** can be used to compare and describe the two Mn centres in complex **13**. Also, the coordination of the ligands in complex **13** is intriguing in a way that three ligands are coordinated to one Mn centre via one of their carboxylate oxygen atoms in *cis* orientation and the second carboxylate oxygen atoms are coordinated to another Mn centre in *syn-anti* bridging coordination mode. The octahedral geometric environment of each Mn centre is completed by three aqua oxygen atoms in *cis* orientation with one lattice water molecule. In **QIHQUT**, one of the carboxylate oxygen atoms of the *p*-nitrobenzoate ligands is coordinated in monodentate *trans* mode while the second carboxylate oxygen atom is uncoordinated. The octahedral coordination around Mn centre is completed by four aqua oxygen atoms with one lattice water molecule, as shown in figure 5-10.¹⁴⁹

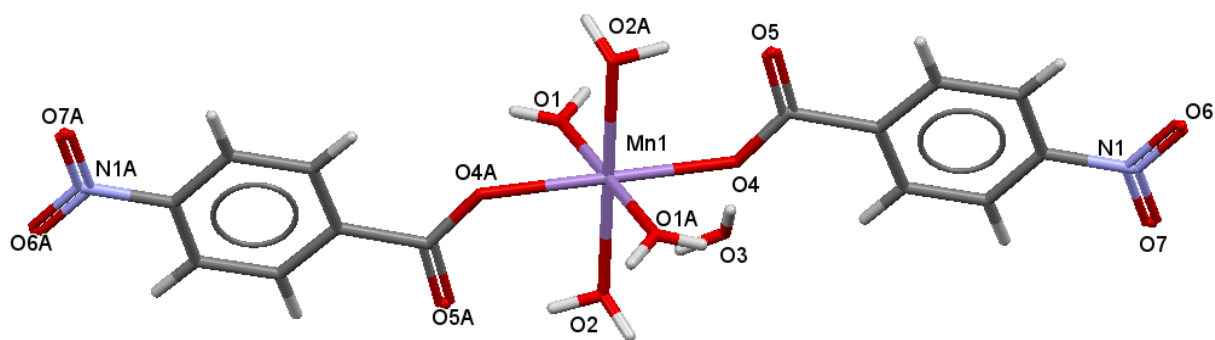


Figure 5-10: Molecular structure of **QIHQUT**.¹⁴⁹

In complex **13**, the Mn1 – O_{water} bond lengths are significantly longer than two of the three Mn1 – O_{carb} bond lengths. For Mn2 centre, the Mn2 – O_{water} bond lengths are significantly longer than the Mn2 – O_{carb} bond lengths without exception. The bond distance of the carboxylate oxygen atom that is coordinated to Mn centre in *anti*-coordination mode appears longer than that of those that are coordinated in the *syn* coordination mode. Also, the longest bond distances are for the carboxylate oxygen atoms that are attached to Mn²⁺ in *syn* topology position relative to the second C – O. This helps to explain the distortion in the octahedral geometry environment of the two Mn²⁺ centres in which some of the bonds of the coordinating atoms are more elongated than each other.

In **QIHQUT**, the Mn atom is situated on a twofold axis and displays pseudo-octahedral coordination. The O_{carb} is coordinated to the Mn centre in *syn* monodentate coordination mode, while it is in *syn-anti* bridging coordination mode in complex **13**.

Mn1 centre		Mn2 centre		QIHQUT	
Distance	(Å)	Distance	(Å)	Distance	(Å)
Mn1 – O1	2.1893(9)	Mn2 – O4	2.1261(10)	Mn1 – O1	2.180(1)
Mn1 – O3	2.1235(9)	Mn2 – O8	2.2549(9)	Mn1 – O2	2.195(1)
Mn1 – O5	2.2759(10)	Mn2 – O9	2.1027(10)	Mn1 – O4	2.184(1)
Mn1 – O6	2.1832(10)	Mn2 – O11	2.2276(10)	Mn1 – O1A	2.180(1)
Mn1 – O7	2.1716(9)	Mn2 – O12	2.1540(10)	Mn1 – O2A	2.195(1)
Mn1 – O10	2.1465(11)	Mn2 – O14	2.1582(9)	Mn1 – O4A	2.184(1)
O1 – C1	1.2791(16)	O9 – C15	1.2567(18)	O4 – C1	1.272(2)
O2 – C1	1.2386(18)	O10 – C15	1.2707(17)	O5 – C1	1.235(1)
O3 – C8	1.2775(17)	O12 – C22	1.2795(17)	O4A – C1A	1.272(2)
O4 – C8	1.2477(17)	O13 – C22	1.2456(18)	O5A – C1A	1.235(1)

Table 5-2: Bond distances of atoms coordinating around the two Mn centres and the C – O distances in complex **13** and in **QIHQUT**.¹⁴⁹

The Mn – O_{carb} distance is 2.184(1) Å in **QIHQUT** with a C – O distance of 1.272 Å for the O_{carb} coordinated to Mn centre and 1.235(1) Å for the non-coordinating O_{carb}. In complex **13**,

the Mn – O_{carb} distances around the two Mn centres vary from 2.103(1) Å to 2.1893(9) Å and the C – O distances range from 1.239(2) Å to 1.280(2) Å with the O_{carb} coordinated to Mn centre in *anti*-coordination mode longer than the O_{carb} coordinated to Mn centre in *syn* coordination mode, as listed in table 5-2.¹⁴⁹

The Mn – Mn interlayer distance in the polymeric network of complex **13** is 8.118(6) Å as represented in figure 5-11 while the Mn – Mn interlayer distance in **QIHQUT** is 7.330 Å.

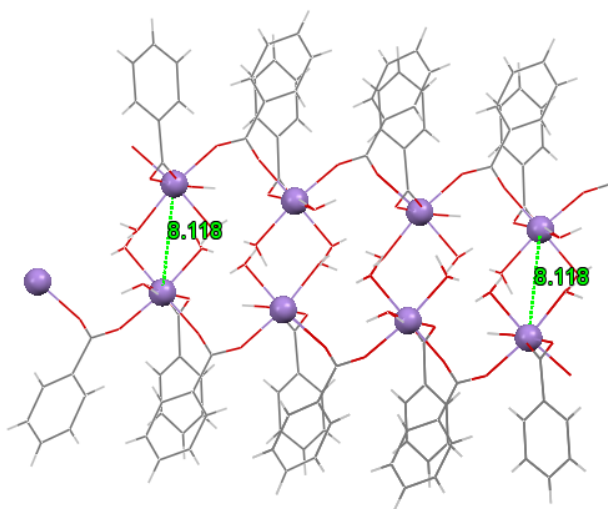


Figure 5-11: View down interlayer space of complex **13** showing the shortest Mn – Mn interdistance to be 8.118(6) Å represented with green dotted lines.

In **QIHQUT**, the bond angle O1 – Mn1 – O4A = 86.28°, O1 – Mn1 – O2A = 96.34° and O2A – Mn1 – O4 = 89.94°. All the *trans* angles are 180° by symmetry. These angles are well within the range of the angles around the two metal centres in complex **13**. However, the lack of an inversion centre at Mn²⁺ in complex **13** means that none of the *trans* angles are 180°, as listed in table 5-3.

Selected bond angles of the atoms coordinating around Mn²⁺ in complex **13** are listed in table 5-3.

Angle	(°)	Angle	(°)
O1 – Mn1 – O5	89.74(4)	O4 – Mn2 – O8	86.11(4)
O3 – Mn1 – O1	90.46(4)	O9 – Mn2 – O11	85.92(4)
O3 – Mn1 – O5	86.57(4)	O4 – Mn2 – O12	88.95(4)
O3 – Mn1 – O6	93.66(4)	O12 – Mn2 – O11	94.00(4)
O10 ¹ – Mn1 – O7	89.92(4)	O9 – Mn2 – O4	95.99(4)
O3 – Mn1 – O10 ¹	100.37(4)	O9 – Mn2 – O8	95.10(4)
O7 – Mn1 – O1	89.46(4)	O9 – Mn2 – O12	93.11(4)
O7 – Mn1 – O5	83.11(4)	O12 – Mn2 – O14	84.98(3)
O7 – Mn1 – O6	87.55(4)	O14 – Mn2 – O8	87.56(3)
O10 ¹ – Mn1 – O6	86.44(4)	O14 – Mn2 – O11	85.13(3)
O10 ¹ – Mn1 – O1	86.93(4)	O11 – Mn2 – O8	90.69(4)
O6 – Mn1 O5	96.48(4)	O4 – Mn2 – O14	93.08(4)
O3 – Mn1 – O7	169.68(4)	O9 – Mn2 – O14	170.69(4)
O10 ¹ – Mn1 – O5	172.31(3)	O12 – Mn2 – O8	170.81(4)
O6 – Mn1 – O1	172.73(4)	O4 – Mn2 – O11	176.40(4)

Symmetric code: ¹-1+x, +y,+z;²1+x,+y,+z

Table 5-3: Bond angles of atom coordinating around the two Mn²⁺ centres in complex 13.

There are four types of H-bonding in complex **13**. The first H-bond type is between the coordinated carboxylate oxygen atoms and O_{water} molecules coordinated to the same Mn²⁺ with distances of O8...O10 = 2.784(1) Å and O4...O6 = 2.825(1) Å. The second H-bond type is between two O_{water} molecules coordinated to different metal centres, with O5...O14 distance of 2.783(1) Å. H-bond type three is between a coordinated O_{water} molecule and lattice O_{water} with O6...O15 distance of 2.707(1) Å and H-bond type four is between the uncoordinated O_{carb} and the lattice O_{water} with O13...O16 distance of 2.693(1) Å, as shown in figure 5-12.

In **QIHQUT**, there are three types of H-bonding. The first H-bond type is between the coordinated O_{water} and the uncoordinated O_{carb} with the distance of O2...O5A = 2.621 Å. H-bond type two is between the coordinated O_{carb} and the oxygen atom of the lattice O_{water} with the distance of O3...O4 = 2.764 Å and H-bond type three is between the coordinated O_{water}

and lattice O_{water} with the distance of $O2 \dots O3 = 2.968 \text{ \AA}$, as shown in figure 5-12.¹⁴⁹

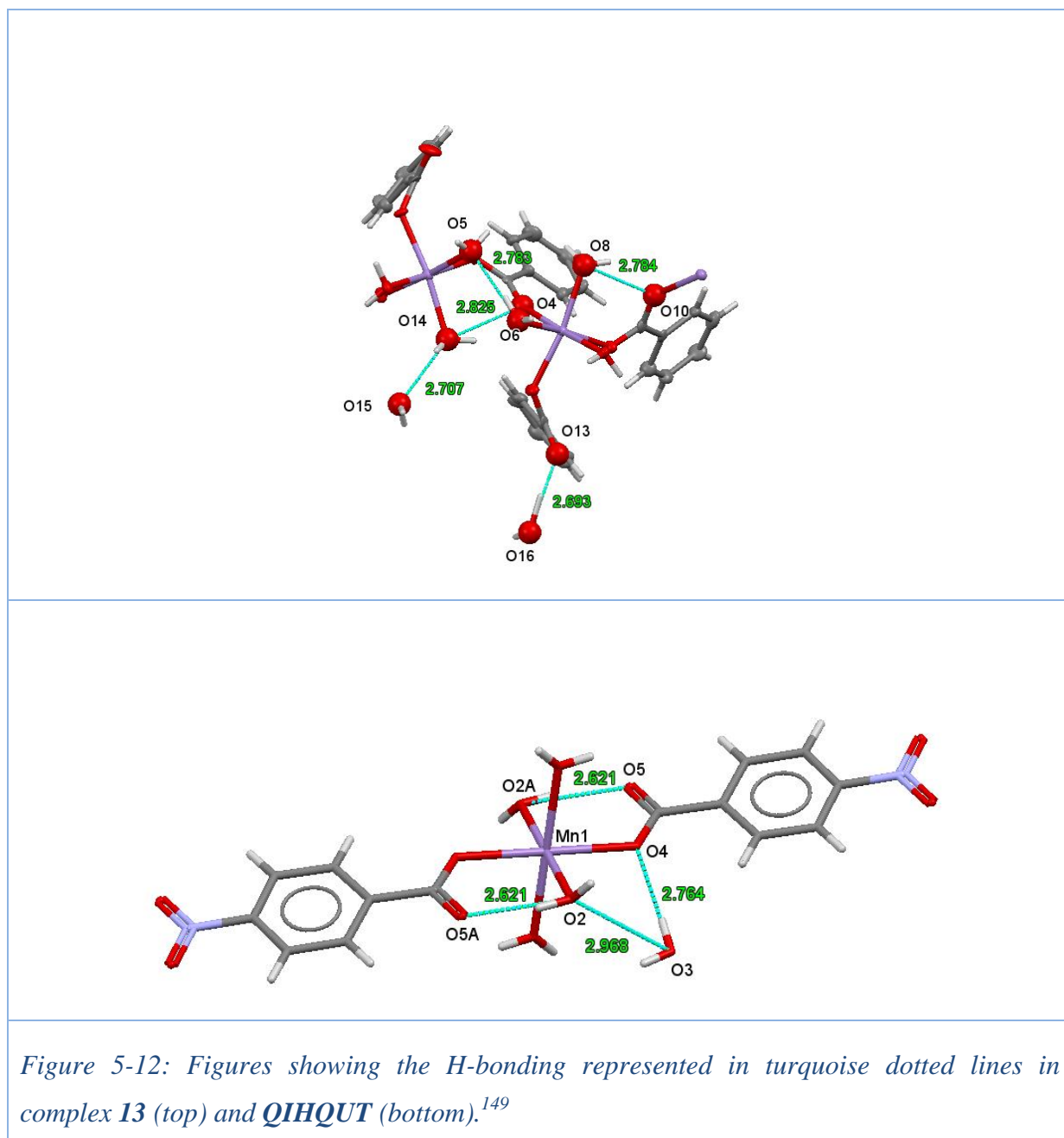


Figure 5-12: Figures showing the H-bonding represented in turquoise dotted lines in complex **13** (top) and **QIHQUT** (bottom).¹⁴⁹

5.2.2. Structure Determination of $[\text{Mn}_2(\text{C}_6\text{H}_5\text{CO}_2)_4(\text{H}_2\text{O})_4]_n$

5.2.2.1. Introduction

Colourless, plate-shaped crystals of complex **14** were obtained by heating manganese(II) carbonate and sodium benzoate in a ratio 1:2 in deionized water. A sketch of the complex is presented in figure 5-13 and shows each Mn centre coordinated to four benzoate ligands and two water molecules.

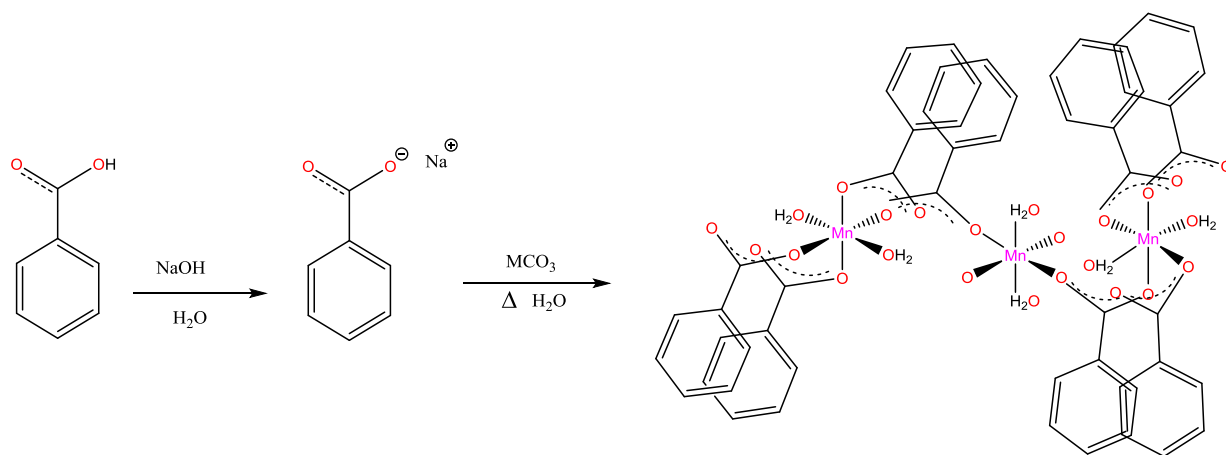


Figure 5-13: Schematic of the reaction that produced complex **14**.

Single crystal analysis was carried out at 150 K. This resulting structure could not be matched to any known structure in the Cambridge Crystallographic Database.

5.2.2.2. Crystal Structure Determination of Complex **14**

The measurement was carried out on an Agilent SuperNova Kappa geometry 4-circle diffractometer using the graphite monochromated Mo $\text{K}\alpha$ radiation, $\lambda = 0.71073 \text{ \AA}$ at 150 K. Complex **14** crystallizes in the triclinic crystal system and P-1 space group.

A full list of crystal parameters and structure determination details as well as an illustration of complex **14** and selected bond lengths and angles are presented below.

	14
Empirical formula	$[\text{Mn}_2(\text{C}_6\text{H}_5\text{CO}_2)_4(\text{H}_2\text{O})_4]_n$
Formula weight	333.19
Temperature (K)	150
Crystal system	Triclinic
Space group	P-1
a (Å)	7.4393(4)
b (Å)	12.9936(5)
c (Å)	14.0870(11)
α (°)	91.238(5)
β (°)	97.493(6)
γ (°)	90.010(4)
Volume (Å ³)	1349.75(14)
Z	4
D_x Mg / m ⁻³)	1.640
μ (mm ⁻¹)	1.00
F(000)	684.0
Crystal size (mm)	0.23 × 0.23 × 0.04
Crystal Shape	Plate, Colourless
R factor (%)	5.69

Table 5-4: Crystal data collection of complex 14.

The asymmetric unit of complex **14** comprises three crystallographically independent Mn²⁺ centres. Each Mn²⁺ centre adopts a distorted octahedral geometric environment with four equatorial carboxylate oxygen atoms and two axial aqua oxygen atoms as shown in figure 5-14.

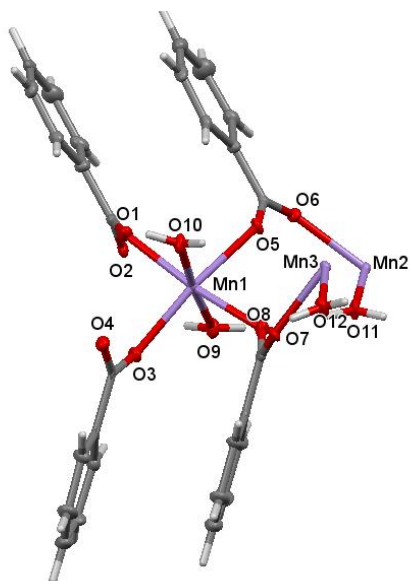


Figure 5-14: An asymmetric unit of complex 14.

The full structure presented in figure 5-15 and shows that each of the three Mn centres, Mn1, Mn2, and Mn3 are coordinated to four benzoate and two water ligands.

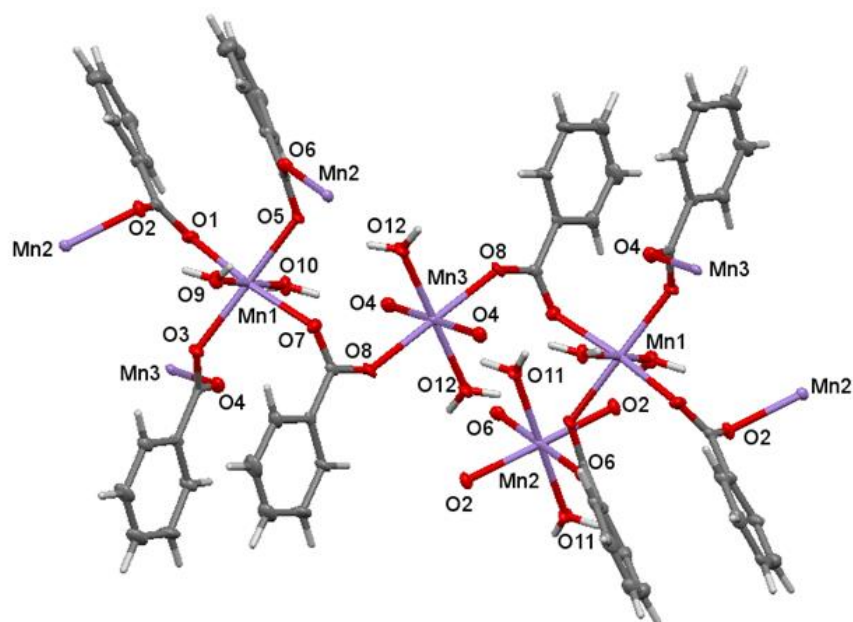
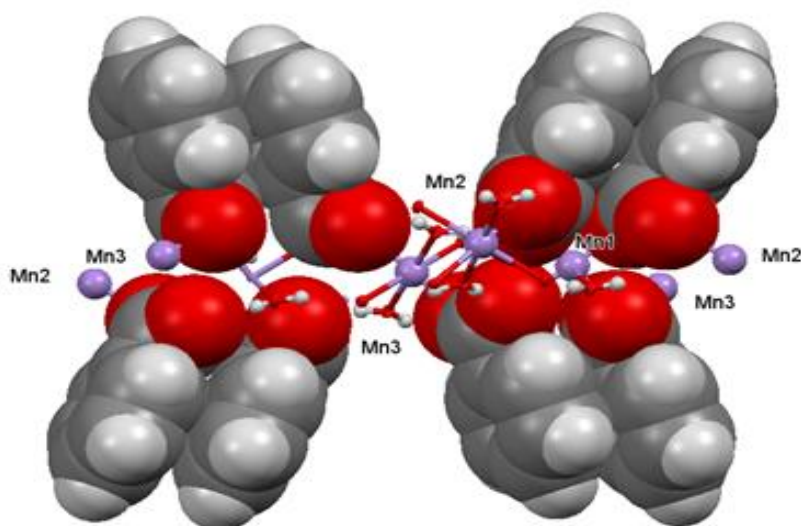


Figure 5-15: Molecular structures of complex 14.

In complex **14**, the carboxylate groups display *syn-anti* bridging coordination configurations in which the two neighboring rings face each other because there is no space for them to sit on the crystallographic plane as shown in figure 5-16. This is applicable to all pairs of phenyl rings around the three Mn²⁺ centres in complex **14**.



*Figure 5-16: Space fill structure of complex **14** showing two neighbor rings facing each other due to the *syn-anti* bridging coordination mode of the carboxylate groups to the Mn²⁺ centres.*

The Mn1 centre is coordinated by equatorial O1, O3, O5, O7 benzoate donor atoms, and two axial aqua oxygen atoms, O9 and O10. These six oxygen atoms coordinating around Mn1 centre are not symmetrical. The axial oxygen atoms O_{water} distances are 2.189(3) Å and 2.191(3) Å while the equatorial O_{carb} oxygen atoms distances are 2.175(4) Å, 2.180(3) Å, 2.183(4) Å and 2.185(4) Å to the d⁵ metal centre.

The Mn2 centre has inversion symmetry and is coordinated by equatorial benzoate donor atoms, O2, O2¹, O6 and O6¹ at distances of 2.172(4) Å and 2.180(3) Å and two axial aqua oxygen atoms; O11 and O11¹ at 2.181(3) Å.

Also, the Mn3 centre is centrosymmetric with equatorial carboxylate O4, O4¹, O8, O8¹ with the distances of 2.181(3) Å and 2.162(3) Å and axial oxygen atoms of H₂O molecule, O12 and O12¹ with the distances of 2.179(3) Å, as listed in table 5-4.

The C – O distances of the carboxylate groups show significant variation. This is as a result of the geometric environments around each Mn centre.

Complex **14** can be compared with *catena*-((μ_7 -trimellitato)-(μ_3 -hydroxo)-diaqua-dimanganese(ii) dihydrate); Mn₂(OH)(H₂O)₂(BTC).2H₂O, which is one of the structures studied as part of an investigation into the ‘role of temperature and time in the formation of infinite – M – O – M – linkages and isolated clusters in MOFs: A few illustrative examples’ and deposited in the database as **XOHSUJ**.⁵³

XOHSUJ was prepared from a typical reaction of the mixture containing manganese(II)acetate tetrahydrate, 1,2,4-benzenetricarboxylic acid, imidazole, and potassium hydroxide in water at 110 °C for 24 hours. It is a three-dimensional network with two crystallographically independent Mn²⁺ ions, one trimetallic anion, one μ_3 -OH and two coordinated and two extra framework water molecules, as shown in figure 5-17.⁵³

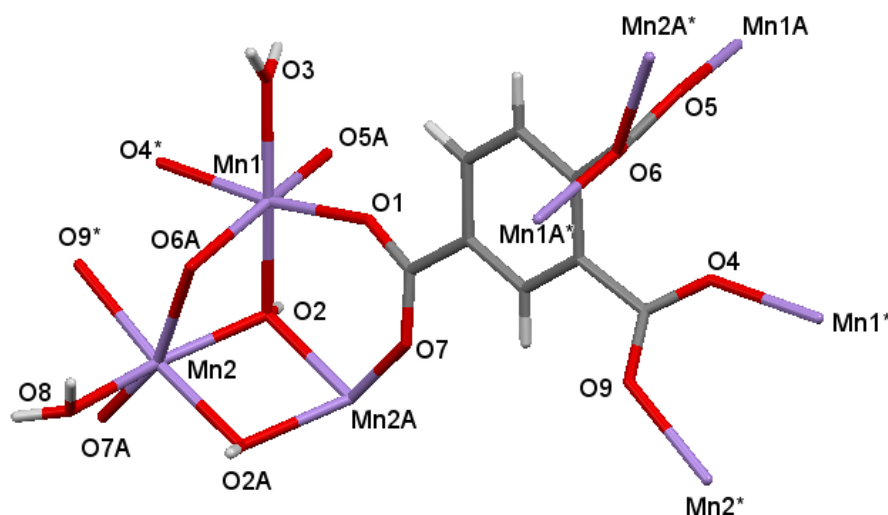


Figure 5-17: Molecular structure of **XOHSUJ**.⁵³

Although the starting materials and the crystallization methods used in preparing complex **14** and **XOHSUJ** are different, the Mn centre geometric environments are similar except for the

presence of the bridging –OH group in **XOHSUJ**. The structure of complex **14** has four equatorial carboxylate oxygen atoms and two axial aqua oxygen atoms while **XOHSUJ** has one aqua oxygen atom and one bridging –OH group around the Mn1 centre and two bridging –OH groups around the Mn2 centre, as shown in figure 5-17.⁵³

In complex **14**, two out of the three six-coordinate Mn centres are situated on crystallographic inversion centres, while **XOHSUJ** contains two crystallographically independent Mn atoms, Mn1 and Mn2. The –OH group links Mn1, Mn2 and Mn2a and one of the carboxylate oxygen atoms links Mn1 and Mn2. The Mn clusters thus formed and connected by trimellitate anions into a three-dimensional structure with one-dimensional channels occupied by two extra framework water molecules.⁵³

When complex **14** is packed and viewed down the crystallographic *b* axis in figure 5-18, the coordinating water molecules, which have been highlighted as space-filling atoms, can be seen to be arranged in such a way that they are facing each other so that they look like they occupy a tunnel.

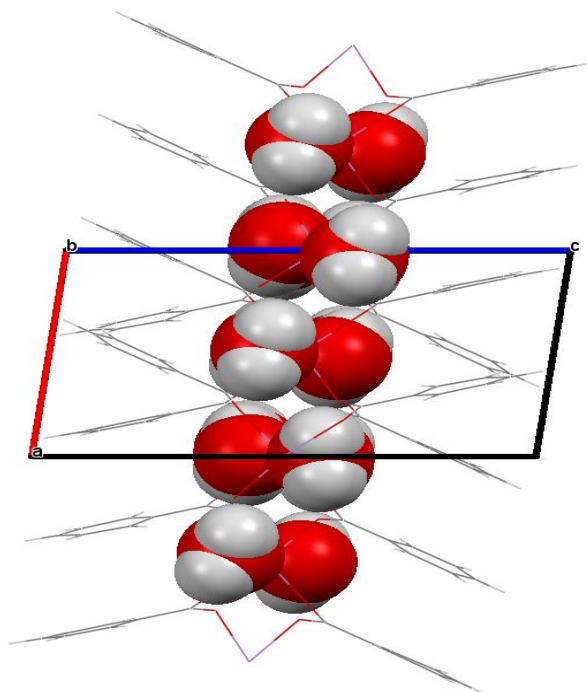


*Figure 5-18: A Packed figure of complex **14** showing a single view of coordinating water in the middle channel highlighted.*

In the distorted octahedral geometric environment of Mn1 in **XOHSUJ**, the Mn – O_{carb} bond distances of the equatorial carboxylate oxygen atoms are 2.084(4) Å, 2.197(4) Å, 2.209(3) Å and 2.246(3) Å while the Mn – O_{water} is 2.185(3) Å and Mn – O_{hydroxyl} is 2.166(3) Å. Some of these Mn – O_{carb} in **XOHSUJ** are longer than those in complex **14**, as listed in table 5-4. The Mn – O_{water} distances are not significantly different while the Mn – O_{hydroxyl} is shorter than Mn – O_{water}.⁵³

Around the Mn2 centre, the three Mn – O_{carb} bond distances are 2.143(3) Å, 2.194(4) Å, and 2.473(2) Å. The Mn – O_{water} distance is 2.180(3) Å while the Mn – O_{hydroxyl} distances are 2.187(4) Å and 2.129(3) Å. The longest Mn – O_{carb} distance is 2.473(2) Å is for the bridging carboxylate group, linking Mn1 and Mn2 to each other while the short Mn – O_{hydroxyl} distance is 2.129(3) Å for the bridging hydroxyl group linking Mn1 and Mn2A to each other.⁵³

In **XOHSUJ**, the carboxylate groups of the tricarboxylate ligand are bonded to the Mn centres in *syn-anti* bidentate coordination mode with the C – O distances of 1.252(4) Å, 1.258(5) Å, 1.252(5) Å and 1.256(5) Å, 1.245(5) Å and 1.258(5) Å respectively. These distances are in the same range as those for the carboxylate groups in the unsubstituted benzoate ligands in complex **14**.⁵³

Distance	(Å)	Distance	(Å)	Distance	(Å)
Mn1 – O1	2.183(4)	Mn2 – O2 ¹	2.181(3)	Mn3 – O4 ¹	2.179(4)
Mn1 – O3	2.186(4)	Mn2 – O2 ²	2.181(3)	Mn3 – O4 ⁴	2.179(4)
Mn1 – O5	2.180(3)	Mn2 – O6 ³	2.172(4)	Mn3 – O8	2.162(3)
Mn1 – O7	2.175(4)	Mn2 – O6	2.172(4)	Mn3 – O8 ⁵	2.162(3)
Mn1 – O9	2.191(3)	Mn2 – O11	2.180(3)	Mn3 – O12 ⁵	2.181(3)
Mn1 – O10	2.189(3)	Mn2 – O11 ³	2.180(3)	Mn3 – O12	2.181(3)

Symmetry code: ¹-1+x,+y,+z;²1-x,2-y,1-z;³-x,2-y,1-z;⁴1-x,1-y,1-z;⁵-x,1-y,1-z.

Table 5-4: Bond distances of the atoms coordinating around the three Mn²⁺ centres in complex **14**.

The interatomic Mn – Mn distances in complex **14** are Mn1 – Mn2 = 4.901 Å, Mn2 – Mn3 = 6.497 Å, and Mn1 – Mn3 = 4.975 Å. These distances are longer than the Mn – Mn distances in **XOHSUJ** with Mn1 – Mn2 = 3.3346(8) Å, Mn1 – Mn2A = 3.662(1) Å, Mn2 – Mn2A = 3.348(1) Å and Mn1 – Mn1A = 5.442(1) Å. The shorter values in **XOHSUJ** are expected to be favourable for magnetic studies, however those in complex **14**, while not so favourable, still merit magnetic investigation, as recommended in future work.⁵³

The shortest interlayer Mn – Mn distance in complex **14** is 14.087 Å and the longest 16.767 Å, as shown in figure 5-19. The interlayer distances between the Mn centres in **XOHSUJ** are shorter, ranging from 11.229(2) Å to 11.653(1) Å.

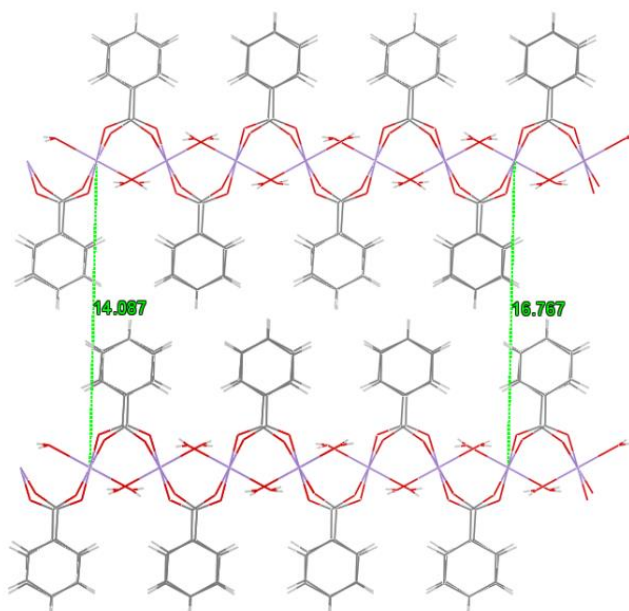


*Figure 5-19: View down interlayer space of complex **14** showing the shortest Mn-Mn inter-distance to be 14.087 Å and the highest Mn-Mn inter-distance to be 16.767 Å represented with green dotted lines.*

In the distorted octahedral geometric environment of Mn1 in **XOHSUJ**, the acute angles are 81.3(1) °, 82.2(1) °, 85.9(1) ° and 87.9(1) ° while the angle of the bridging carboxylate is higher with the value of 97.4(1) ° and 98.3(1) ° respectively. The *trans* angles are 164.8(1) °, 170.5(1) ° and 171.4(1) °. None of the angles is 180 °, as expected because of the lack of a

crystallographic inversion centre at Mn1. There is a similar trend of bond angle values in the Mn2 centre because of the distortion in the octahedral geometric environment of the two crystallographically Mn²⁺ centres in **XOHSUJ**.⁵³ These angles are similar to those in complex **14**, as listed in table 5-5.

Atoms	Angle (°)	Atoms	Angle (°)
O1 – Mn1 – O3	89.57(11)	O6 ³ – Mn2 – O2 ²	83.65(13)
O1 – Mn1 – O9	100.73(15)	O6 ³ – Mn2 – O2 ¹	96.34(13)
O1 – Mn1 – O10	82.82(14)	O6 – Mn2 – O11	95.95(14)
O3 – Mn1 – O9	82.18(15)	O6 – Mn2 – O11 ³	84.05(14)
O3 – Mn1 – O10	100.95(14)	O6 ³ – Mn2 – O6	180.0
O5 – Mn1 – O1	94.94(14)	O11 – Mn2 – O11 ³	180.0
O5 – Mn1 – O9	88.84(15)	O2 ¹ – Mn2 – O2 ²	180.0
O5 – Mn1 – O10	87.84(14)	O8 – Mn3 – O12	84.05(14)
O7 – Mn1 – O3	95.33(14)	O8 – Mn3 – O12 ⁵	95.95(14)
O7 – Mn1 – O5	81.50(11)	O4 ⁴ – Mn3 – O12	90.30(14)
O7 – Mn1 – O9	88.39(15)	O4 ⁴ – Mn3 – O ⁵	89.70(15)
O7 – Mn1 – O10	87.88(14)	O8 ⁵ – Mn3 – O4 ²	83.91(13)
O7 – Mn1 – O1	170.18(14)	O8 ⁵ – Mn3 – O4 ⁴	96.09(13)
O5 – Mn1 – O3	170.58(13)	O8 – Mn3 – O8 ⁵	180.0
O10 – Mn1 – O9	175.34(11)	O4 ² – Mn3 – O4 ⁴	180.0
O11 ³ – Mn2 – O2 ¹	90.33(15)	O12 – Mn3 – O12 ⁵	180.0(2)
O11 ³ – Mn2 – O2 ²	89.67(15)		

Symmetry code: ¹1-x,2-y,1-z; ²1+x,+y,+z; ³-x,2-y,1-z; ⁴1-x,1-y,1-z; ⁵-x,1-y,1-z; ⁶1+x,+y,+z

Table 5-5: Bond angles of the atoms coordinating around the three Mn centres in complex **14**.

The four H-bonds in complex **14** are between the carboxylate oxygen atom of one metal centre and coordinating water molecule on a neighboring metal centre with the distances of O2....O9 = 2.835(5) Å, O4....O10 = 2.821(5) Å, O5....O12 = 2.854(5) Å and O7....O11 = 2.832(5) Å, as shown in figure 5-20.

In **XOHSUJ**, H-bond is between the two carboxylate oxygen atoms coordinated to two individual Mn centres, Mn1, and Mn2 with the distance of O4....O9* = 2.225(4) Å.⁵³

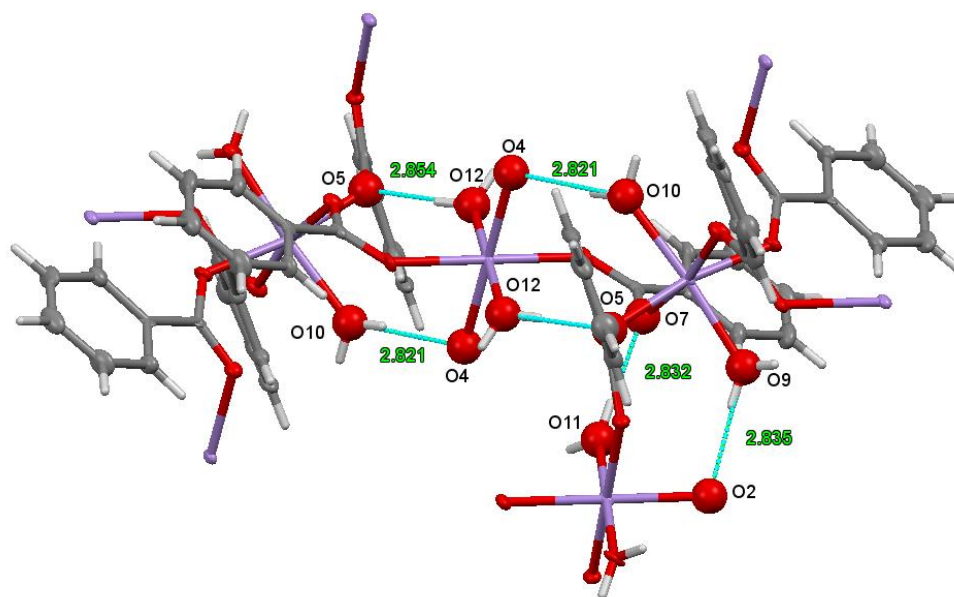


Figure 5-20: H-bonds in complex 14.

Figure 5-21 shows complex **14** as a 2D coordination polymer chain with three crystallographically independent Mn centres.

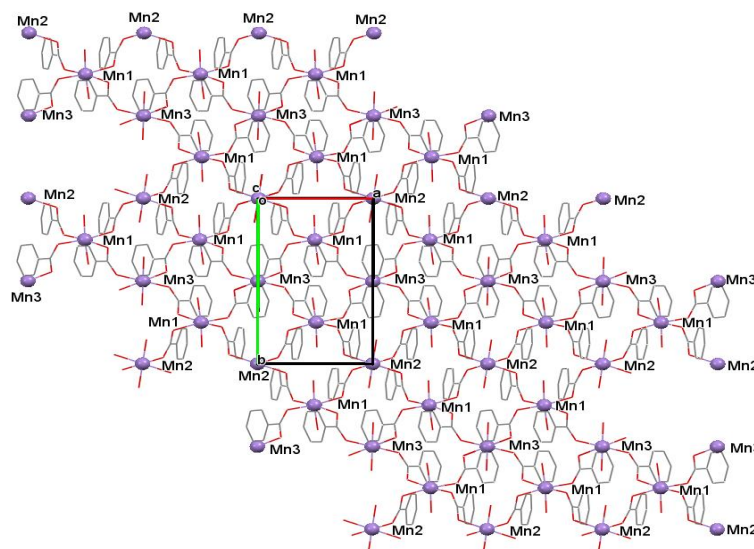


Figure 5-21: The 2D coordination polymer chain of complex **14** with the three crystallographically independent Mn centres labeled. Hydrogen atoms are omitted.

The eight phenyl rings attached to the three metal centres are arranged so that they form pairs of neighboring parallel rings with separations of 3.715 Å and 3.784 Å, as shown in figure 5-22. These distances show that there is $\pi \dots \pi$ interaction between neighboring rings.

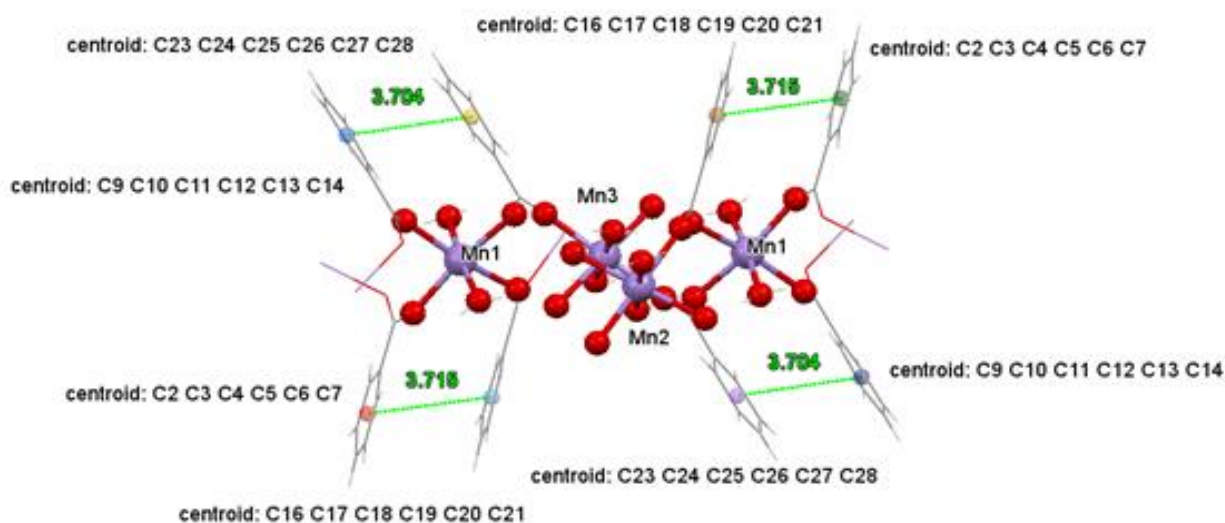


Figure 5-22: Figure showing the distances between the symmetrical rings attached to the metal centres in complex **14**.

5.3. Summary

In the reactive crystallization of sodium benzoate with manganese, four manganese complexes were obtained from the two experimental setups.

X-ray single crystal analysis revealed that three out of the four complexes obtained in the experimental setup in this chapter are identical, complex **13** while the fourth single crystal, complex **14** crystallizes at a different crystal system and space group.

The two main structures analyzed for the purpose of this study are novel manganese benzoate complexes, which are compared with manganese complexes which were prepared with different ligands and methods of preparation.

Complex **13** crystallizes in the monoclinic crystal system and $P2_1/n$ space group where **P** is a Primitive lattice, 2_1 is a rotation by 180° around b axis and a translation by $b/2$ while n is n -glide which consists of a reflection in the ac plane and a translation by $a/2 + c/2$.

Complex **14** crystallizes at triclinic crystal system and $P-1$ space group where **P** is Primitive lattice which contains only one symmetry operation, namely; an inversion centre.

The two manganese benzoate complexes have not been previously studied and cannot be matched to a known structure in the Cambridge Crystallographic Database but were compared with other manganese complexes that had been studied to a high standard.

Complexes **13** and **14** are polymeric chains and 2D sheets respectively with interesting metal-ligands connection networks. In complex **13**, the ligand acts in a bidentate manner so that the two carboxylate oxygen atoms of one ligand are bonded to different Mn centres. Three benzoate ligands are attached to each Mn centre in complex **13** with three coordinating water molecules in *cis* orientation completing the arrangement, as shown in figure 5-23. The uncoordinated lattice water is also included in the crystal structure.

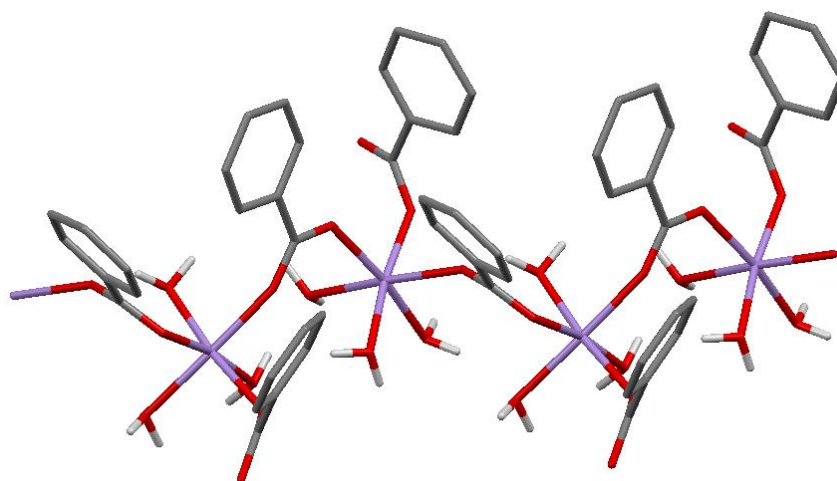


Figure 5-23: Figure showing the connection between Mn^{2+} centres and the ligands in complex 13.

There is an interesting H-bonded water chain in complex 13. This is not similar to those obtained in the hydrated CuAMB complexes 7 and 8 in chapter 4. This H-bonded water chain is not linear when viewed down crystallographic a -axis, as shown in figure 5-24.

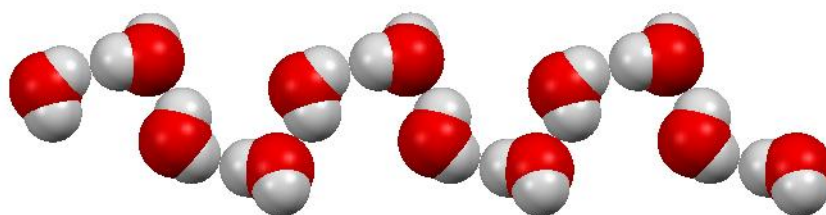


Figure 5-24: 1D nonlinear H-bonded water chain in complex 13.

In complex 14, there are three crystallographically independent Mn^{2+} centres. One of the Mn^{2+} centres is in a special position. Each Mn^{2+} centre sees four benzoates and each benzoate sees two Mn^{2+} centres. The octahedral geometric environment of Mn^{2+} was completed with two coordinated water molecules in *trans* orientation. In a similar fashion to those in complex

13, each carboxylate oxygen atom in complex **14** is coordinated to two different Mn centres, as shown in figure 5-25.

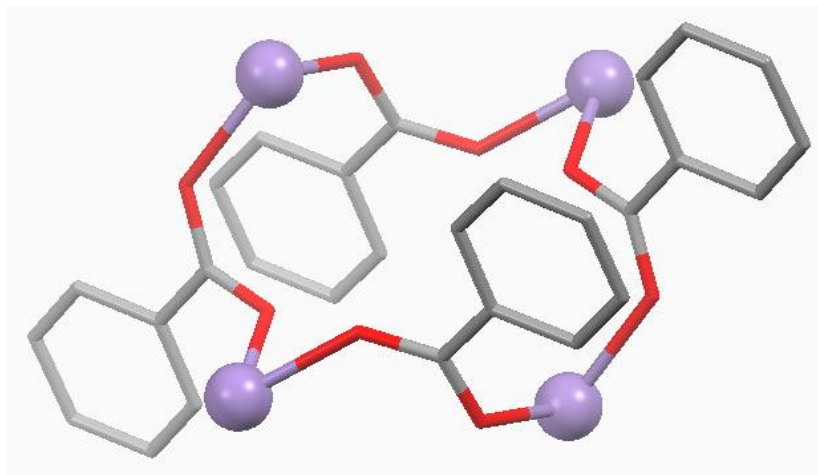


Figure 5-25: Figure showing the connection between the Mn^{2+} centres and the ligands in complex 14.

There is no lattice water in complex **14** but the coordinated water molecules formed H-bonded water chains, as shown in figure 5-26, which have some similarity to those seen in complexes **7** and **8** in chapter 4.

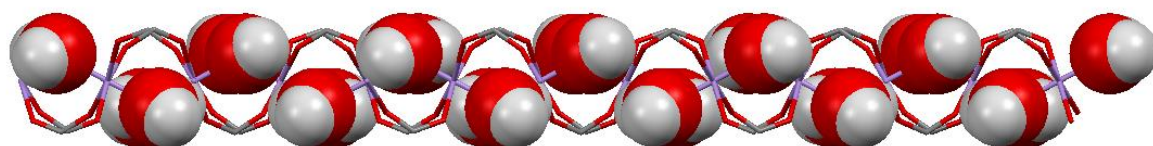


Figure 5-26: Figure showing the packing of the coordinated water molecules viewed down crystallographic a-axis in complex 14.

Chapter 6
Experimental

6.1. General Experimental Methods

The crystals under study were obtained from either solution methods at room temperature or at a high temperature in solution or slow evaporation to dryness.

6.2. Solvents and Reagents

All the reagents; ligands and metal salts used for this study were commercially available and used without further purification.

The solvents, dimethylformamide (DMF), methanol (MeOH) and deionized water were used as supplied unless stated otherwise.

6.3. Reactive Crystallization of Complexes 1, 2, 3 and 4

6.3.1. Reactive Crystallization of Metal Halides: $ZnCl_2$ and $CoCl_2 \cdot 6H_2O$ with Five Substituted Benzoic Acid Ligands in Water, in DMF and in 50:50 Water/Methanol

Crystallization reactions were carried out by reacting metal halides with five different substituted benzoic acid ligands in H_2O , in DMF and in 50:50 $H_2O/MeOH$. The molarity of the metal halide and the ligand solutions were both 0.1 M.

The substituted benzoic acids used and their molecular formulae are listed in table 6-1.

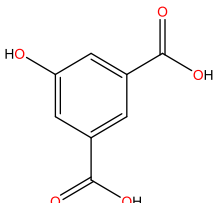
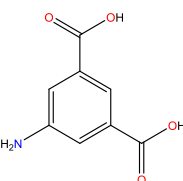
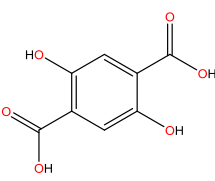
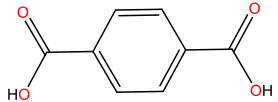
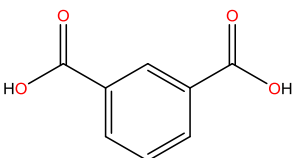
No.	Substituted Benzoic Acids	Structure of Ligands	Mw g/mol.	Mass g/mol.
1.	5-hydroxyisophthalic acid		182.13	0.091
2.	5-aminoisophthalic acid		181.15	0.090
3.	2,5-dihydroxyterephthalic acid		198.13	0.099
4.	Terephthalic acid		166.13	0.083
5.	Isophthalic acid		166.13	0.083

Table 6-1: Table of substituted benzoic acid, their molar mass (g) and the mass (g).

6.3.2. Reactive Crystallization of Zinc Chloride (ZnCl_2) with Five Substituted Benzoic Acid Ligands

Experiment 1

ZnCl_2 (0.544 g, 0.004 mol.) was dissolved in deionized water (40 ml) and was stirred to make a 0.1 M stock solution of ZnCl_2 .

5-hydroxyisophthalic acid (0.091 g, 0.0005 mol.) was dissolved in a 0.1 M solution of ZnCl_2 (5 ml). The metal halide stock solution and the ligand solution were mixed together to produce a solution containing Zn^{2+} and 5-hydroxyisophthalic acid in the molar ratio 1:1. The aqueous solutions were left for four weeks to give the aqueous ions an opportunity to self-assemble into a coordination polymer.

The above reaction was repeated with ZnCl_2 and the remaining four substituted benzoic acid at the same molarity as shown in table 6-1.

The experiment above was repeated in DMF and in 50:50 water/methanol solvent at the same molarity.

6.3.3. Reactive Crystallization of Cobalt(II)Chloride Hexahydrate ($\text{CoCl}_2 \cdot 6\text{H}_2\text{O}$) with Five Substituted Benzoic Acid

Experiment 2

$\text{CoCl}_2 \cdot 6\text{H}_2\text{O}$ (0.714 g, 0.003 mol.) was dissolved in deionized water (40ml) to make a 0.1 M stock solution of $\text{CoCl}_2 \cdot 6\text{H}_2\text{O}$.

5-hydroxyisophthalic acid (0.091 g, 0.0005 mol.) was dissolved in 5 ml of 0.1 M stock solution of $\text{CoCl}_2 \cdot 6\text{H}_2\text{O}$ (0.0005 mol.). The aqueous solutions were left for four weeks.

The above reaction was repeated with $\text{CoCl}_2 \cdot 6\text{H}_2\text{O}$ and the remaining four substituted benzoic acids at the same molarity as shown in table 6-1.

The set of experiments above was repeated in DMF and in 50:50 $\text{H}_2\text{O}/\text{MeOH}$ solvent at the same molarity.

After carrying out the set of the two crystallization reactions above, the reaction vessels were left for one week at room temperature. No crystals were observed when viewed under the microscope. The samples were left for another week and viewed under the polarised microscope. At the end of week two, it was observed that numerous particles were floating on the surface.

By week four, single crystals were obtained from three sample containers at room temperature. The crystals appeared to be of good quality and extinguished well under crossed polarizers. They were immersed in viscous oil (Fomblin oil). A single crystal was picked under the polarising microscope and was fitted onto a loop. The loop was placed onto a goniometer head and fitted onto the diffractometer. All measurement was obtained at a temperature of 150 K. This temperature causes the Fomblin oil to freeze. The crystals obtained in this set of experiments were subjected to single crystal analysis. Complex **1** was obtained from experiment 1 and complex **3** was obtained from experiment 2.

6.3.4. Reactive Crystallization of Different 1st-row 3d Transition Metals and 5-aminoisophthalic acid in Water and in 50:50 H₂O/MeOH

5-aminoisophthalic acid is a beige powder (white to cream granular powder) which is insoluble in water. Its molecular formula is NH₂(C₆H₃)(CO₂H)₂ with a molecular weight of 181.15 g/mol. It contains two carboxyl group attached to the benzene ring at the first and third position with the amine group attached at the 5th position on the phenyl ring as shown in figure 6-1.

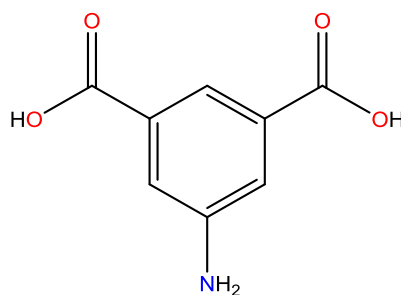


Figure 6-1: ChemSketch of 5-aminoisophthalic acid.

In this set of crystallization reactions, seven 1st-row 3d transition metals were reacted with the 5-aminoisophthalic acid in separate reaction vessels. Two sets of crystallization experiments were carried out on each 1st-row 3d transition metals. Experiment 1 refers to the crystallization reaction in water and Experiment 2 refers to the crystallization reaction in 50:50 H₂O/MeOH.

Full details of the vanadium chloride reaction are given. The remaining 1st-row 3d transition metals used the identical method. The quantities used are tabulated in table 6-2.

Experiment 1

5-aminoisophthalic acid (0.181 g, 0.001 mol.) and a sodium hydroxide pellet (0.08 g, 0.002 mol.) was dissolved in deionized water (50 ml) and mixed vigorously to make a 0.02 M stock solution of 5-aminoisophthalic acid and 0.04 M of sodium hydroxide solution. 5-aminoisophthalic acid is insoluble in water but became soluble after adding sodium hydroxide.

Vanadium(III)chloride (0.157 g, 0.001 mol.) was dissolved in deionized water (50 ml) and was mixed vigorously to make a 0.02 M metal solution.

A 10 ml metal halide solution and 10 ml of the ligand stock solution were mixed together to produce a solution containing V³⁺ and 5-aminoisophthalic acid in the molar ratio 1:1. The aqueous solutions were left for four weeks to give the aqueous ions an opportunity to self-assemble into a coordination polymer.

The above reaction was repeated with seven more 1st-row 3d transition metals and 5-aminoisophthalic acid at the same concentration, as shown in table 6-2.

Metals	Formula	Molar mass g/mol.	Mass used g/mol.
Copper(II)chloride	CuCl ₂	134.45	0.134
Cobalt(II)chloride hexahydrate	CoCl ₂ .6H ₂ O	273.93	0.237
Zinc(II)chloride	ZnCl ₂	136.31	0.136
Iron(II)chloride	FeCl ₂	126.75	0.126
Vanadium(III)chloride	VCl ₃	157.30	0.157
Nickel(II)chloride	NiCl ₂	129.599	0.129
Cobalt(II)chloride	CoCl ₂	129.839	0.129
Zinc acetate dihydrate	Zn(CH ₃ COO) ₂ .2H ₂ O	219.50	0.219

Table 6-2: 1st-row 3d transition metals, their molecular weight (g) and the mass (g).

Experiment 2

The entire procedures for experiment 1 above were repeated with the same 1st-row 3d transition metals listed in table 6-2 and 5-aminoisophthalic acid at the same concentration in 50 ml: 50 ml H₂O/MeOH.

It was observed that all but one sample formed a precipitate which was deposited too rapidly to form single crystals. These materials were further characterized using Powder X-ray Diffractometry (PXRD) and were discovered to be amorphous materials. Only one sample produced material suitable for X-ray single crystal analysis. Though it contained VCl₃ in solution, the crystals which were deposited were the sodium complex, complex **4** as revealed by single crystal X-ray analysis.

6.4. Reactive Crystallization of Anhydrous and Hydrated $M(\text{AMB})_n$

6.4.1. The Small-scale Crystallization of MSO_4 , where $M = \text{Cu, Co, Zn, and Ni}$ Hydrates with NaAMB from Aqueous Solution in order to screen for mixed Metal Compounds, Polymorphs, and Solvate

The set of experiments in this section are to examine the different metal to ligand ratio, bimetallic reaction, different concentration, and various metals in small-scale crystallization using an optical microscope to monitor the reaction and single crystal diffractometer.

1st-row 3d transition metal sulfates ranging from Mn(II) to Zn(II) were used as a pure crystallization reaction and as a bimetallic reaction.

Series of crystallization reaction was set up with different 1st-row 3d transition metals and NaAMB at different concentration.

Preliminary Experiment: 1

2-amino-3-methyl benzoic acid (0.151 g, 0.001 mol.) and sodium hydroxide pellet (0.04 g, 0.001 mol.) were dissolved in 10 ml deionized water with constant stirring using a magnetic stirrer at room temperature to give a 0.1 M stock solution of sodium aminobenzoate. A clear solution was obtained. 1 ml of the 0.1 M stock solution of sodium aminobenzoate was dissolved in 50 ml deionized water to make a 0.02 M solution of sodium benzoate.

Copper(II) sulfate pentahydrate (0.062 g, 0.00025 mol.) was dissolved in 50 ml deionized water to make a 0.005 M solution of CuSO_4 .

The two solutions were reacted together to produce a solution containing Cu^{2+} and NaAMB in the molar ratio 1:4. The reaction mixtures were left over four weeks to give the aqueous ions sufficient time to self-assemble into a coordination polymer.

The above experimental procedure was repeated for five other 1st-row 3d transition metals. The molar mass and grams of metal used are listed in table 6-3.

No.	3d transition metals	Mw g/mol.	Mass g/mol.
1.	CuSO ₄ .5H ₂ O	249.677	0.062
2.	MnSO ₄ .1H ₂ O	169.009	0.042
3.	FeSO ₄ .5H ₂ O	241.984	0.060
4.	CoSO ₄ .7H ₂ O	281.094	0.070
5.	NiSO ₄ .7H ₂ O	280.854	0.070
6.	ZnSO ₄ .7H ₂ O	161.436	0.040

Table 6-3: Table of 1st-row 3d transition metals, their molar mass (g) and the mass (g) used.

At high concentration and at a more dilute reaction, MnSO₄.1H₂O and FeSO₄.7H₂O did not form any crystals when in solution and when allowed to evaporate to dryness.

Experiment 2

The sample containers were labeled **A** to **K**. Each sample container contained NaAMB with the bimetallic solution of CuSO₄ and ZnSO₄ at different volume starting from **A** which contains 10 ml NaAMB with 10 ml CuSO₄ and 0 ml ZnSO₄ to **K** which contained 10 ml NaAMB with 0 ml CuSO₄ and 10 ml ZnSO₄.

A further preliminary experiment was carried out by reacting NaAMB and ZnSO₄ at a lower concentration.

2-amino-3-methyl benzoic acid (0.030 g, 0.0002 mol.) and sodium hydroxide pellet (0.008 g, 0.0002 mol.) were dissolved in 10 ml deionized water with constant stirring using a magnetic stirrer at room temperature to make a 0.02 M solution of NaAMB.

ZnSO₄.7H₂O (0.032 g, 0.0002 mol.) was dissolved in 10 ml of deionized water to make a 0.002 M of ZnSO₄.

The two solutions were mixed together to produce a solution containing Zn^{2+} and NaAMB in the molar ratio 1:1. The solution mixtures were left for over four weeks to give the aqueous ions an opportunity to self-assemble into a coordination polymer.

At the highest concentration, NaAMB and $ZnSO_4 \cdot 7H_2O$ did not grow any crystal and even when allowed to evaporate to dryness, a single crystal obtained was 2-amino-3-methyl benzoic acid (AMB), the starting material as revealed by single crystal analysis. But at a more dilute reaction, the morphology of crystals formed changes. A lot of colourless needle crystals were seen. An identical structure of VOSSAX, $[Zn(OH)(C_8H_8NO_2)]_n$ was obtained.

Main / Further Experiment

For further experiments, sets of crystallization reaction were carried out by reacting 10 ml of 0.1 M NaAMB with 10 ml mixed 0.005 M metal solution such as NaAMB with $CuSO_4$ and $ZnSO_4$, at various volumes as shown in table 6-4 in a way that the total volume of the mixture was always 20 ml.

The sample containers were labeled **A** to **K**. Each sample container contains NaAMB with the bimetallic solution such as $CuSO_4$ and $ZnSO_4$ at different volume starting from **A** which contains 10 ml NaAMB with 10 ml $CuSO_4$ to **K** which contains 10 ml NaAMB with 10 ml $ZnSO_4$ as shown in table 6-4 and were left for some weeks to give the aqueous ions sufficient time to self-assemble into a coordination polymer.

Solution	A	B	C	D	E	F	G	H	I	J	K
$CuSO_4$ / ml	10	9	8	7	6	5	4	3	2	1	0
$ZnSO_4$ / ml	0	1	2	3	4	5	6	7	8	9	10

Table 6-4: Table of molar ratios mixture of $CuSO_4$ and $ZnSO_4$ in the bimetallic reaction.

The above bimetallic crystallization reactions were repeated by reacting NaAMB with $CuSO_4$ and $CoSO_4$, and NaAMB with $CuSO_4$ and $NiSO_4$ at the same molarity.

In the bimetallic crystallization reaction series, various crystals were obtained. Sample bottles for single crystal analysis were selected based on the morphological changes and dichroic changes of the crystals obtained.

The different determination of anhydrous CuAMB complex **5a** was obtained from the crystallization reaction of the aqueous solution of 10 ml NaAMB and 10 ml CuSO₄.

Complex **5b** was obtained from the crystallization reaction of the aqueous solution of 10 ml NaAMB with 5 ml CuSO₄ and 5 ml ZnSO₄.

Complex **5c** was obtained from the crystallization reaction of the aqueous solution of 10 ml NaAMB with 2 ml CuSO₄ and 8 ml CoSO₄.

Also, the three different types of hydrate CuAMB complexes **6**, **7** and **8** were obtained from these set of bimetallic crystallization reaction series.

Complex **6** was obtained when few drops of the aqueous solution of 10 ml NaAMB and 10 ml CuSO₄ were placed in the Petri Dish and were allowed to slowly evaporate to dryness overnight.

Complex **7** was obtained from a mixture of 10 ml aqueous solution of NaAMB with 8 ml CuSO₄ and 2 ml ZnSO₄.

Complex **8** was obtained from the bimetallic crystallization reaction of a 10 ml aqueous solution of NaAMB with 7 ml CuSO₄ and 3 ml NiSO₄. This clear green solution of NaAMB_z and Cu_xNi_y gave two different shapes of crystals; a needle shape crystals and a plate shape crystals. The plate shape crystal is thin and brown but not a good crystal because there was no diffraction when mounted on the single crystal diffractometer. The needle crystals are thick and have a light green colour.

The anhydrous ZnAMB complex **9** was obtained from the reactive crystallization of NaAMB and ZnSO₄ at the molar ratio 1:2.

Likewise, hydrate and anhydrous CoAMB complexes **10** and **11** were obtained from the mono crystallization reaction of NaAMB and CoSO₄ from the same crystallization condition.

Complex **10** was obtained from the slow evaporation of few drops of reactive crystallization of aqueous solutions of Co²⁺ and NaAMB in the molar ratio 1:2.

Complex **11** was obtained from the reactive crystallization of aqueous solutions of Co^{2+} and NaAMB in the molar ratio 1:2. In solution, light pink and reddish pink single crystals were obtained.

Finally, in solution, light green and colourless single crystals of hydrate NiAMB complex **12** were obtained from the aqueous solution of NaAMB and NiSO_4 in the molar ratio 1:2.

6.5. Small-scale Crystallization of MnSO_4 and MnCO_3 Hydrates with Benzoic Acid from Aqueous Solution in order to screen for Polymorphs and Solvates

Sequel to the crystallization reaction of NaAMB with some of the 1st-row 3d transition metals in their +2 oxidation state in chapter 4 in which Mn^{2+} did not grow any crystals at different concentrations, two sets of manganese benzoate reaction in deionized water was set up. Experiment 1 is for the crystallization reaction of sodium benzoate and manganese (II) sulfate monohydrate in deionized water at different molarity and various millimeters. Experiment 2 is the crystallization reactions of manganese (II) carbonate anhydrous and sodium benzoate in deionized water in the molar ratio 1:2 above room temperature.

Experimental 1

Benzoic acid (1.22 g, 0.01 mol.) and sodium hydroxide (0.4 g, 0.01 mol.) were dissolved in 10 ml deionized water with constant stirring using a magnetic stirrer at room temperature to give a 1 M stock solution of sodium benzoate. A clear solution was obtained.

A 1 ml of the 1 M stock solution of sodium benzoate was dissolved in 50 ml deionized water to make a 0.02 M solution of sodium benzoate.

Manganese(II) sulfate monohydrate (0.084 g, 0.0005 mol.) was dissolved in 50 ml deionized water to make a 0.01 M stock solution of MnSO_4 .

The Mn^{2+} and sodium benzoate solution in the molar ratio 1:2 were reacted together in different ratios (v/v) as shown in table 6-5. The reaction mixture was left over six weeks to give the aqueous ions sufficient time to self-assemble into a coordination polymer.

Solution	A	B	C	D	E	F	G	H	I
$\text{C}_6\text{H}_5\text{COONa}$ / ml	9	8	7	6	5	4	3	2	1
$\text{MnSO}_{4(\text{aq})}$ / ml	1	2	3	4	5	6	7	8	9

Table 6-5: Mixture Scheme of the 0.02 M of $\text{C}_6\text{H}_5\text{COONa}$ and 0.01 M of MnSO_4 in ml.

A few drops of the solution in each sample container were dropped in the weighing boat and were allowed to evaporate to dryness overnight.

For Experiment 1, colourless crystalline materials with similar shapes were obtained in all the weighing boats and were scraped out using a spatula. Good crystals were picked with the help of a polarized microscope from weighing boat D which contained 6 ml of 0.02 M C_6H_5COONa and 4 ml of 0.01 M $MnSO_4$. The single crystal obtained was subjected to single crystal analysis and gave $[Mn_2(C_7H_9O_4)_4]_n$ complex **13**.

Week by week, no crystal was obtained in solution in all the reaction vessels. After eight weeks, the screw tops of the sample bottles were removed to allow the solution to slowly evaporate to dryness. After 16 weeks, single crystals similar to complex **13** were seen in all the sample bottles. Crystals suitable for single crystal analysis were picked from the sample bottle that contained 3 ml 0.02 M C_6H_5COONa and 7 ml 0.01 M $MnSO_4$. The crystal was subjected to single crystal analysis and turned out to be the same structure as complex **13** but the data obtained for this structure were of poor quality and were not processed further.

Experiment 2

Benzoic acid (1.22 g, 0.01 mol.) and sodium hydroxide (0.4 g, 0.01 mol.) were dissolved in 10 ml deionized water with constant stirring with a magnetic stirrer at room temperature to give a 1 M stock solution of sodium benzoate. A clear solution was obtained.

A 1 ml of the 1 M stock solution of sodium benzoate was dissolved in 50 ml deionized water to make a 0.02 M solution of sodium benzoate. Manganese(II)carbonate anhydrous (0.057 g, 0.0005 mol.) was dissolved in 50 ml deionized water to make a 0.01 M solution of $MnCO_3$.

The two solutions were reacted together to produce a solution containing Mn^{2+} and C_6H_5COONa in the molar ratio 1:2. The reaction was heated and stirred for a few hours because manganese carbonate is quite insoluble. The solids that remained are most likely manganese carbonate and were filtered off. The clear solution obtained (filtrate) was allowed to evaporate to dryness. As some unreacted manganese carbonate had been removed, some benzoic acid crystals contaminated the product.

For Experiment 2, after two weeks, three different crystals of different habit were obtained. These three crystals were subjected to single crystal analysis at 150 K and 293 K respectively. Single crystal analysis revealed that two of the crystal structures obtained is the same as complex **13** obtained in experiment 1 and the third crystal, complex **14** crystallizes at a different crystal system and space group.

6.6. X-ray Structure Determination

Corrected reflection intensities were harvested from diffraction images collected on four different diffractometers; An Agilent Supernova Kappa geometry 4-circle diffractometer using the Mo K α radiation, $\lambda = 0.71073 \text{ \AA}$ at 150 or 293 K respectively; Oxford diffraction Xcalibur2 equipped with Sapphire2 using the Mo K α radiation, $\lambda = 0.71073 \text{ \AA}$ at 150 or 293 K respectively; Bruker Prospector diffractometer equipped with Cu K α radiation, $\lambda = 1.54184 \text{ \AA}$ at 150 or 293 K respectively; The last diffractometer is XtaLAB AFC11 (RINC): Kappa single diffractometer using the Mo K α radiation, $\lambda = 0.71073 \text{ \AA}$ at 150 or 293 K respectively using CrysAlisPro. X-ray images were recorded on a CCD detector and stored.

The X-ray images were exported to Olex2¹⁵⁰ for further processing, including structure solution via SHELXT¹⁵¹ and least square refinement using SHELXL.¹⁵¹⁻¹⁵² The non-hydrogen atoms were refined anisotropically while all hydrogen atoms were refined isotropically.

MERCURY program was used to display the structure, manipulate it, view the crystal polymeric expansion and calculate the selected bond lengths and angles.¹⁵³

The CAMBRIDGE CRYSTALLOGRAPHIC DATABASE (CCD) and CONQUEST program were used to compare the structure with the existing structure and to check if each of the structures had been studied previously and deposited into the Database.¹⁵⁴⁻¹⁵⁶

D8 Powder Diffractometer was used on powder samples for structural characterization of materials. The resulting fingerprints were exported to EVA for further processing.

Chapter 7

Conclusion and Suggestion for Future Work

7.1. Conclusion

The crystallization reaction of carboxylate based ligands and 1st-row 3d transition metals have been previously studied to a high standard and were known to have produced coordination polymers (CPs) and metal-organic frameworks (MOFs). In this research work, selecting suitable carboxylate based ligands either monodentate or multidentate organic ligands under an appropriate condition was considered.

The crystallization reaction of 1st-row 3d transition metal and the bimetallic crystallization reaction with a carboxylate based ligand that produced layered structures and polymeric chains were synthesized and structurally characterized.

AMB consist of one carbonyl group which can strongly bind to metal ions and thus may produce various structural topologies. The NH₂ group which is next to the carbonyl group took part in the geometry environment of some of the metal complexes obtained such as in the structure of the anhydrous CuAMB and CoAMB unlike the methyl group which is next to the NH₂ group did not get involved in the geometry environment of any of the metal complexes obtained in this research work. The effect of the methyl group in the packing diagram of the complexes obtained was discussed.

In these research works, despite the use of different starting materials, methods, and concentrations in the crystallization reaction of NaAMB with 1st-row 3d transition metals either as a pure metal or as bimetallic solutions containing Cu/Zn, Cu/Co, Cu/Ni, we have proved that the different determinations of the identical anhydrous CuAMB complexes **5a**, **5b**, and **5c** obtained in this study are the same as the structure of Copper 3-Methylantranilate [Bis(2-amino-3-methylbenzoato) copper(II)]: [Cu(C₈H₈NO₂)₂]_n which had been studied to a high standard and deposited into the Cambridge Crystallographic Database as **DUKTIM**. **DUKTIM** was characterized at room temperature (293 K) whereas the three determinations of anhydrous CuAMB complexes **5a**, **5b** and **5c** were characterized at a lower temperature of 150 K, and there were no significant changes in cooling. Likewise, the three different novels hydrated CuAMB complexes **6**, **7** and **8** were obtained from the bimetallic reaction in chapter 4.

In the bimetallic crystallization reaction, the Cu^{2+} displaced Zn^{2+} , Co^{2+} , and Ni^{2+} because Cu^{2+} is a strong Lewis Acid, though the addition of Zn^{2+} promotes morphological and dichroic colour changes of the crystal structure formed.

The expected results from the bimetallic reactive crystallization; $\text{Cu}_x\text{Zn}_y\text{AMB}_z$, $\text{Cu}_x\text{Co}_y\text{AMB}_z$, and $\text{Cu}_x\text{Ni}_y\text{AMB}_z$ respectively were not obtained. Instead, anhydrous and hydrated CuAMB structures were obtained in all the cases even when a small amount of Cu was added such as in the case of the anhydrous CuAMB structure complex **5c**.

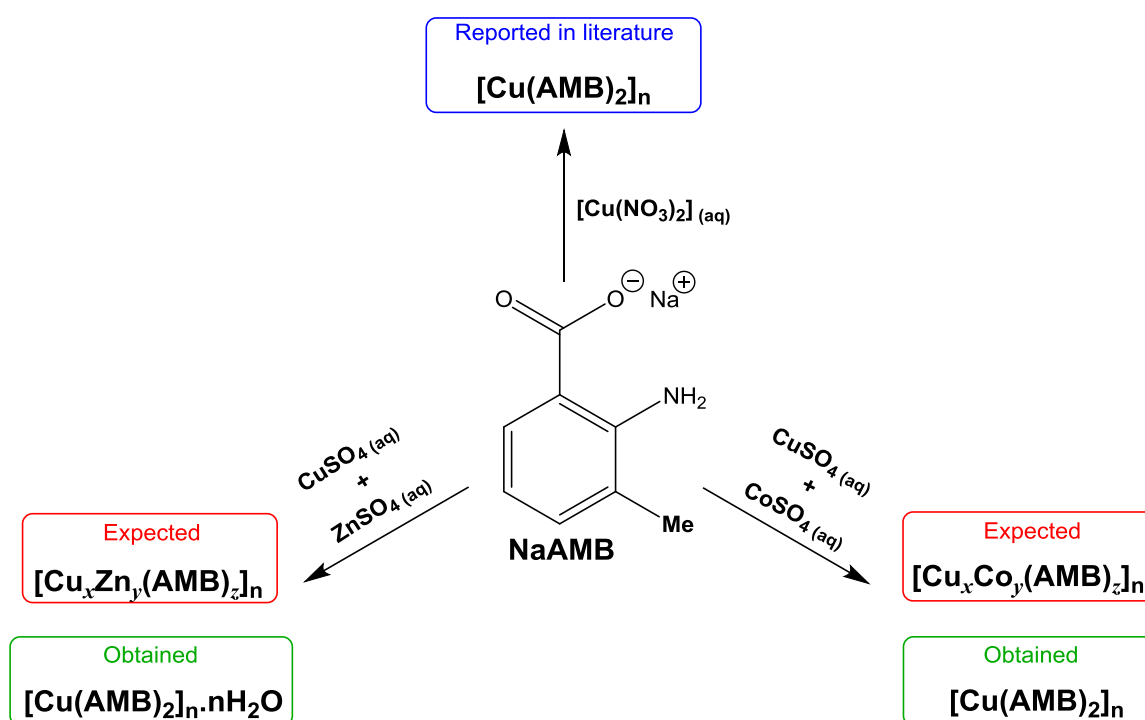


Figure 7-1: Schematic of the bimetallic reaction setup and the crystals obtained.

Figure 7-1 shows the schematic of the reactive crystallization of NaAMB with the 1st-row 3d transition metal and the bimetallic reaction of 1st-row 3d transition metals, the expected results, the reported crystal, and the resulting crystals obtained.

The NaAMB and 1st-row 3d transition metals reaction also produced one novel anhydrous ZnAMB complex **9** of high quality. This was compared with a structure deposited in the Cambridge Crystallographic Database as **CAZXXQ**, which was isomorphous with complex

9 but lacked a methyl group. Complex **9** was also compared to the anhydrous $[\text{Cu}(\text{AMB})_2]_n$ complex **5c**. Though the arrangement around the metal and the ligand are identical, the different metals used gave different unit cells and space groups.

Novel hydrated and anhydrous CoAMB complexes **10** and **11** were also obtained and characterized.

One novel hydrated NiAMB complex **12** was obtained, characterized and compared to other Ni complexes deposited in the database.

The rationale behind these set of experiments was to study the effect of varying the Cu/Zn, Cu/Co and Cu/Ni ratios which gave us the anhydrous layered structure, the hydrate layered structure, and the dimer. This was monitored, studied and reported in this study.

The sets of crystallization reactions of NaAMB and 1st-row 3d transition metals gave the idea of setting up the crystallization reaction of sodium benzoate and manganese (chapter 5). Since $\text{Mn}(\text{AMB})_2$ crystal structures were not obtained in chapter 4. This reaction produced two coordination polymers of manganese benzoate with coordinated water and uncoordinated water molecules.

The method used in this thesis, solution method, is a more convenient crystallization method than hydrothermal or aqueous diffusion which are the most common methods used for the crystallization of coordination polymers and MOFs in previous studies.

7.2. Suggestion for further work

The research intends to continue to study the 1st-row 3d transition metals with different carboxylate based ligands by carrying out a survey of the Cambridge Crystallographic Database to establish the variation in geometry.

To study the design, the properties and the coordination modes of all the carboxylate ligands used and cited in this study.

The topology of the anhydrous CuAMB and the hydrated CuAMB water system are of great interest. Hence, investigation of the fact that favours the crystallization of different CuAMB phases requires a careful experimental study of variant factors such as concentration, pH and rate of evaporation.

To study the effect of the CH₃ group in AMB by trying out some of the reactions done with AMB with the un-methylated ligand as seen in the published ZnAMB complex, **CAZXXOQ**.

To carry out a reaction that will support the displacement/replacement of the coordinated H₂O in complexes **7** and **8** with another linker to form a 3D MOFs.

To employ a spectroscopy method to study and observe the effect of Jahn-Teller Distortion in all the Cu²⁺ complexes.

Also, to study what each layer of the lamellar structure of the novel compounds obtained in this study behaves like.

Lastly, to study the magnetic coupling of each of the novel complexes obtained in this study, to measure the magnetic properties of each layer of the 2D coordination polymers to see if there is communication between the metals centre and the layers.

Appendix 1

Electronic Supporting Information

The materials listed below can be found in the attached CD.

1. CIF Files of all the structures presented within this thesis.
2. PDF files of all the structures presented within this thesis.

List of Crystal Structures obtained in this Study.

Chapter	Complex	Identifying Code	Molecular Formulae	Status
Chapter 3.	1	Argp392	$[\text{Zn}(\text{C}_8\text{H}_5\text{NO}_4)(\text{H}_2\text{O})]_n$	Published as UFULEM
	2	Xrgp97	$(\text{C}_8\text{H}_6\text{O}_6).(\text{Me}_2\text{NCHO})$	Novel
	3	Xrgp94	$[\text{Co}(\text{C}_8\text{H}_4\text{O}_6)(\text{C}_3\text{H}_7\text{NO})_2(\text{H}_2\text{O})_2]_n$	Published as SEWXIE
	4	Orgp307	$[\text{Na}_2(\text{C}_8\text{H}_6\text{NO}_4)_2(\text{C}_8\text{H}_7\text{NO}_4)_2(\text{H}_2\text{O})_6]$	Published as WIGWEP
Chapter 4.	5a	Argp1130	$[\text{Cu}(\text{C}_8\text{H}_8\text{NO}_2)_2]_n$	Published as DUKTIM
	5b	Argp1132	$[\text{Cu}(\text{C}_8\text{H}_8\text{NO}_2)_2]_n$	
	5c	Argp1144	$[\text{Cu}(\text{C}_8\text{H}_8\text{NO}_2)_2]_n$	
	6	Argp1131	$[\text{Cu}(\text{C}_8\text{H}_8\text{NO}_2)_2\text{H}_2\text{O}]_2$	Novel
	7	Argp1133	$\{[\text{Cu}(\text{C}_8\text{H}_8\text{NO}_2)_2]_2 \cdot \frac{8}{3}\text{H}_2\text{O}\}_n$	Novel
	8	Argp1141	$\{[\text{Cu}(\text{C}_8\text{H}_8\text{NO}_2)_2]_2 \cdot \frac{13}{5}\text{H}_2\text{O}\}_n$	Novel
	9	Orgp340	$[\text{Zn}(\text{C}_8\text{H}_8\text{NO}_2)_2]_n$	Novel
	10	Orgp343	$\{[\text{Co}(\text{C}_8\text{H}_8\text{NO}_2)_2] \cdot \text{H}_2\text{O}\}_n$	Novel
	11	Exp_35	$[\text{Co}(\text{C}_8\text{H}_8\text{NO}_2)_2]_n$	Novel
	12	Rrgp20	$\text{Ni}(\text{C}_8\text{H}_8\text{NO}_2)(\text{H}_2\text{O})_2 \cdot 2\text{H}_2\text{O}$	Novel
Chapter 5.	13	Irgp9	$[\text{Mn}_2(\text{C}_6\text{H}_5\text{CO}_2)_4(\text{H}_2\text{O})_6] \cdot (\text{H}_2\text{O})_2$	Novel
	14	Argp1198	$[\text{Mn}_2(\text{C}_6\text{H}_5\text{CO}_2)_4(\text{H}_2\text{O})_4]_n$	Novel

Appendix 2

Structures referenced in this study from the Cambridge Crystallographic database and their CCDC numbers.

No.	CCDC Name	CCDC number
1.	UFULEM	188588
2.	AJAHOI	215246
3.	DUSJUX	788331
4.	FEGBEB	1562387
5.	SEWXIE	1455285
6.	NUZJAV	1439603
7.	WIGWEP	654706
8.	POQTUL	690441
9.	DICHAY	1140247
10.	DUKTIM	1146385
11.	PONLEJ	1236757
12.	OABZCU	1225222
13.	VOSSAX	1286523
14.	CAZXOQ	1121318
15.	ABZACO10	1100295
16.	EKEXEY	779475
17.	YIGGEB	663653
18.	DEJXUO	1559306
19.	DAMBNI	1135969
20.	NUNRUK	777896
21.	AMEBAC	1102561
22.	NAFGEI	751494
23.	QUJJUB01	739083
24.	QIHQUT	161364
25.	XOHSUJ	678766
26.	OMESUV	773910
27.	GIHFOV	1855729
28.	BEHBOG	212689

References

1. C.-T. Chen and K. S. Suslick, *Coord. Chem. Rev.*, 1993, **128**, 293-322.
2. M. Y. Masoomi and A. Morsali, *Coord. Chem. Rev.*, 2012, **256**, 2921-2943.
3. Y.-Y. Liu, J. Li, J-F. Ma, J.-C. Ma and J. Yang *CrystEngComm.*, 2012, **14**, 169-177.
4. C. Janiak, *Dalton Trans.*, 2003, 2781–2804.
5. Z. Wu, W. Sun, Y. Chai, W. Zhao, H. Wu, T. Shia and X. Yang, *CrystEngComm.*, 2014, **16**, 406-414.
6. P. Kar, R. Biswas, Y. Ida, T. Ishida, and A. Ghosh, *Cryst. Growth Des.*, 2011, **11**, 5305-5315.
7. L. Yang, L. Liu, C. Lian, M. Liu, Z. Xu, L.-C Wang and X. Guo, *Dyes and Pigments*, 2015, **122**, 246-256.
8. P. Kar, Y. Ida, T. Ishida and A. Ghosh, *CrystEngComm.*, 2013, **15**, 400–410.
9. Y.-C. He, N. Xu, F.-H. Zhao, W.-Q. Kan, H.-R. Liu and J. You, *Inorg. Chem. Comm.*, 2017, **86**, 78-81.
10. M. Tabatabaee, R. M. Hoseini, and M. Parvez, *Synthesis and Reactivity in Inorganic, Metal-Organic, and Nano-Metal Chemistry*, 2014, **44**, 775-780.
11. C.-D. Wu, C.-Z. Lu, H.-H. Zhuang and J.-S. Huang, *Allgemeine Chem.*, 2002, **628**, 1935-1937.
12. A. Aijaz, P. Lama and P. K. Bharadwaj, *Inorg. Chem.*, 2010, **49**, 5883-5889.
13. S.-D. Li, L. P Lu and F. Su, *Chinese J. Struct. Chem.*, 2016, **35**, 1920-1928.
14. F.-N. Shi, M. S. Reis, P. Brandao, A. M. Souza, V. Felix, and J. Rocha, *Trans. Met. Chem.*, 2010, **35**, 779-786.
15. R. Al-Hashemi, N. Safari, V. Amani, S. Amani, and S. W. Ng, *J. Iran Chem. Soc.*, 2014, **11**, 341-349.

16. Y. Chai, Z. Yan, W. Sun, X. Zhao, Z. Wua, W. Zhao and X. Yang, *Inorganica Chimica Acta*, 2014, **410**, 76–81.
17. H. Günay, A. T. Çolak, O. Z. Yeşilel, T. Tunç and F. Çolak, *J. Molecular Structure*, 2015, **1099**, 108-113.
18. Z. N. Chen, S. X. Liu, J. Qiu, Z. M. Wang, J. L. Huang and W. X. Tang, *J. Chem. Soc., Dalton Trans.*, 1994, 2989-2992.
19. M. W. Wemple, H.-L. Tsai, S. Wang, J. P. Claude, W. E. Streib, J. C. Huffman, D. N. Hendrickson, and G. Christou, *Inorg. Chem.*, 1996, **35**, 6437-6449.
20. J. L. Derissen, *Acta Cryst.*, 1974, **B30**, 2764-2765.
21. C. B. Aakeroy, N. R. Champness, and C. Janiak, *CrystEngComm.*, 2010, **12**, 22–43.
22. M. J. Winter, *d-block chemistry*, Oxford University Press, Oxford, UK, Second ed., 2015.
23. J.-X. Li and Z.-X. Du, *J. Coord. Chem.*, 2016, **69**, 2563-2572.
24. J. A. Kaduk, *Acta Cryst.*, 2002, **B58**, 815-822.
25. N. Lah and R. Clérac, *Inorg. Chem. Comm.*, 2014, **41**, 62-64.
26. J. A. McCleverty, *Chemistry of the First-row Transition Metals*, Oxford University Press, Oxford, England, 1999.
27. D. Nicholls, *Complexes and First-row Transition Elements*, Macmillan, London, 1974.
28. J. R. Gispert, *Coordination chemistry*, Wiley-VCH, Weinheim, 2008.
29. A. Saha, P. Majumdar and S. Goswami, *J. Chem. Soc., Dalton Trans.*, 2000, 1703-1708.
30. S. F. A. Kettle, *Coordination Compounds*, Nelson, London, 1969.
31. N. N. Greenwood, *Chemistry of the Elements*, Butterworth-Heinemann, Oxford, 2nd ed., 1997.

32. G. E. Rodgers, *Brooks/Cole Cengage Learning*, 2011, 3rd ed.
33. A. L. Companion and M. A. Komarynsky, *J. Chem. Ed.*, 1964, **41**, 257-262.
34. S. R. Batten, N. R. Champness, X.-M. Chen, J. Garcia-Martinez, S. Kitagawa, L. Ohrstrom, M.O'Keeffe, M. P. Suh and J. Reedijk, *CrystEngComm.*, 2012, **14**, 3001-3004.
35. I. M. L. Rosa, M. C. S. Costa, B. S. Vitto, L. Amorim, C. C. Correa, C. B. Pinheiro, and A. C. Doriguetto, *Cryst. Growth Des.*, 2016, **16**, 1606-1616.
36. C.-L. Chen, A. M. Goforth, M. D. Smith, C.-Y. Su and H.-C. zur Loye, *Angew. Chem.*, 2005, **44**, 6673 –6677.
37. W. W. Lestari, P. Lonneck, H. C. Streit, F. Schleife, C. Wickleder and E. Hey-Hawkin, *Inorgan.Chimi. Acta*, 2014, **421**, 392-398.
38. M. Eddaoudi, H. Li and O. M. Yaghi, *J. Am. Chem. Soc.*, 2000, **122**, 1391-1397.
39. J. L. C. Rowsell and O. M. Yaghi, *Microporous and Mesoporous Materials*, 2004, **73**, 3-14.
40. Y. Wang, L.-J. Zhang, R. Zhang, Y. Jin, Y. Wang, Y.-H. Xing, F.-Y. Bai and L.-X. Sun, *Cryst. Growth & Des.*, 2017, **17**, 6531-6540.
41. X.-M. Zhang, D.-D. Ding, W. Gao, and J.-P. Liu, *Inorgan.Chimi.Acta*, 2013, **394**, 494-500.
42. L. E. Kreno, K. Leong, O. K. Farha, M. Allendorf, R. P. Van Duyne and J. T. Hupp, *Chem. Rev.*, 2012, **112**, 1105-1125.
43. A. Cheansirisomboon, J. Silanas-Uber, C. Massera, O. Roubeau, S. Youngme and P. Gamez, *Eur. J. Inorg. Chem.*, 2014, 4385-4393.
44. L. S. Flores, S. P. Alcantara, G. C. G. de Lima, M. I. Yoshida and C. C. Corrêa, *Vibrational Spectroscopy*, 2016, **86**, 302-310.
45. J. Y. Lu and A. Babb, *Inorgan.Chimi. Acta*, 2001, **318**, 186-190.

46. N. Getachew, Y. Chebude, I. Diaz and M. Sanchez-Sanchez, *J. Porous Mater.*, 2014, **21**, 769-773.
47. M. D. Allendorf, C. A. Bauer, R. K. Bhaktaa and R. J. T. Houk, *Chem. Soc. Rev.*, 2009, **38**, 1330-1352.
48. U. Mueller, M. Schubert, F. Teich, H. Puetter, K. Schierle-Arndt and J. Pastre, *J. Mater. Chem.*, 2006, **16**, 626-636.
49. C. Zhou, L. Longley, A. Krajnc, G. J. Smales, A. Qiao, I. Erucar, C. M. Doherty, A. W. Thornton, A. J. Hill, C. W. Ashling, O. T. Qazvini, S. J. Lee, P. A. Chater, N. J. Terrill, A. J. Smith, Y. Yue, G. Mali, D. A. Keen, S. G. Telfer and T. D. Bennett, *Nature Comm.*, 2018, **9**, 5042.
50. T. K. Prasad, D. H. Hong, and M. P. Suh, *Chem. Eur. J.*, 2010, **16**, 14043-14050.
51. H. Furukawa, K. Cordova, M. O'Keeffe and O. M. Yaghi, *Science*, 2013, **341**, 974.
52. M. Li, D. Li, M. O'Keeffe, and O. M. Yaghi, *Chem. Rev.*, 2014, **114**, 1343-1370.
53. P. Mahata, M. Prabu and S. Natarajan, *Inorg. Chem.*, 2008, **47**, 8451-8463.
54. H.-C Zhou, J. R. Long and O. M. Yaghi, *Chem. Rev.*, 2012, **112**, 673-674.
55. M. Kurmoo, *Chem. Soc. Rev.*, 2009, **38**, 1353-1379.
56. D. Farrusseng, S. Aguado and C. Pinel, *Angew. Chem. Int. Ed.*, 2009, **48**, 7502-7513.
57. P. Falcaro, R. Ricco, A. Yazdi, I. Imaz, S. Furukawa, D. MasPOCH, R. Ameloot, J. D. Evans and C. J. Doonan, *Coord. Chem. Rev.*, 2016, **307**, 237-254.
58. R. Zou, A. I. Abdel-Fattah, H. Xu, Y. Zhao and D. D. Hickmott, *CrystEngComm.*, 2010, **12**, 1337-1353.
59. L. Ma, C. Abney and W. Lin, *Chem. Soc. Rev.*, 2009, **38**, 1248-1256.
60. S.-J. Jian, Q.-Q. Han, H.-X. Yang and X.-R. Meng, *Acta Cryst.*, 2016, **C72**, 530-535.
61. A. R. Millward and O. M. Yaghi, *J. Am. Chem. Soc.*, 2005, **127**, 17998-17999.

62. H. B. T. Jeazet, C. Staudt and C. Janiak, *Dalton Trans.*, 2012, **41**, 14003–14027.
63. F. Wang, C. Dong, C. Wang, Z. Yu, S. Guo, Z. Wang, Y. Zhao and G. Li, *New J. Chem.*, 2015, **39**, 4437-4444.
64. M. O’Keeffe, M. A. Peskov, S. J. Ramsden and O. M. Yaghi, *Acc. Chem. Res.*, 2008, **41**, 1782-1789.
65. K. S. Taber, *Chemistry Education Research and Practice*, 2001, **2**, 123-158.
66. J. K. Gilbert, O. D. Jong, R. Justi, D. F. Treagust, H. Jan and V. Driel, *Chem. Ed., Towards Research-based Practice*. Science & Technology Education Library, **17**, Springer, Dordrecht, 2002.
67. C. A. Hunter and J. K. M. Sanders, *J. Am. Chem. Soc.*, 1990, **112**, 5525-5534.
68. C. Janiak, *J. Chem. Soc., Dalton Trans*, 2000, 3885–3896.
69. G. R. Desiraju, *Angew. Chem. Int. Ed.*, 1995, **34**, 2311-2327.
70. G. R. Desiraju, *Acc. Chem. Res.*, 2002, **35**, 565-573.
71. C. B. Aakeröy and K. R. Seddon, *Chem. Soc. Rev.*, 1993, **22**, 397-407.
72. G. Xu, J. Lu, P. Guo, Z. Zhou, Z. Du and Y. Xie, *CrystEngComm.*, 2013, **15**, 4473-4478.
73. M. F. C. Ladd. and R. A. Palmer, *Structure Determination by X-ray Crystallography*, Springer Science+Business Media, LLC, 1993, 3rd ed.
74. J. P. Glusker, *Crystal Structure Analysis: A Primer*, Oxford University Press, Oxford, England, 3rd ed., 2010.
75. C. Marin and E. Dieguez, *Orientation of Single Crystals by Back-reflection Laue Pattern Simulation*, World Scientific, Singapore, 1999.
76. M. A. Withersby, A. J. Blake, N. R. Champness, P. A. Cooke, P. Hubberstey and M. Schroder, *J. Am. Chem. Soc.*, 2000, **122**, 4044-4046.

77. C. Hammond, *Introduction to Crystallography*, Oxford University Press, Oxford, 1990.
78. C. William, *Crystal Structure Analysis: Principles and Practice*, Oxford University Press, Oxford, 2001.
79. W. H. Zachariasen, *Theory of X-ray Diffraction in Crystals*, Dover, New York, 1967.
80. C. Hammond, *The Basics of Crystallography and Diffraction*, Oxford University Press, Oxford, 2nd ed., 2001.
81. C. Hammond, *Introduction to Crystallography*, Oxford U.P., Royal Microscopical Society, Oxford, Rev. ed., 1992.
82. A. J. C. Wilson, *Elements of X-ray Crystallography*, Addison-Wesley, Reading (Mass.), 1970.
83. R. Davey and J. Garside, *From Molecules to Crystallizers*, Oxford University Press, Oxford, 2000.
84. P. G. Jones, 1981, **17**, 222-225.
85. B. Spingler, S. Schnidrig, T. Todorova and F. Wild, *CrystEngComm.*, 2012, **14**, 751-757.
86. K.-W. Benz, *Introduction to Crystal Growth and Characterization*, Wiley, Hoboken, 2014.
87. R. W. Boyd, *Nonlinear Optics*, Academic Press, Amsterdam, 2nd ed., 2003.
88. H. Hope, *J. Appl. Cryst.*, 1971, **4**, 333.
89. A. L. Mackay, *J. Mol. Struct. (Theochem)*, 1995, **336**, 293-303.
90. C. Hammond and C. Hammond, *The Basics of Crystallography and Diffraction*, Oxford University Press, 2015.
91. J. M. Robertson, *Phys. Soc. Rep. Prog. Phys.*, 1937, **4**, 332-367.

92. W. C. Phillips, M. Stanton, A. Stewart, H. Qian, C. Ingersoll, and R. M. Sweet, *J. Appl. Cryst.*, 2000, **33**, 243-251.
93. W. Clegg, *Crystal Structure Determination*, Oxford University Press, Oxford, 1998.
94. A. L. Patterson, *Z. Kristallogr.*, 1935, **90**, 517-542.
95. I. Usón and G. M. Sheldrick, *Current Opinion in Structural Biology*, 1999, **9**, 643-648.
96. V. K. Pecharsky, *Fundamentals of Powder Diffraction and Structural Characterization of Materials*, Springer US, Boston, MA, 2009.
97. B. Fultz, *Transmission Electron Microscopy and Diffractometry of Materials*, Springer Berlin Heidelberg, Berlin, Heidelberg, 4th ed. 2013.
98. R. E. Dinnebier and S. J. L. Billinge, *Powder Diffraction: Theory and Practice*, Royal Society of Chemistry, Cambridge, 2008.
99. R. A. Vaia and W. Liu, *J. Poly. Sci. Part B: Polymer Physics*, 2002, **40**, 1590-1600.
100. P. Fraundorf and S. Lin, *Microscopy and Microanalysis*, 2004, **10**, 1356-1357.
101. J. I. Langford and D. Louer, *Rep. Prog. Phys.*, 1996, **59**, 131-234.
102. A. Buckley, N. B. Chapman, M. R. J. Dack, J. Shorter, and H. M. Wall, *J. Chem. Soc.*, 1968, **B**, 631-638.
103. S. M. Boudreau and H. M. Haendler, *Acta Cryst.*, 1986, **C42**, 980-982.
104. R. W. Taft and R. D. Topsom, *Prog. Phys. Org. Chem.*, 1987, **16**, 1-83.
105. M. E. Braun, C. D. Steffek, J. Kim, P. G. Rasmussen, and O. M. Yaghi, *Chem. Comm.*, 2001, 2532-2533.
106. C.-K. Xia, Y.-L. Wu and J.-M. Xie, *Z. Anorg. Allg. Chem.*, 2011, **637**, 282-288.
107. P. Fiedler, S. Bohm, J. Kulhanek and O. Exner, *Org. Biomol. Chem.*, 2006, **4**, 2003-2011.

108. S. Bohm, P. Fiedler, and O. Exner, *New. J. Chem.*, 2004, **28**, 67–74.
109. A. G. Whittaker, *Phys. Chem.*, BIOS: Oxford, 2000.
110. R. S. Berry, S. A. Rice, and J. Ross, *Phys. Chem.*, 2nd ed., Oxford University Press: New York, 2000.
111. R. G. Mortimer, *Phys. Chem.*, 3rd ed., Academic: Amsterdam, 2008.
112. C.-D. Wu, C.-Z. Lu, W.-B. Yang, H.-H. Zhuang and J.-S. Huang, *Inorg. Chem.*, 2002, **41**, 3302-3307.
113. S. M. Boudreau and H. M. Haendler, *Acta Cryst.*, 1992, **C48**, 615-618.
114. T.-J. M. Luo and G. T. R. Palmore, *Cryst. Growth Des.*, 2002, **2**, 337-350.
115. P.-W. Cheng, C.-F. Cheng, Y. Chun-Ting and C.-H. Lin, *Acta Cryst.*, 2010, **E66**, o1928.
116. Zhangliugen, *CSD Private Communication: Experimental Crystal Structure Determination*, DOI: 10.5517/ccdc.csd.cc1pfslh, 2017, CCDC **1562387**.
117. R.-H. Zeng, Z.-Q. Fang, F. Sun, L.-S. Jiang, Y.-W. Tang, *Acta Cryst.*, 2007, **E63**, m1813-m1814.
118. A. Karmakar and J. B. Baruah, *Inorg. Chem. Comm.*, 2009, **12**, 140-144.
119. G. M. Brown and R. E. Marsh, *Acta Cryst.*, 1963, **16**, 191-202.
120. I. Kumar, P. Bhattacharya, and K. H. Whitmire, *J. Organomet. Chem.*, 2015, **794**, 153-167.
121. I. Kumar, P. Bhattacharya, and K. H. Whitmire, *Am. Chem. Soc.*, 2014, **33**, 2906–2909.
122. F. Wiesbrock and H. Schmidbaur, *J. Am. Chem. Soc.*, 2003, **125**, 3622-3630.
123. T. I. A. Gerber, D. Luzipo and P. Mayer, *J. Coord. Chem.*, 2004, **57**, 1399-1403.
124. H. Irving and R. J. P. Williams, *J. Chem. Soc.*, 1953, **0**, 3192-3210.

125. S. Alvarez, *Dalton Trans.*, 2013, **42**, 8613-8636.
126. H. M. Haendler, *Acta Cryst.*, 1986, **C42**, 147-149.
127. X. Ma, S. Cambré, W. Wenseleers, S. K. Doorn and H. Htoon, *Phys. Rev. Lett.*, 2017, **118**, 027402.
128. B. A. Lange and H. M. Haendler, *J. Solid State Chem.*, 1975, **15**, 325-332.
129. S. M. Boudreau, R. A. Boudreau, and H. M. Haendler, *J. Solid State Chem.*, 1983, **49**, 379-384.
130. I. R. Amiraslanov, Kh. S. Mamedov, E. M. Movsumov, F. N. Musaev and G. N. Nadzhafov, 1979, **20**, 917-922.
131. M. A. Nadeem, M. Bhadbhade and J. A. Stride, *Dalton Trans.*, 2010, **39**, 9860–9865.
132. H.-Q. Hao, M.-X. Peng and Z.-Y. Chen, *Acta Cryst.*, 2007, **E63**, m2605.
133. Y.-C. He, N. Xu, F.-H. Zhao, W.-Q. Kan, H.-R. Liu and J. You, *Inorg. Chem. Comm.*, 2017, **86**, 78-81.
134. I. R. Amiraslanov, Kh. S. Mamedov, E. M. Movsumov, F. N. Musaev, A. N. Shnulin, and G. N. Nadzhafov, 1979, **19**, 420-425.
135. H. Necefoglu, O. Aybirdi, B. Tercan, Y. Suzenc and T. Hokelek, *Acta Cryst.*, 2010, **E66**, m585–m586.
136. T. Hokelek, H. Dal, B. Tercan, E. Tenlik, and H. Necefoglud, *Acta Cryst.*, 2010, **E66**, m891–m892.
137. M. Sertcelik, B. Tercan, E. Sahin, H. Necefoglu and T. Hokelek, *Acta Cryst.*, 2009, **E65**, m326-m327.
138. T. Hokelek, H. Dal, B. Tercan, F. E. Ozbek, and H. Necefoglu, *Acta Cryst.*, 2009, **E65**, m466–m467.

139. N. Necefoglu, E. Cimen, B. Tercan, E. Ermis, and T. Hokelek, *Acta Cryst.*, 2010, **E66**, m361–m362.
140. M. Mascal, L. Infantes, and J. Chisholm, *Angew. Chem. Int. Ed.*, 2006, **45**, 32-36.
141. B. Dutta, J. Datta, S. Maity, C. Sinha, D. Sun, P. P. Ray, M. H. Mir, *Phys. Chem. Chem. Phys.*, 2018, **20**, 24744-24749.
142. L. E. Cheruzel, M. S. Pometun, M. R. Cecil, M. S. Mashuta, R. J. Wittebort, R. M. Buchanan, *Angew. Chem.*, 2003, **115**, 5610-5613.
143. S. Pal, N. B. Sankaran, A. Samanta, *Angew. Chem. Int. Ed.*, 2003, **42**, 1741-1743.
144. L. Infantes and S. Motherwell, *CrystEngComm.*, 2002, **4**, 454-461.
145. M. P. Lightfoot, F. S. Mair, R. G. Pritchard, J. E. Warren, *Chem. Comm.*, 1999, 1945-1956.
146. M. V. Veidis, G. H. Schreiber, T. E. Gough and G. J. Palenik, *J. Am. Chem. Soc.*, 1969, **91**, 1859-1860.
147. M. Gerloch, *Inorg. Chem.*, 1981, **20**, 638-640.
148. Q. Gao, M.-Y. Wu, Y.-G. Huang, W. Wei, Q.-F. Zhang and M.-C. Hong, *Aust. J. Chem.*, 2010, **63**, 286-292.
149. O. Kristiansson, *Z. Kristallogr.*, 2001, **216**, 86-88.
150. O. V. Dolomanov, L. J. Bourhis, R. J. Gildea, J. A. K. Howard and H. Puschmann, *J. Appl. Cryst.*, 2009, **42**, 339-341.
151. G. M. Sheldrick, *Acta Cryst.*, 2015, **A71**, 3-8.
152. G. M. Sheldrick, *Acta Cryst.*, 2008, **A64**, 112–122.
153. C. F. Macrae, I. J. Bruno, J. A. Chisholm, P. R. Edgington, P. McCabe, E. Pidcock, L. Rodriguez-Monge, R. Taylor, J. van de Streek and P. A. Wood, *J. Appl. Cryst.*, 2008, **41**, 466–470.
154. F. H. Allen, *Acta Cryst.*, 2002, **B58**, 380-388.

155. F. H. Allen, S. Bellard, M. D. Brice, B. A. Cartwright, A. Doubleday, H. Higgs, T. Hummelink, B. G. Hummelink-Peters, O. Kennard, W. D. S. Motherwell, J. R. Rodgers, and D. G. Watson, *Acta Cryst.*, 1979, **B35**, 2331-2339.
156. C. R. Groom, I. J. Bruno, M. P. Lightfoot, and S. C. Ward, *Acta Cryst.*, 2016, **B72**, 171-179.